Ministère de l'enseignement Supérieur et de la recherche Scientifique

وزارة التعليم العالي والبحث العلمي

Badji Mokhtar Annaba University
Université Badji Mokhtar – Annaba
Faculté des Sciences

Département de Chimie

جامعة باجي مختار – عنابـــة

كـليـة العلوم

قســم الكيمياء

Thèse

Présentée pour obtenir le diplôme de

Doctorat Troisième Cycle

Filière : Chimie

Spécialité : Chimie Pharmaceutique

Par :

BOUONE Yousra Ouafa

Thème :

Synthèse et caractérisation de nouveaux dérivés de β-énaminones et de sulfamides, étude théorique et activité biologique.

Thèse soutenue le 10/07/2024 devant le jury composé de :

N°	Nom et prénom	Grade	Etablissement	Qualité
01	BERREDJEM Malika	Prof.	Université Badji Mokhtar - Annaba	Présidente
02	BOUCHAREB Fouzia	Prof.	Université Chadli Bendjedid - El Tarf	Rapporteur
03	BOUZINA Abdeslem	MCA	Université Badji Mokhtar - Annaba	Co-rapporteur
04	BOUMENDJEL Amel	Prof.	Université Badji Mokhtar - Annaba	Examinatrice
05	ZERROUKI Rachida	Prof.	Université de Limoges - France	Examinatrice
06	OUMEDDOUR Rabah	Prof.	Université 08 mai 1948 - Guelma	Examinateur

Acknowledgements

*The work presented in this thesis was accomplished in the Laboratory of Applied Organic Chemistry (**LCOA**), in the Bioorganic Chemistry group and the Synthesis of Biomolecules and Molecular Modelling group at Badji Mokhtar-Annaba University, Algeria.*

*Words would not be enough to express my gratitude to **Dr. Abdeslem BOUZINA**, PhD at Badji Mokhtar-Annaba University. Thank you for supporting me during my PhD journey, for your advices that were always full of humor and gentleness, for teaching me how to be a chemist and a researcher. Your enthousiasm and optimism never failed to fascinate me and will always be a source of motivation. Thank you for sharing with me your scientific experience. Working with you was a huge oppurtunity.*

*I would like to acknowledge **Prof. Fouzia BOUCHAREB** Professor at Chadli Bendjedid University for her help and assistance.*

*My deep gratitude goes to **Prof. Nour-Eddine AOUF** Professor at Badji Mokhtar-Annaba University, for his unconditional help, support, and encouragement. Thank you for believing in me.*

*My acknowledgment goes to **Prof. Malika BERREDJEM** head of Laboratory of Applied Organic Chemistry for her disponibility and precious aid.*

*I want to address my appreciation to **Prof. Malika IBRAHIM-OUALI** from University of Aix Marseilles for the crystallographic characterization.*

*My thanks goes also to **Prof. Rachida ZERROUKI** from University of Limoges who welcomed me for internship in the "**Laboratoire des Agroressources, Biomolécules et Chimie pour l'innovation en Santé**" in which I learned a lot.*

*Deep thanks to **Dr. Abdelhak DJEMEL** and **Dr. Chaouki BENSOUICI** from the Biotechnology Research Center (CRBt)-Constantine, for their major contribution in the biological evaluation.*

*I would like to thank the jury members for accepting to judge this modest work, including **Prof. Rabah OUMEDDOUR** from University of Guelma, and **Prof. Amel BOUMEDJEL** from Badji Mokhtar-Annaba University.*

"This work is dedicated to my parents; ***Leila*** *and* ***Mohamed****, without them I would have done nothing."*

"To my grandparents ***Malika*** *and* ***Salam****, and my aunt* ***Zouzou*** *who always supported me."*

"To my brother ***Rabeh****."*

"To my bestie ***Assila*** *who was by my side in good and hard times."*

"To my best friends; ***Soundes****,* ***Dhelia****,* ***Amira****."*

"To my labmates and my dear friends with whom I shared the best moments of my PhD journey; ***Rayene****,* ***Racha****,* ***Dounia****,* ***Rayenne****,* ***Rania****,* ***Meriem****,* ***Achraf****,* ***Ouafa****."*

"To all members of the LCOA family who made my journey amusing and informative at the same time."

« Synthesis and characterization of novel β-enaminone and sulfamide derivatives, theoretical study and biological activity. »

Abstract

The work presented in this manuscript lies on two specific families of compounds that shows versatility in both reactivity and pharmacology; β-enaminones and sulfamides.

β-enaminone derivatives were utilized as precursors to three different sets of compounds bearing respectively the β-enaminocarboxamide, the 4-hydroxyquinolone, and the acridine cores.

Synthetic procedures were elaborated and optimized for the three series, in order to give final products in the most improved aspect. Microwave irradiation was employed in the synthesis of 4-hydrooxyquinolone and acridine analogues.

On the other hand, a sulfamide-based small set of compounds was synthesized using sulfanilamide as a starting material.

All synthesized compounds were subjected to characterization using IR, NMR, LC-MS, and X-ray diffraction analysis to provide all the needed structural information.

In vitro studies were conducted to the synthesized molecules including antioxidant tests according to DPPH and ABTS assays for all compounds, as well as the antidiabetic evaluation through α-amylase inhibition for β-enaminocarboxamides.

In silico investigations were accomplished as a complementary study including molecular docking simulation, density functional theory DFT study, and ADME prediction.

Key words : β-enaminones, sulfamides, microwave synthesis, antioxidant agents, α-amylase inhibitors.

« Synthèse et caractérisation de nouveaux dérivés de β-énaminones et de sulfamides, étude théorique et activité biologique. »

Résumé

Le travail présenté dans ce manuscrit repose sur deux familles spécifiques de composés qui montrent une polyvalence à la fois dans la réactivité et la pharmacologie : les β-énaminones et les sulfamides.

Des dérivés de β-énaminones ont été utilisés comme précurseurs pour trois ensembles différents de composés contenant respectivement les motifs de β-énaminocarboxamide, de 4-hydroxyquinolone et d'acridine.

Des méthodologies de synthèse ont été élaborées et optimisées pour les trois séries, afin de synthétiser les produits finaux de façon améliorée. Les irradiations micro-ondes ont été employées dans la synthèse des analogues de 4-hydrooxyquinolone et d'acridine.

D'autre part, une petite série de composés à base de sulfamide a été synthétisé en utilisant la sulfanilamide comme produit de départ.

Tous les composés synthétisés ont été caractérisés en utilisant l'IR, la RMN, la LC-MS et l'analyse de diffraction des rayons X pour fournir toutes les informations structurales nécessaires.

Des études *in vitro* ont été menées sur les molécules synthétisées, comprenant l'évaluation de l'activité antioxydante selon les tests de DPPH et ABTS pour tous les composés, ainsi que l'évaluation de l'activité antidiabétique par inhibition de l'α-amylase pour les β-énaminocarboxamides.

Des investigations *in silico* ont été menées en complément, comprenant une simulation de docking moléculaire, une étude DFT (théorie de la fonctionnelle de la densité) et une prédiction ADME.

Mots clés : β-énaminones, sulfamides, synthèse par micro-onde, agents antioxidants, inhibiteurs de l'α-amylase.

« تحضير وتوصيف مشتقات جديدة من البيتا-إنامينون و السلفاميد، الدراسة النظرية و تقييم النشاط البيولوجي. »

ملخص

العمل المقدم في هذه الأطروحة يعتمد على مجموعتين محددتين من المركبات تظهر أهمية في كل من مجالي التركيب الكيميائي و علم الصيدلة: البيتا-إنامينونات والسلفاميدات.

تم إستخدام مشتقات البيتا-إنامينونات كمركبات أولية لثلاثة مجموعات مختلفة من المركبات تحتوي على عناصر البيتا-إنامينوكاربوكساميد،ال4-هيدروكسيكينولون، والأكريدين. تم تطوير وتحسين منهجيات التركيب العضوي للثلاثة مجموعات للتحصل على المركبات النهائية بشكل جيد. تم إستخدام الإشعاع بالموجات الدقيقة في تركيب نظائر الهيدروكسيكينولون والأكريدين. من ناحية أخرى، تم تركيب سلسلة صغيرة من المركبات المشتقة من السلفاميد بإستخدام السلفانيلاميد كمتفاعل.

تم تحديد الخصائص الهيكلية لجميع المركبات الناتجة بإستخدام التحليل بالأشعة تحت الحمراء، الرنين المغناطيسي النووي، الكروماتوغرافيا السائلة مع مطيافية الكتلة، و حيود الأشعة السينية لتوفير جميع المعلومات البنيوية اللازمة. تم إجراء دراسات في المختبر على الجزيئات المصطنعة، بما في ذلك تقييم النشاط المضاد للأكسدة بإستخدام إختبارات DPPH و ABTS لجميع المركبات، بالإضافة إلى تقييم نشاط البيتا-إنامينوكاربوكساميد ضد داء السكري بتثبيط الألفا-أميليز. تم إجراء دراسات في الحاسوب، بما في ذلك الإلتحام الجزيئي، ودراسة نظرية الكثافة الوظيفية، وتوقع خصائص الADME (إمتصاص، توزيع، أيض، و إخراج الادوية).

كلمات مفتاحية: بيتا-إنامينونات، سلفاميدات، التركيب بالموجات الدقيقة، مضادات الأكسدة، مثبطات الألفا-أميليز.

Table of contents

List of abbreviations

Chemical reagents and solvents

ABTS	2,2′-azinobis(3-ethylbenzothiazoline-6-sulfonic acid
Ac	Acetyl
AcOH	Acetic acid
Ac_2O	Acetic anhydrid
Ar	Aryl
BHA	Butylated hydroxyanisole
BHT	Butylated hydroxytoluene
Bn	Benzyl
CAN	Ceric Ammonium Nitrate
Cbz	Benzyloxycarbonyl
CENS	2-chloroethyl nitrososulfamides
CP	Cyclophosphamide monohydrate
CSI	Chlorosulfonyl isocyanate
DCM	Dichloromethane
DIAD	Diisopropyl azodicarboxylate
DMSO	Dimethyl sulfoxide
DMSO-d_6	Dimethyl sulfoxide-d_6
DPPH	2,2-diphenyl-1-picrylhydrazyl
DPTD	3-Amino-4-[4-(dimethylamino)phenyl]-4,5-dihydro-1,2,5-thiadiazole 1,1-dioxide
Et	Ethyl
EtOH	Ethanol
FAN	Free Amino Nitrogen
***i*Bu**	Isobutyl
$In(OTf)_3$	Indium(III) trifluoromethanesulfonate
***i*Pr**	Isopropyl
Me	Methyl
MeCl	Methyl chloride
MeCN	Acetonitrile
Me_2SO_4	Dimethyl sulfate

MeOH	Methanol
MMC	Mitomycin-C
***n*-Bu**	Butyl
***n*-Bu_4NI**	Tetra-*n*-butylammonium iodide
o/w	Octanol/water
PABA	Para-aminobenzoic acid
$Pd(OAc)_2$-$(PPh_3)_2$	Bis(triphenylphosphine)palladium(II) diacetate
PPh_3	Triphenylphosphine
PTSA	paratoluenesulphonic acid
$Rh_2(Oct)_4$	Rhodium(II) octanoate
tBuONa	Sodium tert-butoxide
TEA	Triethylamine
TFA	Trifluoroacetic acid
THF	Tetrahydrofuran
TMS	Tetramethylsilane
Ts	Tosyl
TsOH	Paratoluenesulphonic acid
ZSM-5	Zeolite Socony Mobil–5

Other abbreviations

ADME	Absorption, Distribution, Metabolism and Excretion
BBB	Blood-Brain Barrier
CA	Carbonic Anhydrase
CaMKII	Calcium/Calmodulin-dependent Protein Kinase II
COX-2	Cyclooxygenase-2
CYP	Cytochrome P450
DEPT	Distortionless Enhancement by Polarization Transfer
DFT	Density-Functional Theory
E	Entgegen
FT	Fourier Transform
FT-IR	Fourier Transform Infrared
GABA	γ-Aminobutyric acid
$GABA_A$	γ-Aminobutyric acid type A
G-gp	P-glycoprotein

GI	Gastrointestinal
HAT	Hydrogen Atom Transfer
hCA	Human Carbonic Anhydrase
HOMO	Highest Occupied Molecular Orbital
HPA	Human Pancreatic α-Amylase
HPLC	High-Performance Liquid Chromatography
HPLC-MS	High-Performance Liquid Chromatography-Mass Spectrometry
IC_{50}	Half-maximal inhibitory concentration
Inh	Inhibition
IR	Infrared
K_i	Inhibitory constant
LC-MS	Liquid Chromatography-Mass Spectrometry
LUMO	Least Unoccupied Molecular Orbital
MCF-7	Michigan Cancer Foundation-7
MEP	Molecular Electrostatic Potential
MIC	Minimum Inhibitory Concentration
M.p	Melting point
MW	Microwave
NMR	Nuclear Magnetic Resonance
ORTEP	Oak Ridge Thermal Ellipsoid Plot
PDB	Protein Data Bank
pH	Potential of hydrogen
R	Rectus
R_f	Retention factor
r.t	Room temperature
S	Sinister
SAR	Structure-Activity Relationship
TLC	Thin Layer Chromatography
TPSA	Topological Polar Surface Area
UV	Ultraviolet
VEGFR2	Vascular Endothelial Growth Factor Receptor
XO	Xanthine Oxidase
XRD	X-Ray Diffraction

Z	Zusammen

Units

cm	Centimeter
cm/s	Centimeter per second
D	Debye
Da	Dalton
eV	Electronvolts
eq	Equivalent
g	Gram
h	Hour
kcal	Kilocalories
kHz	Kilohurtz
mA	Milliamper
min	Minutes
mg	Milligrams
mg/kg	Milligrams per killograms
MHz	Megahurtz
mL	Milliliter
mm	Millimeter
mM	Millimolar
mmol	Millimoles
mol	Moles
nm	Nanometer
ppm	Parts per million
s	Seconds
W	Watt
Å	Angstrom
µL	Microliter
µm	Micrometer
µM	Micromolar
µmol	Micromoles
°C	Degrees Celsius
%	Percent

°	Degrees

List of schemes

Chapter I Overview on β-enaminones

Chapter II Overview on sulfamides and analogues

Chapter III Synthesis of novel β-enaminone and sulfamide derivatives

List of figures

Introduction

Chapter I Overview on β-enaminones

Chapter II Overview on sulfamides and analogues

Chapter III Synthesis of novel β-enaminone and sulfamide derivatives

Chapter IV *In vitro* and *in silico* assessment of novel β-enaminone and sulfamide derivatives

List of tables

Chapter III Synthesis of novel β-enaminone and sulfamide derivatives

Chapter IV *In vitro* and *in silico* assessment of novel β-enaminone and sulfamide derivatives

Chapter V Experimental data

Introduction

For centuries, the primary concern of researchers in the fields of chemistry and medicine has been combating anything that may threaten human health, and finding remedies for deadly diseases through the design of new pharmacologically active and highly effective molecules with the least possible side effects. The need for new drug-candidates increased significantly with the continuous upsurge in pathologies and drug resistance, prompting organic chemists to constantly search, design, and elaborate competent synthetic ways to produce compounds with active pharmacophores from available, simple, and cost-effective starting materials.

The versatility of β-enaminones represent a perfect example on how thousands of molecules can be derived from one molecular core. Indeed, β-enaminones are reactive structures yielding different interesting compounds with advantageous medicinal benefits. That is what made them having a significant importance in the drug design and development of novel drug-candidates [1].

In the present study, the special reactivity of β-enaminones lying in the 'push and pull' feature related to the presence of the conjugated enchainment N-C=C-C=O, was employed to produce three different structural systems; β-enaminocarboxamides, 4-hydroxyquinolone, and acridine analogues.

β-enaminocarboxamides or β-enaminoamides are a combination of β-enaminone and amide groups that have interesting biological effects. For instance, compound **1** was evaluated as an anxiolytic agent acting by allosteric modulation of $GABA_A$ receptors [2]. In a study of 2018, several *Z*-β-enaminones conjugated to amide groups such as compound **2** were described for their promising activities against breast cancer, showing effects on MCF-7 cancer cell line [3]. Furthermore, β-enaminoamides as compound **3** exhibited inhibitory activity against CaMKII which provide a prevention of cardiovascular diseases [4] (**Figure 1**).

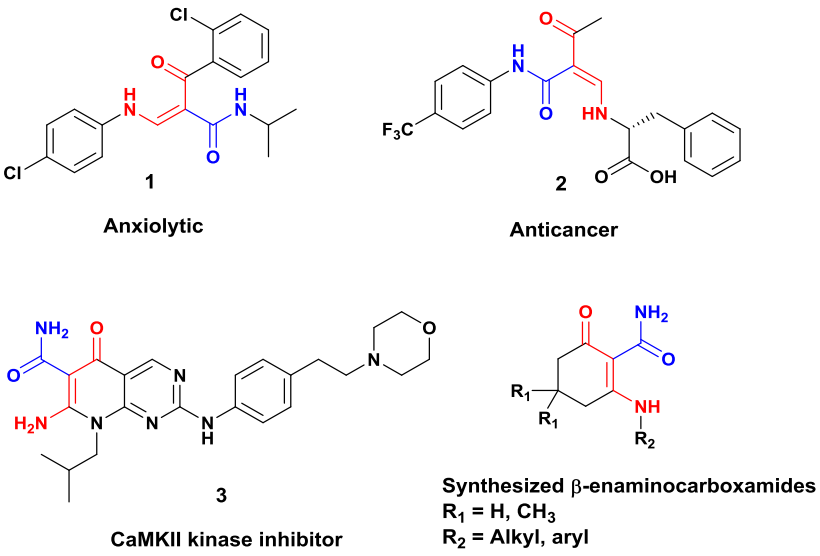

Figure 1. Structure of biologically active β-enaminoamide-containing compounds and the synthesized β-enaminocarboxamides.

Besides acting as precursors to interesting non-cyclic products, β-enaminones have also met expectations in the synthesis of different nitrogen-based heterocycles. Heterocyclic systems containing nitrogen are an integral part of countless natural and synthetic products having various applications in different fields, and have incessantly fulfilled the constant need to therapeutics in the medicinal field [5]. Among the most spread heterocycles, 4-hydroxyquinolones and analogues that have found a large spectrum of uses as antibacterial [6], antiproliferative [7], analgesic [8], antiallergenic [9], and antituberculosis agents [10] (**Figure 2**).

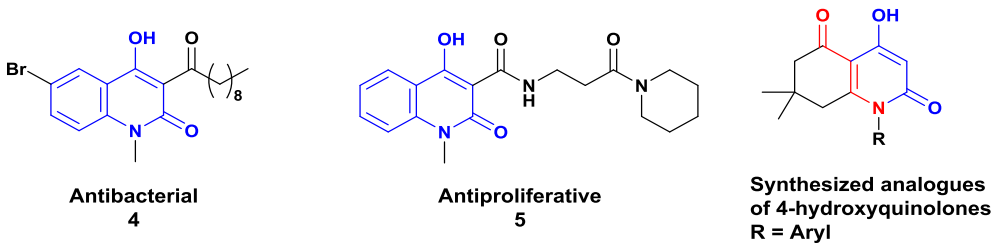

Figure 2. Structures of some active 4-hydroxyquinolones and synthesized analogues of 4-hydroxyquinolones.

Another widely studied heterocyclic ring, acridine and derivatives that have been extensively investigated for their employment in the healing of different pathologies. Pyronaridine **6**, Proflavine **7**, and Amasacrine **8** depicted in **Figure 3** are examples of acridine-based commercialized medicines used respectively as antimalarial, antibacterial, and antineoplastic agents [11].

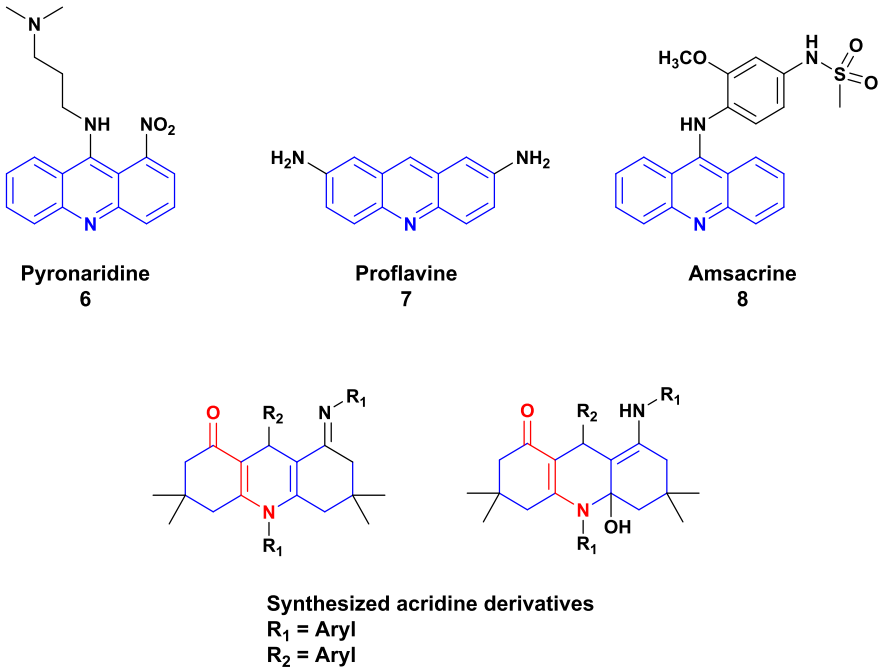

Figure 3. Structures of acridine-based drugs and the synthesized acridine derivatives.

On the other hand, it is needless to say that compounds structurally related to sulfamides have moved medicinal chemistry into another stage with the discovery of sulfanilamide as an extraordinary compound that itself holds several medicinal properties [12]. Sulfamides and analogues have their special place among the multi-target drugs. These drugs have been used as antibacterial [13], antidiabetic [14], and have been recognized as anticancer agents inhibiting different carcinogen drug targets [15], examples of sulfamide-derived molecules having curative gains are shown in **Figure 4**.

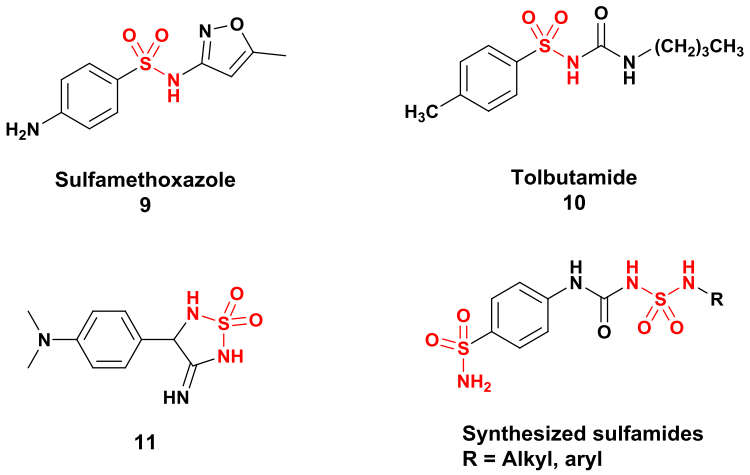

Figure 4. Structures of sulfamide-containing active compounds and the synthesized sulfamide derivatives.

The present manuscript explores the elaboration of efficient synthetic protocols leading to novel compounds derived from β-enaminone and sulfamide as well as the examination of the medicinal potential lying in the achieved molecules.

This thesis includes five different chapters that are structured as follows:

- In the first chapter, we will present a detailed bibliographic study about β-enaminones and their derivatives, giving their numerous applications in both medicinal chemistry as biologically active compounds used in the treatment of pathologies, and in organic synthesis as synthetic chemical intermediates that in diverse conditions could produce different structures.
- In the second chapter, a general overview on sulfamide-based compounds including their uses as active drugs against several diseases will be presented, as well as their reactivity and comportment in different reaction conditions giving diverse non-cyclic and heterocyclic systems.
- In the third chapter, results of our studies will be detailed counting the synthesis of three β-enaminone-derived and one sulfamide-derived series of compounds, the optimization of the corresponding synthetic protocols, and the characterization of the final products using spectroscopic and spectrometric methods namely; IR, ^{1}H NMR, ^{13}C NMR, ^{19}F NMR, and LC-MS, as well as the XRD complete structural elucidation of three derivatives among the synthesized compounds.
- In the fourth chapter, we will discuss the *in vitro* tests results of the antioxidant activity evaluation for all obtained sets of compounds and the evaluation of the antidiabetic activity for the β-enaminocarboxamides. Further, we will conduct a comparative analysis between *in vitro* and *in silico* results based on a molecular docking study. This latter will help predict the binding mode of the studied compounds with both xanthine oxidase and α-amylase enzymes as antioxidant and antidiabetic drug targets respectively. Thereby, explaining the interactions and to identifying key interactions between the active compounds and the cavities of the corresponding enzymes. Furthermore, DFT study will present additional structural properties of the studied compounds. Besides, we will predict pharmacokinetics properties using SwissADME online server.
- In the fifth chapter, all needed information about used reagents, materials, and reaction conditions will be mentioned. In addition, all general procedures leading to each group of compounds will be detailed along with the physico-chemical, spectral, and crystal data of obtained compounds. Moreover, we will present a detailed data of the used methods in the *in vitro* tests as well as the *in silico* studies.

Chapter I

Overview on β-enaminones

1. Chemistry of enaminones

The presence of an amine, ketone, and a double bond all-together in a successive manner within a structure leads to what is called an enaminone moiety. A different disposition of the stated functions gives place to two specific enaminones differentiated by Greek letters α and β (**Figure I.1**). These latter designate the position in which the amine is linked compared to the carbonyl group. As a result, we say α-enaminone **I.1** or β-enaminone **I.2** when the amine is connected to α or β positions respectively.

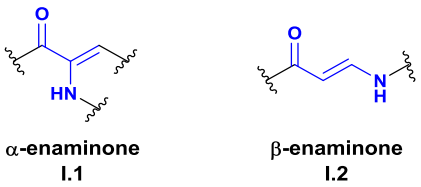

Figure I.1. Structure of α-enaminone and β-enaminone moieties.

The slight difference in structures of α-enaminone and β-enaminone yield differences in reactivity since they have modified electron delocalization forms as shown in **Scheme I.1**. α-enaminone contains two possible mesomeric rearrangements occurring separately; one with the enamine and the other with the α,β-unsaturated carbonyl. While β-enaminone adopts one mesomeric mechanism involving concurrently both enamine and α,β-unsaturated carbonyl. This special electron delocalization is the main reason of the high reactivity observed in β-enaminone-derived molecules particularly their role as nucleophilic agents.

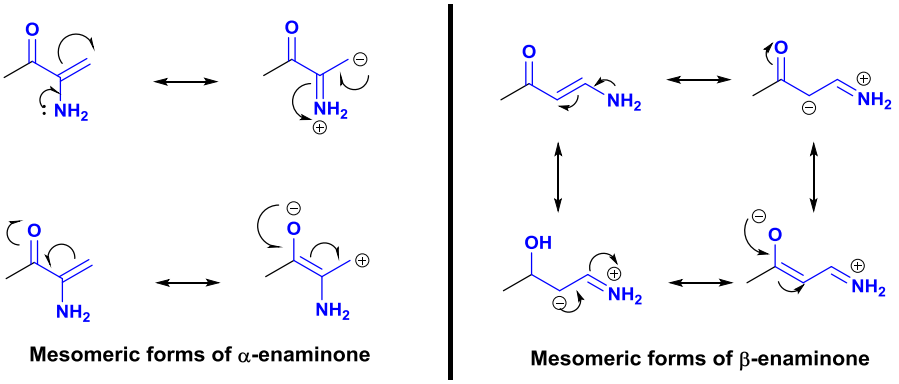

Scheme I.1. Electron delocalization in α- and β-enaminones.

2. Pharmacological effects of β-enaminones

Molecules bearing a β-enaminone scaffold in their structure have been widely investigated as pharmacological agents exhibiting significant biological effects against different pathologies. A selection of the most relevant literature works that discusses the beneficial biological activities of β-enaminone-containing compounds is outlined in the next sections.

2.1. β-enaminones as antibacterial and antituberculosis agents

Among the large number of studies conducted on the antibacterial and antituberculosis activities evaluation of β-enaminone-containing compounds, the study of Bangalore *et al.* [16] that assessed a series of usnic acid coupled to β-enaminones and 1,2,3-triazoles (**Figure I.2**). *Mycobacterium tuberculosis* inhibition was found to be at its topmost in compound **I.3** with a MIC value of 2.5 µM. Other derivatives of the same series presented good antibacterial activity including compound **I.5** that showed inhibitory activity of 41 µM against Gram-positive bacteria "*Bacillus subtilis*" (**Figure I.2).**

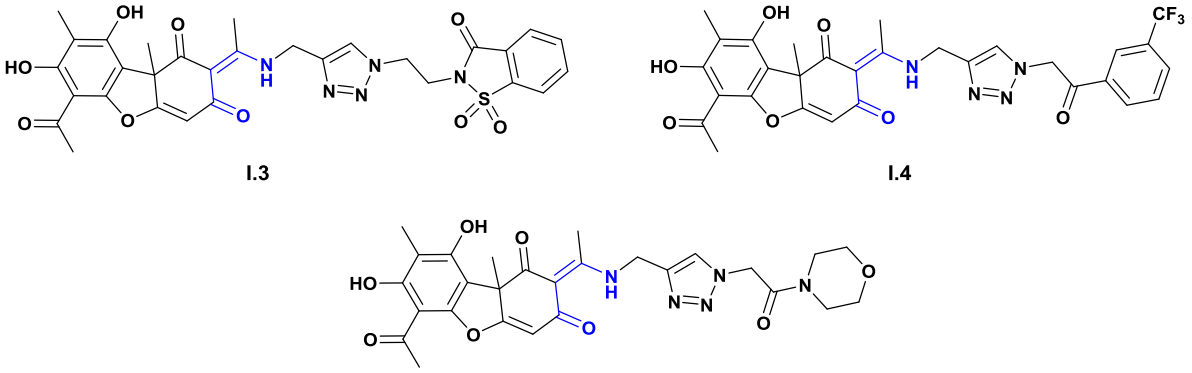

Figure I.2. Strcutures of some antibacterial and antituberculosis agents containing β-enaminone.

2.2. β-enaminones as selective cyclooxygenase-2 inhibitors

In 2019, Kumar *et al.* [17] designed compounds bearing cyclic enaminone moiety as new selective COX-2 inhibitors. Among the studied derivatives, compounds **I.6**, **I.7**, and **I.8** showed the best COX-2 *in vitro* inhibition with IC_{50} respectively equal to 0.513, 0.915, and 0.367 µM and exhibited high selectivity to COX-2 with indexes respectively equal to 74.09, 19.45, and 108.68. In *in vivo* tests, compounds **I.6**, **I.7**, and **I.8** showed potency and were comparable to celecoxib at the dose of 12.5 mg/kg and 25 mg/kg. The promising obtained results in this study highlighted the importance of cyclic enaminones as potent anti-inflammatory agents (**Figure I.3**).

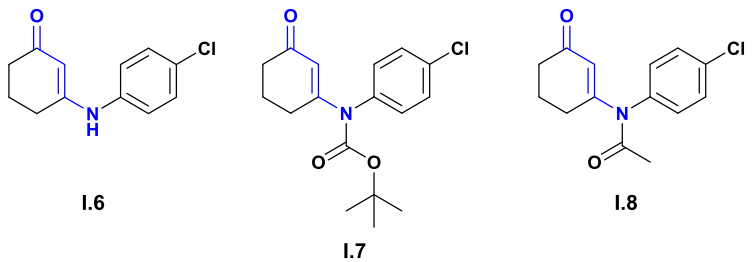

Figure I.3. Structures of some COX-2 inhibitors containing β-enaminone.

2.3. β-enaminones as anticonvulsant agents

β-enaminone moiety has found a significant place between active pharmacophores exhibiting positive anticonvulsant activity, which is supported by several previous studies [18]. The mechanism of action resulting in the anticonvulsant activity was linked to the augmentation of extracellular GABA rates in nervous system. KRS-5-Me-4-OCF_3 (**Figure I.4**) is a lead compound from a set of active anticonvulsant enaminones designed by Wang *et al.* [19]. Modifications in the above-mentioned lead compound using principles of drug design and structure-activity relationship (SAR) studies gave place to novel fluorinated N-benzamide enaminones that were evaluated in a battery of acute preclinical seizure models as reported in the literature by Amaye *et al.* [20]. In continuity to this study, Amaye's group pursued their research on fluorinated N-benzamide enaminones and reported in 2022 the evaluation of similar compounds as anti-seizure agents for the treatment of drug-resistant epilepsy. Results showed that *meta*-substituted trifluoromethyl β-enaminone derivatives **I.9** and **I.10** could block calcium channels of *T*-type by various mechanisms.

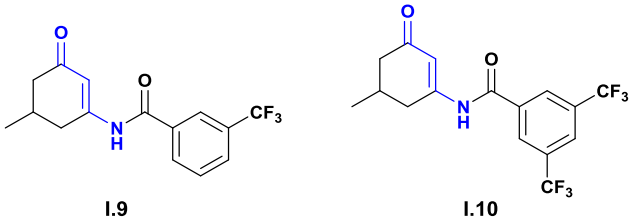

I.9 I.10

Figure I.4. Structures of anticonvulsant β-enaminone derivatives.

2.4. β-enaminones as anticancer agents

Cancer being the second death cause worldwide emerged as a concerning medical condition that needs attention of scientists and researchers in medicinal chemistry. Cancerous diseases could develop in many mechanisms and involves high numbers of physiological proteins, receptors, and enzymes. That is what made the conception of novel anticancer agents a highly needed process [21].

2.4.1. VEGFR2 inhibitors

β-enaminone scaffold is a structural part in many molecules screened for anticancer and antitumor activities, such as compound **I.11** and **I.12** conceived by Ghorab and coworkers (**Figure I.5**) [22]. The present compounds that display similarity with two known antitumor agents; Sorafenib and Sunitinib, showed an interesting potentiality to inhibit VEGFR2 with IC_{50} values respectively equal to 0.12 and 0.29 µM. Docking studies performed by the same group suggested that these analogs possess structural features that allow them to form significant

hydrogen bonds with residues of the VEGFR2 active site. It is noteworthy that carbonyl and amine of the linear β-enaminone moiety contained in compounds **I.11** and **I.12** are both involved in H bonds formation within the cavity of the studied enzyme according to Ghorab *et al.* [22].

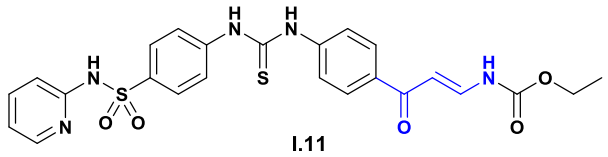

I.11

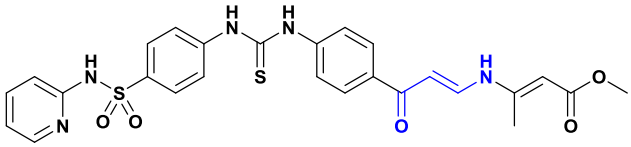

I.12

Figure I.5. Structures of potential VEGFR2 inhibitors bearing β-enaminone moiety.

2.4.2. Carbonic anhydrase inhibitors

Carbonic anhydrase IX (CA IX) is one of the main metallo-enzymes related to tumor growth and was widely explored as a drug target to the development of novel antitumor agents [23]. Eldehna *et al.* [24] investigated in their study the inhibitory ability of newly synthesized **SLC-0111** analogs bearing a linear β-enaminone structure (**Figure I.6**) towards different isoforms of the human carbonic anhydrase hCA family, namely; hCA I, II, IV and IX which were all inhibited by most compounds. Further, the studied series showed a special selectivity towards hCA IX over hCA II especially compound **I.13** and **I.14** with selectivity indexes respectively equal to 1498 and 1689. Besides these compounds, other linear enaminone-containing molecules were investigated as anticancer agents through inhibition of hCA including compound **I.15** that also incorporates the carboxylic acid moiety, showed efficiency against isoforms hCA IX (K_i = 0.83 µM) and hCA XII (K_i = 2.4 µM) [25].

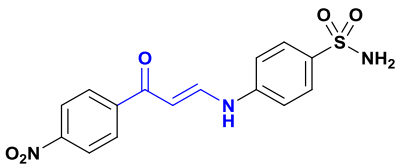

I.13

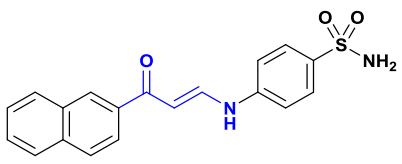

I.14

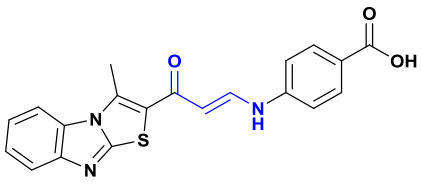

I.15

Figure I.6. Structure of β-enaminone-containing hCA inhibitors.

3. Synthesis of β-enaminones

β-enaminones with its importance in both medicinal chemistry and organic synthesis have widely attracted attention of scientists, that is what prompted elaboration of several synthetic protocols in order to produce these type of molecules.

In the following sections, we will present a compilation of the most commonly used as well as the recent synthetic pathways leading to β-enaminones.

3.1. Condensation reaction of β-diketones and amines

The condensation reaction of β-diketones such as dimedone and cycohexanedione with different primary and secondary amines is the most described procedure for the synthesis of β-enaminones. This procedure follows a certain mechanism in which the amine being nucleophilic attacks one of the carbonyl in diketones considered as highly electrophilic leading to an enaminone compound after elimination of one water molecule.

A high number of scientific works was dedicated to this reaction, starting from the ones using conventional methods to others that involves more optimized and greener conditions.

Application of reflux conditions to generate β-enaminones was described multiple times in different researches including the work described by Eddington *et al.* [26] that reported the synthesis of diverse β-enaminones from trifluoro diketones and substituted benzylamines in absolute ethanol of ethyl acetate as a solvent. Apraku and Okoro [27] carried a modified procedure that led to analogous molecules through condensation of trifluoro diketones and different substituted phenylamines in CH_2Cl_2 in the presence of paratoluenesulphonic acid and acetic acid (**Scheme I.2**).

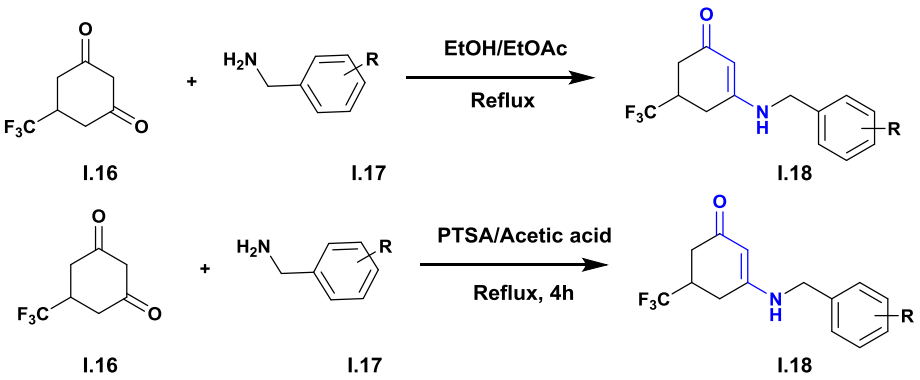

Scheme I.2. β-enaminone synthesis from β-diketones and amines.

Stefani *et al.* [28] attempting an easier way for producing β-enaminones opted for a simple condensation between β-ketoesters or β-diketones with different amines at room temperature in an aqueous milieu.

In view of the high interest lying in β-enaminones as synthetic intermediates, several optimization efforts were pursued to easily provide these molecules. Accordingly, quite a lot of catalysts were employed citing; onion extracts [29], $Bi(TFA)_3$ [30], $CeCl_3.7H_2O$ [31], $CoCl_2.6H_2O$ [32], $LaCl_3$ [33], CAN [34], Pd(0) [35], FAN [36], $NaAuCl_3$ [37], and ZSM-5 [38]. Microwave activation is one of the most used methods in the current organic chemistry laboratories for its high efficiency in terms of providing excellent yields of several compounds in a remarkably short time [39]. This method proved its usefulness in the synthesis of β-enaminones from diketones and amines in solvent-, support-, and catalyst-free conditions as shown in the work of Andrade *et al.* [40] (**Scheme I.3**).

Researches surrounding β-enaminones synthesis from β-diketones and amines under microwave irradiation continued to arise during the last years and included the use of solid supports such as silica, montmorillonite clay K_{10}, and KSF [41-43] making it the fastest procedure to follow in order to produce β-enaminones in excellent yields.

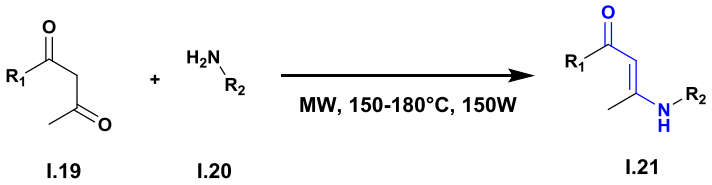

Scheme I.3. Microwave-assisted synthesis of β-enaminones.

3.2. Photochemical reaction of vinyl azides and aldehydes

Photochemical synthesis has gained considerable interest in the recent years as an innovative method with numerous advantages that resides in the replacement of thermal activation, as well as obtain reaction selectivity, scalability, and reproducibility.

Paveliev *et al.* [44] used photochemical activation to generate enaminones in 15–72% yields from vinyl azide and aldehyde derivatives. The reaction was mediated by decatungstate photocatalyst under batch and flow conditions (**Scheme I.4**).

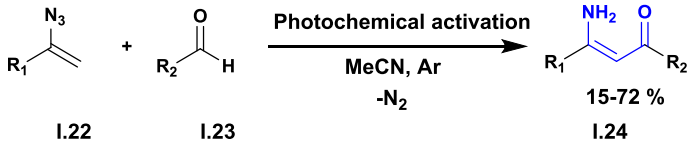

Scheme I.4. Photochemical synthesis of β-enaminones.

3.3. Rearrangement of 1,2,3-triazoles under rhodium catalyst

Acyclic β-enaminones could be obtained from rearrangement of 1,2,3-triazoles in the presence of a catalytic amount of $Rh_2(Oct)_4$ as represented in **Scheme I.5** The stated synthetic pathway is privileged by its rapidity and greenness which is related to microwaves utilization [45].

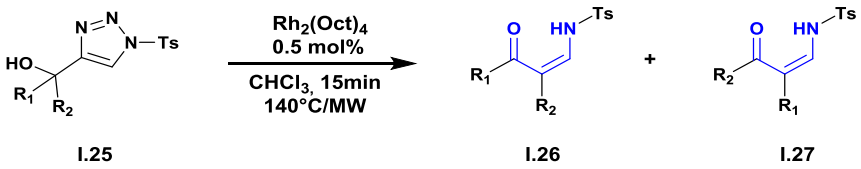

Scheme I.5. β-enaminones formation through rearrangement of 1,2,3-triazoles.

3.4. Electrochemical reaction of vinyl azides and α-ketoacids

Synthesis *via* electrochemistry is considered as one of the advanced green chemistry method in which the source of activation comes from the power connected to electrodes. This power results in the transfer of electrons from the electrode to the reaction mixture, thereby creating a constant circuit that takes a reaction to completion. Kong *et al.* [46] employed this strategy to produce enaminones starting from vinyl azides and α-keto acids as presented in **Scheme I.6**.

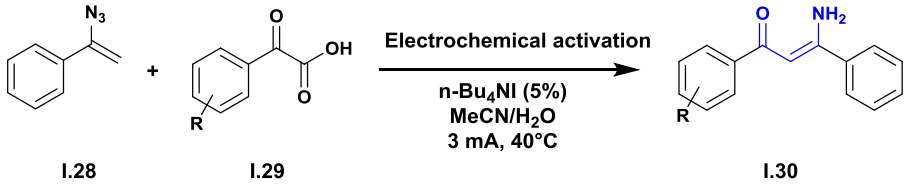

Scheme I.6. Electrochemical synthesis of β-enaminone derivatives from vinyl azides and α-ketoacids.

3.5. Isomerization of propargylic hydroxylamines

Gayon *et al.* [47] aiming for the synthesis of isoxazoles and pyrimidines derivatives from propargylic hydroxylamines have reacted these latter in acetonitrile as a solvent under basic conditions (NaOH 10 mol%) at 50°C during 1h of reaction time. Unexpectedly, Gayon and colleagues have observed a rearrangement instead of a cyclization that resulted in the formation of N-protected β-enaminones in their *Z* isomers (**Scheme I.7**) as well as a negligible amount of imines conjugated to alkyne group. The yields of *Z*-β-enaminones were found to be varying from moderate to excellent [29-90%]. Moderate yields were attributed to the presence of sterically hindered substituents linked to the alkyne group, what made this procedure an interesting and unusual way to produce β-enaminones from propargylic hydroxylamines substituted with small constituents in a relatively short time and with selectivity of *Z* isomers over *E* isomers.

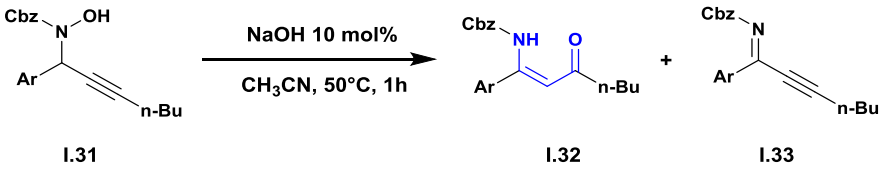

I.31 I.32 I.33

Scheme I.7. Synthesis of *Z*-enaminones from isomerization of propargylic hydroxylamines.

3.6. Reactions of keto-alkynes and propargylic amines

Different β-enaminone derivatives were produced through condensation between keto-alkynes and propargylic amines under reflux in methanol (**Scheme I.8)** [48]. This procedure has been recognized as effective for the synthesis of N-propargylic β-enaminones serving as reactive synthetic intermediates for the preparation of different heterocyclic systems including pyridine rings.

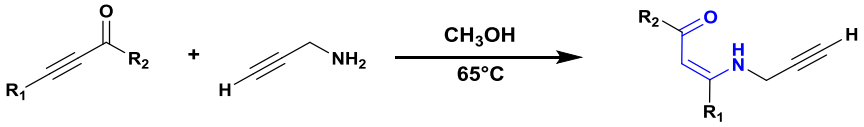

I.34 I.35 I.36

Scheme I.8. Synthesis of β-enaminones from propargylic amines.

4. Applications of β-enaminones as synthetic intermediates

The special reactivity of β-enaminones made them widely employed in the synthesis of different structures. Next sections will include a modest selection of previously reported syntheses of different systems from β-enaminone precursors, highlighting their significant importance as electrophilic and nucleophilic agents.

4.1. Acridines

In 2012, To *et al.* [49] used β-enaminone derivatives in a one pot multicomponent reaction that included different β-enaminones, aldehydes, and cyclic β-diketones catalyzed by $In(OTf)_3$. This reaction afforded acridinediones in excellent yields after stirring for 2 to 3h at a temperature of 100°C (**Scheme I.9**).

The reaction occurred according to an addition in which the β-enaminone and the cyclic β-diketones played the role of nucleophilic agents that attacked the carbonyl of the aldehyde derivative forming an asymmetrical carbon. β-enaminone moiety prioritized by two nucleophilic sites promoted the final cyclization with its azote atom that led to the formation of acridine ring.

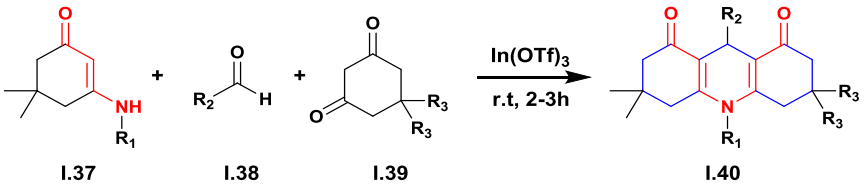

Scheme I.9. General procedure for the synthesis of acridine derivatives from β-enaminones.

4.2. Pyridines

β-enaminones substituted by a propargyl group in the azote position served as precursors to pyridines in a number of researches such as the one published in 2015 by Karabiyikoglu *et al.* [48]. Authors elaborated an easy strategy to promote the formation of a pyridine ring; this strategy consisted of the use of iodine that reacted with the alkyne group to create a highly electrophilic tricycle. The double bond in the β-enaminone enchainment with its high nucleophilicty engendered by electron delocalization attacked the formed electrophilic site, thereby produced the pyridine heterocycle. The stated strategy gave excellent yields of pyridine derivatives (**Scheme I.10**).

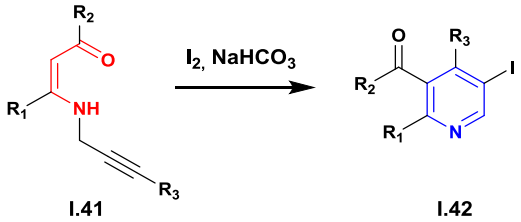

Scheme I.10. General procedure for the synthesis of pyridines from β-enaminones.

4.3. Quinolines

Quinolines were achieved from β-enaminones, amines, and DMSO through the metal free procedure reported in 2019 by Jiang and coauthors [50]. This procedure led to several quinoline-based derivatives in moderate to good yields (**Scheme I.11**).

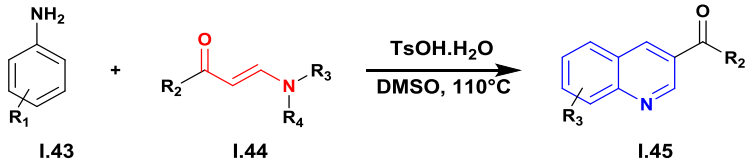

Scheme I.11. General procedure for the synthesis of quinolones from β-enaminones.

4.4. Indoles

Indole rings could also be attained when reacting 2-chloroaryl enaminones in the presence of a 5:2 mixture of $NaNH_2$ and tBuONa as presented in the work of Caubere *et al.* [51]. Indoles is a product of an intramolecular cyclization in which the double bond of the enaminone moiety

is activated by proton delocalization of azote resulting in a nucleophilic attack at the *ortho* position of the aryl ring (**Scheme I.12**).

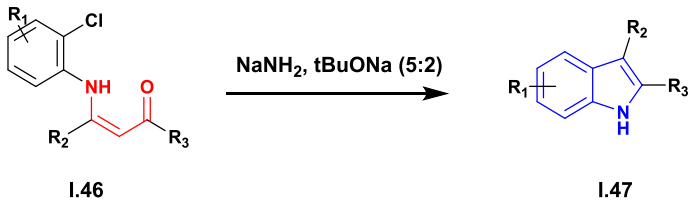

I.46 I.47

Scheme I.12. General procedure for the synthesis of indoles from β-enaminones.

4.5. Indenoindoles

Among the diverse nitrogen-based heterocycles that are accessible from β-enaminones, the indenoindole tetracycle. The work of Jiang and coworkers [52] reported the microwave three-component reaction of β-enaminones **I.48**, ninhydrin **I.49**, and acetic anhydride producing the final indenoindoles **I.50** in excellent yields exceeding 60% (**Scheme I.13**).

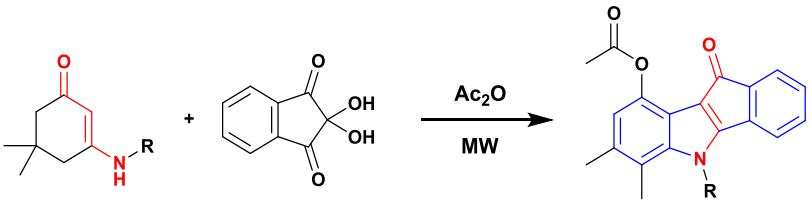

I.48 I.49 I.50

Scheme I.13. General procedure for the synthesis of indenoindoles from β-enaminones.

4.6. Carbazoles

Carbazole analogues are formed by an intramolecular cyclization of β-enaminones adopting a similar mechanism pathway as indole formation [53]. This procedure involves the use of palladium-based catalyst $Pd(OAc)_2$-$(PPh_3)_2$ in the presence of sodium bicarbonate $NaHCO_3$ (**Scheme I.14**).

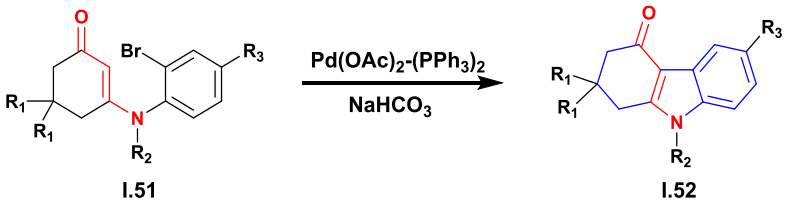

I.51 I.52

Scheme I.14. General procedure for the synthesis of carbazoles from β-enaminones.

Conclusion

In this chapter, we conducted a bibliographic overview on β-enaminones and derivatives. The study englobed a general description of the chemistry of enaminones and their special reactivity as well as their role in medicinal research through presenting different pharmacologically active

compounds bearing this skeleton. We also mentioned the role of β-enaminones among the organic chemistry area as reactive synthetic intermediates leading to different interesting structural systems by presenting synthetic pathways of several heterocyclic rings from β-enaminone-containing reagents. This bibliography ideally introduces the reported work in the present thesis that lies on the use of β-enaminones to yield three different families of compounds.

Chapter II

Overview on sulfamides and analogues

1. Chemistry of sulfamides

A sulfamide moiety can be defined by a sulfone group attached to two amines giving the (N-SO_2-N) enchainment. A small modification in this structure gives three different analogues of sulfamides; in this way, the suppression of one amine group define a sulfonamide function with the structure (N-SO_2), the addition of an aromatic ring to this latter gives place to an arylsulfonamide (Ar-SO_2-N), named benzenesulfonamide when it is attached to a substituted benzene ring. While the addition of a CO-NH to a sulfonamide group results in a widely studied pharmacophore named sulfonylurea exhibiting the structural enchainment of (N-CO-N-SO_2) (**Figure II.1**).

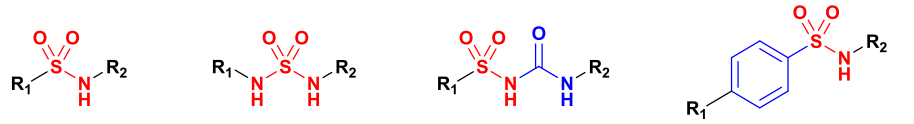

Figure II.1. General structure of sulfamide and analogues.

2. Pharmacological effects of sulfamides and analogues

Sulfamides and analogues with their special structure bioisosteric to urea constitute a remarkably large class of compounds exhibiting different pharmacological activities since the early eras of medicinal chemistry and represent a widespread pharmacophore in a high number of commercialized drugs [54].

A selection of some biological activities presented by sulfamide-based compounds will be outlined in the following sections.

2.1. Antibacterial activity

Among the earliest identified activities of sulfamides and analogues, the antibacterial activity found in the Prontosil **II.5** that was then commercialized from Bayer laboratories (**Figure II.2**). This discovery that owed a Nobel price to G. Domagk was followed by the contribution of both Jacques and Thérèse Tréfouel in the finding of sulfanilamide **II.6** from Prontosil decomposition (**Scheme II.1**). The antibacterial activity was attributed essentially to the sulfanilamide moiety considered as an analogue of *para*-aminobenzoicacid (PABA) **II.7**, a property that allowed sulfanilamide to efficiently inhibit the bacterial dihydropteroate synthase resulting in a bacteriostatic activity [55].

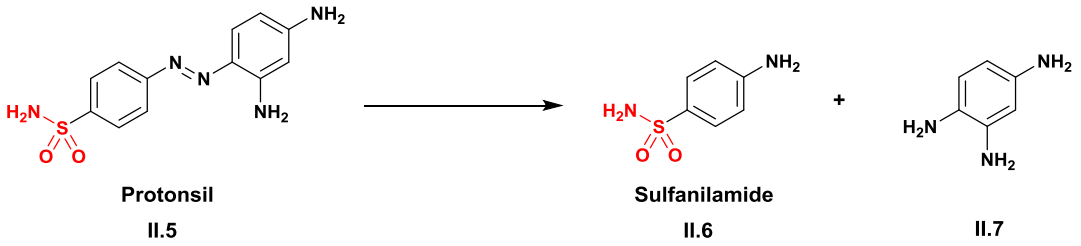

Scheme II.1. Decomposition of Protonsil to sulfanilamide.

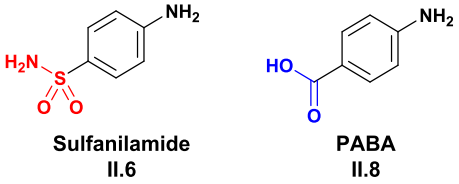

Figure II.2. Structures of sulfanilamide and PABA.

Since the discovery of the antibacterial feature of sulfanilamide, a considerable number of sulfanilamide analogues were conceived to enlarge the spectrum of the treated infectious diseases. Sulfamethoxazole **II.9** and Sulfadiazine **II.10** figures as the most known sulfonamide-based antibacterial agents (**Figure II.3**) [13].

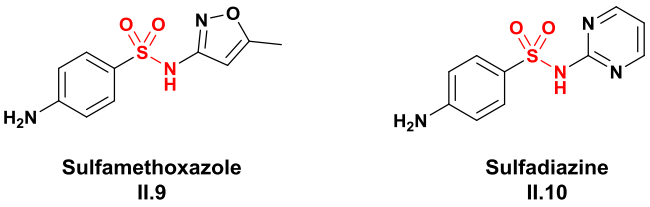

Figure II.3. Structures of some antibacterial sulfonamide derivatives.

Other recently reported compounds containing (N-SO_2-N) pharmacophore revealed antibacterial activity against Gram positive and negative bacteria such as compounds **II.11**, **II.12**, and **II.13** (**Figure II.4**) [56].

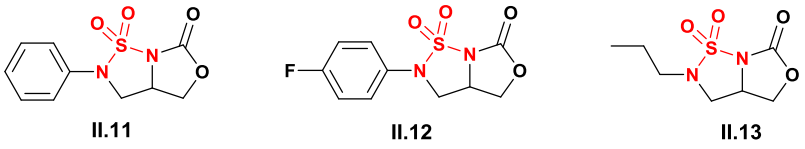

Figure II.4. Structures of some antibacterial (N-SO_2-N)-based compounds.

2.2. Anti-inflammatory activity

Sulfamide analogues including arylsulfonamides have shown an increasing interest as anti-inflammatory with the conception of coxibs as Valdecoxib **II.14** and Celecoxib **II.15** that have been commercialized as nonsteroidal anti-inflammatory drugs (**Figure II.5**) [57].

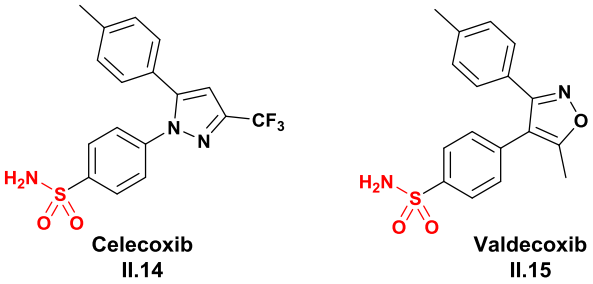

Figure II.5. Structures of anti-inflammatory sulfonamide derivatives.

2.3. Antidiabetic activity

Among the sulfamide analogues that present an antidiabetic effect, the well-known pharmacophore; sulfonylurea (N-CO-N-SO_2). These compounds represent a class of orally active hypoglycemic drugs and have been utilized in managing type 2 diabetes for many years. They act by enhancing the release of insulin by pancreatic β cells. The discovery of sulfonylureas as hypoglycemic agents dates back to a clinical observation in the 1940s by Janbon and Loubatières, who noted the blood sugar-lowering effect of a sulfanilamide derivative while treating bacterial infections [58].

Extensive research on sulfonylureas has led to the discovery of new derivatives. Carbutamide **II.16** was the initial orally active sulfonylurea derivative developed for hypoglycemia treatment, followed by Tolbutamide **II.17**, which was synthesized by substituting the NH_2 group with its bioisostere CH_3. Further compounds have been identified, comprising a second generation of sulfonylureas such as Glimepiride **II.18** (**Figure II.6**) [59].

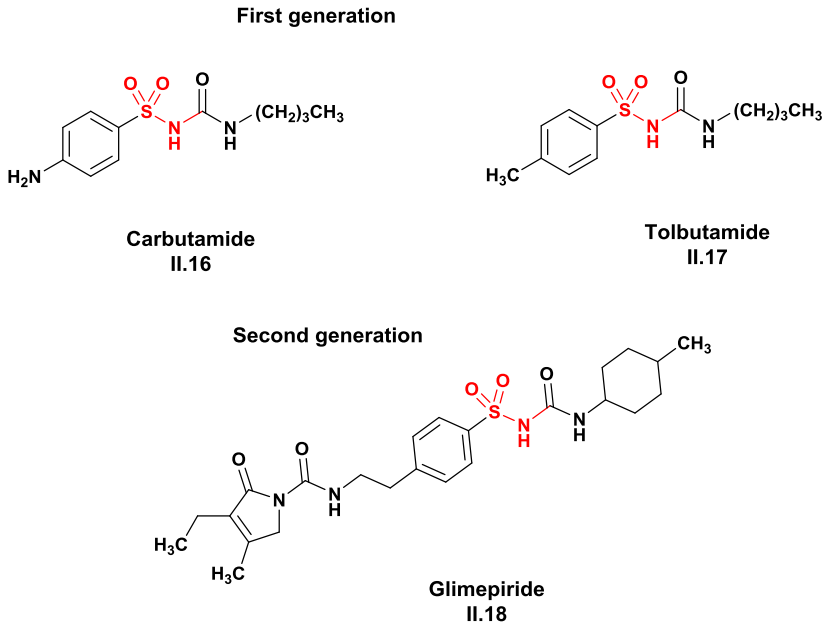

Figure II.6. Structure of hypoglycemic sulfonylurea derivatives.

2.4. Anticancer activity

A recent comprehensive study on 3-Amino-4-[4-(dimethylamino)phenyl]-4,5-dihydro-1,2,5-thiadiazole 1,1-dioxide (DPTD) revealed its potential cytotoxic, cytostatic, and genotoxic effects on human blood lymphocyte cultures, along with its metabolites. Additionally, DPTD emerges as a promising candidate for anticancer therapy, either as a standalone treatment or in combination with other drugs [60]. Şekeroğlu *et al.* [61] have provided evidence suggesting that DPTD could be utilized in combined cancer therapy. Co-administration of DPTD with MMC or CP may lead to enhanced cytotoxic and genotoxic outcomes, possibly due to synergistic effects. One of these sulfamide-based anticancerous compounds; derivative **II.19** illustrated in **Figure II.7**.

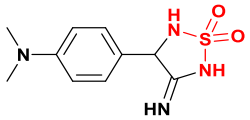

II.19

Figure II.7. Structure of a sulfamide-based anticancerous agent.

3. Synthetis of sulfamides and analogues

3.1. Reaction of α-aminoesters and sulfonyl chloride

Danek *et al.* [62] described the synthesis of symmetric N,N'-disubstituted sulfamides from aromatic α-aminoesters in the presence of sulfonyl chloride and pentane. The corresponding sulfamides were obtained with yields ranging from 71 to 85% (**Scheme II.2**).

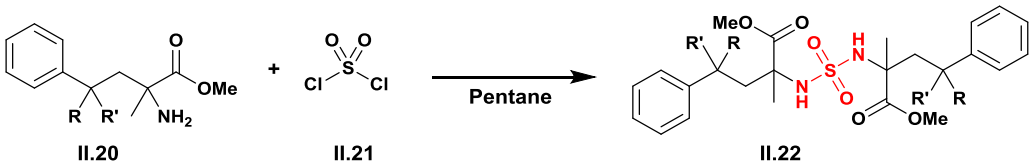

II.20 **II.21** **II.22**

Scheme II.2. Synthesis of sulfamides from α-aminoesters.

3.2. Reaction of nucleophile reagents and chlorosulfonyl isocyanate

Abdaoui *et al.* [63] prepared alkylating agents; 2-chloroethyl nitrososulfamides (CENS), using CSI as the starting reagent. This synthesis involves four steps (carbamoylation-sulfamoylation followed by a Mitsunobu alkylation, deprotection, and finally nitrosation), and these compounds were obtained with yields ranging from 47 to 58% (**Scheme II.3**).

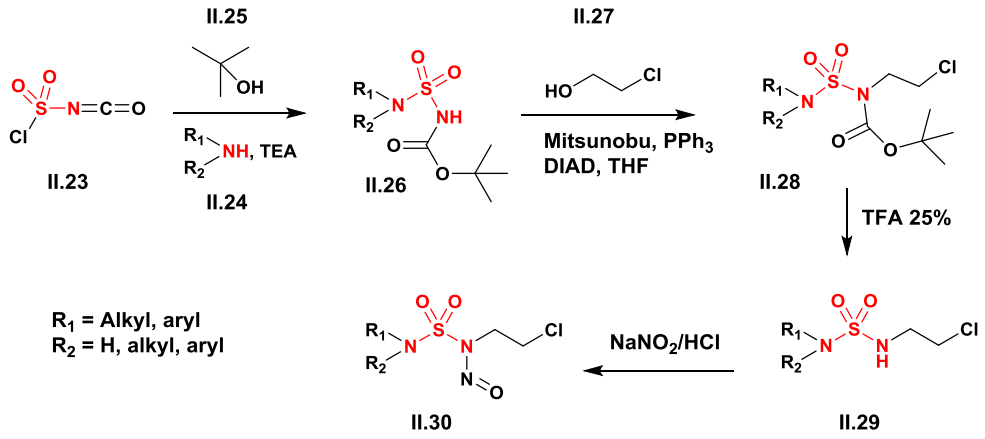

Scheme II.3. Sulfamide synthesis from CSI.

The acylation of indoles **II.31** with chlorosulfonyl isocyanate occurs at position 3, leading to the formation of sulfonyl chlorides **II.33** (**Scheme II.4**) [64].

The reaction of sulfonyl chlorides with amines proceeds through a nucleophilic substitution of the chlorine, resulting in the formation of indole sulfamides **II.35** (**Scheme II.4**) from the structure of the initial compounds.

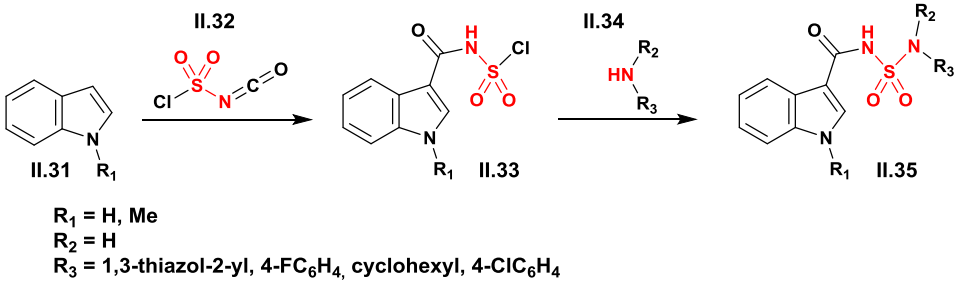

Scheme II.4. Sulfamide synthesis from CSI and indoles.

3.3. Reaction of amines and sulfur dioxide

Sulfamide derivatives were easily achieved in the work described by Leontiev *et al.* [65] through the simple one-step reaction of SO_2 gas with different aromatic anilines (**Scheme II.5**). The obtainment of final symmetrical sulfamides is conditioned upon the use of amine bases that activates sulfur dioxide rendering it a readily usable reagent. This procedure is effective not only in the synthesis of symmetrical sulfamides but also was employed in generating the corresponding sulfamide polymers.

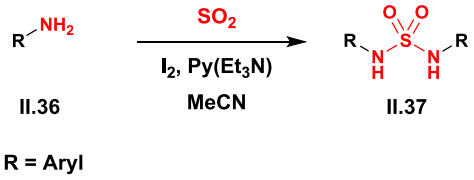

Scheme II.5. Sulfamide synthesis from sulfur dioxide.

4. Reactivity and applications of sulfamide derivatives as synthetic intermediates

4.1. Sulfamides in N-substitution reactions

Sulfonamides and sulfamides contain nitrogen atoms that can act as reactive nucleophiles, enabling acetylation reactions catalyzed by an acid, alkylation catalyzed by a base, chlorination, and cyanoethylation as presented in **Scheme II.6** [66].

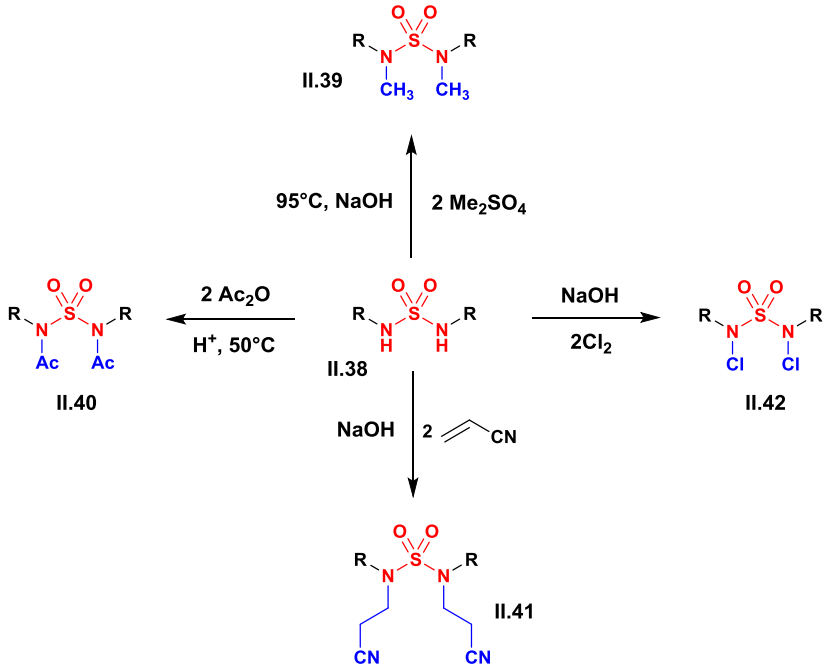

Scheme II.6. N-substitution of sulfamides.

4.2. Synthesis of bis aziridines

Treating N,N'-bis(1-alkyl-2-chloroethyl)sulfamides **II.43** under basic conditions (K_2CO_3) at mild conditions leads to the formation of bis-aziridinylsulfonyls [67], this reaction perfectly highlights the high reactivity of sulfamides towards electrophilic sites contained in the same structure leading to an intracyclization (**Scheme II.7**).

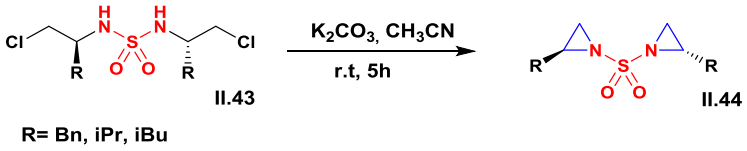

Scheme II.7. Synthesis of bis-aziridines from sulfamides.

4.3. Synthesis of cyclosulfamides

Bouzina *et al.* [68] described the synthesis of cyclic sulfamides *via* a three-component reaction similar to Biginelli reaction involving aldehydes, cyclohexanedione, and simple sulfamide instead of urea. This procedure conducted under microwave irradiation catalyzed by acetic acid

and sulfuric acid gave the desired compounds in excellent yields (**Scheme II.8**). The anti-Alzheimer activity of the synthesized derivatives was evaluated through inhibition assessment of acetylcholinesterase enzyme [69].

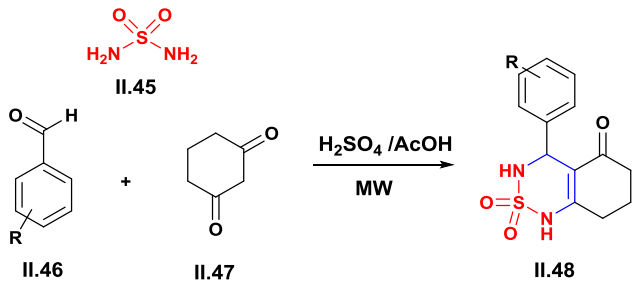

Scheme II.8. Cyclosulfamides synthesis *via* multicomponent reaction.

4.4. Sulfamide reaction with carbonyls

The high nucleophilicity of sulfamide azotes can be clearly confirmed when reacted to carbonyl-containing functional groups such as esters, as well as their reaction with nitriles.

A considerable amount of work has been done by Stud and his colleagues on these reactions and related reactions of sulfamides, with some of them depicted in **Scheme II.9**. Some of the heterocycles obtained can be considered as analogues of pyrimidine and purine [66].

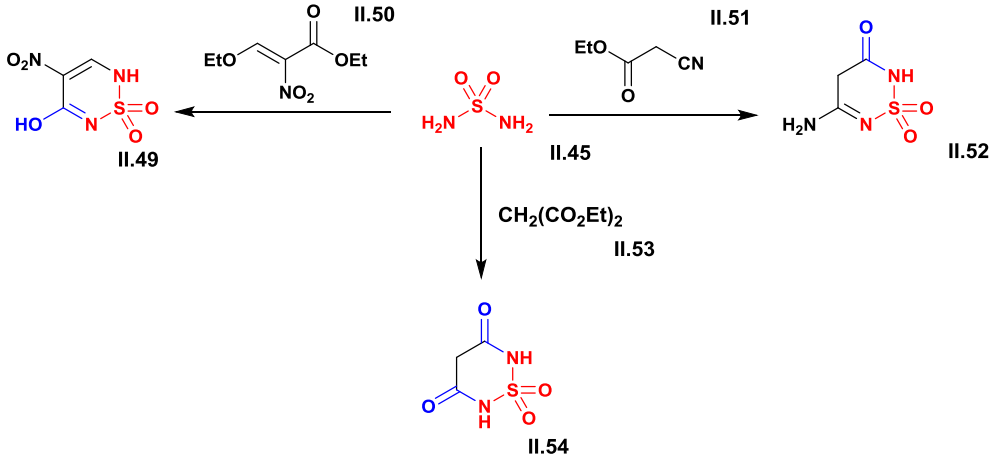

Scheme II.9. Reaction of sulfamides with carbonyl-containing reagents.

Conclusion

In this chapter, we have provided a bibliographic overview of sulfamides in the broad sense of the term. We have mentioned the structural motifs that can derive from a sulfamide as well as their pharmacological activities. We have cited several methods for synthesizing sulfamides as well as their reactivity towards different reagents.

Chapter III

Synthesis of novel β-enaminone and sulfamide derivatives

Accessing novel compounds that can serve as potential drug candidates is the primary objective of drug design and development. Many methods are employed in order to obtain promising active substances, such as synthesizing novel compounds with similarities to known commercialized drugs, which are often synthesized or extracted from medicinal plants.

Conceiving novel molecules by modifying the skeleton of known compounds is a relatively complicated process, in which the scientist needs to prioritize several factors including good yields, cost-effectiveness, eco-friendliness, as well as the simplicity and feasibility of the elaborated protocol. In order to achieve the before-mentioned factors; using simple, reactive, and easily achievable starting materials is a great choice. That is what incited us to the use of β-enaminone-containing derivatives as starting materials, which could be effortlessly accessed by a simple condensation reaction [70]. Further, this kind of molecules possess an interesting enchainment of atoms that results in an enhanced reactivity and consequently helps access numerous acyclic and heterocyclic systems [71].

Another promising precursor for the synthesis of potentially active compounds is sulfanilamide; a well-known and acknowledged sulfamide derivative that is considered as an active drug itself [72]. The use of sulfanilamide as a starting material effectively enables the production of novel compounds with enhanced biological activities [73].

In this chapter, we will discuss our results obtained from the employment of β-enaminones and sulfanilamide as starting materials resulting in the synthesis of four different series of compounds; β-enaminocarboxamides, 4-hydroxyquinolone analogues, acridines, and sulfamide derivatives.

1. β-enaminone derivatives

β-enaminone derivatives used in this study were synthesized according to the method described by our group (**Scheme III.1**) [74]. This latter involves the use of ultrasonic irradiation, which is a green, ecofriendly, and easy alternative for preparing β-enaminones, compared to the classic protocol [75]. Final products were generated from the condensation of dicarbonylic compounds (cyclohexanedione/dimedone) and various primary amine in the presence of copper bromide (CuBr) as a heterogeneous catalyst. After removal of the catalyst, a series of 22 β-enaminones were obtained in excellent yields, by recrystallization in diethyl ether.

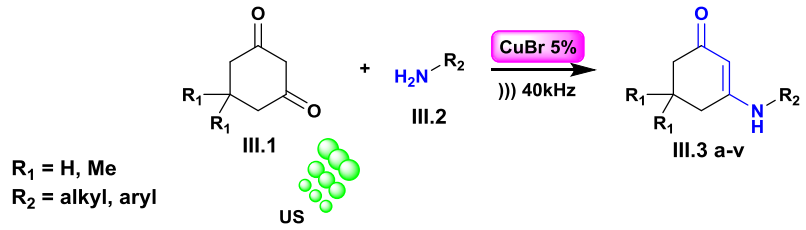

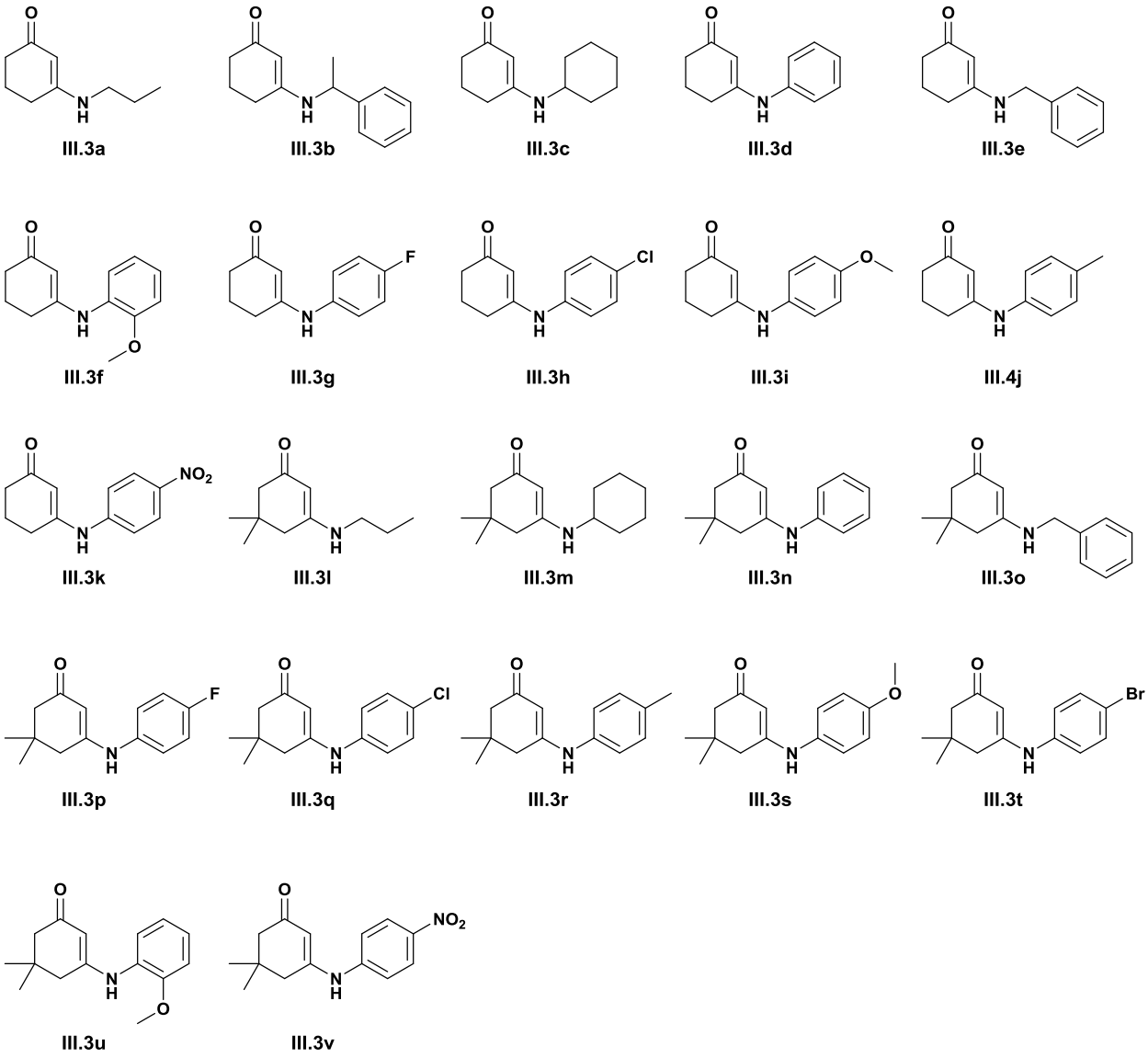

Scheme III.1. Green synthesis of β-enaminones.

A plausible mechanism of β-enaminones formation outlined in **Scheme III.2**. Carbonyl of the β-diketone is activated by copper bromide yielding an enhancement in elecrophilicity. The amine derivative perfoms a nucleophilic attack on the activated carbonyl yielding an intermediate. This step is followed by the elimination of water molecule and the recovery of the CuBr catalyst resulting in the corresponding β-enaminone derivative.

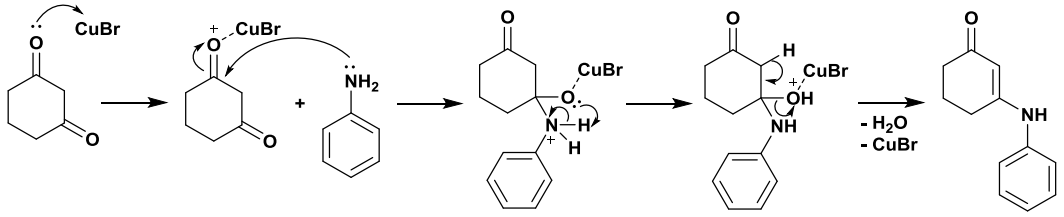

Scheme III.2. Plausible mechanism of β-enaminones formation.

Resulting β-enaminones possessing an interesting reactivity, served as precursors to the synthesis of three different series of molecules; β-enaminocarboxamide, 4-hydroxyquinolone analogues, and acridine analogues (**Scheme III.3**).

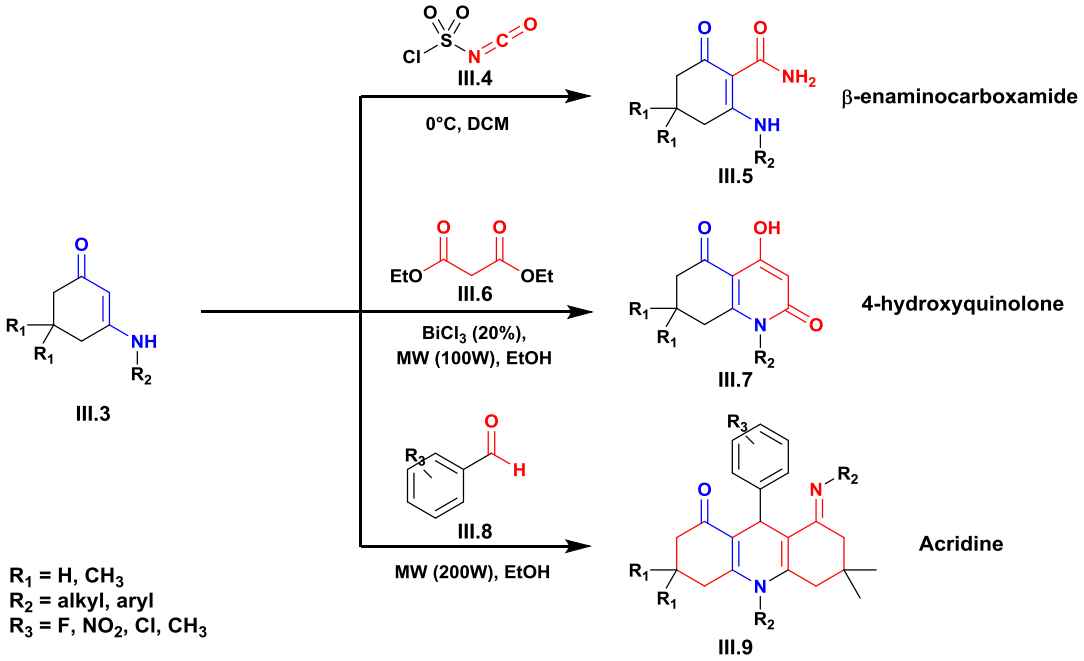

Scheme III.3. Synthesis of β-enaminocarboxamides, 4-hydroxyquinolones, and acridines from β-enaminone derivatives.

2. β-enaminocarboxamides

β-enaminocarboxamides, also known as enaminoamides, hold an increasing interest in the conception of active drug-candidates [76]. Indeed, many molecules containing the enaminoamide moiety were investigated for their therapeutic aspects [2-4]. The synthesis of β-enaminocarboxamides was ensured by the condensation of β-enaminone derivatives and chlorosulfonyl isocyanate (CSI) at 0°C in DCM as a solvent (**Scheme III.4**). No catalyst was employed. After 2 hours, methanol was added. The completion of the reaction was indicated by TLC, in which we noticed a new product with a decreased polarity compared to the starting material. A purification through column chromatography was required to obtain the final products in good yields.

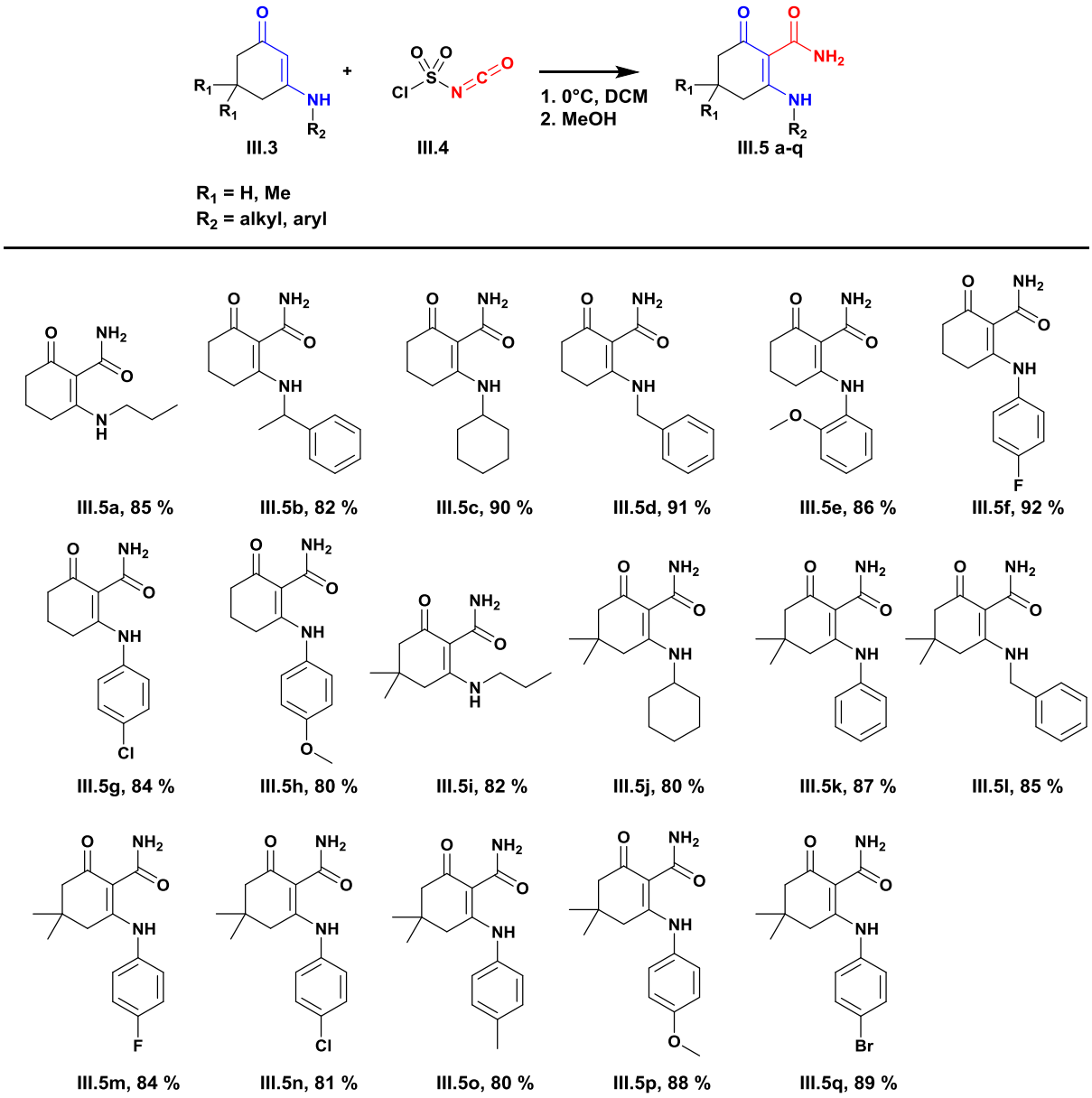

Scheme III.4. Synthesis of β-enaminocarboxamides.

2.1. Mechanistic proposal

A mechanism describing the formation of β-enaminocarboxamides is outlined in **Scheme III.5**. The double bond of the β-enaminone **III.3a** was activated by the mesomeric effect of the azote and engendered an addition in the function of isocyanate that generated an intermediate with chlorosulfonyl motif **III.10**. The enaminone moiety was recovered after an imine-enamine equilibrium. Then, methanol was added to the chlorosulfonyl-containing intermediate **III.11** by an addition-elimination mechanism followed by the removal of SO_3 and MeCl molecules that gave the desired compound.

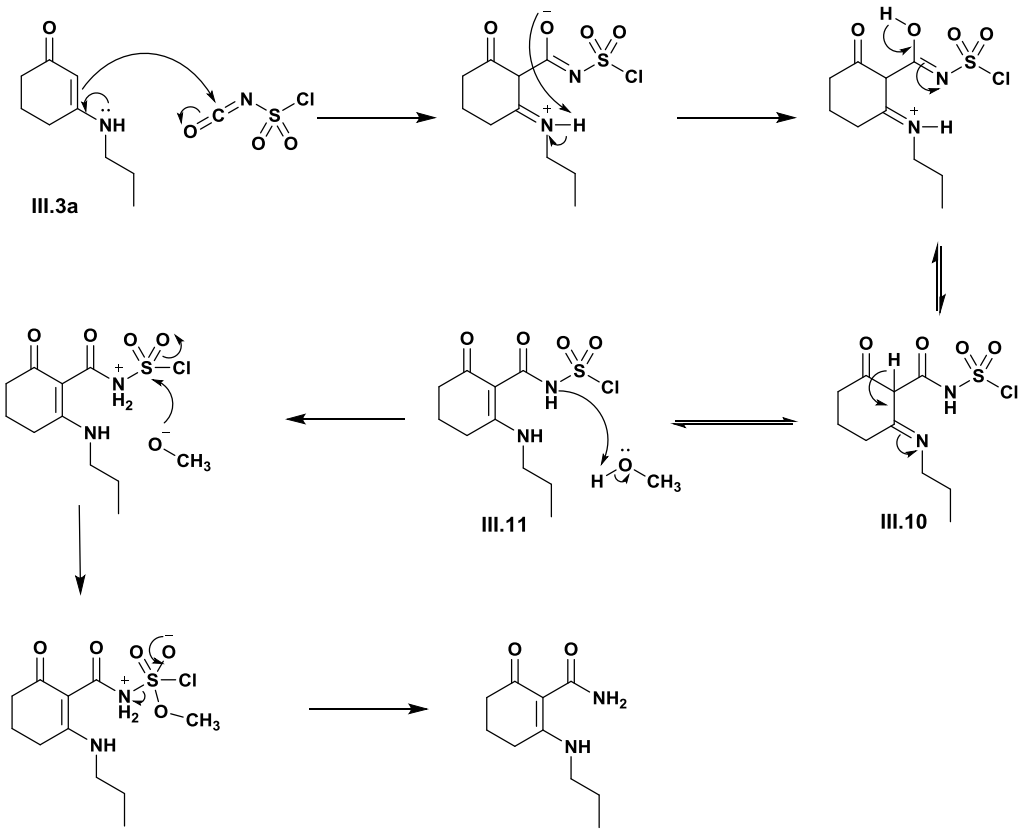

Scheme III.5. Mechanistic proposal for the formation of β-enaminocarboxamides.

2.2. Spectral characterization of β-enaminocarboxamides

Final β-enaminocarboxamides were characterized using ^{1}H NMR, ^{13}C NMR, and IR spectroscopy.

In ^{1}H NMR, structures were confirmed by:

- The presence of a signal at 12-14 ppm as a singlet or doublet corresponding to the secondary amine proton. The dishielded displacement in which these protons appeared could be attributed to the presence of an intramolecular H-bond. It also can be observed that signals of amines in aromatics were more deshielded than the aliphatic ones.

- Two singlets were noticed in the ranges of [5.41-7.31] and [7.72-11.54] ppm, which corresponds to the primary amide protons, which shows the chemical nonequivalence of these protons. It can be assumed that the formation of hydrogen bonds made the primary amide protons nonequivalent, similarly with the study of gorobet *et al.* [77]

In ^{13}C NMR, structures were confirmed by:

- Peaks at [186.70-196.91] ppm that corresponds to ketone carbon.

- Peaks between 171.79 and 173.78 ppm that indicates the presence of the amide.

- Two peaks in the ranges of [93.64-101.07] and [171.11-173.12] ppm that corresponds to the double bonds.

In IR, structures were confirmed by the presence of:

- Absorption bands ranged between 3206 and 3419 cm^{-1} which is indicative of the N-H bonds of both amine and amide groups.

- Sharp and intense bands comprised between 1606 and 1755 cm^{-1} which designates carbonyl bonds of amide and ketone functions.

- Bands ranging between 1591-1541 cm^{-1} indicating the absorption of conjugated double bonds C=C.

In LC-MS:

- Mass spectrum exhibited a molecular peak corresponding to [M+1].

- Purity of the products were verified using liquid chromatography showing a purity greater than 96%.

Compound **III.5n** is taken as a model and its spectra are outlined in **Figures III.1-III.4**.

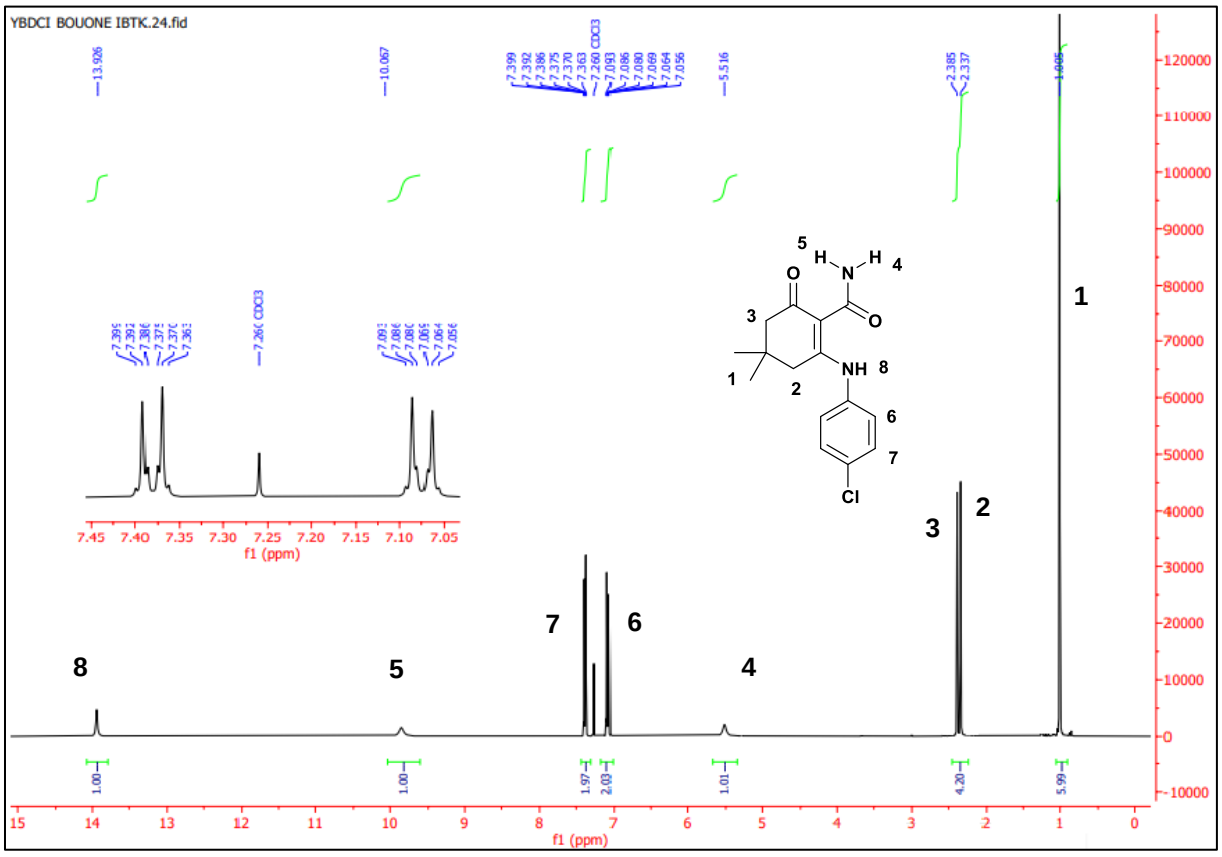

Figure III.1. ^{1}H NMR spectra of compound **III.5n**.

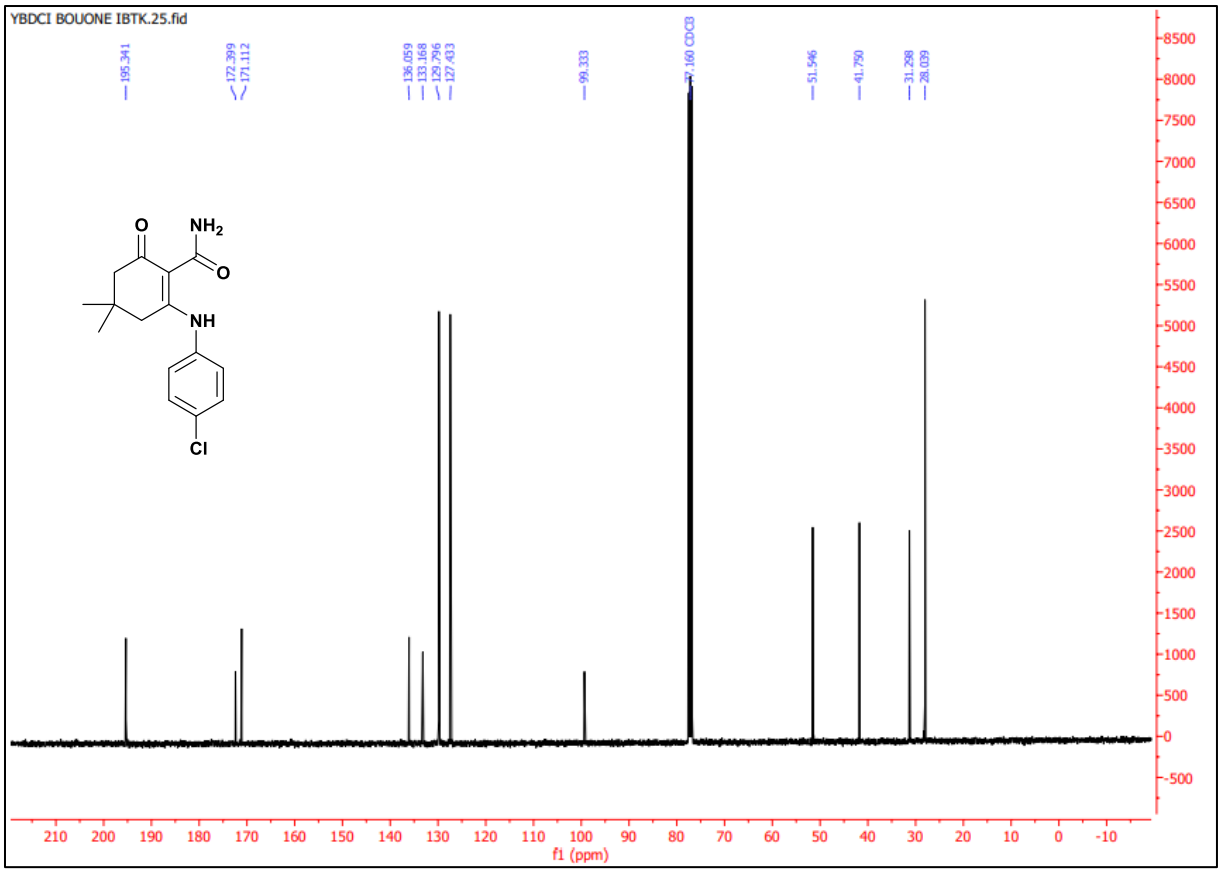

Figure III.2. ^{13}C NMR spectrum of compound **III.5n**.

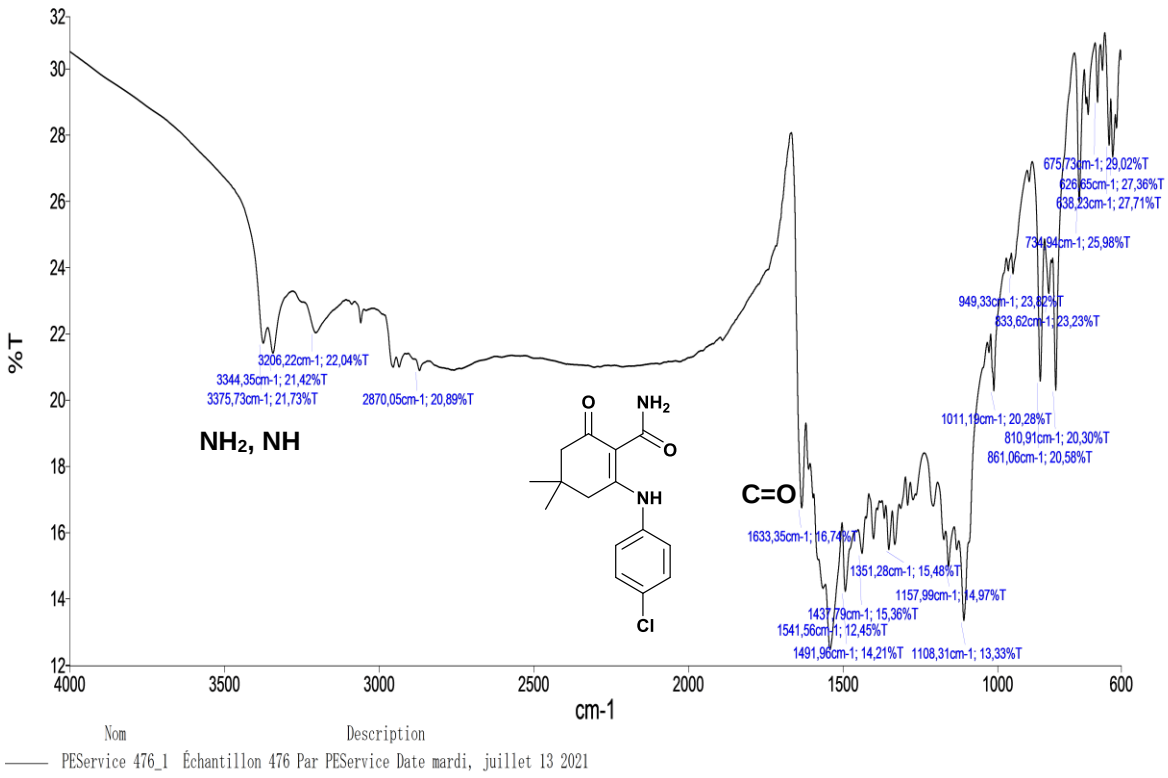

Figure III.3. IR spectrum of compound **III.5n**.

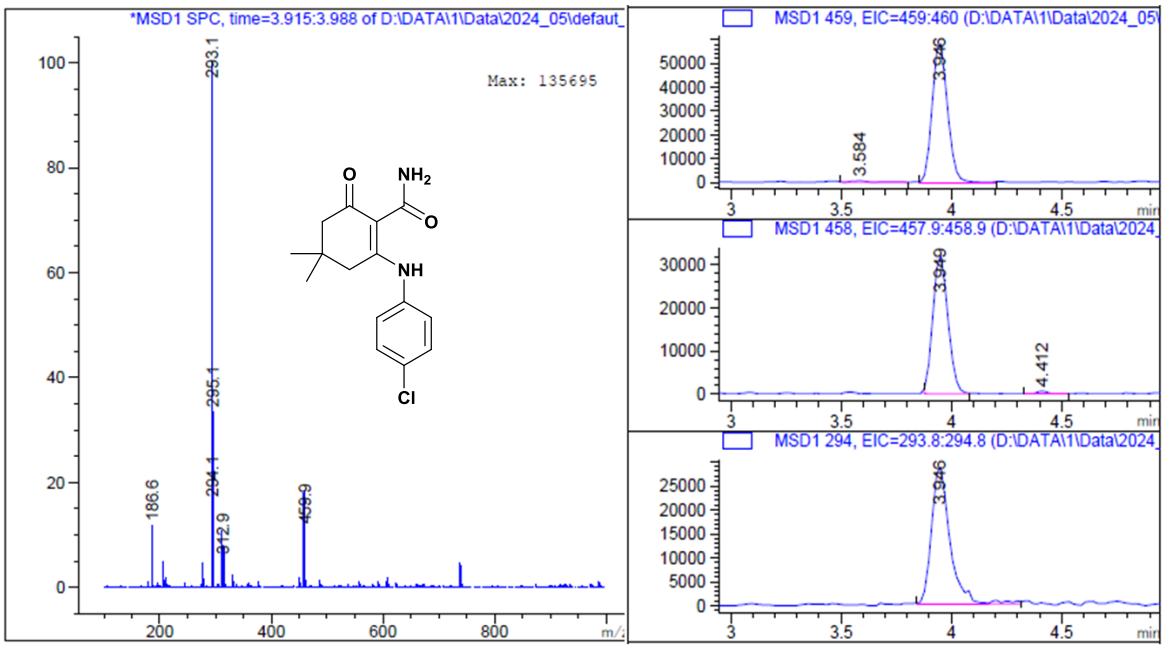

Figure III.4. LC-MS spectrum of compound **III.5n**.

2.3. Crystallographic study for compound III.5h

Compound **III.5h** was obtained in a pure crystalline form suitable for XRD analysis, and a structural study was accomplished (**Figure III.5**).

The asymmetric unit contains one molecule of **III.5h** that crystallizes in monoclinic system and corresponds to the C2/c space group.

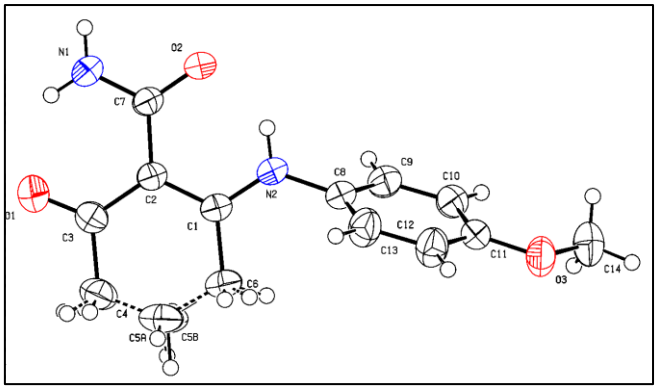

Figure III.5. ORTEP diagram for **III.5h**.

Analysis of the structure using Mercury software [78] clearly indicates intramolecular interactions presence that resides in two hydrogen bonds with lengths equal to 1.98 and 1.80 Å (**Figure III.6**) and engendered the formation of two planar pseudo-cycles with S(6) graph set motif. These findings explain the nonequivalence of the primary amide protons, as well as the dishielded displacement of secondary amine proton, and emphasize the before-mentioned ^{1}H NMR observations.

Further, intermolecular interactions were detected as well in the crystalline structure, citing two H bonds (2.15 Å) between every two molecules of **III.5h** forming a dimer [79]. The dimerization of compound **III.5h** provoked the creation of a cycle with $R^2_2(8)$ graph set motif (**Figure III.6**).

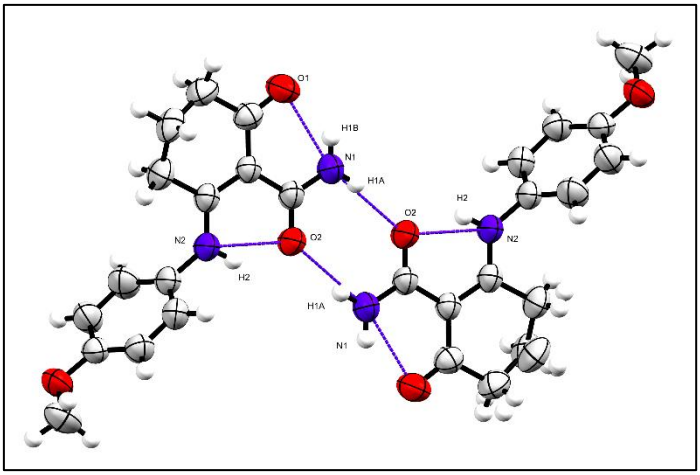

Figure III.6. 3D representation of the dimer formed by molecules of compound **III.5h**.

Other intermolecular contacts were noticed in the structure with lengths comprised between 2.68 and 2.86 Å (**Table III.1**).

Molecules repartition in the crystal structure as well as H bonds, intra and intermolecular contacts are represented as packing diagrams (**Figure III.7**).

Table III.1. Properties of H bonds for compound **III.5h**.

D-H…A	***d*(D-H)**	***d*(H…A)**	***d*(D-A)**	**D-H-A**	**Symmetry**
N_1-H_{1B}…O_1	0.860	1.980	2.648	139.89	x,y,z
N_2-H_2…O_2	0.860	1.800	2.519	139.89	x,y,z
N_1-H_{1A}…O_2	0.860	2.151	2.992	165.81	x,y,z, 1-x,2-y,1-z
C_9-H_9…O_3	0.930	2.687	3.396(2)	133.7	x,y,z, 1.5-x,-1/2+y,1/2-z
C_{13}-H_{13}…O_1	0.930	2.685	3.600(2)	168.0	x,y,z, 1-x,1-y,1-z
C_{5A}-H_{5AA}…C_{11}	0.970	2.854	3.692(2)	145.2	x,y,z, -1/2+x,-1/2+y,z
C_{12}-H_{12}…C_7	0.930	2.794	3.665(2)	156.3	x,y,z, -1/2+x,1/2+y,z
C_{5A}-H_{5AB}…C_{10}	0.970	2.837	3.664(2)	143.6	x,y,z, 1-x,y,1/2-z

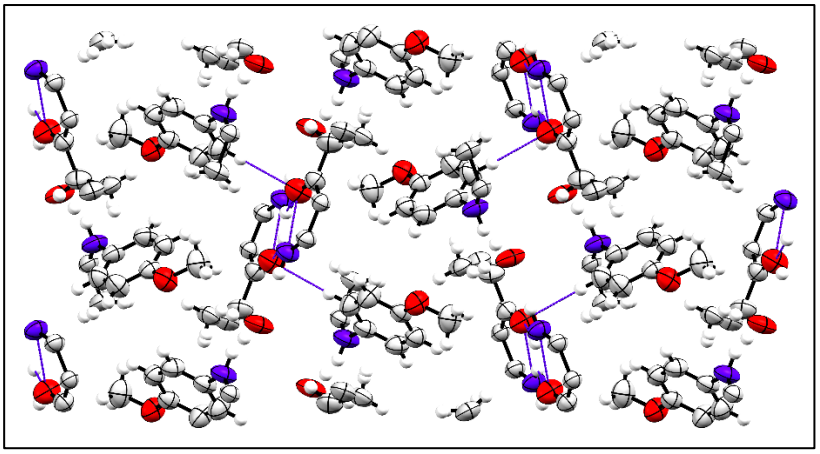

(a)

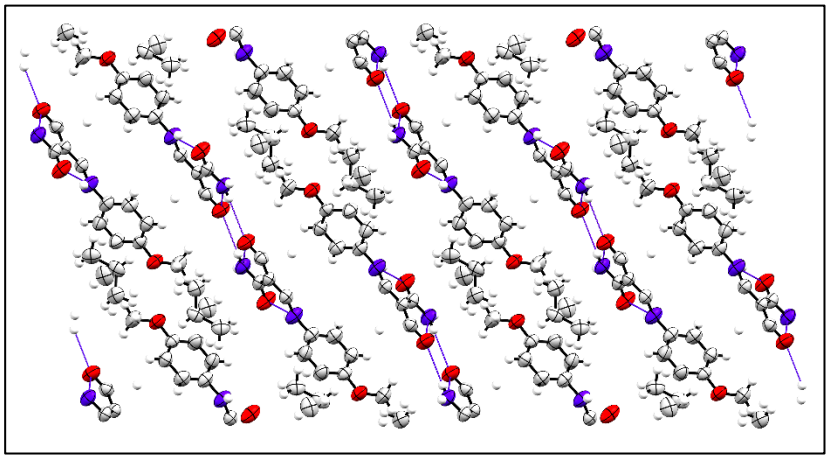

(b)

Figure III.7. Packing diagrams viewed along (a) and (b) axes for compound **III.5h**.

3. 4-hydroxyquinolone analogues

The general method for synthesizing 4-hydroxyquinolone analogues is evocated in **Scheme III.6**. This protocol that is advantaged with its rapidity and respect for the environment is based on the condensation of simple and available reagents; namely previously prepared β-enaminones and commercialized diethyl malonate in the presence of ethanol. Reaction mixture was then subjected to microwave irradiation as an activation tool and catalyzed by bismuth chloride ($BiCl_3$). These reaction conditions were achieved after optimization of the reaction involving compound **III.3d** as a model substrate as indicated in **section 3.1**.

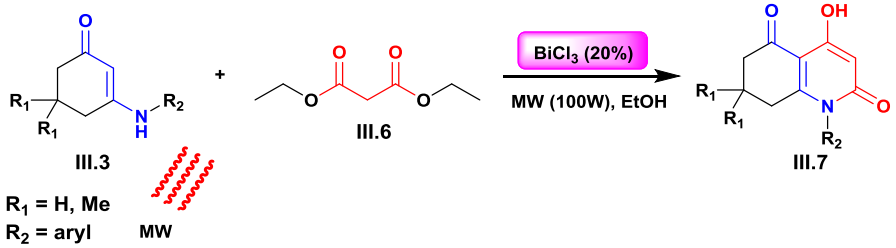

Scheme III.6. Synthesis of 4-hydroxyquinolone analogues.

3.1. Optimization of reaction conditions

In order to obtain satisfactory reaction conditions for the synthesis of 4-hydroxyquinolone analogues with improved yields, we selected a model reaction (**Scheme III.7**) including the β-enaminone **III.3d** and diethyl malonate in different classic and green reaction conditions.

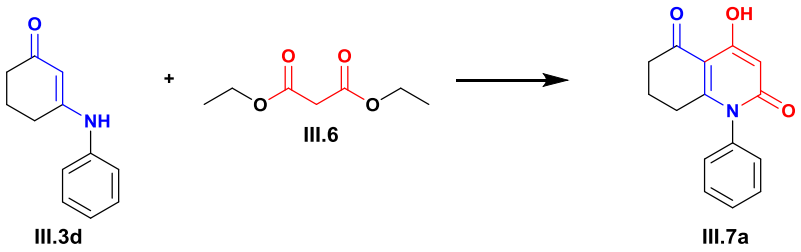

Scheme III.7. Typical synthesis of 4-hydroxyquinolone analogues.

As a first attempt, we reacted compound **III.3d** and diethyl malonate **III.6** at room temperature without the use of any catalyst. Ethanol was added to solubilize the mixture and make it homogeneous. The control of the reaction progress using TLC showed that no product was obtained even after 48h. However, once the reaction was put at high temperature (120°C) employing refluxing, the formation of a new product with a small yield have been noticed after 48h (**Table III.2**).

In view of the increasing interest of microwave irradiation as a source of activation in organic synthesis of interesting compounds that relies on its remarkable rapidity compared to conventional technics, as well as its improved yields, we have been encouraged to try our reaction, employing microwave as an alternative to classic heating.

As a result, this modification was gainful and the desired product was achieved with a relatively better yield and a minimized reaction time, which shifted from 48 hours to 12 minutes only.

Table III.2. Optimization of conditions for the synthesis of 4-hydroxyquinolone analogues.

Entry	Method	Solvent	Duration	Yield (%)
1	Room temperature	EtOH	48h	--
2	High temperature	EtOH	48h	6
3	Microwave	--	12min	20

The obtainment of better results using microwave prompted us to continue improving reaction conditions by employing several catalysts as presented in **Table III.3**.

Table III.3. Optimization of reaction time and catalyst.

Entry	Catalyst	Duration (min)	Yield (%)
1	$BiCl_3$ (20%)	8	48
2	$Zn[OOCCH_3]_2$	8	35
3	SiO_2	15	29
4	K-10	16	24
5	$ZnCl_2$	9	40
6	CsI	10	35
7	CuBr	10	38
8	$AgNO_3$	11	40

Using silicon dioxide and montmorillonite K-10 (Entry 3, 4) showed slight improvements in yields, which can be neglected since it was accompanied with an increase of reaction time. Then, several metal-based catalysts were experienced including : zinc acetate, cesium iodide, copper bromide, and silver nitrate (Entry 2, 6-8) that promoted the final products with better yields ranging between 35 and 40 % and a shorter reaction time of 8 to 11 minutes.

In our quest for efficient catalysts, we turned our focus to $BiCl_3$, known for its accessibility and small harmfulness. Notably, it is also ecologically friendly [80]. Lewis acid catalysts containing Bismuth has gathered significant attention and found widespread application in numerous reactions, particularly in heterocycles synthesis [80,81]. Encouraged by these advantages, we investigated $BiCl_3$ effect on the progression of the reaction (**Table III.3**). It was noticed that $BiCl_3$ use gave better results with 48% yield and 8 minutes reaction time.

Polar solvents show a key role in generating heat *via* microwave radiation through the dipolar polarization mechanism. Molecules with significant dipolar moments, when exposed to the electric field generated by microwaves, exhibit continuous rotation, thereby generating thermal energy [82]. We investigated the impact of solvents, starting with the most environmentally friendly option: water. However, the reaction did not proceed due to the immiscibility of the reagents with water. Therefore, we selected alternative polar solvents for trying in our reaction, including ethanol, methanol, and acetone, as detailed in **Table III.4**.

Table III.4. Solvent effect on reaction rate.

Entry	Solvent	Duration (min)	Yield (%)
1	Ethanol	5	55
2	Methanol	6	50
3	Acetone	8	46
4	Solvent-free	8	48

Acetone failed to enhance either the yields or the reaction periods. Likewise, methanol had minimal impact on the reaction time. Ethanol significantly increased the yield and reduced the reaction duration (**Table III.4**).

Under these promising conditions, various significant substituents were introduced on the aromatic ring of β-enaminones. (**Scheme III.8**).

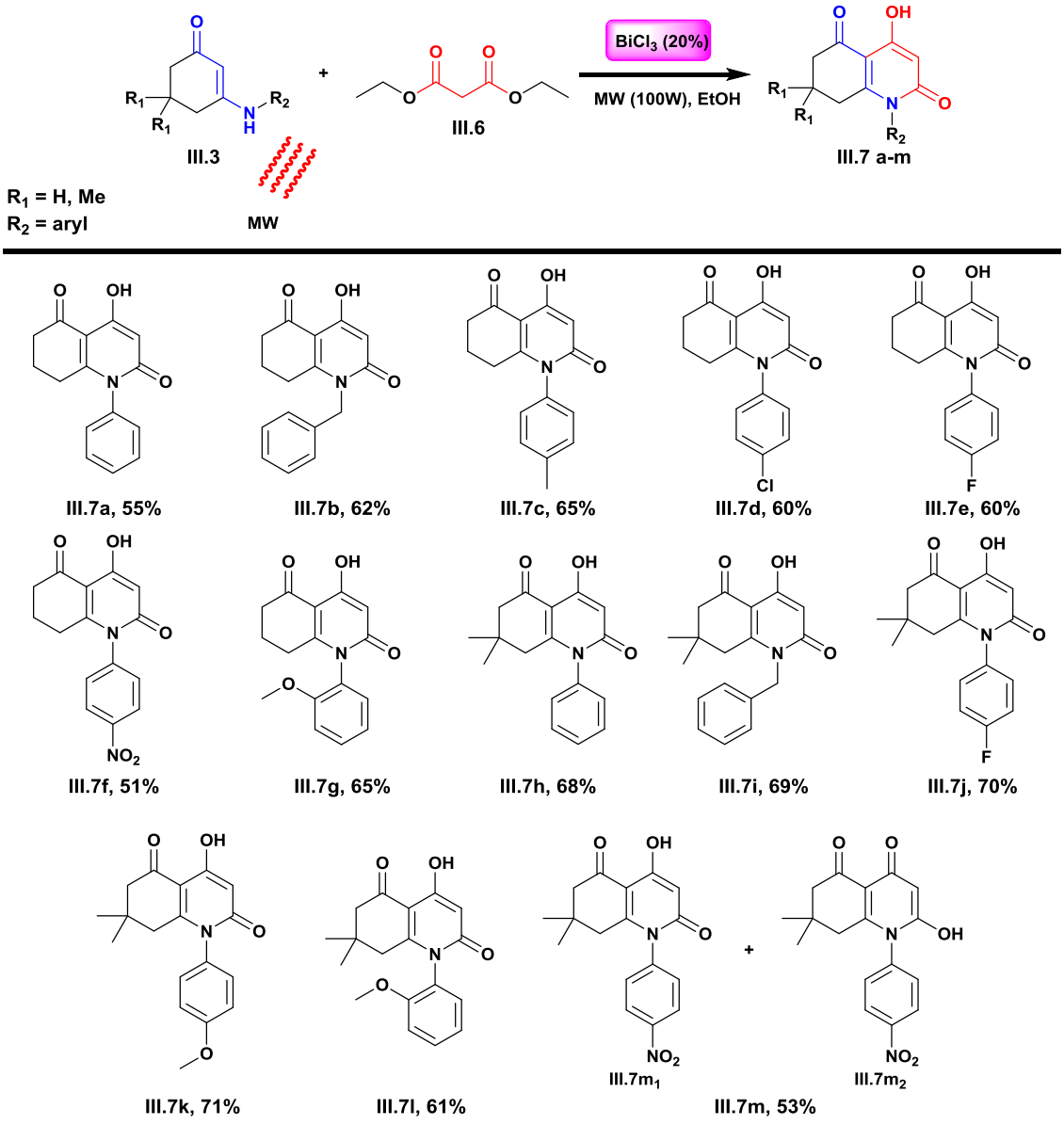

Scheme III.8. Synthesized derivatives of 4-hydroxyquinolone analogues.

The type of substituents used notably affected the obtained yields. In general, β-enaminones derived from dimedone exhibited higher yields. Furthermore, the inclusion of electron-rich groups, such as CH_3 and OCH_3 groups in the *p* and *o* positions (**III.7c**, **III.7g**, **III.7k**, **III.7l**), increased yields by enhancing the nucleophilicity of NH. Conversely, the introduction of a nitro group in the *p* position (**III.7f**, **III.7m**) decreased NH reactivity, leading to lower yields.

The reason for the low yields observed is the incomplete reaction, leaving a portion of the β-enaminone unreacted. Moreover, extending the reaction time beyond 15min is not advisable as it may lead to the degradation of the final product.

3.2. Mechanistic proposal

Initially, $BiCl_3$ activates diethylmalonate **III.6**, resulting in augmenting its electrophlicity. Subsequently, the β-enaminone **III.3d**, which contains two active sites, undergoes a nucleophlic attack by C=C bond. This reaction liberates an ethanol molecule. Upon catalyst recovery, an intermediate is obtained **III.12**. This intermediate is also activated by $BiCl_3$, subsequently attacked by the secondary amine of the β-enaminone, forming a heterocyclic compound **III.13**. Another EtOH molecule is liberated, and $BiCl_3$ is recovered giving **III.7a** (**Scheme III.9**).

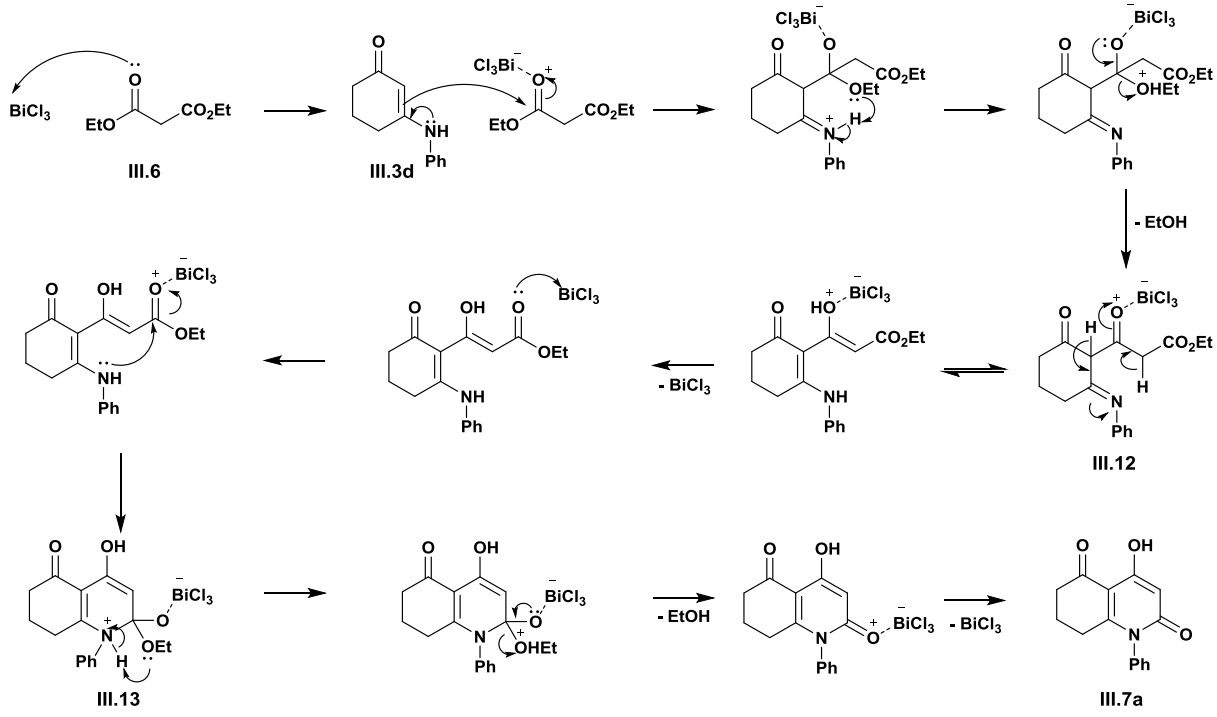

Scheme III.9. Proposed mechanism for the synthesis of 4-hydroxyquinolone analogues catalyzed by bismuth chloride.

3.3. Spectral characterization of 4-hydroxyquinolone analogues

Structures of synthesized compounds were confirmed using spectroscopic and spectrometric methods including ^{1}H, ^{13}C NMR, IR, DEPT, and LC-MS.

In ^{1}H NMR, we noticed:

- Singlets at (12.37-12.78 ppm) that corresponds to the enolic hydroxyl.
- The proton attached to Cα appeared as a singlet at [5.61-5.87] ppm.

In ^{13}C NMR:

- Signals at the range of [95.58-98.16] ppm that indicates the Cα.
- Carbonyls appeared at [201.27-202.60] ppm and [162.36-164.41] ppm respectively.
- The C-OH appeared at [166 .71-168.20] ppm.

In FT-IR spectrum, structures were confirmed by:

- OH stretching at [3236-3449] cm^{-1}.
- Ketone and carboxamide fonctions confirmed by [1647-1738] cm^{-1}, and C=C bonds absorbed at a range of [1511-1650] cm^{-1}.

In LC-MS:

- Mass spectrum exhibited a molecular peak corresponding to [M+1].
- Purity of the products were verified using liquid chromatography showing a purity greater than 96%.

Compound **III.7c** is taken as a model, and the corresponding spectra are depicted in **Figures III.8-III.12**.

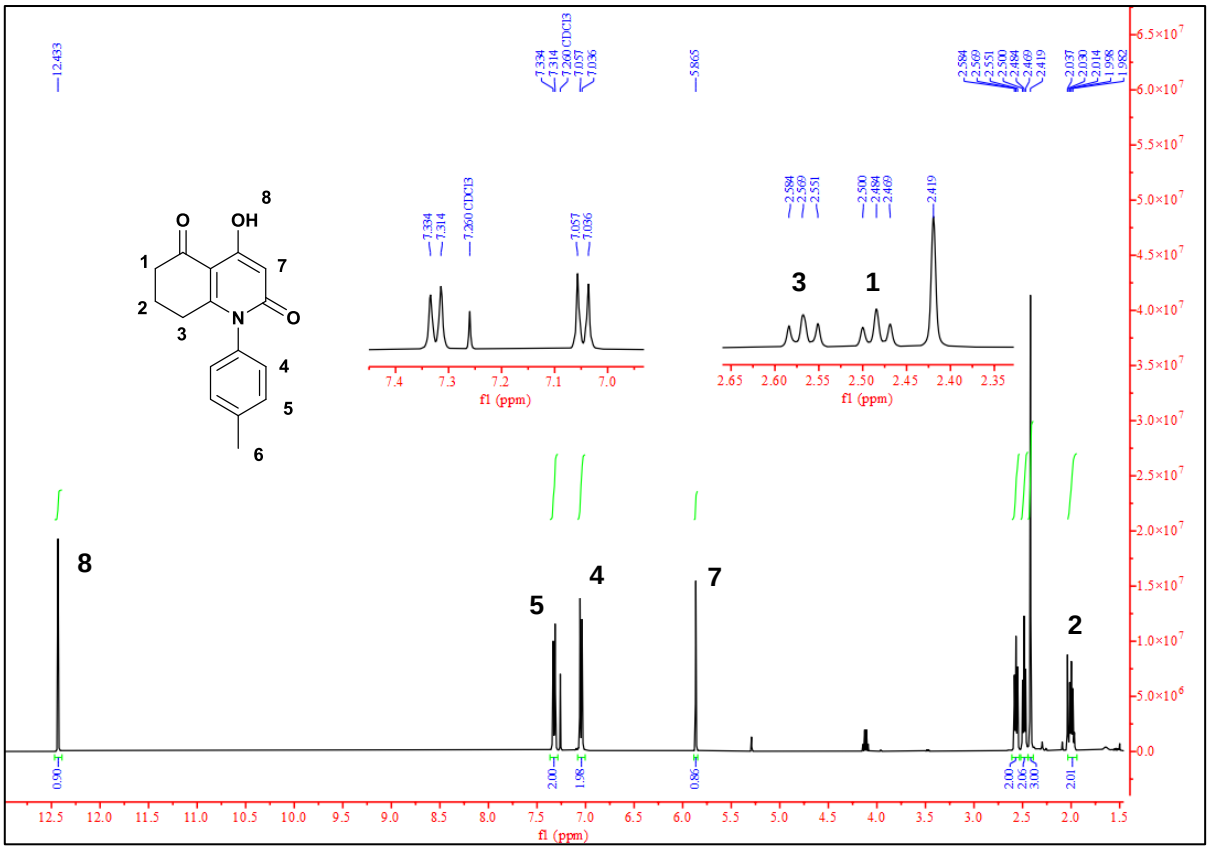

Figure III.8. ^{1}H NMR spectra of compound **III.7c**.

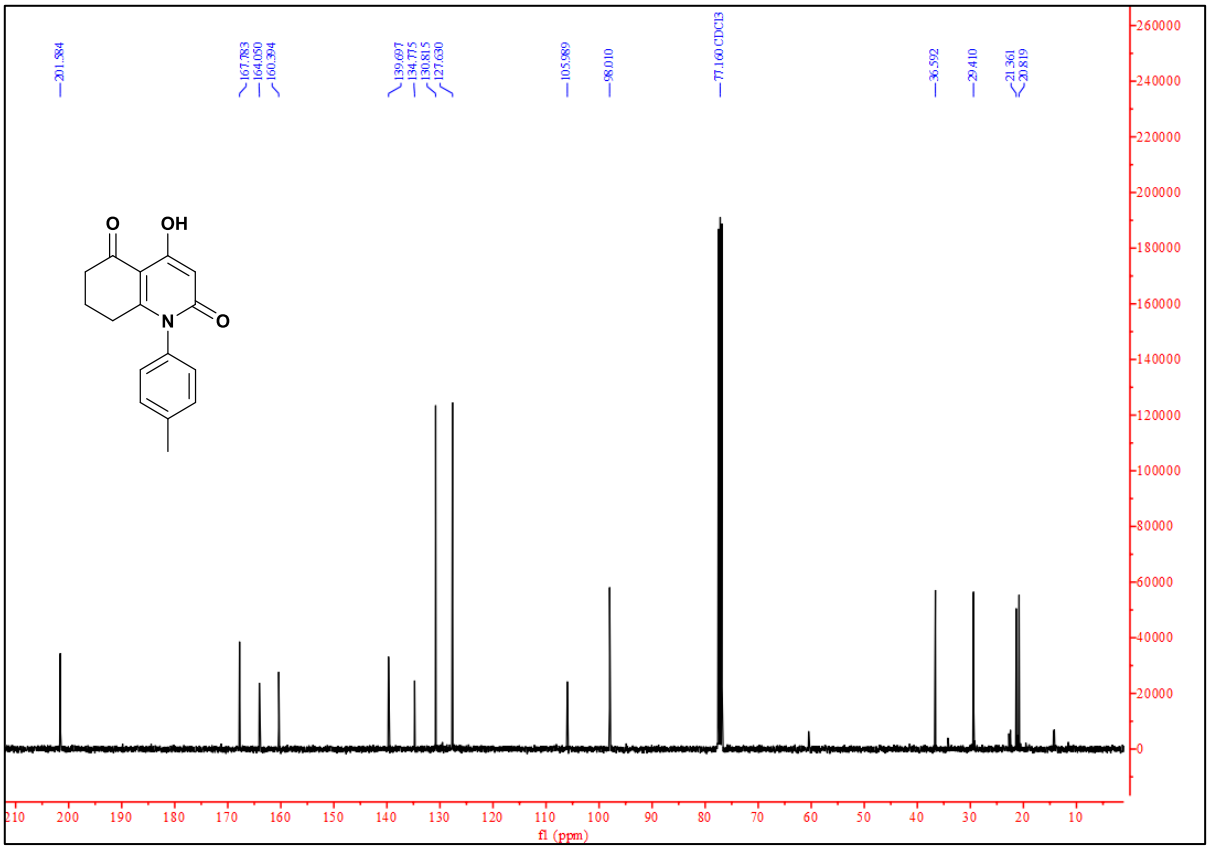

Figure III.9. ^{13}C NMR spectra of compound **III.7c**.

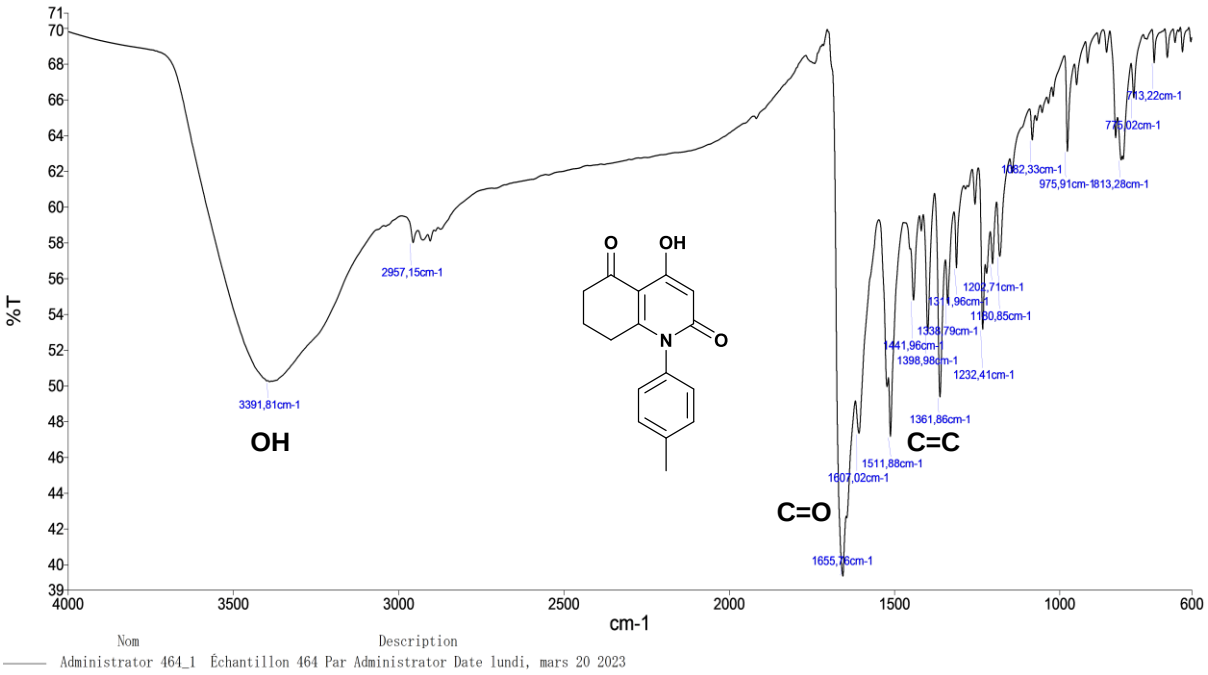

Figure III.10. IR spectra of compound **III.7c**.

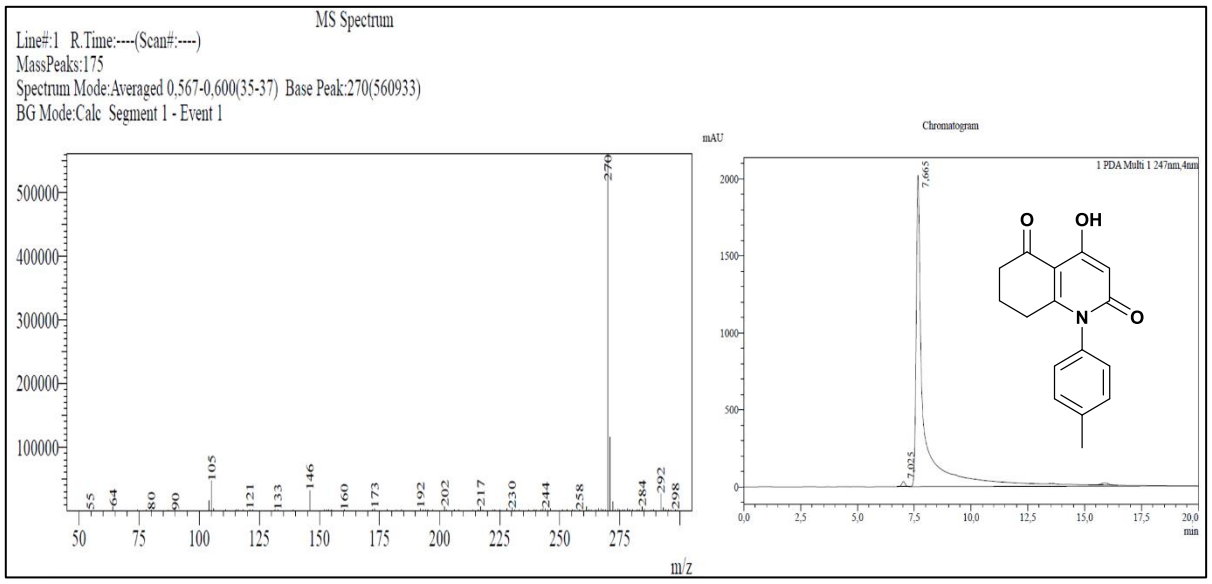

Figure III.11. LC-MS spectra of compound **III.7c**.

Figure III.12. DEPT spectra of compound **III.7c**.

In contrast to other, *p*-nitrosubstituted derivative **III.7m** gave two forms, as illustrated in **Figure III.13**. This suggests an equilibrium between two enolic forms: 4-hydroxyhydroquinoline-2,5-dione (**III.7m$_1$**) and 2-hydroxyhydroquinoline-4,5-dione (**III.7m$_2$**).

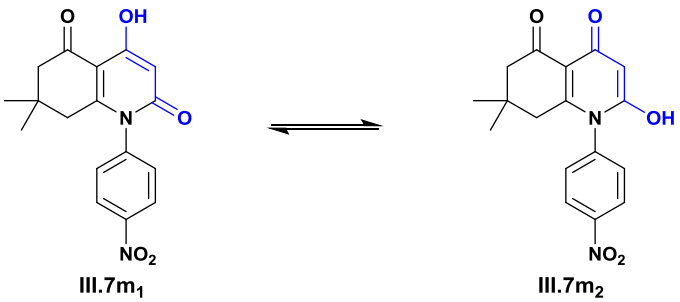

Figure III.13. The two tautomers of compound **III.7m**.

With comprehensive analysis of proton NMR spectrum (**Figure III.14**), which displayed awaited signals, it was noted that identical signals were also present with slightly different shifts and lower intensities. This observation led to the conclusion of the presence of two tautomeric forms.

Ratio between the two enolic forms was determined through integral observation of the ^{1}H NMR spectrum of compound **III.7m**. The results indicated a ratio of 5:1, with 4-

hydroxyhydroquinoline-2,5-dione **III.7m$_1$** being the major form, constituting nearly 83% of the mixture.

Further analysis of the ^{1}H-NMR results (**Figure III.14**) for the 4-hydroxyhydroquinoline-2,5-dione **III.7m$_1$** form revealed two singlets at 5.87 and 12.36 ppm, corresponding to the enolic OH at position 4 and the proton attached to C(α), respectively. These findings are consistent with the NMR results obtained for the other synthesized compounds. However, the enolic proton in the minor form, 2-hydroxyhydroquinoline-4,5-dione **III.7m$_2$**, exhibited a singlet with more deshielded chemical shift (13.99 ppm), which can be related to the negative mesomeric electron delocalization induced by the electron-withdrawing nitro group located in the para position of the aromatic ring.

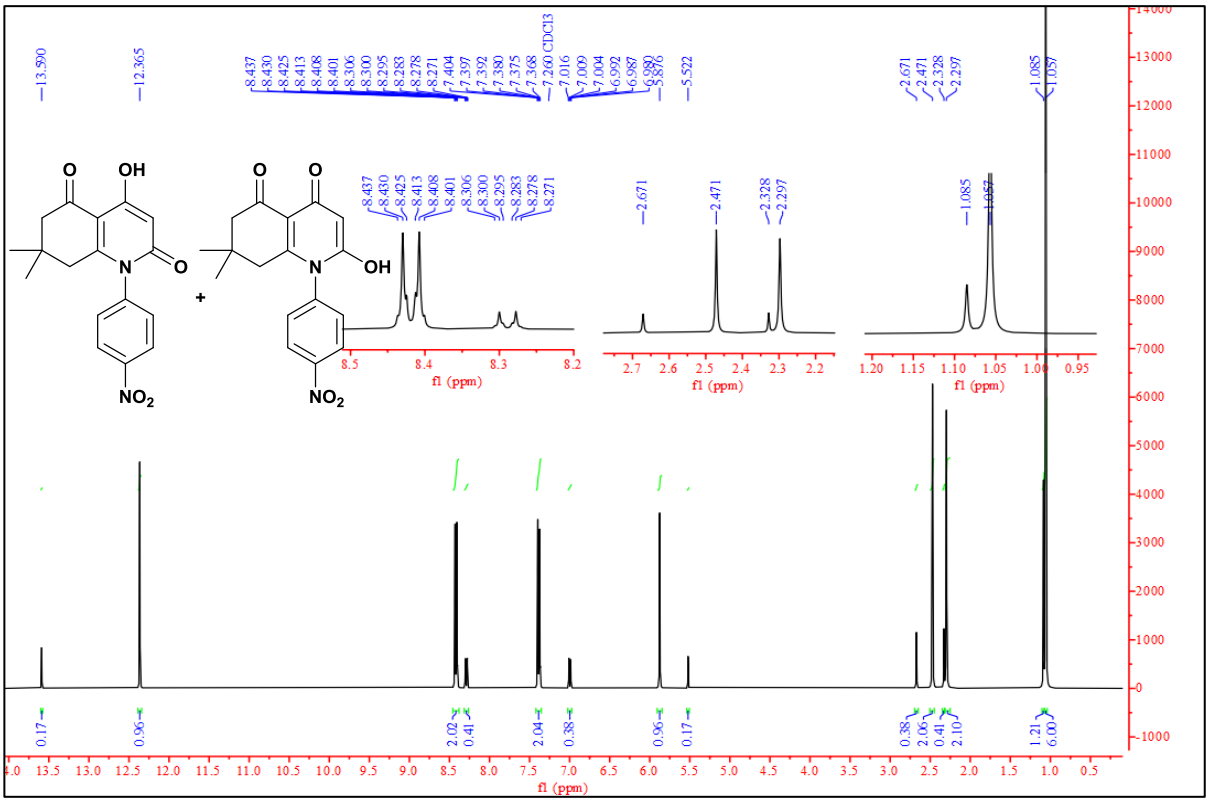

Figure III.14. ^{1}H NMR spectrum of compound **III.7m**.

3.4. Crystallographic study for compound III.7i

A suitable crystal of compound **III.7i** underwent X-ray study. It was revealed that the asymmetric unit consists of one molecule of 8-hydroxy-3,3-dimethyl-5-(phenylamino)-3,4-dihydronaphthalene-1,6(2H,5H)-dione **III.7i**, which crystallizes in the triclinic crystal system with the P-1 space group.

The ORTEP, depicted in **Figure III.15**, highlights the structural arrangement. Notably, the reaction of β-enaminone and diethyl malonate yielded the enolic tautomer rather than the

dicarbonylic one. The presence of the enol group facilitated the formation of an intramolecular hydrogen bond (O_2-H_2…O_1) between the enolic proton and the carbonyl moiety in the substituted cyclohexenone ring, with a bond length of 1.818 Å. This interaction resulted in a pseudocycle with a S(6) graph-set motif.

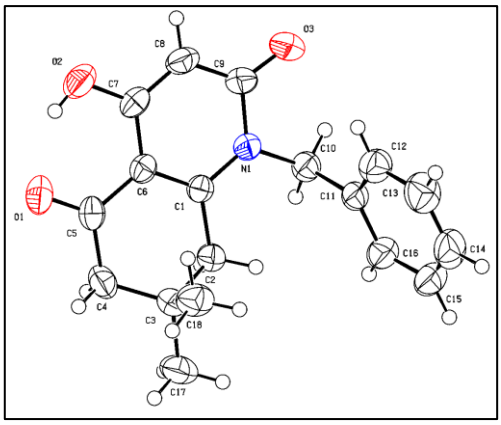

Figure III.15. ORTEP of compound **III.7i**.

The crystal structure is reinforced by intermolecular interactions of the C-H…O type, as detailed in **Table III.5**, with lengths ranging from 2.424 to 2.695 Å. These interactions form three distinct graph sets, comprising two infinite chains and a ring with a $R^2_2(8)$ graph-set motif. Additionally, an extra intermolecular interaction is observed between two identical oxygen atoms (O_1…O_1) with a length of 3.008 Å.

These interactions enhance the cohesion of the crystal structure, effectively linking the components together. The crystal packing diagram, depicted in **Figure III.16**, provides insight into the distribution of the structural components within the crystal.

Additionally, a hydrophobic interaction is observed in the structure, characterized by pi-pi stacking between the benzylic aromatic rings.

Table III.5. Properties of H bonds for compound **III.7i**.

D-H…A	***d*(D-H)**	***d*(H…A)**	***d*(D-A)**	**D-H-A**	**Symmetry**
O_2-H_2…O_1	0.820	1.818	2.553(2)	148.46	x,y,z
C_{14}-H_{14}…O_1	0.930	2.593	3.495(2)	163.7	x,y,z, x,y,-1+z
C_{15}-H_{15}…O_2	0.930	2.695	3.595(2)	163.0	x,y,z , -1+x,y,-1+z
C_8-H_8…O_3	0.930	2.424	3.344(2)	169.94	x,y,z, 2-x,1-y,2-z

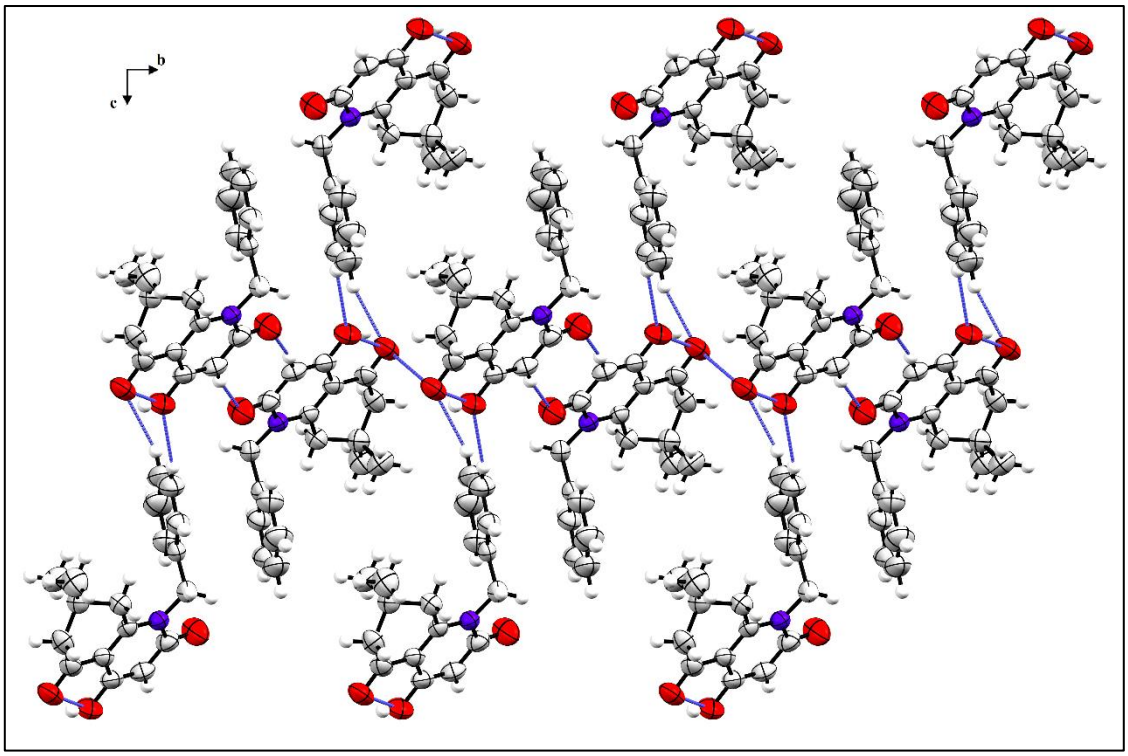

Figure III.16. Packing diagram of compound **III.7i** viewed along (a) axis.

4. Acridine derivatives

Acridines and their derivatives form a diverse category of heterocycles renowned for their utility across various domains [83,84], especially in medicinal applications. They demonstrate a wide range of functions as bioactive compounds combating numerous diseases including Alzheimer's [85-87], leukemia [88], and malaria [89]. Our focus was on developing novel acridines derived from β-enaminones through an environmentally friendly, rapid, and sustainable synthesis method, as depicted in **Scheme III.10**.

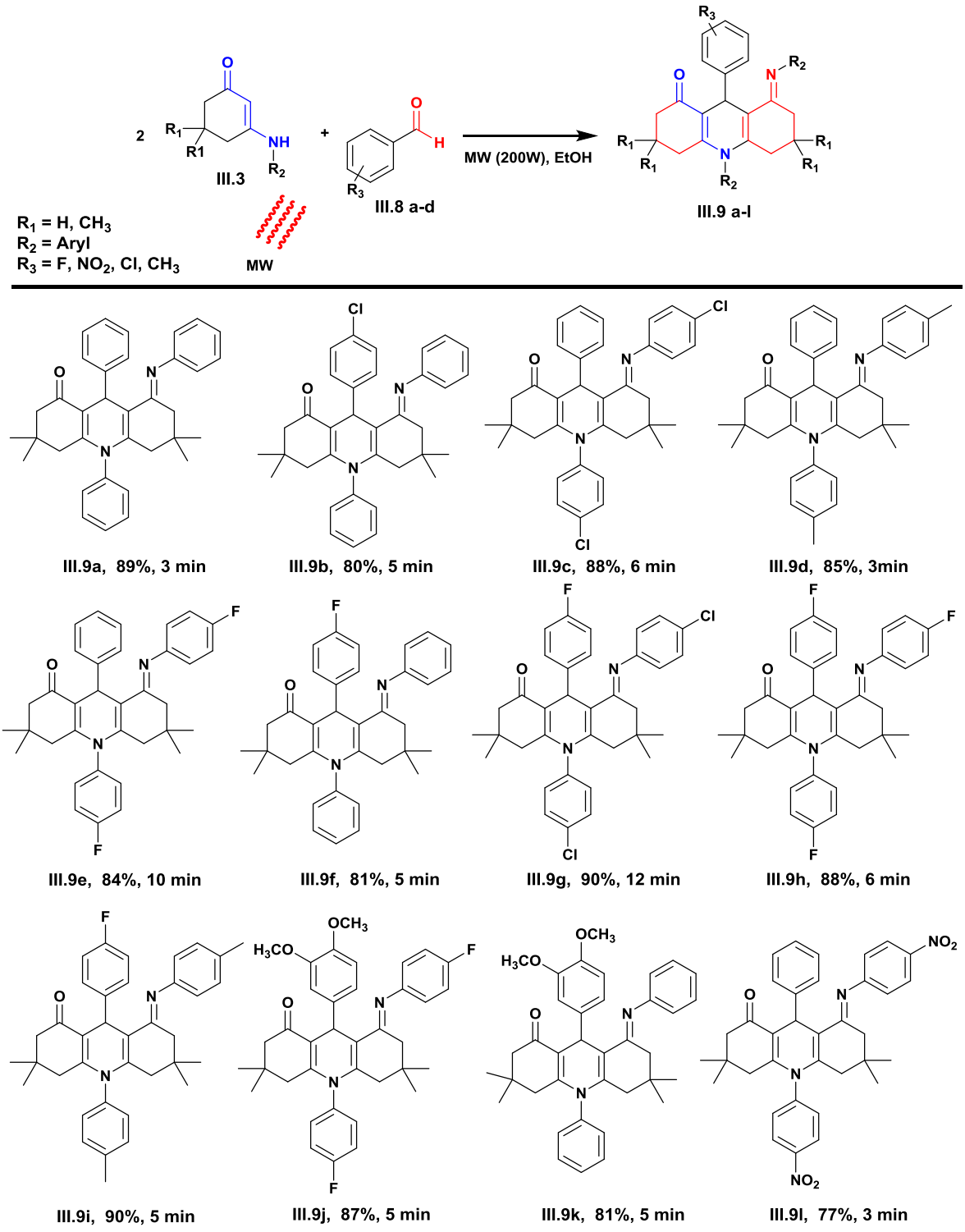

Scheme III.10. Synthetis of acridine analogues.

The use of *ortho*-substituted aldehyde derivatives led to novel hydroxylated acridine analogues **III.14**, due to the steric effect that prevented the elimination of H_2O (**Scheme III.11**).

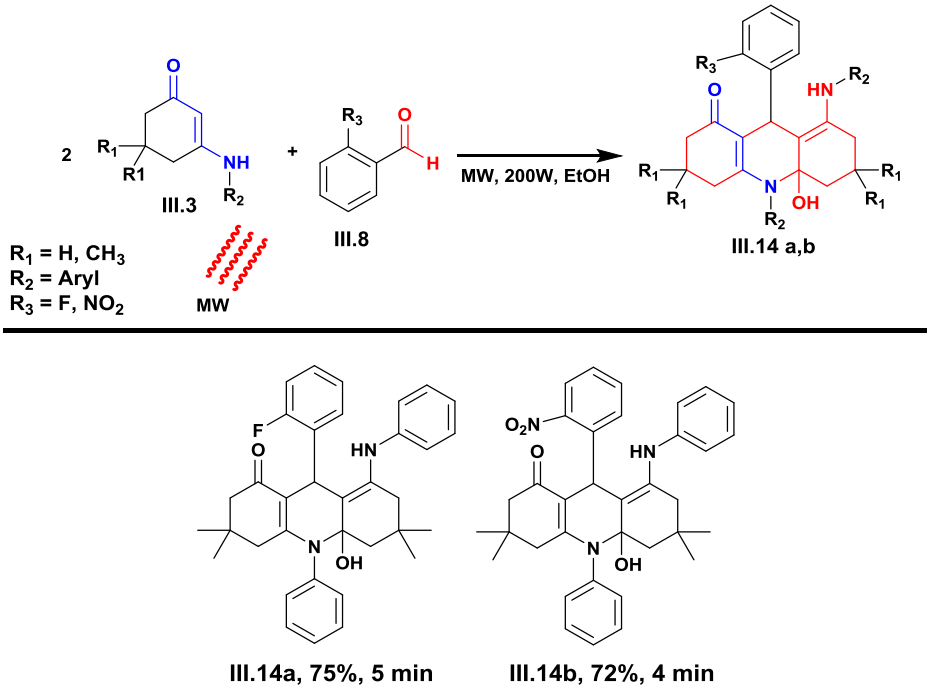

Scheme III.11. Synthesized hydroxyl-containing acridine derivatives.

4.1. Spectral characterization of acridine derivatives

All structures were confirmed using spectroscopic and spectrometric methods citing ^{1}H, ^{13}C NMR, IR, and LC-MS.

In ^{1}H NMR spectrum, the following signals were perceived:

- A singlet corresponding to the proton linked to the asymmetrical carbon with a chemical shift ranged between 5.38 and 5.62 ppm.

- The presence of all the aromatic rings in structures was confirmed by analyzing integrations of signals that appeared in the aromatic region of spectra

In ^{13}C NMR spectrum, we confirmed the structure of synthesized compounds by the presence of peaks at 194.81–198.61 ppm and 163.06–164.43 ppm that corresponds to C=O (ketone) and C=N (imine) carbons respectively.

In infrared spectrum, indicative bands were observed including:

- Intense absorption bands at 1638.11–1713.14 cm^{-1} corresponding to C=O bonds.

- Intense sharp bands were located in the region between 1591.03 and 1614.66 cm^{-1} that are related to the absorption of imine double bonds C=N.

In LC-MS:

- Mass spectra always exhibited a molecular peak that corresponds to [M+23] or [M+1].

- Purity of the products were verified using liquid chromatography showing a purity greater than 96%.

Compound **III.9i** is taken as a model, and the correspondind spectra are depicted in **Figures III.17-III.20**.

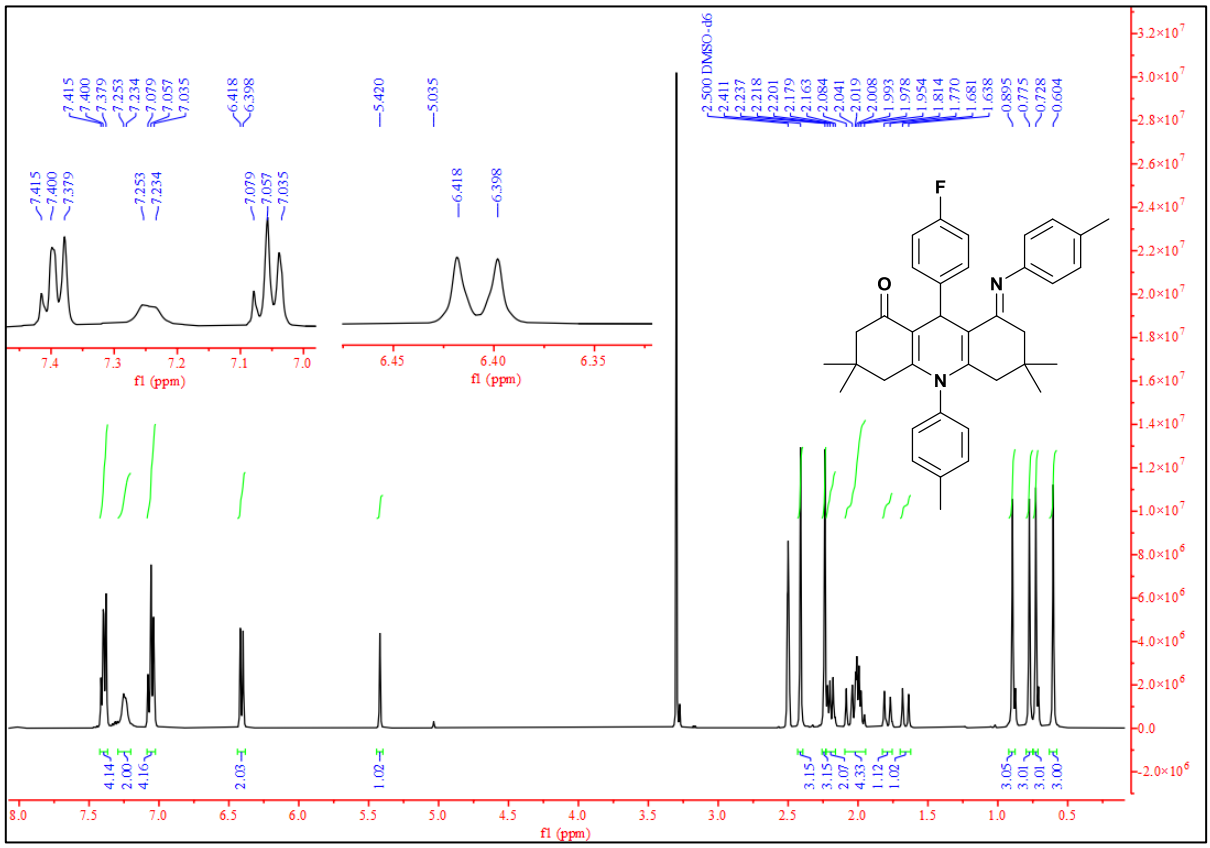

Figure III.17. ^{1}H NMR spectrum of compound **III.9i**.

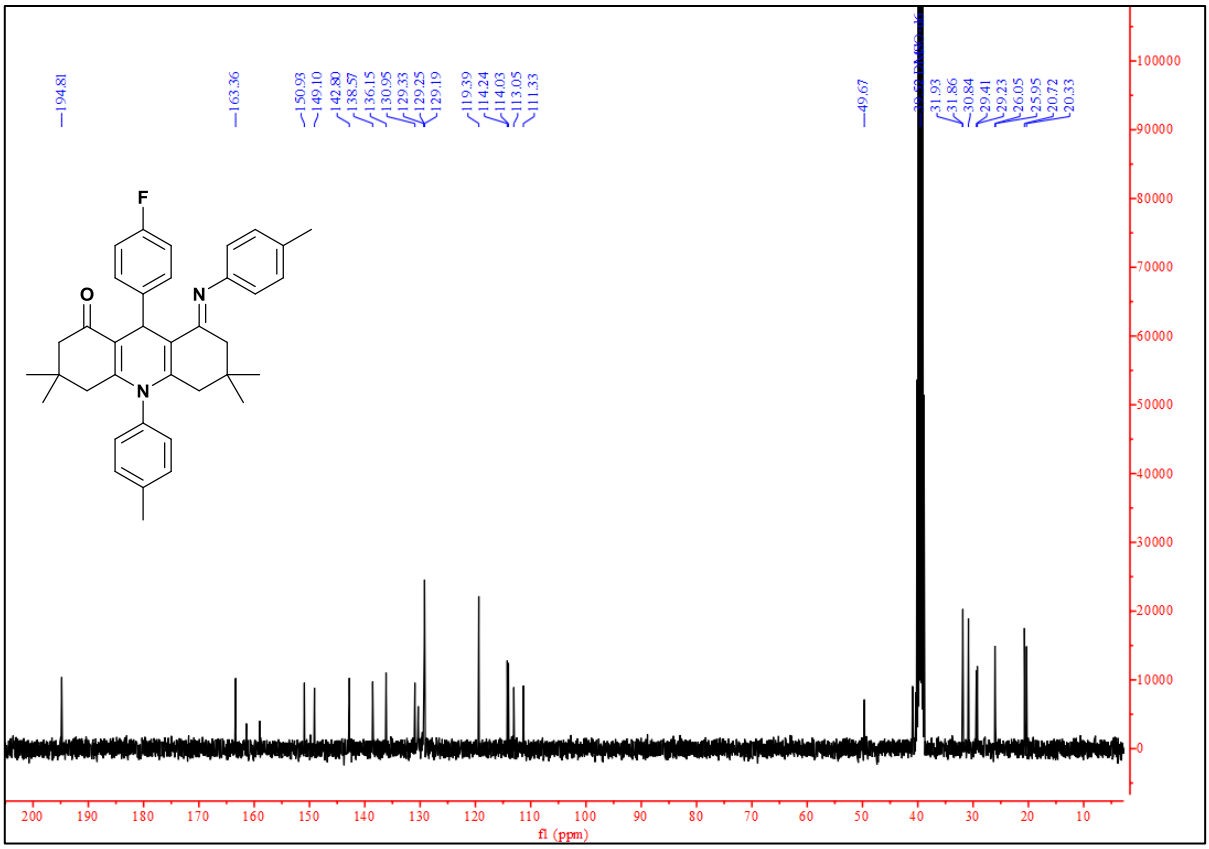

Figure III.18. ^{13}C NMR spectrum of compound **III.9i**.

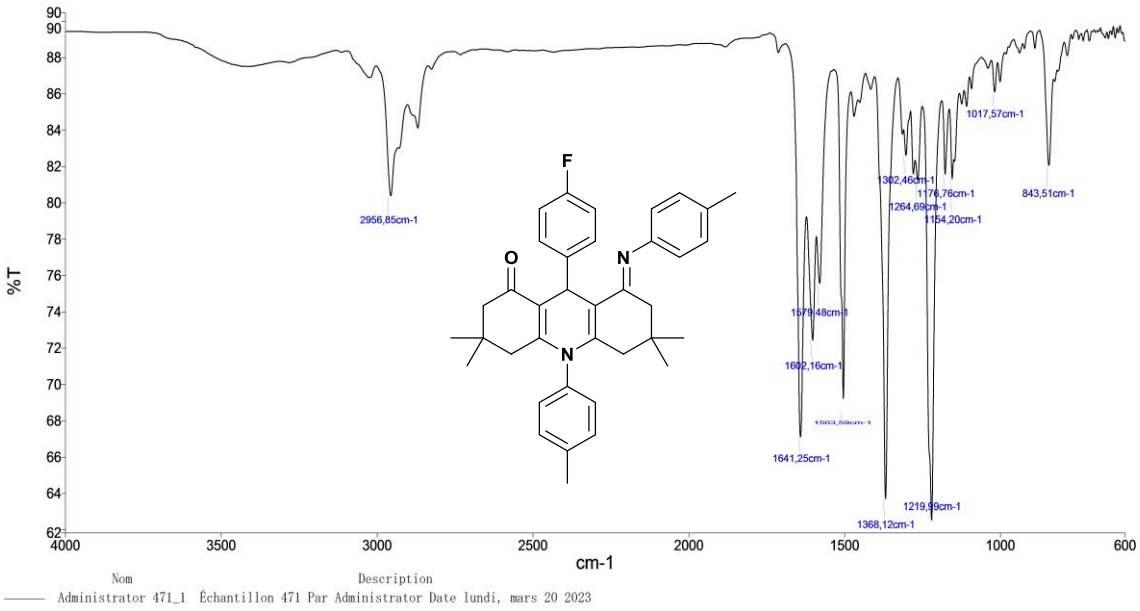

Figure III.19. Infrared spectrum of compound **III.9i**.

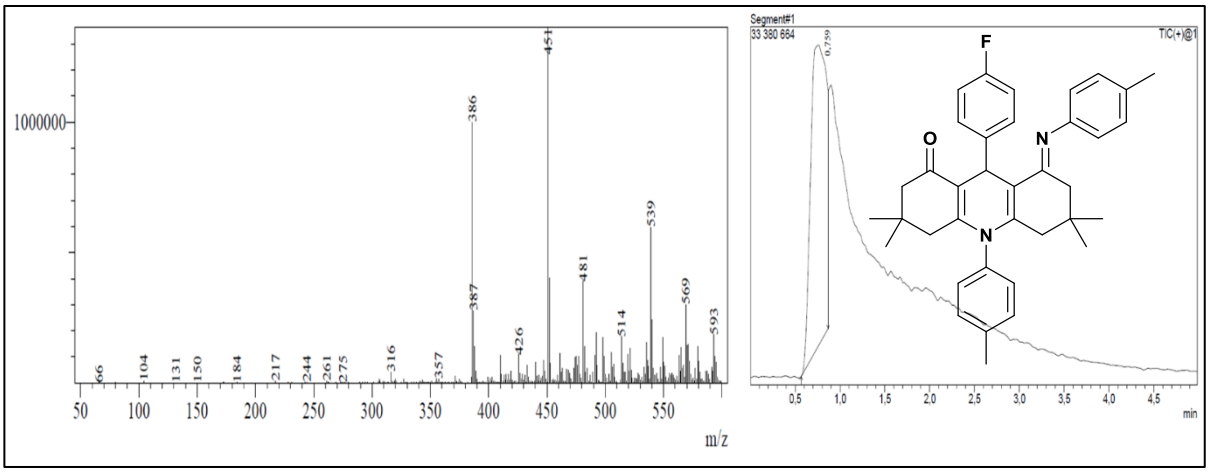

Figure III.20. LC-MS spectrum of compound **III.9i**.

Structures of hydroxylated acridine derivatives were confirmed by ^{1}H, ^{13}C NMR, and IR.

In proton NMR, a singlet at 10.26 and 10.11 ppm, indicating the presence of the proton connected to the conjugated nitrogen atom NH, while the chiral carbon H appeared in the region of 5 ppm. Additionally, the presence of OH was inferred from the observation of a signal around 2.8 ppm of the ^{1}H NMR spectrum and a broad band 3200 cm^{-1} in infrared spectrum.

Spectra of compound **III.14a** are shown in figures **III.21**-**III.24**.

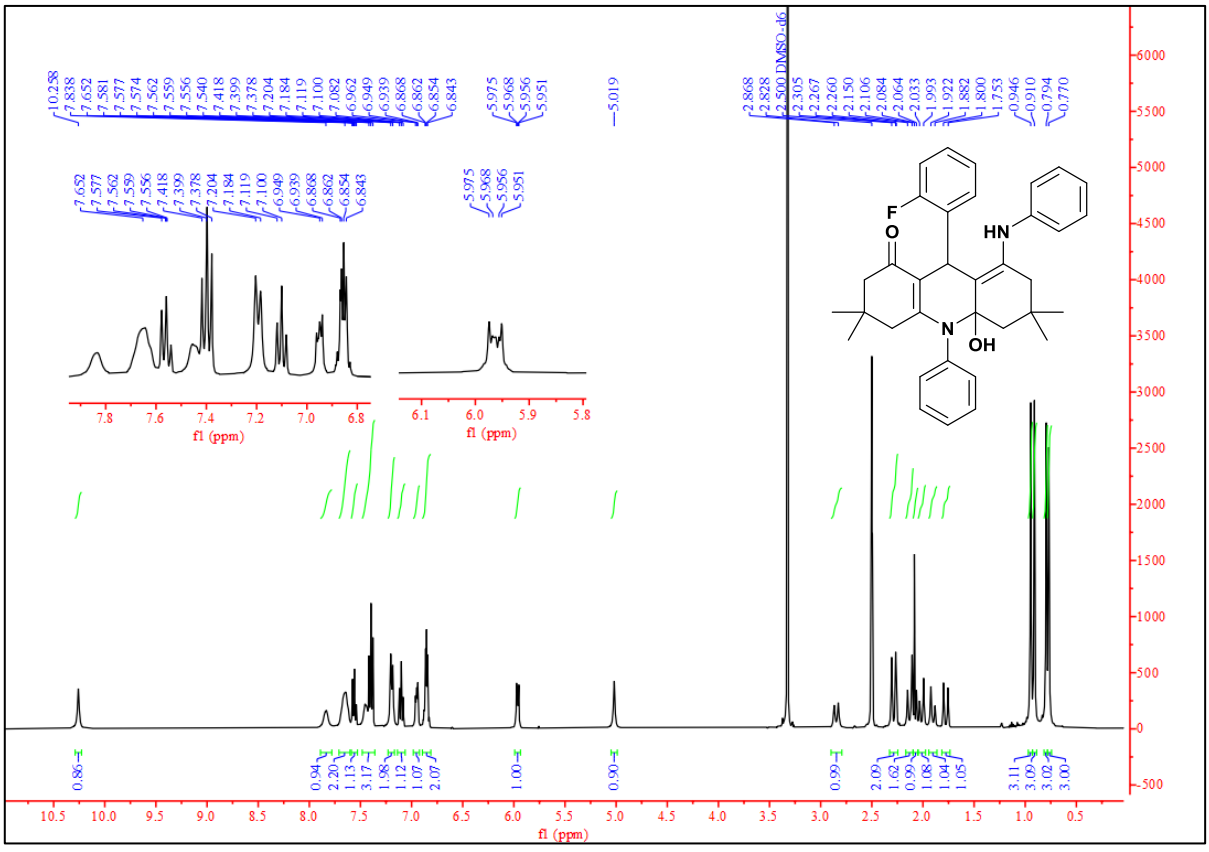

Figure III.21. ^{1}H NMR spectrum of compound **III.14a**.

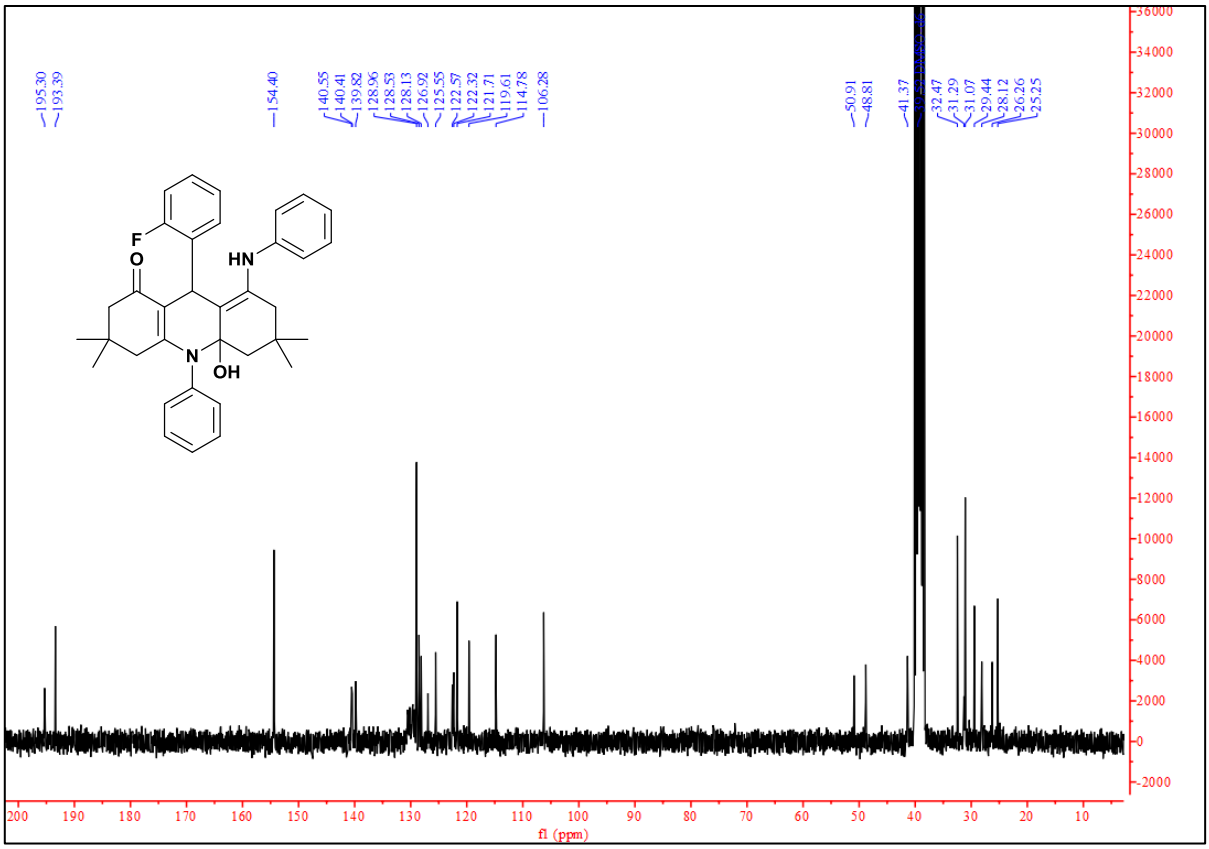

Figure III.22. ^{13}C NMR spectrum of compound **III.14a**.

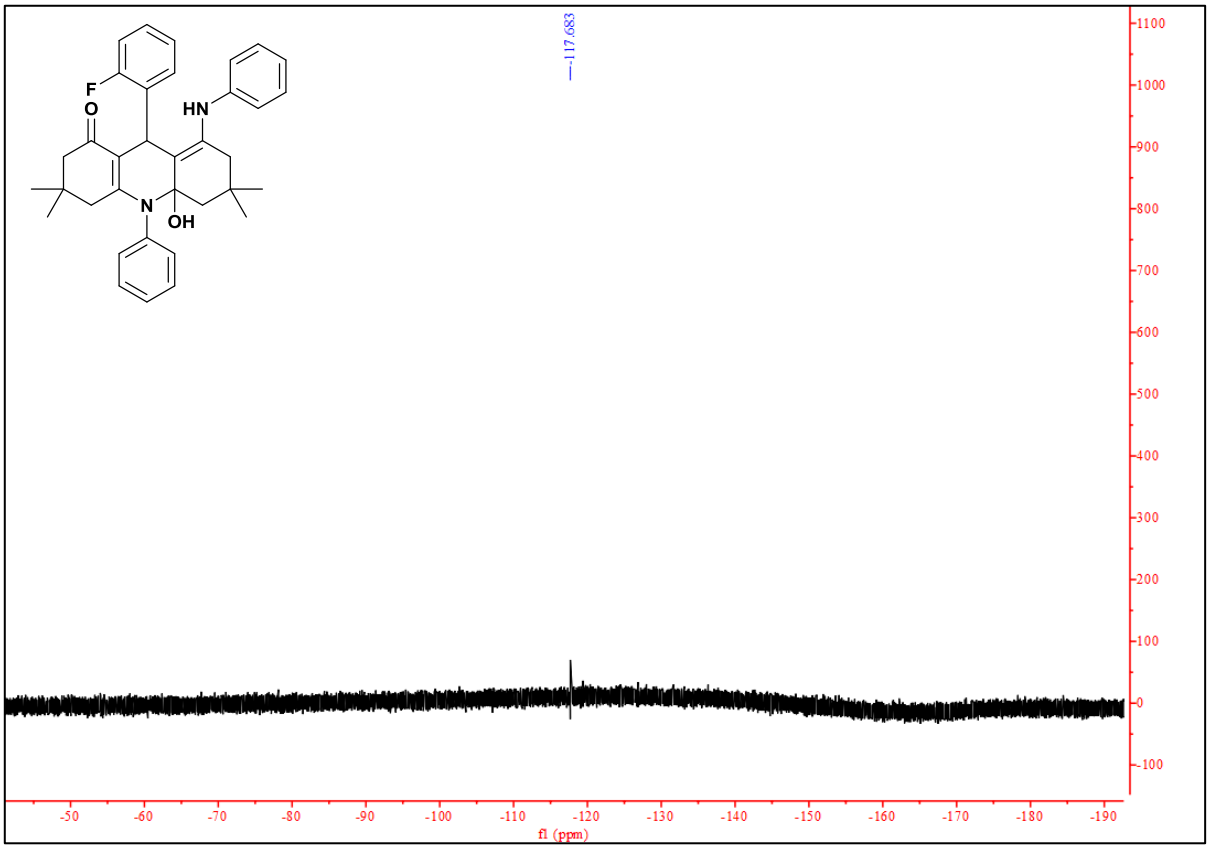

Figure III.23. ^{19}F NMR spectrum of compound **III.14a**.

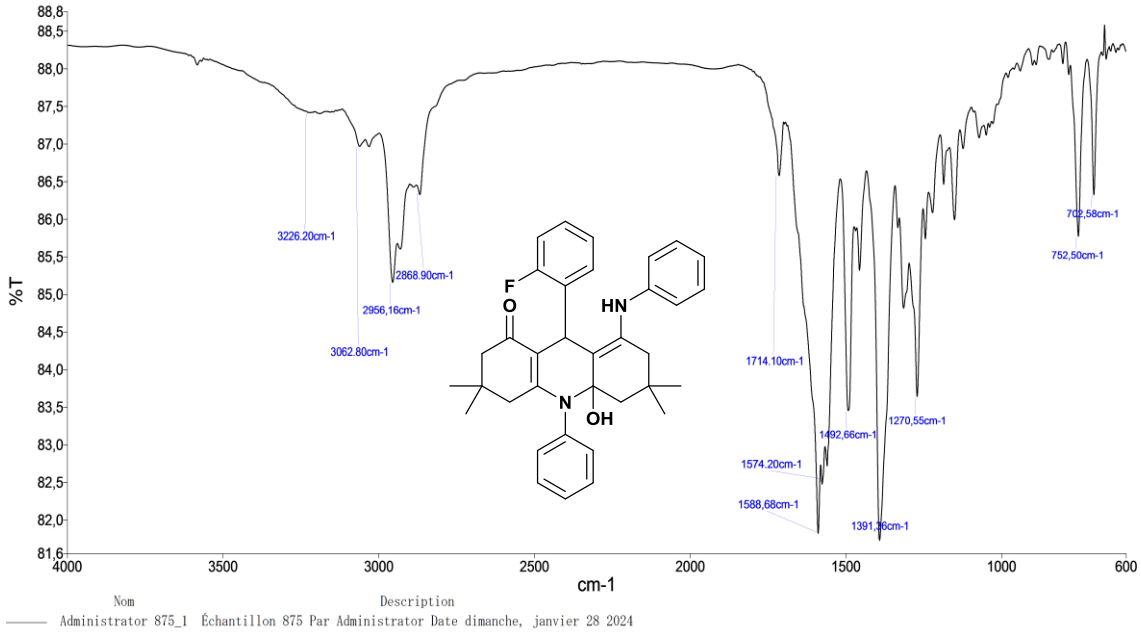

Figure III.24. IR spectrum of compound **III.14a**.

4.2. Crystallographic study for compound III.9d

Compound **III.9d** was crystallized through slow evaporation of methanol/dichloromethane mixture, which resulted in the formation of yellow crystals suitable for XRD analysis. The structure of compound **III.9d** was fully characterized as shown in the corresponding ORTEP diagram (**Figure III.25**).

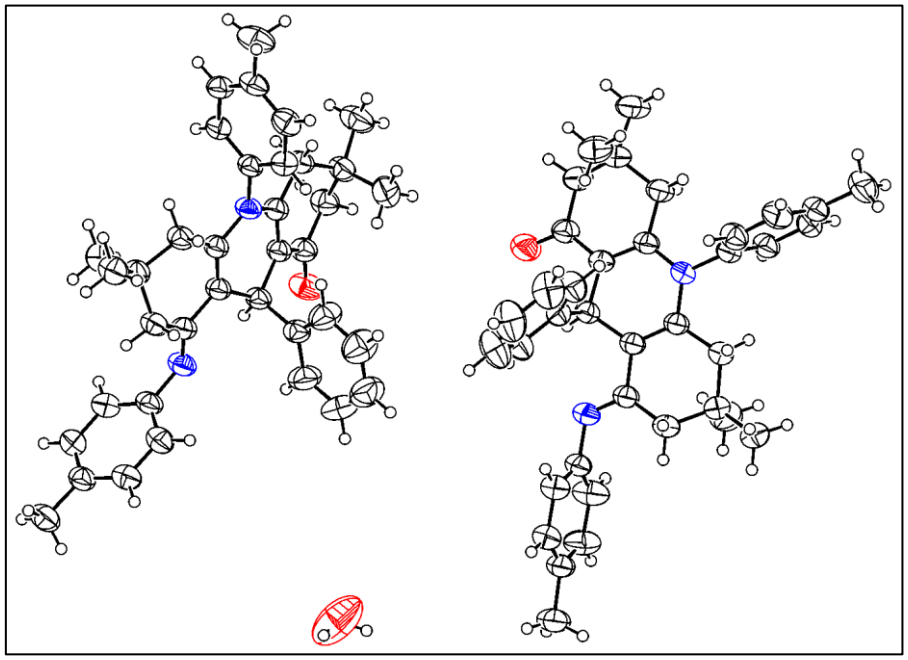

Figure III.25. ORTEP diagram of compound **III.9d**.

The crystal structure's asymmetric unit comprises two molecules of compound (E)-3,3,6,6-tetramethyl-9-phenyl-10-(p-tolyl)-8-(p-tolylimino)-3,4,5,6,7,8,9,10-octahydroacridin-1(2H)-one **III.9d** and one water molecule (**Figure III.25**). The presence of two spatially distinct molecules in the asymmetric unit is primarily attributed to the presence of a chiral carbon, resulting in the formation of the S and R stereoisomers as a racemic mixture (**Figure III.26**).

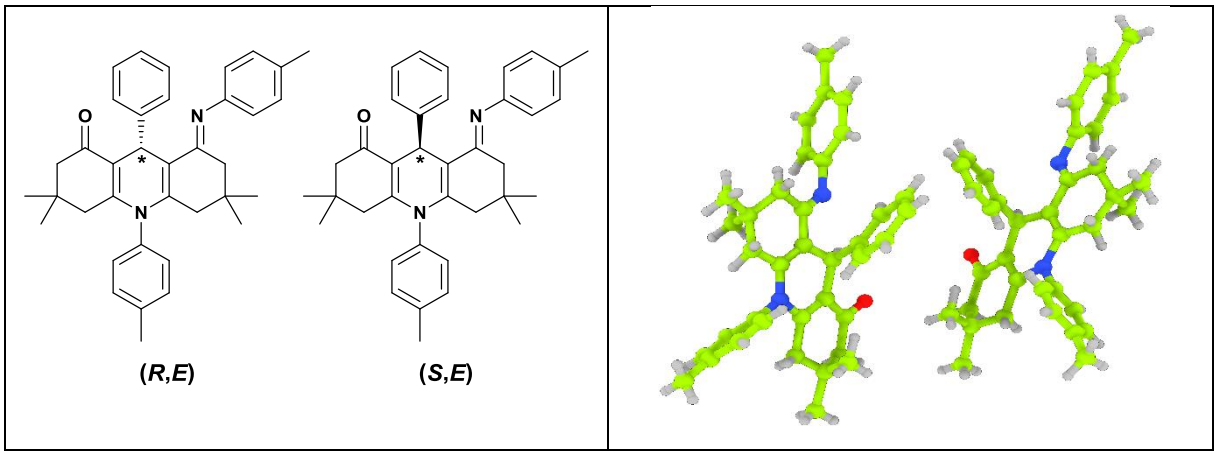

Figure III.26. 2D (left) and 3D (right) views of the two stereoisomers of compound **III.9d**.

The overall observation of the ORTEP diagram depicted in **Figure III.25** demonstrates that the atoms and groups of compound **III.9d** reveal a specific rearrangement in space, corresponding to the *E* geometric conformation in relation to the imine double bond. The cohesion of the crystal structure is reinforced by the presence of short contacts between various atoms of the molecules, as indicated in **Table III.6**.

Table III.6. Short contacts in the crystal structure of compound **III.9d**.

D-H…A	*d*(D-H)	*d*(H…A)	*d*(D-A)	D-H-A	Symetrie
C_{61}-H_{61B}…O_1	**0.960**	2.536	3.364(3)	144.5	x,y,z ; x,y,-1+z
C_{21}-H_{21A}…O_2	**0.960**	2.503	3.347(3)	146.7	x,y,z ; 1+x,y,z
O_3-H_{3C}…O_2	**0.85**	2.550	3.15(1)	129	x,y,z ; 1-x,1-y,1-z
C_5-H_{5A}…C_{74}	**0.970**	2.886	3.850(4)	173.0	x,y,z ; 1-x,1-y,1-z

5. Sulfamide derivatives

One of the most known pharmacophore since the earliest history of pharmaceutical science; the sulfamide moiety. Sulfamides and derivatives occupies a huge part of commercialized medicines especially as antibacterial [90]. Herein, we report the synthesis of sulfamide derivatives from available sulfanilamide, CSI, and amines (**Scheme III.12**).

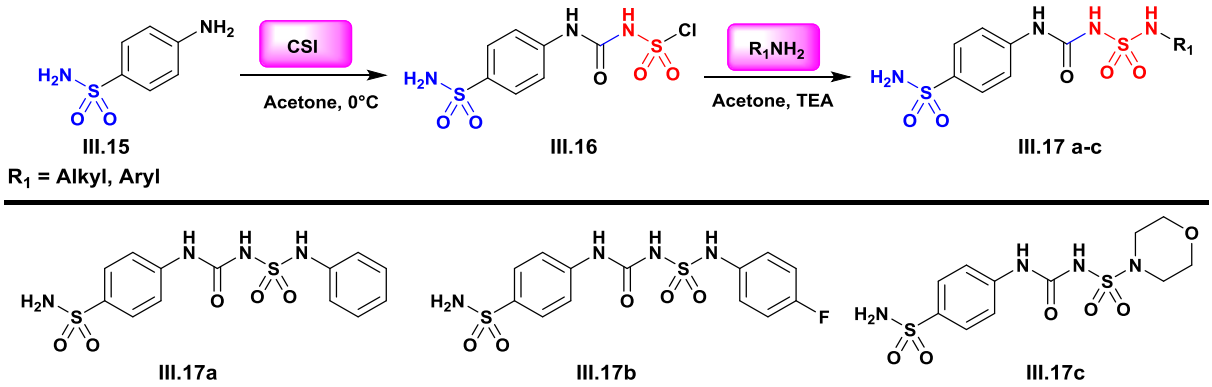

Scheme III.12. Synthesis of sulfamide derivatives.

5.1. Spectral characterization of sulfamide derivatives

Sulfamides were characterized with methods including ^{1}H, ^{13}C NMR, and IR.

In ^{1}H NMR, several significant signals were observed counting signals corresponding to the aromatic protons, as well as a singlet around 7 ppm that is related to NH_2 Group.

In ^{13}C NMR, all required signals were perceived.

In IR, absorption bands corresponding to NH_2 were located around 3238 cm^{-1}, and aromatic C-H bonds absorbed near to 3075 cm^{-1}. Further, the presence of SO_2 function was confirmed by two intense sharp bands around 1100 and 1300 cm^{-1}.

Spectra of compound **III.17a** are depicted in figures **III.27-III.29**.

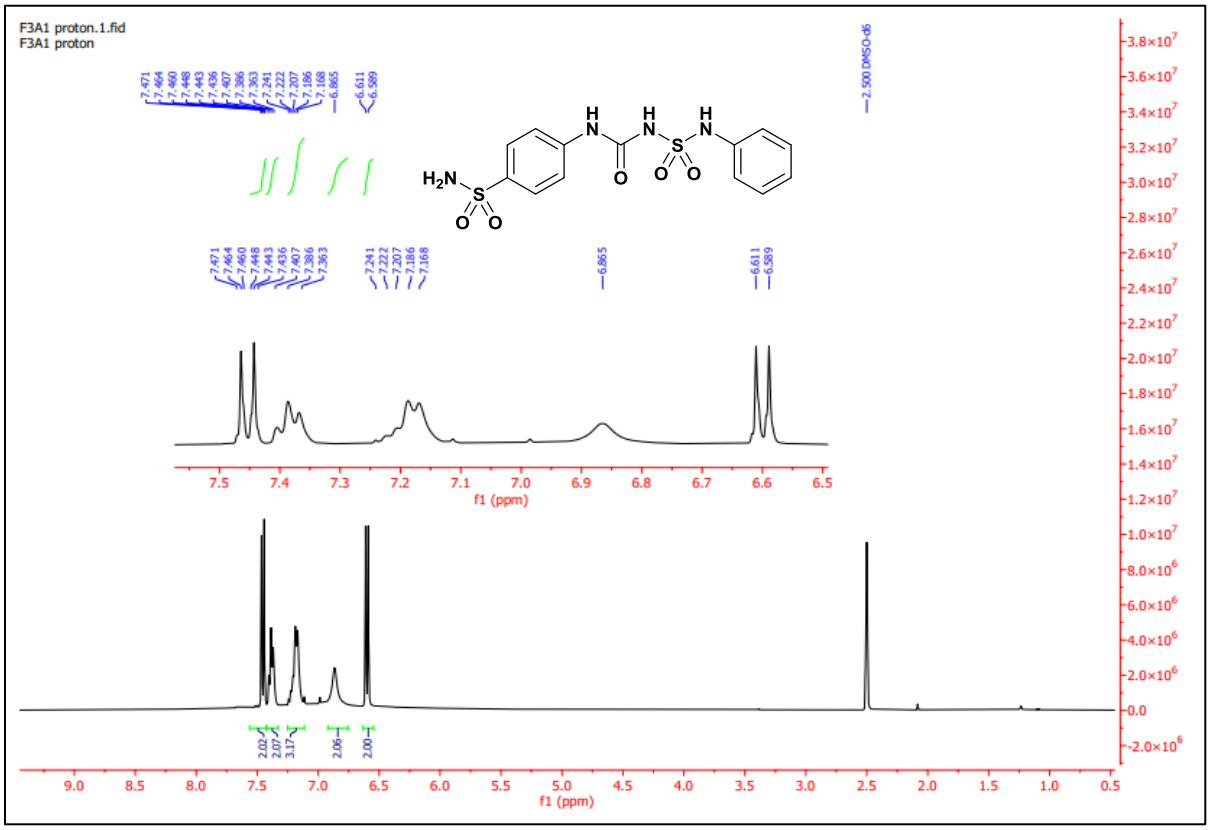

Figure III.27. ^{1}H NMR spectrum of compound **III.17a**.

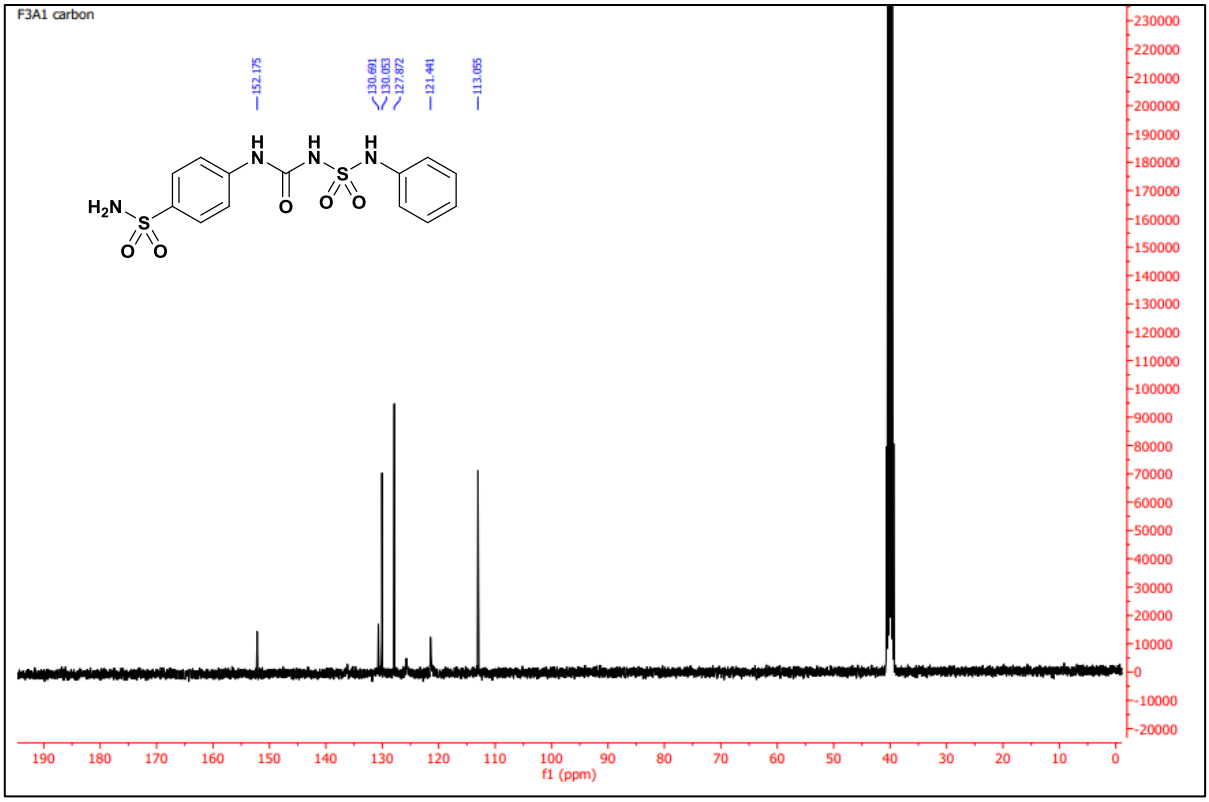

Figure III.28. ^{13}C NMR spectrum of compound **III.17a**.

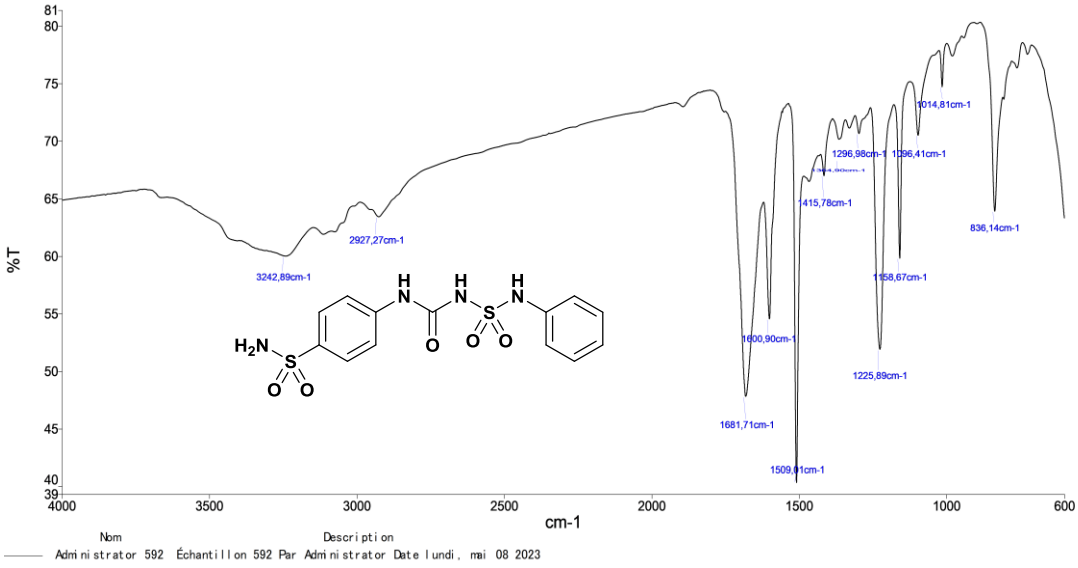

Figure III.29. IR spectrum of compound **III.17a**.

Conclusion

In this chapter, we detailed the synthesis of four distinct series of molecules comprising promising pharmacophores. Among these series, three were derived from chemical transformations on β-enaminone derivatives.

The first one, β-enaminocarboxamides that resulted from the condensation of β-enaminones and chlorosulfonyl isocyanate in dichloromethane affording the final products with excellent yields (80-92 %).

The second series consisted of 4-hydroxyquinolone analogues that were obtained through condensation of β-enaminones and diethyl malonate using microwave synthesis combined to heterogeneous catalysis ($BiCl_3$). This method yielded products with satisfactory yields ranging between 51% and 71%.

The third series comprised acridine derivatives, synthesized by reacting β-enaminones with aldehydes in a catalyst-free condition under microwave irradiation yielding 72 to 90 % of the desired compounds.

Furthermore, sulfanilamide was used in the synthesis of a fourth series of compounds containing sulfamide moiety. Sulfanilamide was condensed to chlorosulfonyl isocyanate yielding a carbamate intermediate, which was subsequently reacted with an amine.

Structural confirmation of all final products was achieved through spectral analysis, including infrared (IR), proton and carbon nuclear magnetic resonance (NMR) spectroscopy. Furthermore, three of these compounds underwent X-ray diffraction studies for further validation of their structures.

Chapter IV

In vitro and in silico assessment of novel β-enaminone and sulfamide derivatives

After a successful synthesis process of a drug-candidate, this latter is subjected to many crucial steps to confirm its ability to become a molecule with potent medicinal effects. Among these steps, *in silico* assessment that consists of a deep study giving information about the structural features of a molecule through DFT calculations, its aptitude to inhibit a drug target through molecular docking and dynamics simulations, and its ability to become a bioavailable drug through pharmacokinetics and toxicity prediction as well as drug-likeness investigation. Another stage of evaluating the capacity of a synthesized organic substance to become a drug-candidate is the *in vitro* tests, which gives a clearer insight of the biological activity in more applied and experimental aspects.

In this chapter, we will present the results of the *in vitro* tests conducted on our synthesized families of compounds counting antioxidant activity evaluation for all the mentioned series, and α-amylase inhibition for β-enaminocarboxamides. Every biological investigation will be followed by an *in silico* study that will include a molecular docking against a suitable target, an ADME prediction, and a DFT study to comprehend structural characteristics of synthesized compounds especially the most active ones.

1. *In vitro* and *in silico* assessment of β-enaminocarboxamides

1.1. *In vitro* evaluation and molecular docking of antioxidant and α-amylase inhibition activities

Antioxidant scavenging ability of synthesized β-enaminocarboxamides **III.5** was completed according to DPPH assay.

DPPH scavenging assay is a recognizable method that detects antioxidant substances that acts as proton donors [91]. The DPPH scavenging ability of prepared β-enaminocarboxamides **III.5** was evaluated and the results are shown in **Table IV.1**.

Compounds **III.5(a,i,n,p)** revealed a weak radical scavenging activity with an IC_{50} beyond 10 µmol/mL and compounds **III.5(b**,**d**,**e**,**h**,**j**,**l)** exhibited moderate antioxidant activity with IC_{50} ranging between 4.54 ± 1.17 and 9.65 ± 1.75 µmol/mL while derivatives **III.5(c**,**g**,**m)** showed relatively better results than the before-mentioned compounds.

The most promising antioxidant activity among the studied compounds appeared in compound **III.5k** that demonstrated an IC_{50} = 1.38 ± 0.73 µmol/mL better than the standard BHT (IC_{50} = 2.05 ± 0.09 µmol/mL), and compound **III.5o** that showed a clearly enhanced IC_{50} = 0.55 ± 0.04 µmol/mL than both the utilized standards citing BHT (IC_{50} = 2.05 ± 0.09 µmol/mL), and BHA (IC_{50} = 0.98 ± 0.02 µmol/mL).

The antidiabetic activity of β-enaminocarboxamides was evaluated through estimation of their inhibitory capacity against α-amylase enzyme using acarbose as a standard. IC_{50} values in **Table IV.1**.

IC_{50} values of all compounds **III.5(c,e,h,i,m,n,p)** were beyond 10 µmol/mL indicating a feeble α-amylase inhibition. Moreover, compound **III.5k** (IC_{50} = 6.60 ± 0.78 µmol/mL) showed an activity slightly close to the one exhibited by the standard acarbose.

It is worth mentioning that six derivatives **III.5(b,d,g,j,l,o)** among the synthesized β-enaminocarboxamides displayed remarkable results by showing IC_{50} less than the standard, in a range varying between 1.07 ± 0.03 and 4.10 ± 0.46 µmol/mL. These results are encouraging especially for compound **III.5j** that presented the best potency in α-amylase inhibition.

In order to elaborate a correlation between experimental and theoretical results, and to learn more about the binding mode of studied β-enaminocarboxamides within the active sites of both xanthine oxidase (XO) and human pancreatic α-amylase (HPA) as antioxidant and antidiabetic drug targets respectively, we aimed for a molecular docking simulation that involves two corresponding PDB files: **3NRZ** (XO in complex with hypoxanthine) [92] and **1B2Y** (HPA in complex with acarbose) [93]. Achieved results are summarized in **Table IV.1**.

Table IV.1. IC_{50} values (mean ± SD) and docking scores of β-enaminocarboxamides.

Compound	Antioxidant activity		α-amylase inhibition	
	IC_{50} (µmol/mL)	Docking score (kcal.mol^{-1})	IC_{50} (µmol/mL)	Docking score (kcal.mol^{-1})
III.5a	>10	-6.02	>100	-5.74
III.5b	4.67 ± 0.53	-6.02	1.32 ± 0.21	-6.00
III.5c	3.11 ± 0.13	-6.00	17.02 ± 6.31	-6.43
III.5d	9.65 ± 1.75	-6.11	1.28 ± 0.11	-6.32
III.5e	4.54 ± 1.17	-5.85	32.35 ± 16.79	-6.01
III.5g	3.12 ± 0.06	-6.74	4.10 ± 0.46	-6.10
III.5h	4.67 ± 0.39	-6.00	23.81 ± 4.79	-5.93
III.5i	>10	-5.77	27.43 ± 8.60	-6.18
III.5j	7.09 ± 0.23	-4.83	1.07 ± 0.03	-6.36
III.5k	1.38 ± 0.73	-6.33	6.60 ± 0.78	-6.12
III.5l	5.70 ± 0.53	-6.42	1.19 ± 0.09	-6.20
III.5m	3.51 ± 0.15	-6.22	22.58 ± 8.45	-5.80
III.5n	>10	-6.23	11.90 ± 2.40	-6.04
III.5o	0.55 ± 0.04	-6.86	3.12 ± 0.17	-5.60
III.5p	>10	-6.00	14.56 ± 4.88	-5.20
BHA	0.98 ± 0.02	-	-	-

BHT	2.05 ± 0.09	-	-	-
Acarbose	-	-	5.65 ± 0.016	-9.20
Hypoxanthine	-	-6.07	-	-

Synthesized β-enaminocarboxamides when docked to XO showed docking scores ranging from -4.83 to -6.86 kcal.mol^{-1}. Among the studied compounds, seven derivatives exhibited a docking score better than the co-crystallized ligand (Hypoxanthine), namely compounds **III.5(d,g,k,l,m,n,o)**. The best docking score was noticed in compound **III.5o** that showed the most potent IC_{50} value in antioxidant DPPH assay.

Many significant interactions were noticed between the docked compounds and the active site of XO including hydrogen bonds with residues such as Glu802, Asn768, and Lys771 (**Figure IV.1**). Main parts of the molecule that were involved in hydrogen bonds formation with residues of XO cavity, carbonyl group of the ketone function as H-bond acceptor and N-H of both secondary amine and primary amide functions as H-bond donors.

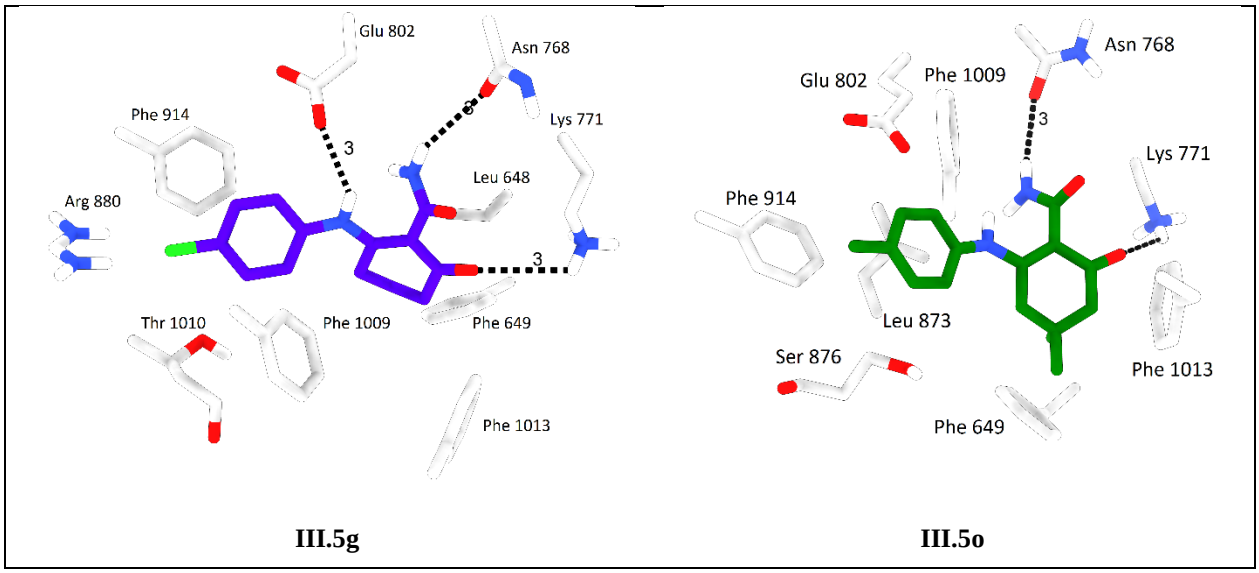

Figure IV.1. 3D views of compounds **III.5g** and **III.5o** docked to XO active site.

On the other hand, docking of β-enaminocarboxamides with HPA resulted in docking scores located between -5.20 and -6.43 kcal.mol^{-1}. Most potent derivatives in the *in vitro* test specifically compounds **III.5(b,d,j,l)** with IC_{50} under 2 µmol/mL displayed docking scores respectively equal to -6.00, -6.32, -6.36, and -6.20 kcal.mol^{-1}. Presented interactions between β-enaminocarboxamides and HPA active site consisted of H-bonds (**Figure IV.2**) with several residues citing Tyr62, Gln63, Asp197, Glu233, and Asp300. The presence of the primary amide group in the structure of synthesized β-enaminocarboxamide derivatives enhanced the activity since both CO and NH_2 were strongly involved in H-bonds formation with the active site of HPA respectively as H-bond acceptor and donor.

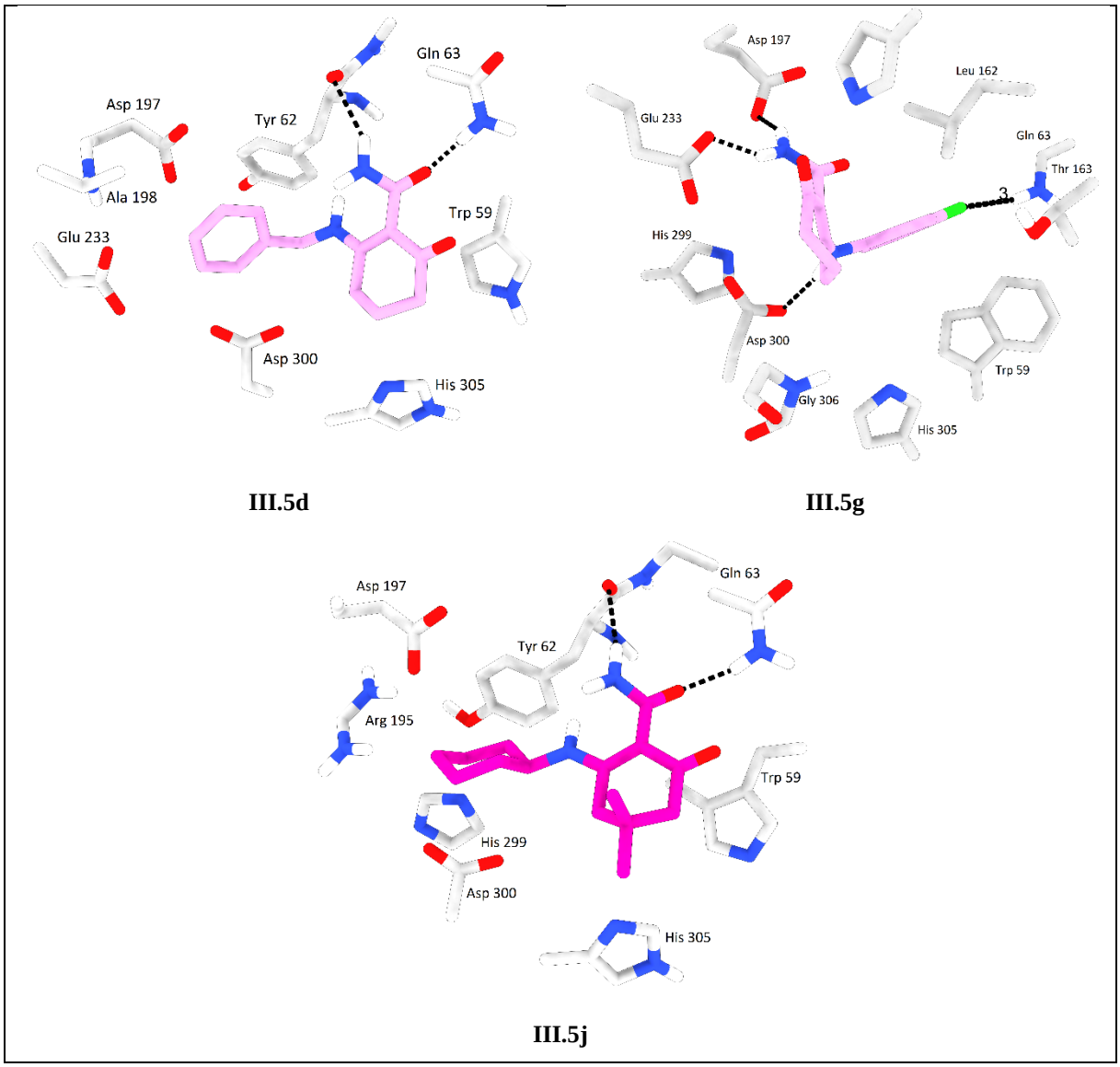

Figure IV.2. 3D views of compounds **III.5(d,g,j)** docked to HPA active site

1.2. ADME prediction

In order to predict the behavior of the synthesized β-enaminocarboxamides as administrated drugs, an *in silico* investigation was carried out using online server SwissADME [94] that helped generate different parameters related to pharmacokinetics as shown in **Table IV.2**.

Table IV.2. ADME parameters of β-enaminocarboxamides generated with SwissADME.

Entry	Molecular weight (g/mole)	Rotatable bonds	H-bond donor	H-bond acceptor	Log Po/W iLogP	Log S ESOL	GI	BBB	Log Kp (cm/s)	TPSA (Å²)
III.5a	196.25	4	2	2	1.76	-1.85	High	No	-6.30	72.19
III.5b	258.32	4	2	2	1.69	-3.10	High	No	-5.97	72.19
III.5c	236.31	3	2	2	1.77	-2.75	High	No	-5.90	72.19
III.5d	244.29	4	2	2	1.85	-2.77	High	No	-6.17	72.19

III.5e	260.29	4	2	3	1.75	-2.89	High	No	-6.24	81.42
III.5f	248.25	3	2	3	1.42	-2.97	High	Yes	-6.08	72.19
III.5g	264.71	3	2	2	2.02	-3.40	High	Yes	-5.81	72.19
III.5h	260.29	4	2	3	1.48	-2.89	High	No	-6.24	81.42
III.5i	224.30	4	2	2	1.94	-2.55	High	No	-5.89	72.19
III.5j	264.36	3	2	2	2.19	-3.10	High	Yes	-5.87	72.19
III.5k	258.32	3	2	2	1.68	-3.13	High	Yes	-6.02	72.19
III.5l	272.34	4	2	2	2.16	-3.10	High	Yes	-6.14	72.19
III.5m	276.31	3	2	3	1.65	-3.64	High	Yes	-5.66	72.19
III.5n	292.76	3	2	2	1.84	-4.07	High	Yes	-5.39	72.19
III.5o	272.34	3	2	2	1.82	-3.78	High	Yes	-5.45	72.19
III.5p	288.34	4	2	3	1.84	-3.56	High	No	-5.82	81.42

Many important parameters have been successfully predicted using the SwissADME predictive tool; skin permeability coefficient. The latter is a crucial predictive value that can quantifie the transport of a molecule through the outer layer of the epiderm, indicating the level of skin absorption [95]. Thus, molecules' skin permeability increases when Log Kp values are more negative [94]. Solubility in water is a fundamental property that affect the drug-candidate even before entering the human body; indeed, a great solubility in water could facilitate formulation of the drug. Further, a soluble molecule can be easily absorbed by the organism [94].

An other important parameter; the lipophilicity, which can be considered as the opposite of water solubility. Lipophilic molecules have an advantage in crossing biological membranes because they are attracted to lipids, a feature that facilitates absorption and enhance bioavailability. Yet, achieving the right balance between lipophilicity and solubility in water is the key to avoid problems in the formulation process [96]. Therefore, Log P indicating lipophilicity and Log S referring to water solubility should not exceed 5 and 6 respectively [94]. Solubility in water estimated with Log S (ESOL) ranged between -1.85 and -4.07, while skin permeability coefficient K_p between -5.39 and -6.30 cm/s.

All prepared compounds were predicted to be orally bioavailable according to Lipinski's rule of five [97] by presenting a molecular weight less than 500 Da with a range of [196.25 - 292.76 $g.mol^{-1}$], Log P values less than 5 [1.42 - 2.19], as well as H-bond donors (2) and acceptors (2, 3) less than 5 and 10 respectively. In addition, rotatable bonds of all derivatives are less than 10 varying between 3 and 4.

Bioavailability radars of studied compounds are displayed in **Figure IV.3** giving a first look on their drug-likeness. Results shows that most β-enaminocarboxamides are within the optimal range of lipophilicity, size, polarity, flexibility, solubility, and saturation (pink area).

Figure IV.3. Bioavailability radars of β-enaminocarboxamides predicted using SwissADME.

Recognizing whether compounds interact with P-glycoprotein (P-gp), a key member of ATP-binding cassette transporters, is essential for understanding active efflux across biological membranes. This understanding is particularly pertinent for processes like efflux from the gastrointestinal wall to the lumen or from the brain. P-gp serves a crucial role in protecting the central nervous system (CNS) from foreign substances. The inhibition of P-gp improves all pharmacokinetics properties [94].

None of the studied enaminocarboxamides showed inhibition to P-gp (**Table IV.3**).

Understanding how molecules interact with cytochromes P450 (CYP) is pivotal. These enzymes are essential for metabolizing drugs and facilitating their elimination [94].

Results shows that each enaminocarboxamides derivative is predicted to inhibit at least one type of CYP except compound **III.5i**. Derivative **III.5o** is able to inhibit three cytochromes; CYP1A2, CYP2C19, and CYP3A4 while compound **III.5n** estimated to inhibit all cytochromes except CYP2D6 (**Table IV.3**).

Table IV.3. Predicted behavior of β-enaminocarboxamides towards P-gp and CYP.

	Pharmacokinetics-related proteins					
Compounds	**P-gp substrate**	**CYP1A2 inhibitor**	**CYP2C19 inhibitor**	**CYP2C9 inhibitor**	**CYP2D6 inhibitor**	**CYP3A4 inhibitor**
III.5a	-	+	-	-	-	-
III.5b	-	+	+	-	-	-
III.5c	-	+	-	-	-	-
III.5d	-	+	+	-	-	-
III.5e	-	+	-	-	-	-
III.5f	-	+	-	-	-	-
III.5g	-	+	+	-	-	-
III.5h	-	+	-	-	-	-
III.5i	-	-	-	-	-	-
III.5j	-	-	+	-	-	-
III.5k	-	+	+	-	-	-
III.5l	-	+	+	-	-	-
III.5m	-	+	+	-	-	-
III.5n	-	+	+	+	-	+
III.5o	-	+	+	-	-	+
III.5p	-	+	+	-	-	-

1.3. DFT study

Electronic composition of a molecule is an important factor that is highly linked to its activity as a drug-candidate or reactivity as a synthetic intermediate. A DFT calculation was performed to all of the synthesized β-enaminocarboxamides using Gaussian 09 [98].

The entails the determination of various parameters crucial for assessing chemical reactivity, including the energy gap, kinetic stability, polarizability, chemical softness, chemical hardness (η), electronic chemical potential (μ), electronegativity (χ), electrophilicity index (ω);

Dipolar moment **μ** is an important characteristic that gives information about the polarity of a molecule and its comportment in different states (acidic, basic, or neutral). This information can be useful to predict the behavior of the molecule as a synthetic reagent in diverse reaction conditions, or as a drug candidate within various physiological environments. The more polar is a molecule the higher is its dipolar moment. Dipolar moments of the studied compounds ranged between 2.4260 and 6.1007 D in which compound **III.5e** is the highest and **III.5g** the lowest (**Table IV.4**).

Table IV.4. Molecular descriptors and parameters of studied enaminocarboxamides calculated with B3LYP/6-31G(d,p) method in gas phase.

Entry	μ (D)	E_{HOMO} (eV)	E_{LUMO} (eV)	ΔEgap	(η)	(*S*)	(μ)	(χ)	(ω)
III.5a	4.7475	-5.7792	-0.7244	5.0548	2.5274	0.3957	-3.2518	3.2518	2.0919
III.5b	4.5092	-5.7781	-0.7592	5.0189	2.5094	0.3985	-3.2686	3.2686	2.1288
III.5c	4.9631	-5.7266	0.6898	6.4164	3.2082	0.3117	-2.5184	2.5184	0.9885
III.5d	4.4343	-5.8243	-0.7902	5.0341	2.5171	0.3973	-3.3073	3.3073	2.1728
III.5e	6.1007	-8.0353	2.6811	10.7164	5.3582	0.1866	-2.6771	2.6771	0.6688
III.5f	4.9938	-5.7781	-1.4090	4.3691	2.1845	0.4578	-3.5935	3.5935	2.9557
III.5g	2.4260	-5.9111	-1.4300	4.4812	2.2406	0.4463	-3.6705	3.6705	3.0066
III.5h	5.1361	-5.3849	-1.2036	4.1813	2.0907	0.4783	-3.2942	3.2942	2.5953
III.5i	4.6950	-5.7636	-0.7274	5.0363	2.5181	0.3971	-3.2455	3.2455	2.0915
III.5j	4.8990	-5.7128	-0.6931	5.0197	2.5098	0.3984	-3.2029	3.2029	2.0437
III.5k	4.0229	-5.7770	-1.2147	4.5623	2.2811	0.4384	-3.4958	3.4958	2.6787
III.5l	4.4048	-5.8064	-0.7927	5.0137	2.5069	0.3989	-3.2995	3.2995	2.1714
III.5m	2.9495	-5.8322	-1.2487	4.5835	2.2917	0.4363	-3.5405	3.5405	2.7348
III.5n	2.5106	-5.9005	-1.4166	4.4839	2.2419	0.4460	-3.6586	3.6586	2.9852
III.5o	4.5294	-5.6880	-1.1432	4.5448	2.2724	0.4401	-3.4156	3.4156	2.5669
III.5p	5.3723	-5.5492	-1.0253	4.5239	2.2619	0.4421	-3.2873	3.2873	2.3887

The energy gap between HOMO and LUMO is a significant indicator of the stability of a compound. Frontier Molecular Orbitals (FMOs), play a pivotal role in elucidating ligand-receptor interactions. The HOMO serves as an electron donor, while the LUMO acts as an electron acceptor, facilitating electron transfer; an essential aspect in understanding molecular interactions. These FMOs offer qualitative insights into electron susceptibility, aiding in the comprehension of molecular interactions.

Energy gap values of enaminocarboxamide-based compounds were located in a range of [4.1813-10.7164 eV], the most stable derivative was compound **III.5e**, which is the most polar as well (**Table IV.4**).

Table IV.5. Optimized structures and HOMO/LUMO orbitals of studied β-enaminocarboxamides.

Code	Optimized structure	HOMO	LUMO
III.5a	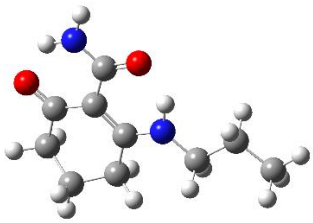	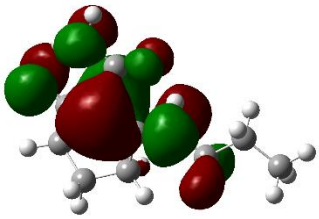	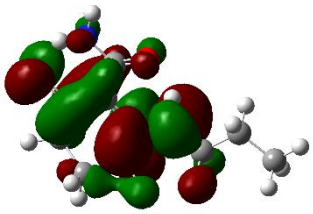
III.5b	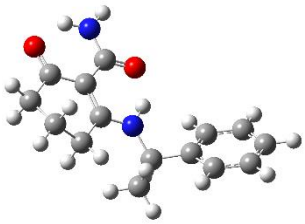	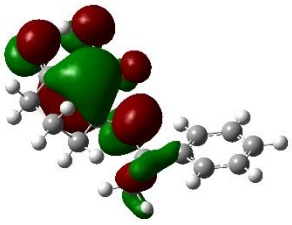	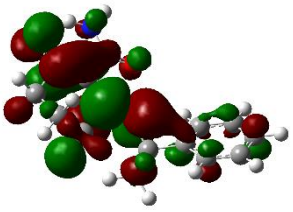
III.5c	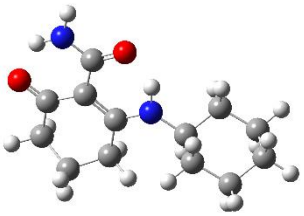	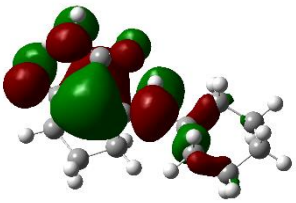	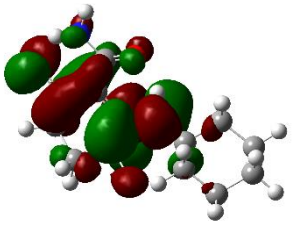
III.5d	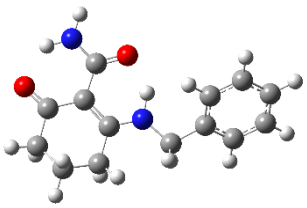	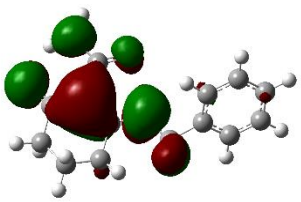	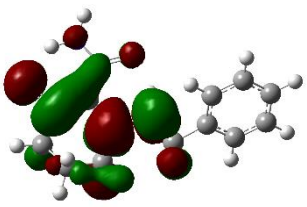

III.5e	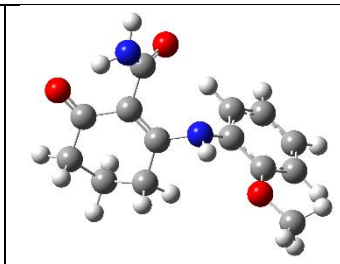	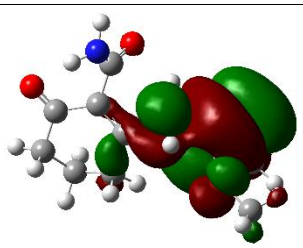	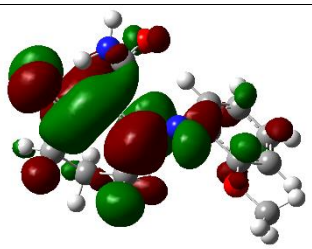
III.5f	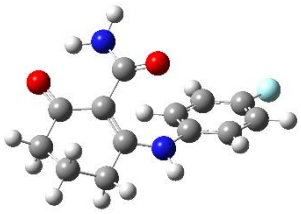	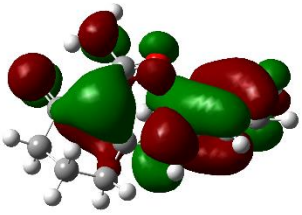	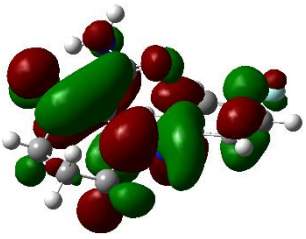
III.5g	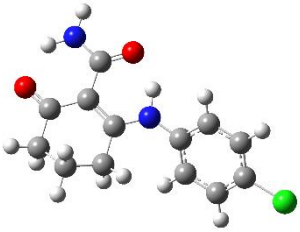	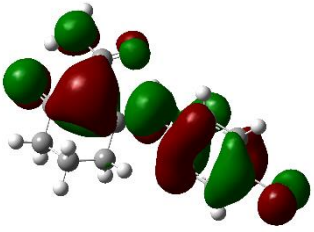	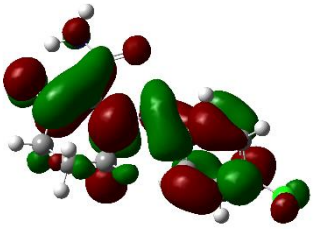
III.5h	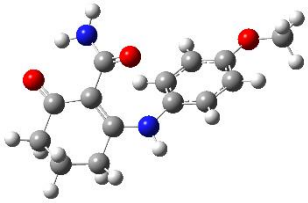	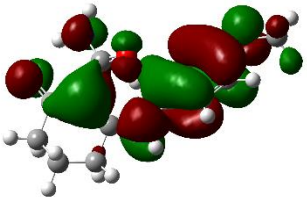	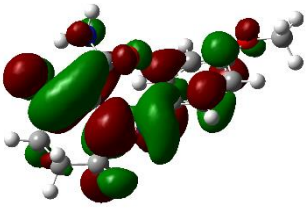
III.5i	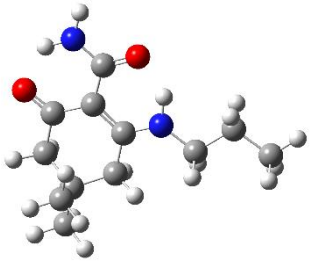	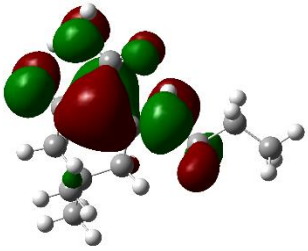	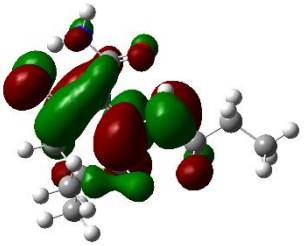
III.5j	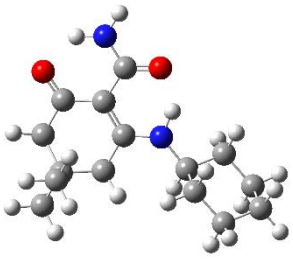	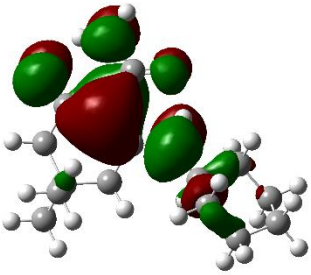	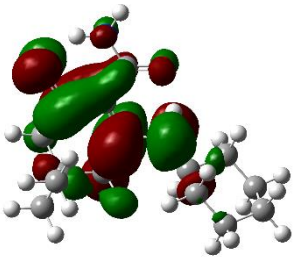

III.5k	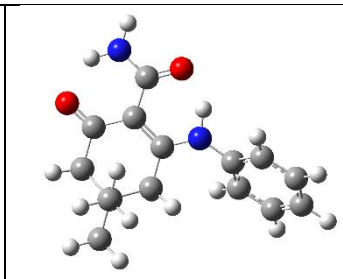	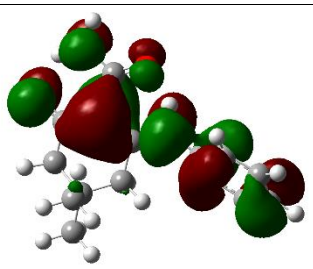	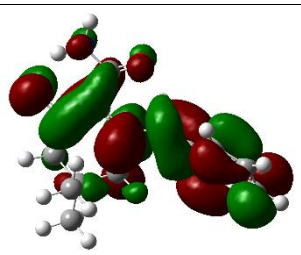
III.5l	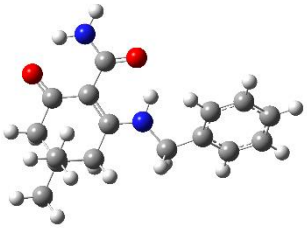	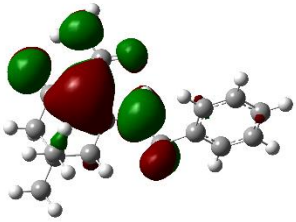	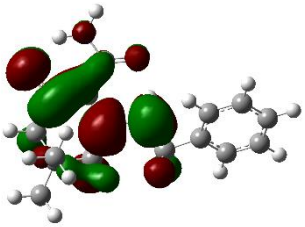
III.5m	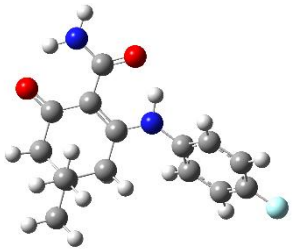	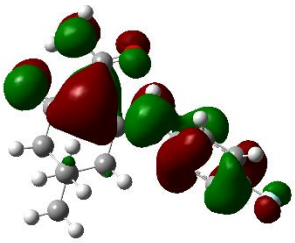	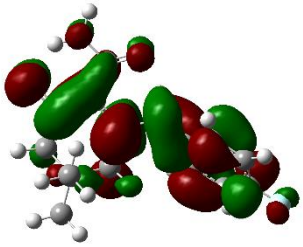
III.5n	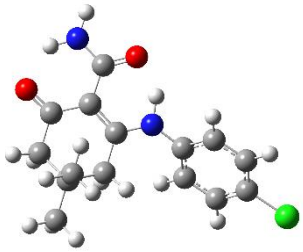	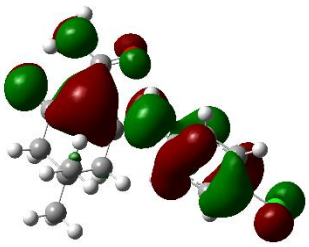	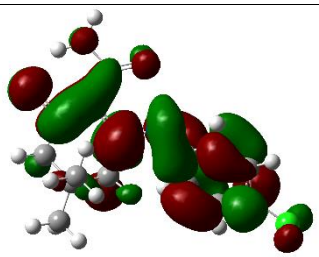
III.5o	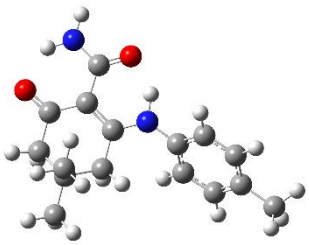	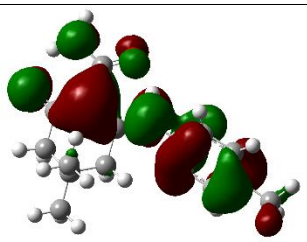	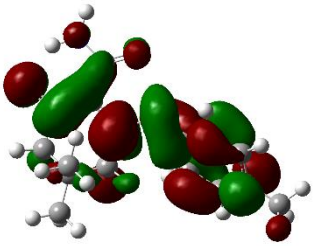
III.5p	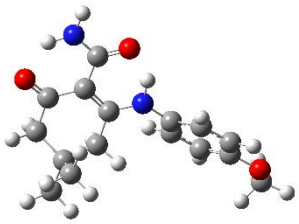	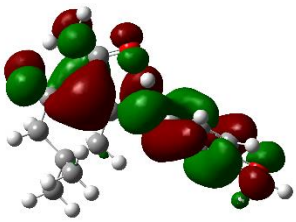	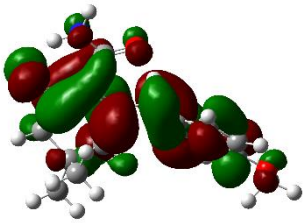

The molecular electrostatic potential (MEP) serves as a reactivity index, revealing both the electrophilic and nucleophilic regions within a molecule. This information proves invaluable in predicting a compound's behavior in relation to a target and within the physiological

environments of an organism. Consequently, the most electron-rich and electron-deficient areas of a compound represent its most reactive parts, enhancing their interaction ability with target molecules. Furthermore, mapping the electrostatic potential surrounding a compound elucidates fluctuations in binding affinity with the receptor's active site.

Molecular electrostatic potential (MEP) maps of studied β-enaminocarboxamides shown in **Figure IV.4** were constructed at B3LYP/6-31G(d,p) level in gas phase in order to have a glance on the nucleophilic and electrophilic parts of the molecules, thereby learn more about their reactivity. The color code of presented maps are lying in a range starting from the deepest red (most nucleophilic regions) and the deepest blue (most electrophilic regions). General observations of the presented MEP shows that the red color is always more located on carbonyl groups of ketone and amide functions that have an enhanced nucleophilicity due to the electronic delocalization engendered by the β-enaminone and β-enaminocarboxamide enchainments. These findings suggests that our synthesized β-enaminocarboxamides could exhibit a possible affinity with proton donors inside cavities of molecular targets leading to the formation of significant interactions and resulting in a biological activity, as noticed in the molecular docking study that showed the formation of H-bonds between carbonyls and active sites of xanthine oxidase and α-amylase.

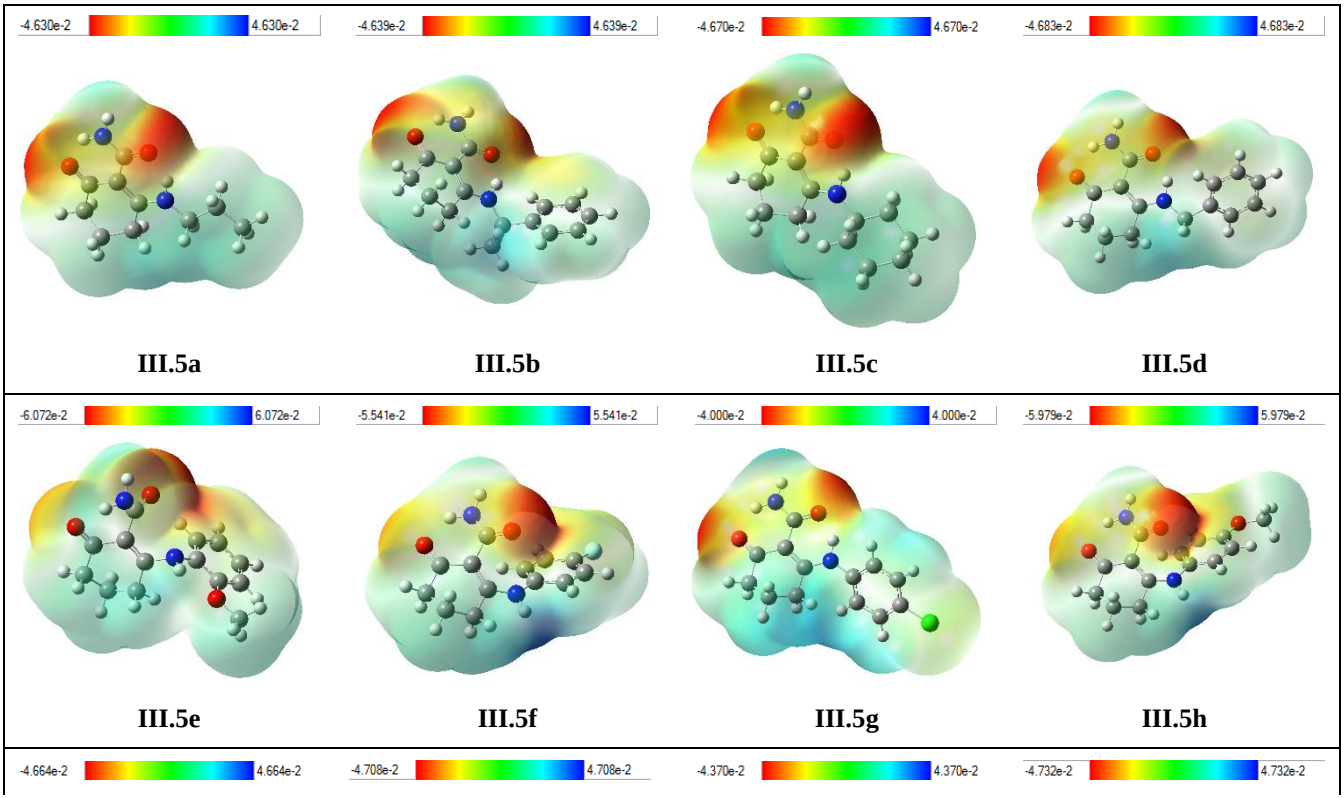

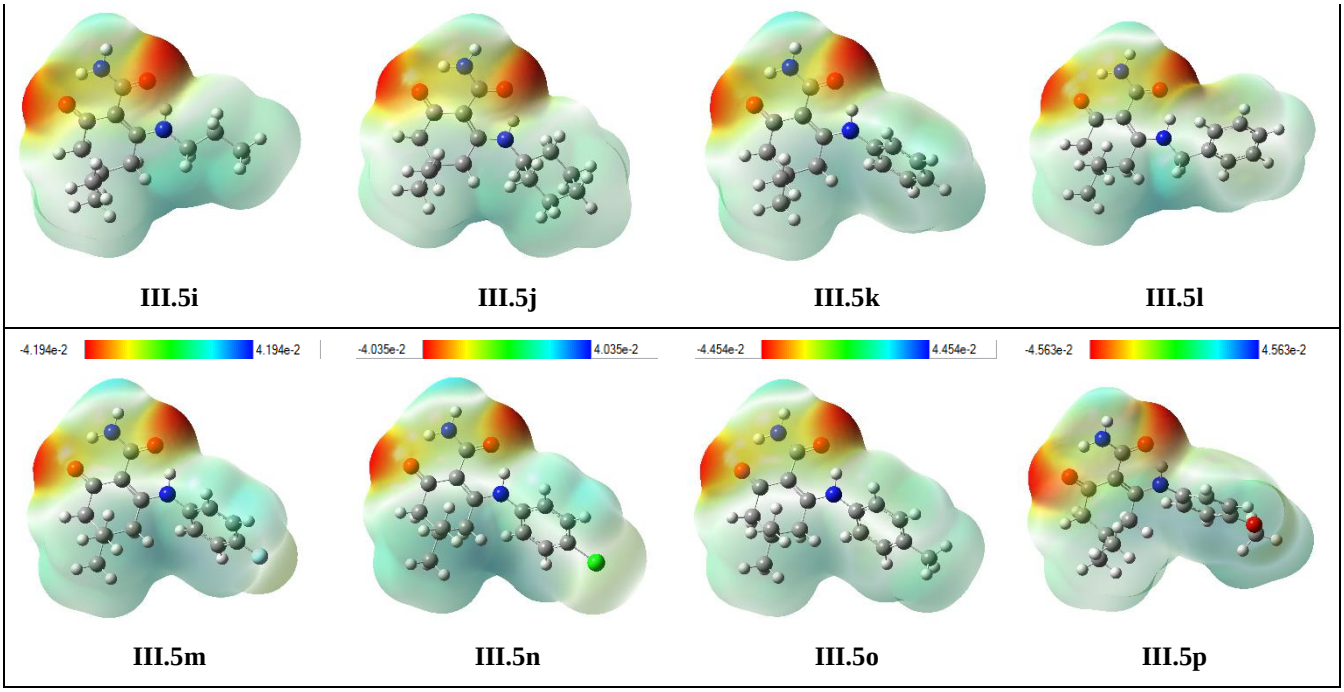

Figure IV.4. MEP maps of synthesized enaminocarboxamides.

2. *In vitro* and *in silico* assessment of 4-hydroxyquinolone analogues

2.1. *In vitro* evaluation and molecular docking of the antioxidant activity

Hydroxyl-containing molecules are known as excellent antioxidant agents [99], that is what prompted us to evaluate the antioxidant activity of 4-hydroxyquinolone analogues using the DPPH and ABTS assays [91,100].

Results of the radical scavenging activity of the synthesized 4-hydroxyquinolone analogues are summarized in **Table IV.6**.

According to DPPH assay results, IC_{50} of compound **III.7h** was estimated to a value greater than 10 µmol/mL, which corresponds to a weak value of antioxidant activity. Further, moderate radical scavenging aptitude was attributed to compounds **III.7(d**,**i**,**j)** that exhibited an IC_{50} lying in the range of [5.08 ± 0.05 – 6.70 ± 0.51 µmol/mL]. However, compounds **III.7(c**,**k**,**l)** showing a 50% inhibition concentration ranging between 2.52 ± 0.16 and 3.77 ± 1.17 µmol/mL are considered as more potent than the above-mentioned derivatives.

Finally, compounds **III.7(a**,**e**,**g)** gave the most encouraging results of radical scavenging ability, exhibiting IC_{50} values respectively equal to 0.99 ± 0.15, 1,98 ± 0.08, and 1.00 ± 0.08 µmol/mL, which are better than the standard BHT (IC_{50} = 2.05 ± 0.09 µmol/mL) and very similar to the standard BHA (IC_{50} = 0.98 ± 0.02 µmol/mL).

On the other hand, ABTS assay results shows that compounds **III.7(c,e,k)** exhibited an IC_{50} higher than 1 µmol/mL, while IC_{50} of **III.7(d,h,i,j)** varied between 0.35 ± 0.02 and 0.76 ± 0.01 µmol/mL.

Compared to the tested 4-hydroxyquinolone analogues, compounds **III.7(a,g,l)** exhibited the best results in ABTS assay with IC_{50} ranging from 0.14 ± 0.01 to 0.22 ± 0.02 µmol/mL, which is in consistency with the DPPH assay findings.

Molecular docking was performed against an antioxidant target (XO in complex with quercetin) PDB: **3NVY** [101] in order to reinforce the experimental results and to explore the binding mode of synthesized 4-hydroxyquinolone analogues. Resulted docking scores are summarized in **Table IV.6**.

Table IV.6. IC_{50} values (mean ± SD) and docking scores of 4-hydroxyquinolone analogues.

Compound	DPPH assay	ABTS assay	Docking score
	IC_{50} (µmol/mL)		(kcal.mol^{-1})
III.7a	0.99 ± 0.15	0.22 ± 0.02	-6.36
III.7c	3.14 ± 1.41	1.58 ± 0.50	-6.43
III.7d	6.70 ± 0.51	0.76 ± 0.01	-7.38
III.7e	1.98 ± 0.08	2.24 ± 0.02	-7.26
III.7g	**1.00 ± 0.08**	**0.14 ± 0.01**	**-7.59**
III.7h	>10	0.35 ± 0.02	-5.60
III.7i	5.08 ± 0.05	0.72 ± 0.01	-5.18
III.7j	6.13 ± 1.51	0.54 ± 0.01	-6.20
III.7k	3.77 ± 1.17	1.18 ± 0.16	-6.18
III.7l	2.52 ± 0.16	0.16 ± 0.02	-6.07
BHA	0.98 ± 0.02	0.04 ± 0.003	-
BHT	2.05 ± 0.09	0.007 ± 0.001	-
Quercetin	-	-	-8.48

Docking scores in complex with XO ranged between -5.18 and -7.59 kcal.mol^{-1} with compound **III.7g** presenting the best docking score. Achieved *in silico* results are in consistency with DPPH and ABTS *in vitro* tests in which compound **III.7g** showed the best IC_{50} values among the synthesized series. Studied derivatives exhibited several meaningful interactions consisting of H-bonds with residues of the active site including Ser876, Leu648, and Lys771 (**Figure IV.5**). Hydroxyl groups in 4-hdroxyquinolone analogues were significantly involved in H-bonds formation as well as the two carbonyl groups contained in the structures.

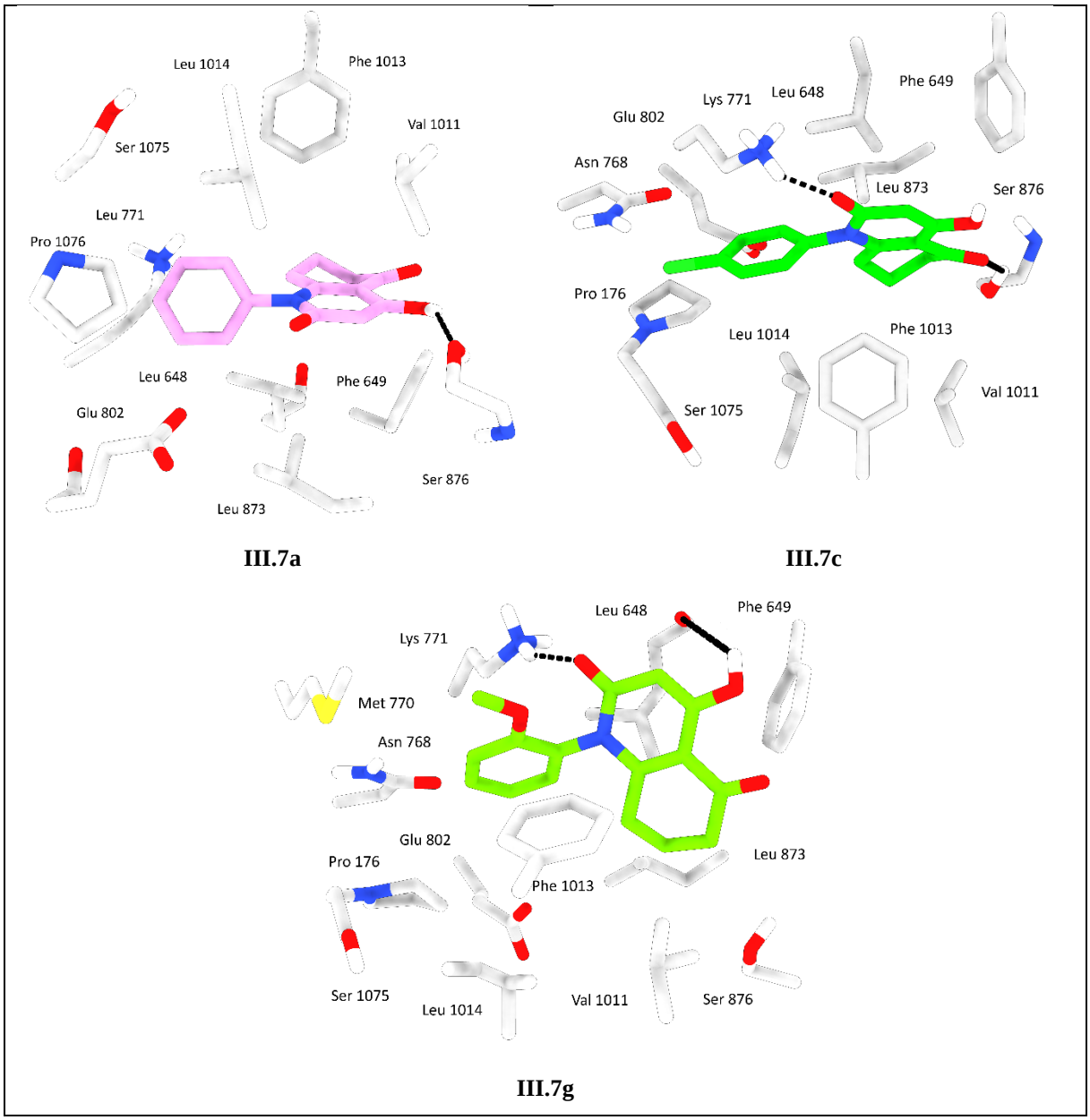

Figure IV.5. 3D view of compounds **III.7(a,c,g)** docked with XO.

2.2. ADME prediction

Phamacokinetic properties of the prepared 4-hydroxyquinolone analogues were estimated using SwissADME as presented in **Table IV.7**.

All derivatives were found to be in the norms of Lipinski's rule of five. Molecular weight lied between 255.27 and 328.32 g.mol^{-1}, which ensures an easy transfer inside the organism. Further, 1 H-bond donor, 3 to 5 H-bond acceptors, and 1 to 2 rotatable bonds were noticed in structures of the investigated compounds. Lipophilicity expressed as Log P was also predicted, results showed a lipophilicity in the range of 1.75 and 2.91 indicating acceptable values for a drug-candidate.

Solubility in water Log S and skin permeability Log K_p are also essential parameters that directly affect the absorption and diffusion of a substance within physiological systems. Herein, Log S ESOL and Log K_p values were respectively situated in a range from -2.85 to -3.70, and from -6.24 to -7.05 cm/s.

Table IV.7. ADME parameters of 4-hydroxyquinolone analogues generated with SwissADME.

Entry	Molecular weight (g/mole)	Rotatable bonds	H-bond donor	H-bond acceptor	Log Po/W iLogP	Log S ESOL	GI	BBB	Log Kp (cm/s)	TPSA (Å²)
III.7a	255.27	1	1	3	1.75	-2.89	High	Yes	-6.66	59.30
III.7b	269.30	2	1	3	2.19	-2.85	High	Yes	-6.79	59.30
III.7c	269.30	1	1	3	1.92	-3.18	High	Yes	-6.49	59.30
III.7d	289.71	1	1	3	2.54	-3.48	High	Yes	-6.42	59.30
III.7e	273.26	1	1	4	2.36	-3.04	High	Yes	-6.70	59.30
III.7f	300.27	2	1	5	2.00	-2.93	High	No	-7.05	105.12
III.7g	285.29	2	1	4	2.44	-2.95	High	Yes	-6.86	68.53
III.7h	283.32	1	1	3	2.19	-3.54	High	Yes	-6.24	59.30
III.7i	297.35	2	1	3	2.78	-3.50	High	Yes	-6.37	59.30
III.7j	301.31	1	1	4	2.75	-3.70	High	Yes	-6.28	59.30
III.7k	313.35	2	1	4	2.91	-3.61	High	Yes	-6.44	68.53
III.7l	313.35	2	1	4	2.73	-3.61	High	Yes	-6.44	68.53
III.7m	328.32	2	1	5	2.33	-3.59	High	No	-6.63	105.12

Bioavailability radars shown in **Figure IV.6** indicate that lipophilicity, size, polarity, solubility, flexibility and saturation are all within the pink area that designate the optimal range of the six factors, and this for most compounds, while compounds **III.7(a,d,e,f)** slightly violated the saturation factor.

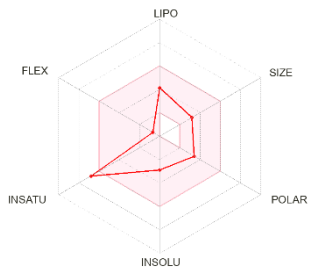

III.7a

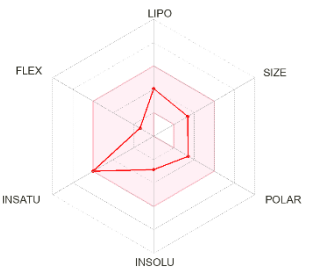

III.7b

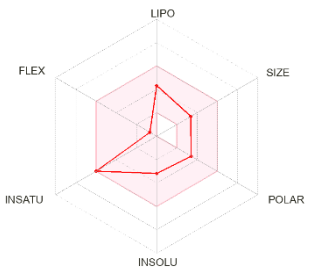

III.7c

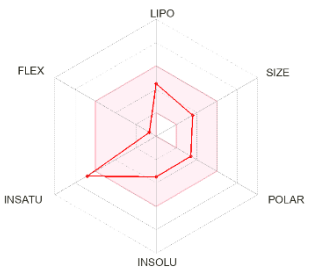

III.7d

Figure IV.6. Bioavailability radars of 4-hydroxyquinolone analogues predicted using SwissADME.

The feature of inhibiting cytochromes P450 and P-gp is a useful way to predict the properties of molecules during the absorption, distribution, metabolism, and excretion processes. This feature was predicted for synthesized 4-hydroxyquinolone analogues as shown in **Table IV.8**. All synthesized compounds were able to inhibit at least one cytochrome P450 with compound **III.7k** inhibiting three CYP, while none of them were identified as substrates of P-gp.

Table IV.8. Predicted behavior of 4-hydroxyquinolone analogues towards P-gp and CYP.

	Pharmacokinetics-related proteins					
Compounds	**P-gp substrate**	**CYP1A2 inhibitor**	**CYP2C19 inhibitor**	**CYP2C9 inhibitor**	**CYP2D6 inhibitor**	**CYP3A4 inhibitor**
III.7a	-	+	-	-	-	-
III.7b	-	+	-	-	-	-
III.7c	-	+	-	-	-	-

III.7d	-	+	-	-	-	-
III.7e	-	+	-	-	-	-
III.7f	-	-	-	-	-	-
III.7g	-	+	-	-	-	-
III.7h	-	+	-	-	-	-
III.7i	-	+	-	-	+	-
III.7j	-	+	-	-	-	-
III.7k	-	+	-	+	-	+
III.7l	-	+	-	-	-	-
III.7m	-	-	-	+	-	-

2.3. DFT study

DFT calculations of 4-hydroxyquinolone analogues **III.7** were performed using Gaussian 09 [6]. Molecular descriptors and different parameters were generated according to the DFT B3LYP 6-31G(d,p) method as shown in **Table IV.9**. Dipolar moments of studied 4-hydroxyquinolone analogues ranged between 2.5369 and 7.3766 D starting from the chlorine-substituted derivative **III.7d** to the methoxy-substituted derivative **III.7k** as the less and most polar compounds respectively. Optimized structures and FMOs graphical representations of all synthesized 4-hydroxyquinolone analogues are summarized in **Table IV.10** The energy gap values between HOMO and LUMO for studied compounds were located in the interval of [3.5620 - 4.7911 eV], in which compound **III.7b** is the most stable among studied derivative.

Table IV.9. Molecular descriptors and parameters of studied 4-hydroxyquinolone analogues.

Entry	μ (D)	E_{HOMO} (eV)	E_{LUMO} (eV)	ΔEgap	(η)	(S)	(μ)	(χ)	(ω)
III.7a	4.0139	-5.9601	-1.2267	4.7334	2.3667	0.4225	-3.5934	3.5934	2.7279
III.7b	3.4469	-6.0167	-1.2256	4.7911	2.3956	0.4174	-3.6212	3.6212	2.7369
III.7c	4.4347	-5.9171	-1.1823	4.7348	2.3674	0.4224	-3.5497	3.5497	2.6613
III.7d	2.5369	-6.1011	-1.3818	4.7193	2.3596	0.4238	-3.7414	3.7414	2.9662
III.7e	2.8784	-6.0475	-1.3124	4.7351	2.3675	0.4224	-3.6799	3.6799	2.8599
III.7f	2.9066	-6.3177	-2.7456	3.5720	1.7860	0.5599	-4.5317	4.5317	5.7491
III.7g	4.9604	-5.8115	-1.0754	4.7361	2.3681	0.4223	-3.4435	3.4435	2.5036
III.7h	4.0406	-5.9416	-1.2104	4.7312	2.3656	0.4227	-3.5760	3.5760	2.7028

III.7i	3.4627	-5.9977	-1.2139	4.7838	2.3919	0.4181	-3.6058	3.6058	2.7179
III.7j	2.9442	-6.0279	-1.2961	4.7318	2.3659	0.4227	-3.6620	3.6620	2.8340
III.7k	7.3766	-5.8115	-1.5742	4.2374	2.1187	0.4720	-3.6929	3.6929	3.2183
III.7l	4.7610	-8.9558	-5.0513	3.9046	1.9523	0.5122	-7.0035	7.0035	12.5621
III.7m	3.0659	-6.2940	-2.7320	3.5620	1.7810	0.5615	-4.5130	4.5130	5.7180

Table IV.10. HOMO and LUMO orbitals for synthesized 4-hydroxyquinolone analogues.

Code	Optimized structure	HOMO	LUMO
III.7a	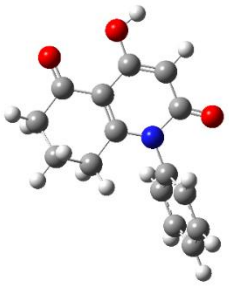	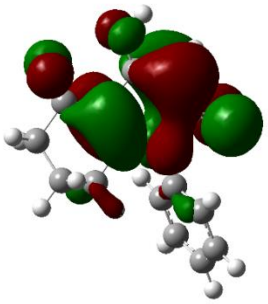	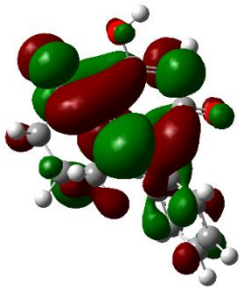
III.7b	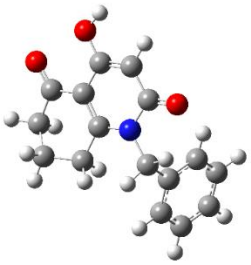	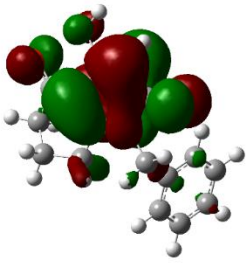	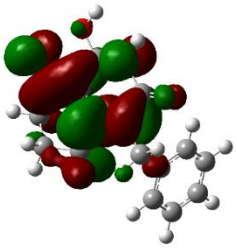
III.7c	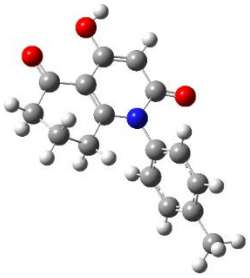	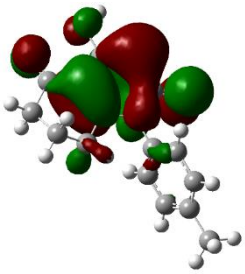	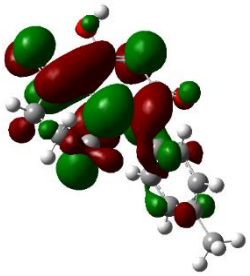
III.7d	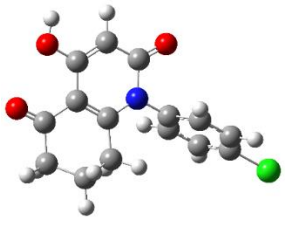	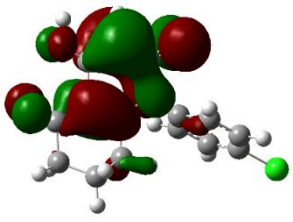	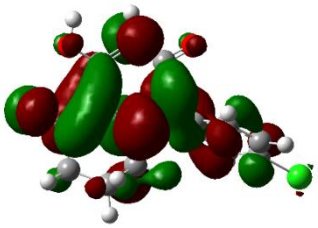
III.7e	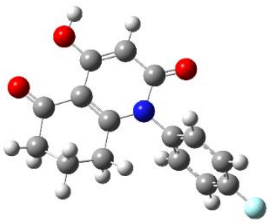	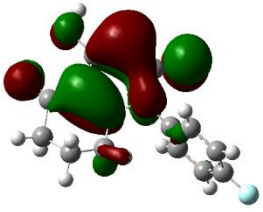	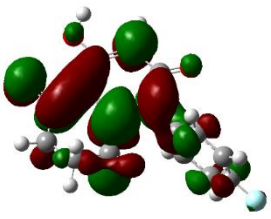

III.7f

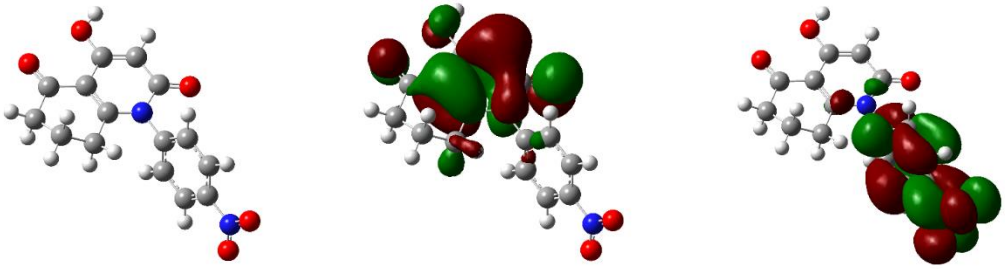

III.7g

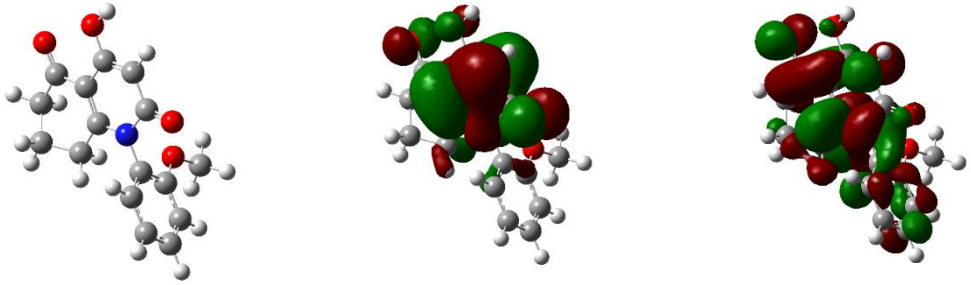

III.7h

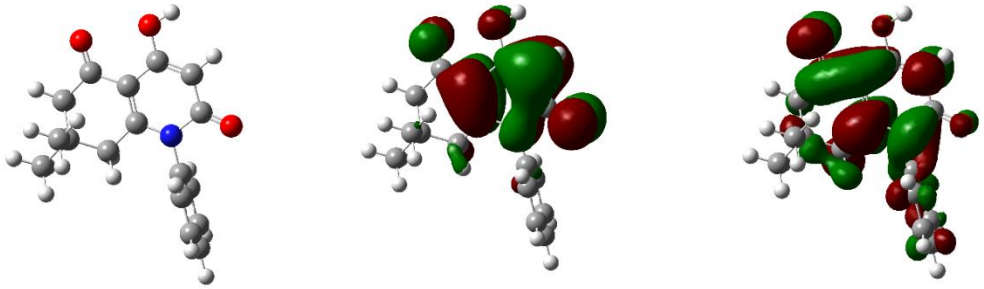

III.7i

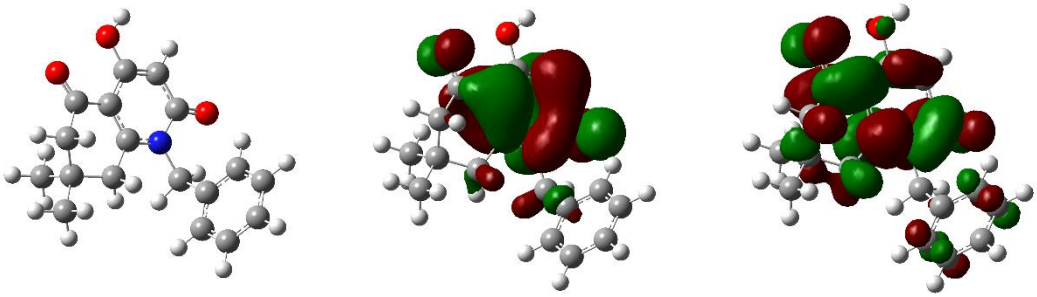

III.7j

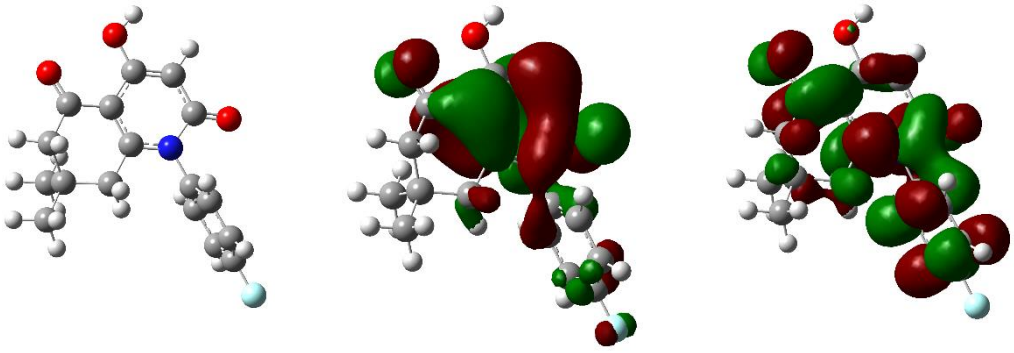

III.7k

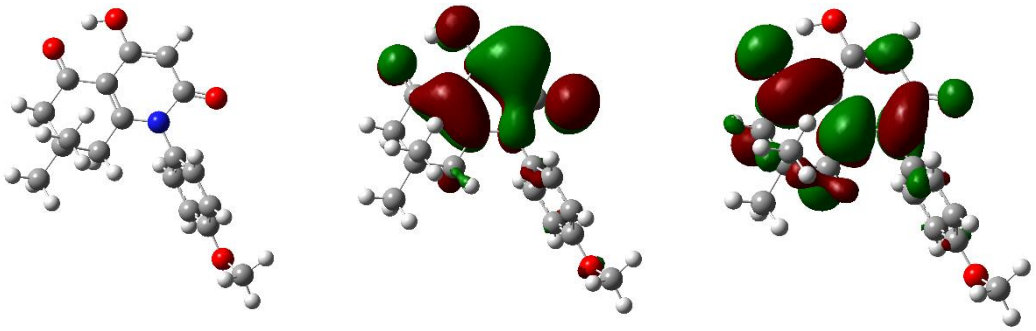

III.7l

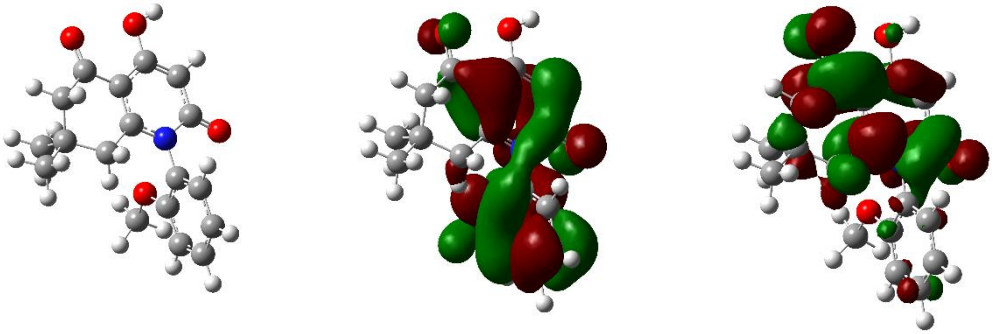

III.7m

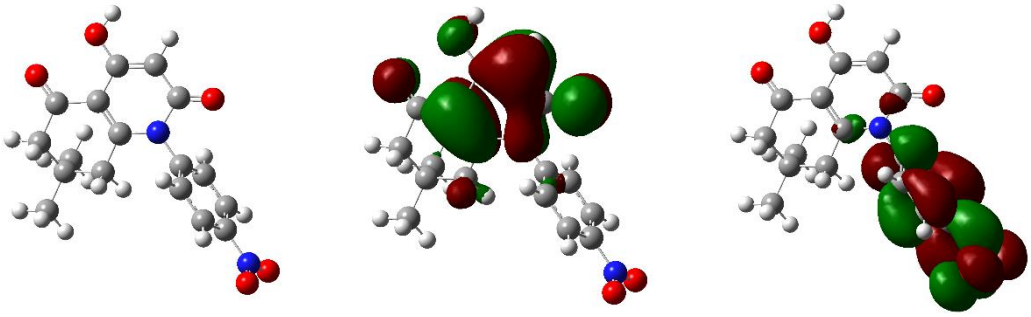

MEP of investigated compounds were represented as maps with color codes lying between the deepest red showing the most nucleophilic parts and the deepest blue showing the most electrophilic ones (**Figure IV.7**). Generally, red color was situated in the carbonyl groups corresponding to ketone and amide moieties. It can be assumed that these groups have a high potency to form interactions by acting as proton acceptors in H-bonds formation. This observation is reliable with the molecular docking results since the two carbonyl groups were involved in H-bonds formation with Xanthine Oxidase active pocket. Moreover, red color corresponding to electron-rich parts of the molecules was also located on the oxygen atom of the hydroxyl group. In addition, blue color that indicates electron-deficient regions was strongly located in hydrogen atoms of the hydroxyl groups suggesting a high electronegativity gap between the two mentioned atoms, thus a significant lability of corresponding hydrogens and the ability of these latter to act as H-bond donor, which was also noticed in molecular docking results.

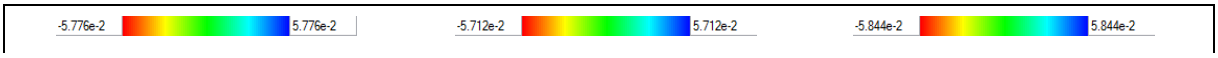

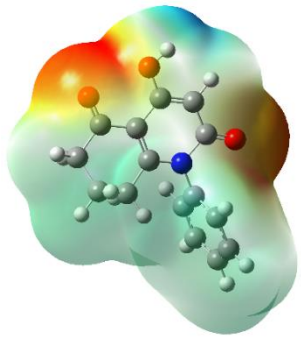

III.7a

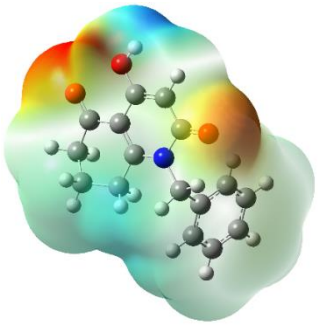

III.7b

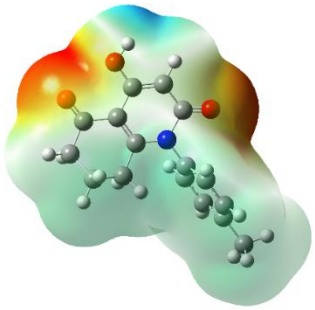

III.7c

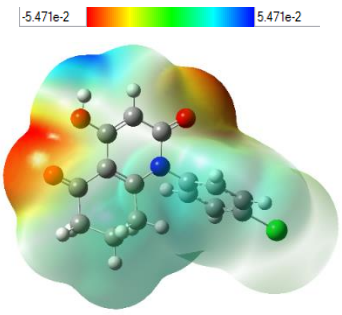

III.7d

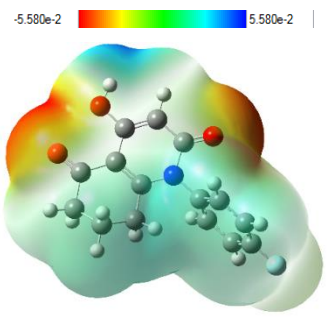

III.7e

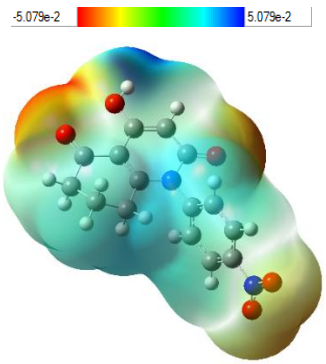

III.7f

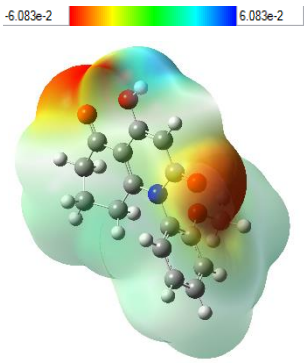

III.7g

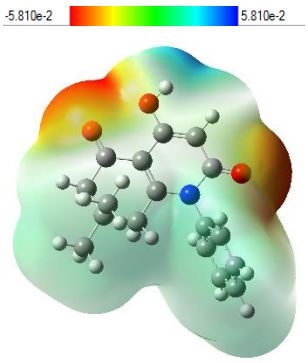

III.7h

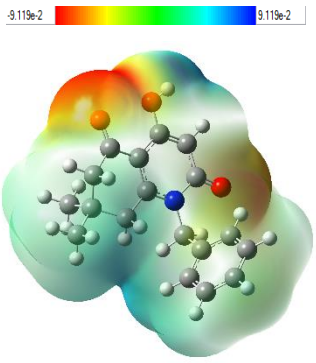

III.7i

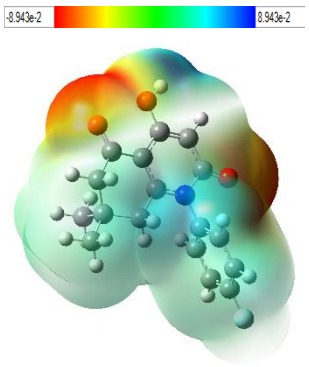

III.7j

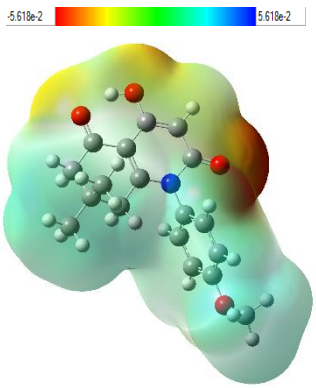

III.7k

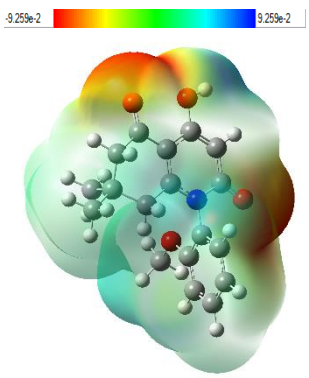

III.7l

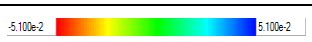

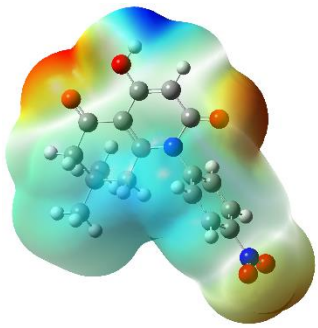

III.7m

Figure IV.7. MEP maps of synthesized 4hydroxyquinolone analogues.

3. *In* vitro and *in silico* assessment of acridine derivatives

3.1. Antioxidant activity

The radical scavenging potential of newly synthesized acridine derivatives was assessed through the DPPH assay, a well-established, cost-effective method for detecting hydrogen donors [91]. The findings revealed that among the examined acridine compounds, only compound **III.9j** and the new hydroxylated derivative **III.14a** displayed antioxidant activity. The inhibition percentages and IC_{50} values of these compounds, along with the standards BHA and BHT, are detailed in **Table IV.11**.

Table IV.11. Inhibition percentages and IC_{50} values (mean ± SD) corresponding to the radical scavenging activities of compound **III.14a**, **III.9j**, and the standards BHA and BHT.

Compound		**III.14a**	**III.9j**	**BHA**	**BHT**
	Concentration (mM)				
% Inhibition in DPPH assay	3.2	85.52 ± 1.29	45.96 ± 4.58	86.48 ± 0.40	69.75 ± 1.54
	1.6	73.15 ± 3.11	37.73 ± 2.49	68.34 ± 1.46	42.01 ± 2.62
	0.8	40.93 ± 10.21	24.80 ± 3.51	46.56 ± 0.69	28.61 ± 1.42
	0.4	30.16 ± 1.57	16.95 ± 4.45	30.34 ± 0.62	16.76 ± 1.76
	0.2	21.59 ± 0.76	7.78 ± 2.44	16.37 ± 0.96	13.36 ± 1.24
	0.1	17.67 ± 0.19	8.28 ± 0.94	11.82 ± 1.44	6.89 ± 5.81
	0.05	12.81 ± 0.60	6.73 ± 2.80	3.81 ± 1.25	1.89 ± 0.78
	IC_{50} µmol/mL	0.99 ± 0.13	1.72 ± 0.23	0.98 ± 0.02	2.05 ± 0.09

Compound **III.14a** demonstrated superior radical scavenging efficacy, exhibiting an inhibition percentage of 85.52 ± 1.29% at a concentration of 3.2 mM. In contrast, compound **III.9j** only achieved 45.96 ± 4.58% inhibition at the same concentration. Additionally, product **III.14a**

exhibited an IC_{50} value of 0.99 ± 0.13 µmol/mL, which is comparable to the standard BHA (IC_{50} = 0.98 ± 0.02 µmol/mL) and surpasses the standard BHT (IC_{50} = 2.05 ± 0.09 µmol/mL). The enhanced radical scavenging capability of compound **III.14a** is likely attributable to the presence of a hydroxyl group, rendering it a proficient proton donor.

3.2. Molecular docking

A molecular docking investigation was conducted as a complementary analysis to the *in vitro* assessments, affirming the antioxidant efficacy of compound **III.14a**. This investigation provided detailed insights into the binding mechanism of **III.14a** within the cavities of the xanthine oxidase enzyme.

The **III.14a**-xanthine oxidase complex (PDB: **3NVY** [101]) demonstrated satisfactory stability, reflected in a docking score of -6.20 kcal/mol, comparable to the Quercetin (**Table IV.12**). Furthermore, compound **III.14a**, displayed significant interactions with the site of the xanthine oxidase enzyme. Specifically, it formed a hydrogen bond with Lys771 and engaged in a hydrophobic interaction through pi-pi stacking with the backbone of Phe1013. Additionally, 'pi-cation' contacts were observed between Lys771 and two aromatic rings of the compound (**Figure IV.8**).

Table IV.12. Docking scores of **III.14a** compared to the reference ligand Quercetin.

Ligands	**Drug targets**
	Xanthine Oxidase (3NVY)
	Docking score (kcal/mol)
III.14a	-6.20
Quercetin	-8.48

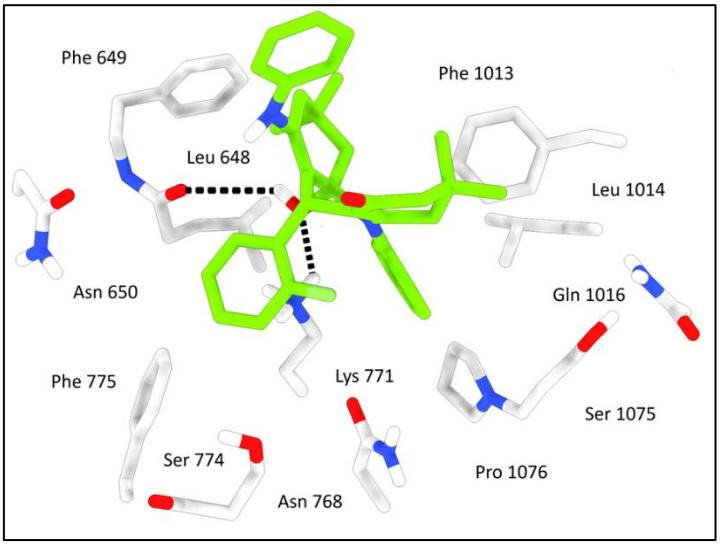

Figure IV.8. 3D binding interactions of the **III.14a** ligand within the cavity of XO.

3.3. DFT study

This study explores the comparison between molecular docking results and the structural properties of compound **III.14a**, employing DFT calculations *via* Gaussian 09 software [98]. Theoretical computations were carried out, affirming the stability of compound **III.14a** through the absence of imaginary frequencies.

The study involves the determination of several parameters essential for measuring chemical reactivity of compound **III.14a**, as outlined in **Table IV.13**.

Moreover, the intriguing dipole moment of 4.17 D in compound **III.14a** can be attributed to the presence of OH and NH in the structure.

The energy gap serves as a crucial parameter for comprehending the electronic structure and reactivity of a compound. A larger energy gap indicates greater stability and reduced reactivity, as it necessitates more energy to excite an electron from the HOMO to the LUMO. Conversely, a smaller energy gap suggests higher reactivity and potential for electron transfer or involvement in chemical reactions.

Compound **III.14a** demonstrates a relatively substantial energy gap of 4.7068 eV, indicating a stable molecular structure with limited electron transfer abilities. This characteristic could significantly influence its chemical reactivity and potential applications across various domains, including pharmaceuticals and materials science.

Table IV.13. The calculated parameters of compound **III.14a** obtained by B3LYP/6-31G (d,p) method in gas phase.

Molecular descriptors	**Log P (o/w)**	**α_{Tot}(Bohr^3)**	**μ(D)**	**E_{HOMO} (eV)**	**E_{LUMO} (eV)**	**ΔEgap (eV)**
III.14a	4.69	380.372333	4.174002	-5,2148	-0,5080	4,7068
Molecular descriptors	**(η)**	**(S)**	**(μ)**	**(χ)**	**(ω)**	
III.14a	2,3534	0,4249	-2,8614	2,8614	1,7396	

A MEP analysis was conducted on compound **III.14a** utilizing the B3LYP method at the 6-31G(d,p) level, visually represented in **Figure IV.9**. The variation in electrostatic potential is depicted using a specific color code range spanning from the deepest red to the deepest blue, denoting nucleophilic and electrophilic sites, respectively.

In summary, this study offers valuable insights into the stability, reactivity, and inhibitory properties of compound **III.14a**, thereby enhancing our understanding of its pharmacological potential.

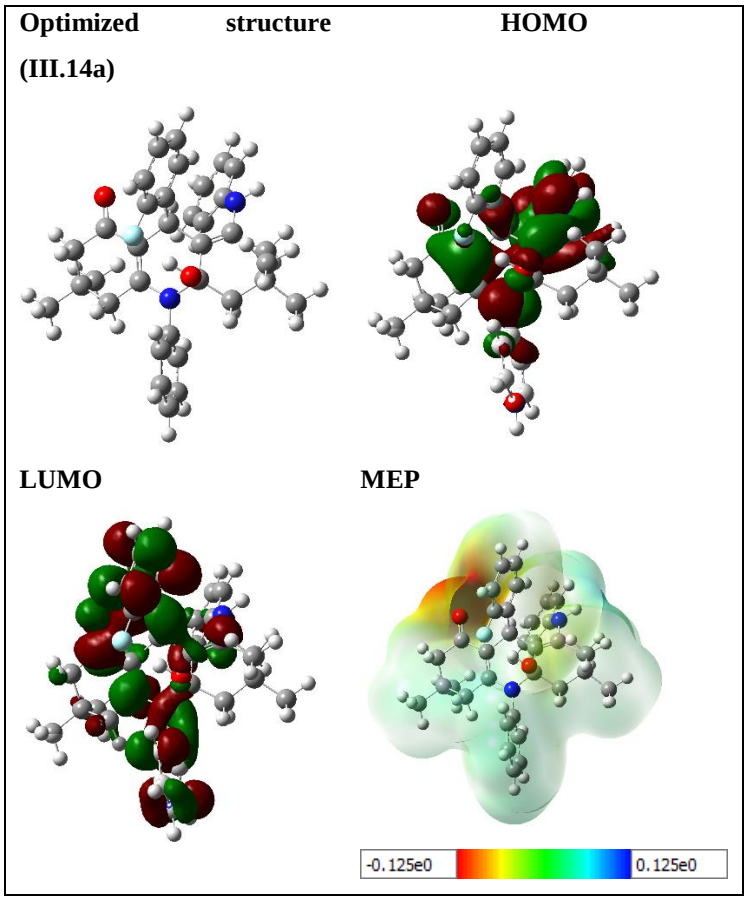

Figure IV.9. Optimized structure, (HOMO, LUMO) orbitals and the MEP of compound **III.14a**.

4. *In vitro* and *in silico* assessment of sulfamide derivatives

4.1. Antioxidant activity

The ability of compound **III.17b** in exhibiting antioxidant activity through HAT mechanism was evaluated according to DPPH assay [91]. As outlined in **Table IV.14**, compound **III.17b** revealed a good radical scavenging activity with an IC_{50} equal to 1.20 ± 0.03 µmol/mL, a promising value. Inhibition percentages increased with the rise of concentration reaching about 81 % at a concentration of 3.2 mM giving better results than BHT (IC_{50} = 2.05 ± 0.09, inh: 69 %) and acceptable results compared to BHA (IC_{50} = 0.98 ± 0.02 µmol/mL, inh: 86 %).

Table IV.14. IC_{50} values (mean ± SD) and inhibition percentages in DPPH assay for compound **III.17b**.

Compound		**III.17b**	**BHA**	**BHT**
	Concentration (mM)			
	3.2	81.07 ± 5.11	86.48 ± 0.40	69.75 ± 1.54
	1.6	56.81 ± 0.79	68.34 ± 1.46	42.01 ± 2.62

% Inhibition in DPPH assay	0.8	35.28 ± 0.69	46.56 ± 0.69	28.61 ± 1.42
	0.4	19.49 ± 1.15	30.34 ± 0.62	16.76 ± 1.76
	0.2	12.84 ± 0.42	16.37 ± 0.96	13.36 ± 1.24
	0.1	8.30 ± 1.36	11.82 ± 1.44	6.89 ± 5.81
	0.05	8.91 ± 1.49	3.81 ± 1.25	1.89 ± 0.78
	IC_{50} µmol/mL	1.20 ± 0.03	0.98 ± 0.02	2.05 ± 0.09

4.2. ADME prediction

ADME parameters for synthesized sulfamide derivatives were generated using SwissADME online server [94] (**Table IV.15**). Compounds **III.17** exhibited a molecular weight ranging between 364.40 and 388.39 $g.mol^{-1}$ (≤ 500 Da), Log P values of 0.25 to 0.99 (≤ 5), 6 to 7 rotatable bonds (≤ 10), 3 to 4 H-bond donors (≤ 5), and 6 to 8 H-bond acceptors (≤ 10). These value respect Lipinski's rule of five that designate an orally administrable drug-candidate [97]. Further, solubility in water was estimated and reached -1.36 to -3.20 that corresponds to good numbers of solubility enhancing transfer within physiological environments. In addition, skin permeability indicated by Log K_p lied between -7.26 to -9.13 cm/s.

Table IV.15. ADME parameters of sulfamides generated with SwissADME.

Entry	Molecular weight (g/mole)	Rotatable bonds	H-bond donor	H-bond acceptor	Log Po/W iLogP	Log S ESOL	GI	BBB	Log Kp (cm/s)	TPSA (Å²)
III.17a	370.40	7	4	6	0.72	-3.20	Low	No	-7.26	164.22
III.17b	388.39	7	4	7	0.99	-3.12	Low	No	-7.57	164.22
III.17c	364.40	6	3	8	0.25	-1.36	Low	No	-9.13	164.66

Bioavailability of the studied compounds was graphically represented as radars (**Figure IV.10**). The three derivatives failed to attain the optimum ranges (pink area) of all six parameters at once. Compound **III.17a** and **III.17b** respected lipophilicity, size, flexibility, and solubility, but violated polarity and saturation indexes. However, compound **III.17c** was located in the optimal intervals of all stated parameters except polarity that was slightly violated.

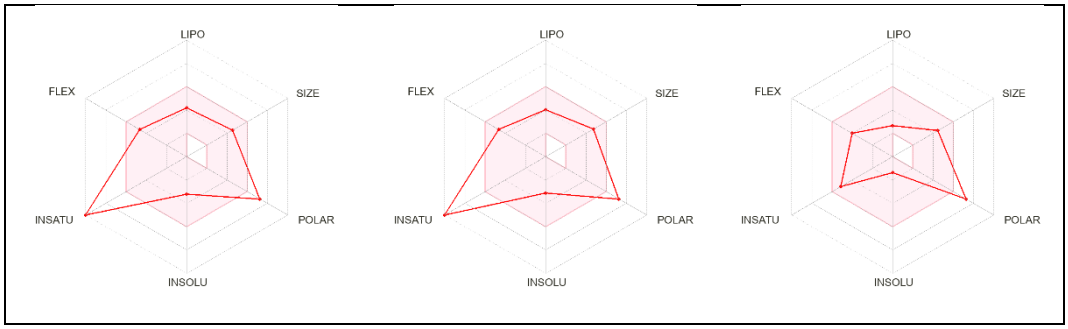

III.17a	III.17b	III.17c

Figure IV.10. Bioavailability radars for synthesized sulfamide derivatives.

The ability of synthesized sulfamide derivatives to inhibit P-gp and cytochromes P450 was predicted using SwissADME. Results shows that both compounds **III.17a** and **III.17b** are substrates to P-gp while only the fluorine-substituted derivative **III.17b** was able to inhibit CYP1A2.

Table IV.16. Predicted behavior of sulfamide derivatives towards P-gp and CYP.

	Pharmacokinetics-related proteins					
Compounds	**P-gp substrate**	**CYP1A2 inhibitor**	**CYP2C19 inhibitor**	**CYP2C9 inhibitor**	**CYP2D6 inhibitor**	**CYP3A4 inhibitor**
III.17a	+	-	-	-	-	-
III.17b	+	+	-	-	-	-
III.17c	-	-	-	-	-	-

Conclusion

In this chapter, *in silico* and *in vitro* studies were conducted to evaluate the biological activity of the synthesized compounds.

In vitro antioxidant activitiy of all the synthesized compounds was evaluated through DPPH or ABTS assays. Results were found to be promising for the β-enaminocarboxamide and 4-hydroxyquinolone analogues especially for compounds **III.5k**, **III.7a**, and **III.7g** that exhibited encouraging IC_{50} values compared to the employed standards. In the series of acridine derivatives, only the hydroxylated compound **III.17b** showed a promising antioxidant activity which was attributed to the presence of OH. One of the synthesized sulfamide derivatives was screened for its antioxidant capacity through DPPH assay showing good results, encouraging the study of further derivatives of the same series.

Antidiabetic activity was also assessed for the first synthesized set of compounds bearing the β-enaminocarboxamide moiety through inhibition of α-amylase enzyme. Attained results showed a high potentiality of β-enaminocarboxamides to inhibit α-amylase especially for compounds **III.5(b,d,g,j,l,o)** that presented remarkable IC_{50} values between 1.07 ± 0.03 and 4.10 ± 0.46 µmol/mL surpassing the one exhibited by Acarbose.

A complementary study consisting of an *in silico* investigation was completed including molecular docking that provided a better insight on how molecules act in the active site of the studied enzymes, as well as a DFT study that helped to understand the structural composition

of compounds, and to assess the most important and reactive regions of the molecules through mapping their electrostatic potential. Finaly, an ADME prediction was performed to apprehend pharmacokinetics properties necessary for the conception of novel drug-candidates.

Chapter V

Experimental data

1. General experimental conditions

1.1. Melting point measurement

Melting points of all final products were measured in open capillary tubes on a Büchi B-545.

1.2. Chromatography

TLC (silica Merck 60 F_{254}) served as a monitoring method for all conducted reactions (Art. 5554).

All reagents (except aliphatic amines and CSI) and obtained products were UV-active (under UV lamp: 254 nm) and were detectible with ninhydrin (10% in Ethanol).

Purification by column purification was conducted with a silica gel Carlo Erba (Silica Gel 60 Å, granulometry: 35-70 μm) or Merck 60 H (Art.9385).

1.3. Nuclear magnetic resonance

(^{1}H NMR) were acquired using a Bruker spectrometer operating at 400 MHz. Chemical shifts are expressed in δ units (ppm) with tetramethylsilane (TMS) serving as the reference (δ 0.00). All coupling constants (*J*) are provided in Hertz. Multiplicity is denoted by one or more of the following: s (singlet), d (doublet), t (triplet), q (quartet), p (pentet), m (multiplet), bs (broad singlet), dd (doublet of doublets), dt (doublet of triplets), td (triplet of doublets), dq (doublet of quartets), ddd (doublet of doublets of doublets).

(^{13}C NMR) spectra were recorded on a Bruker instrument at 100 MHz. Chemical shifts are reported in δ units (ppm) referenced to $CDCl_3$ or DMSO-d_6 (δ 77.0 and 39.0-40.0).

(^{19}F NMR) spectra were acquired using a Bruker spectrometer operating at 282 MHz.

1.4. Infrared

Infrared spectra were recorded on a Perkin Elmer FT-600 spectrometer using sodium chloride cells. The positions of characteristic bands are given in cm^{-1}.

1.5. Liquid chromatography-mass spectrometry (LC-MS)

The purity of the synthesized compounds was assessed *via* HPLC-MS analyses using a Shimadzu Prominence LC analytical system. This comprehensive system included a Shimadzu LC-20AD binary HPLC pump, Shimadzu CTO-10AS column oven, Shimadzu SIL-20ACHT cooling autosampler, Shimadzu CBM-20A system controller, and Shimadzu SPD-20MA diode array detector, all sourced from Shimadzu in Kyoto, Japan. The LC-MS-2020 mass detector, equipped with electrospray ionization, featured a single quadrupole. Quantification occurred on a monolithic Chromolith RP-C18 column (2.1 mm × 50 mm, 1.8 μm particle size) using a

gradient mobile phase transitioning from H_2O/CH_3CN (70:30, v/v) with 0.1% formic acid to H_2O/CH_3CN (10:90, v/v) at a flow rate of 0.5 mL/min. UV monitoring was conducted at 254 nm with a total runtime of 30 minutes.

1.6. Elemental analysis

Microanalysis spectra were conducted using an Elemental Analyzer (Euro E.A. 3000-V3.0-single-2007), with the determined values found to be within the acceptable range of the calculated values.

1.7. Crystallography

Crystallographic data for the studied compounds **III.5h**, **III.7i**, and **III.9d** were obtained using a SuperNova, Dual, Cu at home/near, AtlasS2 four-circle diffractometer equipped with an AtlasS2 CCD detector using Mo Kα (micro-focus sealed tube) radiation (λ = 0.71073 Å) for compounds **III.5h** and **III.7i**, and Cu Kα (micro-focus sealed tube) radiation (λ = 1.54184 Å) for **III.9d**. The crystals were maintained at a temperature of 295K during data collection.

The studied structures were solved with the SHELXT-2014/5 [102**]** solution program by Intrinsic Phasing with Olex2 [103] as the graphical interface. Refinement was performed with SHELXL-2018/3 [104] using full matrix least-squares minimization on F^2. All absorption corrections were conducted with the CrysAlisPro 1.171.42.51a [105**]** using spherical harmonics implemented in SCALE3 ABSPACK scaling algorithm. Crystal structure visualization and construction of crystal packing diagrams were carried out using Mercury 4.0 software [78**]**.

1.7.1. Crystallographic data for compound III.5h

Crystals of compound **III.5h** were obtained through slow evaporation of a dichloromethane solution.

Crystallographic data and experimental details of structural analysis for the studied compound *2-((4-methoxyphenyl)amino)-6-oxocyclohex-1-ene-1-carboxamide* **III.5h** are summarized in **Table V.1**.

CCDC Number: 2217011 contains the supplementary crystallographic data for compound **III.5h**. These data can be obtained free of charge from the Cambridge Crystallographic Data Centre *via* www.ccdc.cam.ac.uk/data_request/cif.

Table V.1. Crystallographic properties of compound **III.5h**.

Formula	$C_{14}H_{16}N_2O_3$	Absorption coefficient (mm^{-1})	0.094
Formula Weight ($g.mol^{-1}$)	260.29	F(000)	1104.0

Crystal habit, Color	Prism, Colorless	Crystal size (mm)	0.4 × 0.18 × 0.14
Crystal system	Monoclinic	θ range for data collection (º)	2.160 - 32.400
Space group	C2/c	Reflections collected	33156
a (Å)	14.2517(5)	Independent reflections	4531
b (Å)	9.7694(3)	R_{int}	0.0353
c (Å)	19.1925(7)	Number of parameters	182
α (°)	90	Goodness-of-fit on F^2	1.046
β (°)	100.784(4)	Final R indices [I ≥ 2σ(*I*)]	R_1 = 0.0578, wR_2 = 0.1570
γ (°)	90	R indices [all data]	R_1= 0.0731 wR_2= 0.1695
Volume (Å^3)	2624.99(16)	Largest difference peak and hole (Å^3)	0.272, -0.260
Z, Z'	8, 0	CCDC deposition no.	CCDC 2217011
Density (calculated) (g.cm^{-3})	1.317		

1.7.2. Crystallographic data for compound III.7i

Crystals of compound **III.7i** were formed by crystallization in hexane.

Crystallographic data and experimental details for structural analysis for the studied compound *8-hydroxy-3,3-dimethyl-5-(phenylamino)-3,4-dihydronaphthalene-1,6(2H,5H)-dione* **III.7i** are summarized in **Table V.2**.

CCDC 2256921, contains the supplementary crystallographic data for compound **III.7i**. These data can be obtained free of charge from The Cambridge Crystallographic Data Centre *via* www.ccdc.cam.ac.uk/data_request/cif.

Table V.2. Crystallographic properties of compound **III.7i**.

Formula	$C_{18}H_{19}NO_3$	Absorption coefficient (mm^{-1})	0.089
Formula weight (g.mol^{-1})	297.34	F(000)	316.0
Crystal habit, color	Prism, colorless	Crystal size (mm)	0.32 × 0.14 × 0.08
Crystal system	Triclinic	θ range for data collection (º)	2.360 - 33.343
Space group	P-1	Reflections collected	19501
a (Å)	6.4370 (3)	Independent reflections	5272
b (Å)	10.9513(4)	R_{int}	0.0259
c (Å)	11.3400(6)	Number of parameters	202
α (°)	102.588 (4)	Goodness-of-fit on F^2	1.043
β (°)	102.906 (4)	Final R indices [I ≥ 2σ(*I*)]	R_1 = 0.0552, wR_2 = 0.1414

γ (°)	91.799 (3)	R indices [all data]	R_1= 0.0799 wR_2= 0.1579
Volume (Å^3)	757.77(6)	Largest differrence peak and hole (Å^{-3})	0 .24, -0.17
Z, Z'	2, 0	CCDC deposition no.	CCDC 2256921
Density (calculated) (g.cm^{-3})	1.3 03		

1.7.3. Crystallographic data for compound III.9d

Crystals of compound **III.9d** were grown using the principle of slow evaporation in which a mixture of dichloromethane and methanol was used. After reaching the saturation point, yellow crystals of compound **III.9d** were formed then removed from the saturated solution, and were subjected to a single crystal X-ray diffraction analysis.

Crystallographic data and experimental details for structural analysis for the studied compound *(E)-3,3,6,6-tetramethyl-9-phenyl-10-(p-tolyl)-8-(p-tolylimino)-3,4,5,6,7,8,9,10-octahydroacridin-1(2H)-one* **III.9d** are summarized in **Table V.3**.

CCDC Number: 2301288 contains the supplementary crystallographic data for compound **III.9d**. These data can be obtained free of charge from the Cambridge Crystallographic Data Centre *via* www.ccdc.cam.ac.uk/data_request/cif.

Table V.3. Crystallographic properties of compound **III.9d**.

Moiety formula	2($C_{37}H_{40}N_2O$), 0.25(H_2O)	Density (calculated) (g.cm^{-3})	1.137
Sum formula	$C_{74}H_{8\ 0.50}N_4O_{2.25}$	Absorption coefficient (mm^{-1})	0.521
Formula Weight (g.mol^{-1})	1061.92	F(000)	1141.0
Crystal habit, Color	Prism, yellow	Crystal size (mm)	0.16 × 0.14 × 0.08
Crystal system	triclinic	θ range for data collection (º)	8.268 to 141.316
Space group	P-1	Reflections collected	24894
a (Å)	11.0058(3)	Independent reflections	11680
b (Å)	17.7046(6)	R_{int}	0.0266
c (Å)	18.5541(6)	Number of parameters	745
α (°)	61.975(3)	Goodness-of-fit on F^2	1.025
β (°)	89.384(3)	Final R indices [I ≥ 2σ(I)]	R_1 = 0.0456, wR_2 = 0.1181
γ (°)	77.656(3)	R indexes [all data]	R_1 = 0.0666, wR_2 = 0.1340
Volume (Å^3)	3100.7(2)	Largest difference peak and hole (Å^3)	0.17, -0.13
Z, Z'	2, 0	CCDC deposition no.	CCDC 2301288

1.8. Ultrasound

Ultrasound-conducted reactions were performed using an ultrasonic bath (FUNGILAB model, 40 kHz, power 250 W). The reactions took place in open glass tubes with dimensions of 25 mm in diameter, 1 mm in thickness, and a volume of 20 mL.

1.9. Products and solvents

The products and solvents utilized in both the reactions and the purification processes of all obtained derivatives were directly employed without undergoing any purification or distillation procedures. Reactions were all monitored using oven-dried glasswares. Anhydrous condition was ensured under nitrogen atmosphere.

2. Synthetic methods

2.1. Synthesis of β-enaminones

The synthesis of β-enaminones was done according to the method described by Redjemia *et al.* [74]. In a glass tube with dimensions of 25 mm in diameter, 1 mm in thickness, and a volume of 20 mL, a mixture containing a dicarbonyl compound (1 mmol), an amine (1 mmol), and CuBr (0.05 mmol) was prepared. The reaction mixture underwent ultrasonication at a frequency of 40 kHz for an appropriate duration at room temperature. The progression of the reaction was monitored by TLC. Upon completion of the reaction, DCM (5 mL) was added. The catalyst was recovered from the residue, and the filtrate was concentrated. Diethyl ether was added to the reaction mixture, and the pure product was allowed to crystallize overnight at 6°C. Finally, the product was filtered and dried.

Spectroscopic characterization of synthesized enaminones were described in the literature [74,106].

2.2. Synthesis of β-enaminocarboxamides

A solution containing β-enaminones (1 mmol) in anhydrous CH_2Cl_2 (5 mL) was slowly added dropwise to a stirred solution of CSI (1.1 mmol) in anhydrous CH_2Cl_2 (5 mL) at 0°C over a duration of 3 minutes. The resulting solution was stirred at room temperature for 2h, followed by the addition of 5 mL of methanol. The formation of the desired compound was monitored by TLC with a solvent system of dichloromethane/methanol (94:06). Subsequently, the solution was concentrated under reduced pressure, and the residue was purified by silica gel column chromatography using a mixture of dichloromethane/methanol (96:04) as the eluent, resulting in the isolation of pure β-enaminocarboxamides in excellent yields.

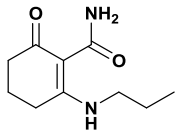

6-oxo-2-(propylamino) cyclohex-1-ene-1-carboxamide III.5a

$C_{10}H_{16}N_2O_2$. **M**: 196.12 g.mol^{-1}. **Aspect:** White powder. **Yield** = 85 %. **M.p** = 164–166 °C. **R_f** = 0.34 (DCM/MeOH, 94:06).

IR (KBr, cm^{-1}): ν = 3283 (NH_2), 2933, 1709 (C=O), 1618 (C=O), 1574 (C=C); **^{1}H NMR (400 MHz, DMSO-*d*$_6$): δ** = 0.93 (t, 3H, *J* = 7.4 Hz, CH_2-CH_3), 1.53-1.62 (m, 2H, CH_2-CH_3), 1.74-1.80 (m, 2H, CH_2-CH_2-CH_2), 2.27 (t, 2H, *J* = 7.1 Hz, CH_2-C), 2.64 (t, 2H, *J* = 6.3 Hz, CH_2-CO), 3.30 (q, 2H, *J* = 7 Hz, CH_2-NH), 6.74 (sl, 1H, CO-NH^a), 9.50 (sl, 1H, CO-NH^b), 12.37 (s, 1H, NH); **^{13}C NMR (101 MHz, DMSO-*d*$_6$): δ** = 11.1, 19.3, 22.2, 26.0, 37.3, 44.3, 98.0, 172.0, 173.6, 193.9. **Anal. Calc. for $C_{10}H_{16}N_2O_2$** C, 61.20; H, 8.22; N, 14.27; Found C, 61.27; H, 8.16; N, 14.23.

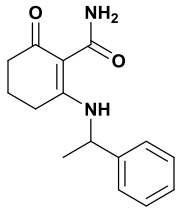

6-oxo-2-((1-phenylethyl)amino)cyclohex-1-ene-1-carboxamide III.5b

$C_{15}H_{18}N_2O_2$. **M**: 258.14 g.mol^{-1}. **Aspect:** Cristal. **Yield** = 82 %. **M.p** = 160–162 °C. **R_f** = 0.37 (DCM/MeOH, 94:06).

IR (KBr, cm^{-1}): ν = 3419 (NH_2), 3244 (NH), 1713 (C=O), 1573 (C=C); **^{1}H NMR (400 MHz, $CDCl_3$): δ** = 1.28 (s, 3H, CH_3), 1.63 (s, 2H, CH_2-CH_2-CH_2), 2.39 (s, 2H, CH_2-CH_2-C), 2.63 (d, 2H, *J* = 14.9 Hz, CH_2-CH_2-CO), 4.78 (s, 1H, CH), 5.52 (sl, 1H, CO-NH^a), 7.29-7.40 (m, 5H, 5CH_{Ar}), 9.86 (sl, 1H, CO-NH^b), 12.76 (s, 1H, NH); **^{13}C NMR (101 MHz, $CDCl_3$): δ** = 19.5, 24.8, 29.8, 37.7, 54.0, 101.0, 125.6, 127.8, 129.2, 142.0, 173.1, 173.5, 195.3. **Anal. Calc. for $C_{15}H_{18}N_2O_2$** C, 69.74; H, 7.02; N, 10.84; Found C, 69.70; H, 7.07; N, 10.89.

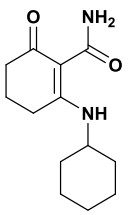

2-(cyclohexylamino)-6-oxocyclohex-1-ene-1-carboxamide III.5c

$C_{13}H_{20}N_2O_2$. **M**: 236.15 g.mol^{-1}. **Aspect:** White powder. **Yield** = 90 %. **M.p** = 179–181 °C. **R_f** = 0.46 (DCM/MeOH, 94:06).

IR (KBr, cm^{-1}): ν = 3357 (NH_2), 1621 (C=O), 1561 (C=C); **^{1}H NMR (400 MHz, DMSO-*d*$_6$): δ** = 1.22-1.41 (m, 5H, $2CH_2$-CH_2(cyclohexyl)), 1.51-1.55 (m, 1H, CH_2(cyclohexyl)), 1.62-1.67 (m, 2H, CH_2-CH_2-CO), 1.73-1.84 (m, 4H, $2CH_2$(cyclohexyl)), 2.26 (t, 2H, *J* = 8 Hz, CH_2-C), 2.68 (t, 2H, *J* = 6.3 Hz, CH_2-CO), 3.58-3.67 (m, 1H, CH-NH), 6.3 (sl, 1H, CO-NH^a), 7.72 (sl, 1H, CO-NH^b), 12.55 (d, 1H, *J* = 8.4 Hz, NH) ;**^{13}C NMR (101 MHz, DMSO-*d*$_6$): δ** = 19.5, 23.6, 24.81, 25.8, 32.6, 37.3, 50.9, 97.9, 172.1, 172.3, 193.9. **Anal. Calc. for $C_{13}H_{20}N_2O_2$** C, 66.07; H, 8.53; N, 11.85; Found: C, 66.13; H, 8.60; N, 11.79.

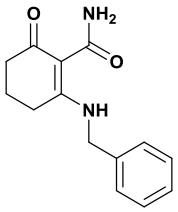

2-(benzylamino)-6-oxocyclohex-1-ene-1-carboxamide III.5d

$C_{14}H_{16}N_2O_2$. **M**: 244.12 g.mol^{-1}. **Aspect:** Yellow powder. **Yield** = 91 %. **M.p** = 144–146 °C. **R$_f$** = 0.44 (DCM /MeOH, 94:06).

IR (KBr, cm^{-1}): ν = 3297 (NH_2), 3034, 1612 (C=O), 1563 (C=C); **^{1}H NMR (400 MHz, DMSO-*d*$_6$): δ** = 1.74-1.80 (m, 2H, CH_2-CH_2-CH_2), 2.28 (t, 2H, *J* = 7.2 Hz, CH_2-C), 2.67 (t, 2H, *J* = 6.3 Hz, CH_2-CO), 4.62 (d, 2H, *J* = 5.7 Hz, CH_2-NH), 6.88 (d, 1H, *J* = 5.0 Hz, CO-NH^a), 7.31-7.35 (m, 3H, $3CH_{Ar}$), 7.38-7.42 (m, 2H, $2CH_{Ar}$), 9.49 (d, 1H, *J* = 5.1 Hz, CO-NH^b), 12.64 (s, 1H, NH); **^{13}C NMR (101 MHz, DMSO-*d*$_6$): δ** = 19.3, 26.2, 37.2, 46.4, 98.6, 127.2, 127.5, 128.7, 137.3, 171.9, 173.7, 194.2. **Anal. Calc. for $C_{14}H_{16}N_2O_2$** C, 68.83; H, 6.60; N, 11.47; Found: C, 68.80; H, 6.55; N, 11.51.

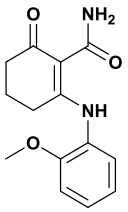

2-((2-methoxyphenyl)amino)-6-oxocyclohex-1-ene-1-carboxamide III.5e

$C_{14}H_{16}N_2O_3$. **M**: 260.12 g.mol^{-1}. **Aspect:** Brown powder. **Yield** = 86 %. **M.p** = 215–217 °C. **R$_f$** = 0.39 (DCM MeOH, 94:06).

IR (KBr, cm^{-1}): ν = 3291 (NH_2), 2925, 1619 (C=O) , 1591 (C=O), 1566 (C=C); **^{1}H NMR (400 MHz, DMSO-*d*$_6$): δ** = 1.71-1.77 (m, 2H, CH_2-CH_2-CH_2), 2.35 (t, 2H, *J* = 6.5 Hz, CH_2-C), 2.56 (t, 2H, *J* = 6.2 Hz, CH_2-CO), 3.83 (s, 3H, O-CH_3), 7.00 (td, 1H, *J* = 7.6, 1.3 Hz, CH_{Ar}), 7.15 (dd, 2H, *J* = 8.3, 1.3 Hz, $2CH_{Ar}$), 7.25-7.35 (m, 2H, $1CH_{Ar}$, CO-NH^a), 9.5 (s, 1H, CO-NH^b), 13.92 (s, 1H, NH); **^{13}C NMR (101 MHz, DMSO-*d*$_6$): δ** = 19.9, 27.6, 37.6, 55.7, 99.5, 112.1,

120.4, 125.7, 126.5, 128.2, 153.2, 171.8, 172.9, 195.0. **Anal. Calc. for $C_{14}H_{16}N_2O_3$** C, 64.60; H, 6.20; N, 10.76; Found: C, 64.54; H, 6.16; N, 10.70.

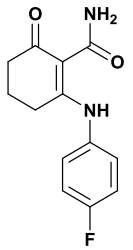

2-((4-fluorophenyl)amino)-6-oxocyclohex-1-ene-1-carboxamide III.5f

$C_{13}H_{13}FN_2O_2$. **M**: 248,10 g.mol^{-1}. **Aspect:** White powder. **Yield** = 92 %. **M.p** = 194–196 °C. **R_f** = 0.25 (DCM /MeOH, 94:06).

IR (KBr, cm^{-1}): ν = 3406 (NH_2), 3258(NH) , 1707 (C=O), 1606 (C=O), 1541 (C=C); **^{1}H NMR (400 MHz, $CDCl_3$): δ** = 1.88-1.94 (m, 2H, CH_2-CH_2-CH_2), 2.62 (t, 2H, *J* = 6.3 Hz, CH_2-C), 2.72 (t, 2H, *J* = 6.4 Hz, CH_2-CO), 6.97-7.22 (m, 5H, 4CH_{Ar}, CO-NH^a), 11.54 (s, 1H, CO-NH^b), 13.24 (s, 1H, NH); **^{13}C NMR (101 MHz, $CDCl_3$): δ** = 19.7, 28.6, 34.0, 94.4, 116.8, 117.0, 127.6, 127.7, 132.1, 172.1, 173.1, 196.8. **Anal. Calc. for $C_{13}H_{13}FN_2O_2$** C, 62.90; H, 5.28; N, 11.28; Found: C, 62.85; H, 5.20; N, 11.22.

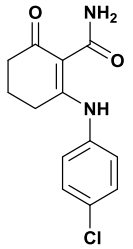

2-((4-chlorophenyl)amino)-6-oxocyclohex-1-ene-1-carboxamide III.5g

$C_{13}H_{13}ClN_2O_2$. **M**: 264,07 g.mol^{-1}. **Aspect:** Yellow powder. **Yield** = 84 %. **M.p** = 214–216 °C. **R_f** = 0.46 (DCM /MeOH, 94:06).

IR (KBr, cm^{-1}): ν = 3303 (NH_2), 1620 (C=O), 1551 (C=C), 1489 (C=C); **^{1}H NMR (400 MHz, $CDCl_3$): δ** = 1.82-1.88 (m, 2H, CH_2-CH_2-CH_2), 2.46 (t, 2H, *J* = 6.8 Hz, CH_2-C), 2.55 (t, 2H, *J* = 6 Hz, CH_2-CO), 5.7 (sl, 1H, CO-NH^a), 7.08 (d, 2H, *J* = 8.8 Hz, 2CH_{Ar}), 7.36 (d, 2H, *J* = 6.8 Hz, 2CH_{Ar}), 9.97 (sl, 1H, CO-NH^b), 13.89 (s, 1H, NH); **^{13}C NMR (101 MHz, $CDCl_3$): δ** = 20.4, 28.7, 38.0, 98.9, 127.7, 129.7, 131.8, 136.3, 172.4, 173.5, 193.8. **Anal. Calc. for $C_{13}H_{13}ClN_2O_2$** C, 58.99; H, 4.95; N, 10.58; Found: C, 58.92; H, 4.99; N, 10.55.

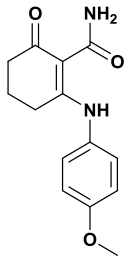

2-((4-methoxyphenyl)amino)-6-oxocyclohex-1-ene-1-carboxamide III.5h

$C_{14}H_{16}N_2O_3$. **M**: 260.12 g.mol^{-1}. **Aspect:** Cristal. **Yield** = 80 %. **M.p** = 186–188 °C. **R_f** = 0.44 (DCM /MeOH, 94:06).

IR (KBr, cm^{-1}): ν = 3346 (NH_2), 3221 (NH), 1613 (C=O), 1585 (C=C), 1565 (C=C); **^{1}H NMR (400 MHz, $CDCl_3$): δ** = 1.79-1.86 (m, 2H, CH_2-CH_2-CH_2), 2.45 (t, 2H, *J* = 6 Hz, CH_2-C), 2.51 (t, 2H, *J* = 6.3 Hz, CH_2-CO), 3.60 (s, 3H, O-CH_3), 5.59 (sl, 1H, CO-NH^a), 6.89 (d, 2H, *J* = 8.8 Hz, 2CH_{Ar}), 7.05 (d, 2H, *J* = 8.8 Hz, 2CH_{Ar}), 9.16 (sl, 1H, CO-NH^b), 13.67 (s, 1H, NH); **^{13}C NMR (101 MHz, $CDCl_3$): δ** = 20.3, 28.6, 38.0, 55.6, 99.8, 114.6, 127.1, 130.2, 158.7, 172.6, 173.0, 195.7. **Anal. Calc. for $C_{14}H_{16}N_2O_3$** C, 64.60; H, 6.20; N, 10.76; Found: C, 64.54; H, 6.27; N, 10.80.

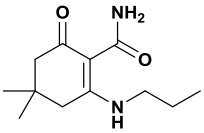

4,4-dimethyl-6-oxo-2-(propylamino)cyclohex-1-ene-1-carboxamide III.5i

$C_{12}H_{20}N_2O_2$. **M**: 224,15 g.mol^{-1}. **Aspect:** Cristal. **Yield** = 82 %. **M.p** = 172–174 °C. **R_f** = 0.39 (DCM /MeOH, 94:06).

IR (KBr, cm^{-1}): ν = 3312 (NH_2), 2963, 1632 (C=O), 1564 (C=C); **^{1}H NMR (400 MHz, $CDCl_3$): δ** = 0.99 (t, 3H, *J* = 7.3 Hz, CH_2-CH_3), 1.04 (s, 6H, 2CH_3), 1.61-1.71 (m, 2H, CH_2-CH_3), 2.27 (s, 2H, CH_2-C), 2.39 (s, 2H, CH_2-CO), 3.26 (q, 2H, *J* = 7.1 Hz, CH_2-NH), 5.41 (sl, 1H, CO-NH^a), 9.82 (sl, 1H, CO-NH^b), 12.30 (s, 1H, NH); **^{13}C NMR (101 MHz, $CDCl_3$): δ** = 11.1, 22.2, 28.0, 30.2, 39.2, 44.7, 50.3, 95.6, 171.8, 172.4, 193.0. **Anal. Calc. for $C_{12}H_{20}N_2O_2$** C, 64.26; H, 8.99; N, 12.49; Found: C, 64.19; H, 8.92; N, 12.55.

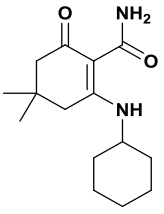

2-(cyclohexylamino)-4,4-dimethyl-6-oxocyclohex-1-ene-1-carboxamide III.5j

$C_{15}H_{24}N_2O_2$. **M**: 264,18 g.mol^{-1}. **Aspect:** Cristal. **Yield** = 80 %. **M.p** = 166–168 °C. **R_f** = 0.32 (DCM /MeOH, 94:06).

IR (KBr, cm^{-1}): ν = 3244 (NH_2), 3059, 1755 (C=O), 1712 (C=O), 1572 (C=C); **^{1}H NMR (400 MHz, $CDCl_3$): δ** = 1.07 (s, 6H, $2CH_3$), 1.23-1.33 (m, 3H, CH_2-CH_2(cyclohexyl)), 1.51-1.64 (m, 3H, CH_2-CH_2(cyclohexyl)), 1.73 (m, 2H, CH_2(cyclohexyl)), 1.78-1.93 (m, 2H, CH_2(cyclohexyl)), 2.53 (s, 2H, CH_2-C), 2.60 (s, 2H, CH_2-CO), 4.11 (q, 1H, *J* = 7 Hz, CH-NH), 5.71 (sl, 1H, CO-NH^a), 7.84 (sl, 1H, CO-NH^b), 8.65 (sl, 1H, NH); **^{13}C NMR (101 MHz, $CDCl_3$): δ** = 14.9, 24.4, 24.8, 28.5, 31.6, 32.5, 43.3, 46.6, 53.5, 55.5, 63.7, 93.6, 171.1, 172.8, 186.7. **Anal. Calc. for $C_{15}H_{24}N_2O_2$** C, 68.15; H, 9.15; N, 10.60; Found: C, 68.10; H, 9.21; N, 10.67.

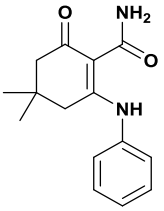

4,4-dimethyl-6-oxo-2-(phenylamino)cyclohex-1-ene-1-carboxamide III.5k

$C_{15}H_{18}N_2O_2$. **M**: 258,14 $g.mol^{-1}$. **Aspect:** White powder. **Yield** = 87 %. **M.p** = 222–224 °C. **R_f** = 0.44 (DCM /MeOH, 94:06).

IR (KBr, cm^{-1}): ν = 3295 (NH_2), 3065, 1615 (C=O), 1552 (C=C); **^{1}H NMR (400 MHz, $CDCl_3$): δ** = 1.00 (s, 6H, $2CH_3$), 2.33 (s, 2H, CH_2-C), 2.41 (s, 2H, CH_2-CO), 5.62 (sl, 1H, CO-NH^a), 7.12-7.42 (m, 5H, $5CH_{Ar}$), 9.78 (sl, 1H, CO-NH^b), 13.91 (s, 1H, NH); **^{13}C NMR (101 MHz, $CDCl_3$): δ** = 28.0, 31.2, 42.1, 51.6, 99.7, 126.1, 127.4, 129.6, 137.5, 171.3, 173.2, 193.2. **Anal. Calc. for $C_{15}H_{18}N_2O_2$** C, 69.74; H, 7.02; N, 10.84; Found: C, 69.79; H, 7.09; N, 10.90.

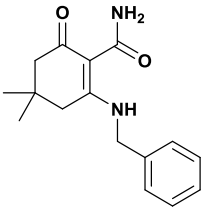

2-(benzylamino)-4,4-dimethyl-6-oxocyclohex-1-ene-1-carboxamide III.5l

$C_{16}H_{20}N_2O_2$. **M**: 272,15 $g.mol^{-1}$. **Aspect:** Cristal. **Yield** = 85 %. **M.p** = 136 – 138 °C. **R_f** = 0.25 (DCM /MeOH, 94:06).

IR (KBr, cm^{-1}): ν = 3220 (NH_2), 3030, 1733 (C=O), 1707 (C=O), 1590 (C=C); **^{1}H NMR (400 MHz, $CDCl_3$): δ** = 1.00 (s, 6H, $2CH_3$), 2.10 (s, 2H, CH_2-C), 2.18 (s, 2H, CH_2-CO), 4.19 (s, 2H, CH_2-NH), 5.12 (s, 1H, CO-NH^a), 5.49 (sl, 1H, CO-NH^b), 7.19 - 7.30 (m, 5H, $5CH_{Ar}$). **Anal. Calc. for $C_{16}H_{20}N_2O_2$** C, 70.56; H, 7.40; N, 10.29; Found: C, 70.61; H, 7.43; N, 10.33.

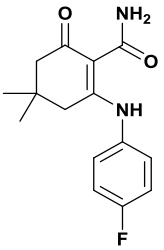

2-((4-fluorophenyl)amino)-4,4-dimethyl-6-oxocyclohex-1-ene-1-carboxamide III.5m

$C_{15}H_{17}FN_2O_2$. **M**: 276,13 g.mol^{-1}. **Aspect:** Yellow powder. **Yield** = 84 %. **M.p** = 192–194 °C. **R_f** = 0.34 (DCM /MeOH, 94:06).

IR (KBr, cm^{-1}): ν = 3313 (NH_2), 1692 (C=O), 1615 (C=O), 1601, 1551 (C=C); **^{1}H NMR (400 MHz, $CDCl_3$): δ** = 1.00 (s, 6H, $2CH_3$), 2.33 (s, 2H, CH_2-C), 2.35 (s, 2H, CH_2-CO), 5.73 (sl, 1H, CO-NH^a), 7.11 (d, 4H, *J* = 6.8 Hz, $4CH_{Ar}$), 9.80 (sl, 1H, CO-NH^b), 13.78 (s, 1H, NH); **^{13}C NMR (101 MHz, $CDCl_3$): δ** = 28.0, 31.2, 41.7, 51.5, 99.1, 116.4, 127.2, 128, 128.4, 130.6, 133.4, 134.0, 160.4, 162.9, 171.6, 172.6, 195.3; **MS: (m/z)** = 277 (M+1); **Anal. Calc. for $C_{15}H_{17}FN_2O_2$** C, 65.20; H, 6.20; N, 10.14; Found: C, 65.24; H, 6.26; N, 10.19.

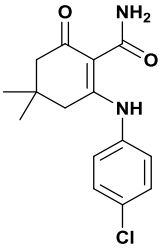

2-((4-chlorophenyl)amino)-4,4-dimethyl-6-oxocyclohex-1-ene-1-carboxamide III.5n

$C_{15}H_{17}ClN_2O_2$. **M**: 292,10 g.mol^{-1}. **Aspect:** White powder. **Yield** = 81 %. **M.p** = 214 – 216 °C. **R_f** = 0.39 (CH_2Cl_2/MeOH, 94:06).

IR (KBr, cm^{-1}): ν = 3375 (NH_2) , 3344 (NH_2), 3206 (NH), 2870, 1633 (C=O), 1541 (C=C), 1491, 1437; **^{1}H NMR (400 MHz, $CDCl_3$): δ** = 1.00 (s, 6H, $2CH_3$), 2.33 (s, 2H, CH_2-C), 2.38 (s, 2H, CH_2-CO), 5.51 (sl, 1H, CO-NH^a), 7.05-7.09 (m, 2H, $2CH_{Ar}$), 7.36-7.39 (m, 2H, $2CH_{Ar}$), 10.06 (sl, 1H, CO-NH^b), 13.92 (s, 1H, NH); **^{13}C NMR (101 MHz, $CDCl_3$): δ** = 28.03, 31.29, 41.75, 51.54, 99.33, 127.43, 129.79, 133.16, 136.05, 171.11, 172.39, 195.34; **MS: (m/z)** = 293 (M+1); **Anal. Calc. for $C_{15}H_{17}ClN_2O_2$** C, 61.54; H, 5.85; N, 9.57; Found: C, 61.49; H, 5.90; N, 9.51.

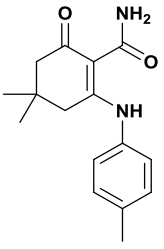

4,4-dimethyl-6-oxo-2-(p-tolylamino)cyclohex-1-ene-1-carboxamide III.5o

$C_{16}H_{20}N_2O_2$. **M**: 272,15 g.mol^{-1}. **Aspect:** Yellow powder. **Yield** = 80 %. **M.p** = 187 – 189 °C. **R_f** = 0.41 (CH_2Cl_2/MeOH, 94:06).

IR (KBr, cm^{-1}): ν = 3377 (NH_2), 3347 (NH_2), 3206 (NH), 3046, 2961, 1631 (C=O), 1514 (C=C), 1512 (C=C), 1438 (C=C); **^{1}H NMR (400 MHz, $CDCl_3$): δ** = 0.99 (s, 6H, $2CH_3$), 2.32 (s, 2H, CH_2-C), 2.37 (s, 3H, CH_3), 2.39 (s, 2H, CH_2-CO), 5.47 (sl, 1H, CO-NH^a), 7.01 (d, 2H, *J* = 4.3 Hz, $2CH_{Ar}$), 7.20 (d, 2H, *J* = 7.9 Hz, $2CH_{Ar}$), 9.95 (sl, 1H, CO-NH^b), 13.81 (s, 1H, NH); **^{13}C NMR (101 MHz, $CDCl_3$): δ** = 21.24, 28.03, 31.18, 41.68, 51.59, 98.90, 125.97, 130.18, 134.82, 137.43, 171.53, 172.55, 195.23; **Anal. Calc. for $C_{16}H_{20}N_2O_2$** C, 70.56; H, 7.40; N, 10.29; Found: C, 70.50; H, 7.45; N, 10.34.

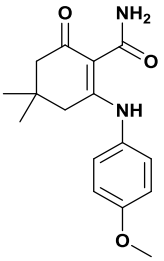

2-((4-methoxyphenyl)amino)-4,4-dimethyl-6-oxocyclohex-1-ene-1-carboxamide III.5p

$C_{16}H_{20}N_2O_3$. **M**: 288,15 g.mol^{-1}. **Aspect:** Cristal. **Yield** = 88 %. **M.p** = 144 – 146 °C. **R_f** = 0.53 (CH_2Cl_2/MeOH, 94:06).

IR (KBr, cm^{-1}): ν = 3335 (NH_2), 2937, 1617 (C=O), 1554 (C=C), 1432 (C=C); **^{1}H NMR (400 MHz, $CDCl_3$): δ** = 0.98 (s, 6H, $2CH_3$), 2.31 (s, 2H, CH_2-C), 2.35 (s, 2H, CH_2-CO), 3.82 (s, 3H, O-CH_3), 5.53 (sl, 1H, CO-NH^a), 6.89-6.93 (m, 2H, $2CH_{Ar}$), 7.02-7.06 (m, 2H, $2CH_{Ar}$), 9.87 (sl, 1H, CO-NH^b), 13.69 (s, 1H, NH); **^{13}C NMR (101 MHz, $CDCl_3$): δ** = 27.41, 31.11, 41.05, 52.01, 54.50, 98.80, 115.83, 126.43, 129.29, 159.56, 171.82, 172.95, 195.55; **MS: (m/z)** = 289 (M+1); **Anal. Calc. for $C_{16}H_{20}N_2O_3$** C, 66.65; H, 6.99; N, 9.72; Found: C, 66.60; H, 6.93; N, 9.69.

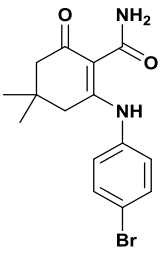

2-((4-bromophenyl)amino)-4,4-dimethyl-6-oxocyclohex-1-ene-1-carboxamide III.5q

$C_{15}H_{17}BrN_2O_2$. **M**: 336,05 g.mol^{-1}. **Aspect:** Cristal. **Yield** = 89 %. **M.p** = 228 – 230 °C. **R_f** = 0.43 (CH_2Cl_2/MeOH, 94:06).

IR (KBr, cm^{-1}): ν = 3345 (NH_2), 3210 (NH), 2958, 1709 (C=O), 1634 (C=O), 1566 (C=C), 1492 (C=C), 1437 (C=C); **^{1}H NMR (400 MHz, $CDCl_3$): δ** = 0.99 (s, 6H, $2CH_3$), 2.32 (s, 2H, CH_2-C), 2.34 (s, 2H, CH_2-CO), 5.54 (sl, 1H, CO-NH^a), 7.09 (d, 2H, *J* = 1.1 Hz, $2CH_{Ar}$), 7.10 (d, 2H, *J* = 1.1 Hz, $2CH_{Ar}$), 9.79 (sl, 1H, CO-NH^b), 13.86 (s, 1H, NH); **^{13}C NMR (101 MHz, $CDCl_3$): δ** = 28.00, 31.18, 41.64, 51.51, 99.14, 116.41, 128.00, 133.48, 160.33, 162.80, 171.46, 172.43, 195.24. **Anal. Calc. for $C_{15}H_{17}BrN_2O_2$** C, 53.43; H, 5.08; N, 8.31; Found: C, 53.39; H, 5.14; N, 8.36.

2.3. Synthesis of 4-hydroxyquinolone analogues

In a microwave reactor, a mixture consisting of diethyl malonate (3 mmol) and β-enaminone (1 mmol) was introduced, dissolved in 1 mL of ethanol as the solvent. To this mixture, 0.2 mmol of $BiCl_3$ was added. The reaction mixture was then subjected to microwave irradiation for an appropriate duration ranging from 5 to 13 minutes. The progression of the reaction was monitored by TLC. Upon completion of the reaction, 5 mL of ethanol was added, and the catalyst was recovered by filtration. The synthesized derivatives were purified *via* column chromatography, using an eluent composed of a 1:1 mixture of ethyl acetate and petroleum ether. The pure fractions were subsequently concentrated under reduces pressure.

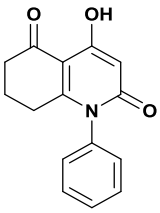

4-hydroxy-1-phenyl-7,8-dihydroquinoline-2,5(1H,6H)-dione III.7a

$C_{15}H_{13}NO_3$. **M**: 255,09 g.mol^{-1}. **Aspect:** Brown powder. **Yield** = 55 %. **M.p** = 162–164 °C. **R_f** = 0.35 (EtOAc/Petroleum ether, 60:40).

IR (KBr, cm^{-1}): ν =3261 (OH), 1710 (C=O), 1592 (C=O), 1574 (C=C); **^{1}H NMR (400 MHz, DMSO-*d_6*): δ** = 1.91 (qt, 2H, *J* = 6.4 Hz, CH_2), 2.43 (t, 2H, *J* = 6.2 Hz, CH_2-C), 2.54 (t, 2H, *J* = 5.6 Hz, 2H, CH_2-CO), 5.63 (s, 1H, CH), 7.23-7.42 (m, 2H, Ar-H), 7.42-7.64 (m, 3H, Ar-H), 12.71 (s, 1H, OH); **^{13}C NMR (101 MHz, DMSO-*d_6*): δ** = 19.9, 28.8, 35.82, 95.8, 104.7, 128.14, 128.9, 129.4, 137.3, 162.1, 162.6, 167.2 202.53; **MS: (m/z) =** 256 (M+1); **Anal. Calc. for $C_{15}H_{13}NO_3$** C, 70.58; H, 5.13; N, 5.49; Found: C, 70.62; H, 5.10; N, 5.44.

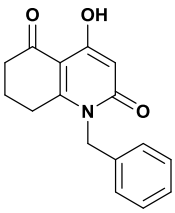

1-benzyl-4-hydroxy-7,8-dihydroquinoline-2,5(1H,6H)-dione III.7b

$C_{16}H_{15}NO_3$. **M**: 269,11 g.mol^{-1}. **Aspect:** Crystal. **Yield** = 62 %. **M.p** = 178–180 °C. **R_f** = 0.41 (EtOAc/Petroleum ether, 60:40).

IR (KBr, cm^{-1}): ν =3373 (OH), 1647 (C=O), 1590 (C=O), 1530 (C=C); **^{1}H NMR (400 MHz, DMSO-*d*$_6$): δ** = 1.94 (qt, 2H, *J* = 6.3 Hz, CH_2), 2.54 (t, 2H, *J* = 6.0 Hz, CH_2-C), 2.91 (t, 2H, *J* = 6.1 Hz, CH_2-CO), 5.35 (s, 2H, N-CH_2), 5.68 (s, 1H, CH), 7.12 – 7.19 (m, 2H, Ar-H), 7.24 – 7.40 (m, 3H, Ar-H), 12.78 (s, 1H, OH); **^{13}C NMR (101 MHz, DMSO-*d*$_6$): δ** = 19.9, 27.1, 35.6, 45.9, 95.6, 105.0, 126.1, 127.2, 128.7, 136.1, 162.2, 162.6, 167.0, 202.6; **Anal. Calc. for $C_{16}H_{15}NO_3$** C, 71.36; H, 5.61; N, 5.20; Found: C, 71.38; H, 5.63; N, 5.18.

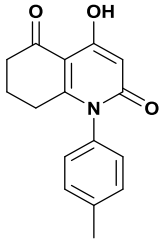

4-hydroxy-1-(p-tolyl)-7,8-dihydroquinoline-2,5(1H,6H)-dione III.7c

$C_{16}H_{15}NO_3$. **M**: 269,11 g.mol^{-1}. **Aspect:** Crystal. **Yield** = 65 %. **M.p** = 222–224 °C. **R_f** = 0.45 (EtOAc/Petroleum ether, 60:40).

IR (KBr, cm^{-1}): ν =3391 (OH), 1655 (C=O), 1607 (C=O), 1511 (C=C); **^{1}H NMR (400 MHz, $CDCl_3$): δ** = 1.94–2.06 (m, 2H, CH_2), 2.42 (s, 3H, CH_3), 2.48 (t, 2H, *J* = 6.2 Hz, CH_2-C), 2.57 (t, 2H, *J* = 6.0 Hz, CH_2-CO), 5.87 (s, 1H, CH), 7.05 (d, 2H, *J* = 8.2 Hz, Ar-H), 7.32 (d, 2H, *J* = 8.0 Hz, Ar-H), 12.43 (s, 1H, OH); **^{13}C NMR (101 MHz, $CDCl_3$): δ** = 20.8, 21.3, 29.4, 36.6, 98.0, 106, 127.63 130.8, 134.7, 139.7, 160.3, 164.0, 167.7, 201.5; **MS: (m/z)** = 270 (M+1); **Anal. Calc. for $C_{16}H_{15}NO_3$** C, 71.36; H, 5.61; N, 5.20; C, 71.31; H, 5.64; N, 5.23.

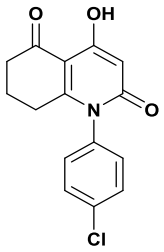

1-(4-chlorophenyl)-4-hydroxy-7,8-dihydroquinoline-2,5(1H,6H)-dione III.7d

$C_{15}H_{12}ClNO_3$. **M**: 289,05 g.mol^{-1}. **Aspect:** Crystal. **Yield** = 60 %. **M.p** = 240–242 °C. **R_f** = 0.62 (EtOAc/Petroleum ether, 60:40).

IR (KBr, cm^{-1}): ν =3258 (OH), 1673 (C=O), 1532 (C=C); **^{1}H NMR (400 MHz, DMSO-*d*$_6$): δ** = 1.92 (qt, 2H, *J* = 6.3 Hz, CH_2), 2.44 (t, 2H, *J* = 6.2 Hz, CH_2-C), 2.54 (t, 2H, *J* = 6.0 Hz, CH_2-CO), 5.64 (s, 1H, CH), 7.32-7.40 (m, 2H, Ar-H), 7.58-7.66 (m, 2H, Ar-H), 12.70 (s, 1H, OH);

^{13}C NMR (101 MHz, DMSO-d_6): δ = 19.9, 28.8, 35.8, 95.8, 104.8, 129.5, 130.2, 133.6, 136.1, 162.1, 162.5, 167.33, 202.53; **MS: (m/z)** = 290 (M+1); **Anal. Calc. for $C_{15}H_{12}ClNO_3$** C, 62.19; H, 4.18; N, 4.83; Found: C, 62.15; H, 4.14; N, 4.80.

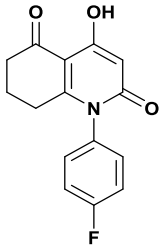

1-(4-fluorophenyl)-4-hydroxy-7,8-dihydroquinoline-2,5(1H,6H)-dione III.7e

$C_{15}H_{12}FNO_3$. **M**: 273,08 g.mol^{-1}. **Aspect:** Crystal. **Yield** = 60 %. **M.p** = 226–228 °C. **R_f** = 0.49 (EtOAc/Petroleum ether, 60:40).

IR (KBr, cm^{-1}): ν =3398 (OH), 1728 (C=O), 1661 (C=O), 1605 (C=C); **^{1}H NMR (400 MHz, $CDCl_3$): δ** = 1.97–2.08 (m, 2H, CH_2), 2.48 (t, 2H, *J* = 6.2 Hz, CH_2-C), 2.58 (t, 2H, *J* = 6.0 Hz, CH_2-CO), 5.86 (s, 1H, CH), 7.13-7.19 (m, 2H, Ar-H), 7.19-7.25 (m, 2H, Ar-H), 12.43 (s, 1H, OH); **^{13}C NMR (101 MHz, $CDCl_3$): δ** = 20.8, 29.4, 36.5, 98.0, 106.1, 117.1, 117.4, 129.8, 129.9, 133.2, 133.2, 160.1, 163.9, 167.9, 201.6; **MS: (m/z)** = 274 (M+1); **Anal. Calc. for $C_{15}H_{12}FNO_3$** C, 65.93; H, 4.43; N, 5.13; Found: C, 65.99; H, 4.47; N, 5.10.

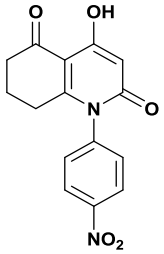

4-hydroxy-1-(4-nitrophenyl)-7,8-dihydroquinoline-2,5(1H,6H)-dione III.7f

$C_{15}H_{12}N_2O_5$. **M**: 300,07 g.mol^{-1}. **Aspect:** Crystal. **Yield** = 51 %. **M.p** = 120–122 °C. **R_f** = 0.5 (EtOAc/Petroleum ether, 60:40).

IR (KBr, cm^{-1}): ν =3351 (OH), 1668 (C=O), 1644 (C=O), 1525 (C=C); **^{1}H NMR (400 MHz, $CDCl_3$): δ** = 2.01–2.09 (m, 2H, CH_2), 2.46 (t, 2H, *J* = 6.2 Hz, CH_2-C), 2.61 (t, 2H, *J* = 6.6 Hz, CH_2-CO), 5.87 (s, 1H, CH), 7.42 (d, 2H, *J* = 8.4 Hz, Ar-H), 8.40 (d, 2H, *J* = 8.3 Hz, Ar-H), 12.43 (s, 1H, OH); **^{13}C NMR (101 MHz, $CDCl_3$): δ** = 20.7, 29.4, 36.5, 98.1, 106.4, 125.4, 129.7, 142.9, 148.4, 158.9, 163.3, 168.2, 201.4; **Anal. Calc. for $C_{15}H_{12}N_2O_5$** C, 60.00; H, 4.03; N, 9.33; Found: C, 60.05; H, 4.08; N, 9.37.

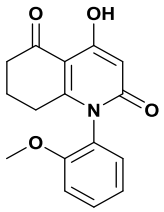

4-hydroxy-1-(2-methoxyphenyl)-7,8-dihydroquinoline-2,5(1H,6H)-dione III.7g

$C_{16}H_{15}NO_4$. **M**: 285,10 g.mol^{-1}. **Aspect:** Crystal. **Yield** = 65 %. **M.p** = 171–173 °C. **R_f** = 0.29 (EtOAc/Petroleum ether, 60:40).

IR (KBr, cm^{-1}): ν =3401 (OH), 1682 (C=O), 1650 (C=O), 1528 (C=C); **^{1}H NMR (400 MHz, DMSO-*d*$_6$): δ** = 1.66–2.05 (m, 2H, CH_2), 2.22–2.35 (m, 2H, CH_2-C), 2.42–2.68 (m, 2H, CH_2-CO), 3.76 (s, 3H, CH_3), 5.61 (s, 1H, CH), 7.10 (td, 1H, *J* = 1.2, 7.6 Hz, Ar-H), 7.23 (dd, 2H, *J* = 1.7, 7.7 Hz, Ar-H), 7.49 (ddd, 1H, *J* = 1.7, 7.4, 8.3 Hz, Ar-H), 12.68 (s, 1H, OH); **^{13}C NMR (101 MHz, DMSO-*d*$_6$): δ** = 19.9, 27.7, 35.8, 55.8, 95.8, 104.6, 112.5, 120.9, 125.4, 129.2, 130.7, 154.0, 162.1, 162.3, 167.2, 202.4; **MS: (m/z)** = 286 (M+1); **Anal. Calc. for $C_{16}H_{15}NO_4$** C, 67.36; H, 5.30; N, 4.91; Found: C, 67.31; H, 5.25; N, 4.87.

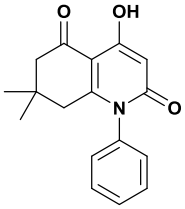

4-hydroxy-7,7-dimethyl-1-phenyl-7,8-dihydroquinoline-2,5(1H,6H)-dione III.7h

$C_{17}H_{17}NO_3$. **M**: 283,12 g.mol^{-1}. **Aspect:** Crystal. **Yield** = 68 %. **M.p** = 210–212 °C. **R_f** = 0.47 (EtOAc/Petroleum ether, 60:40).

IR (KBr, cm^{-1}): ν =3429 (OH), 1676 (C=O), 1592 (C=O), 1536 (C=C); **^{1}H NMR (400 MHz, $CDCl_3$): δ** = 1.03 (s, 6H, $2CH_3$), 2.32 (s, 2H, CH_2-C), 2.44 (s, 2H, CH_2-CO), 5.87 (s, 1H, CH), 7.13 (d, 2H, *J* = 7.2 Hz, Ar-H), 7.11–7.18 (m, 2H, Ar-H), 7.46–7.59 (m, 3H, Ar-H), 12.39 (s, 1H, OH); **^{13}C NMR (101 MHz, $CDCl_3$): δ** = 28.14, 32.63, 42.81, 50.16, 97.91 (CH), 104.99, 128.03, 129.58, 130.26, 137.45, 158.73, 164.13 (N-C=O), 167.62 (C-OH), 201.28 (C=O); **MS: (m/z)** = 284 (M+1); **Anal. Calc. for $C_{17}H_{17}NO_3$** C, 72.07; H, 6.05; N, 4.94; Found: C, 72.10; H, 6.08; N, 4.99.

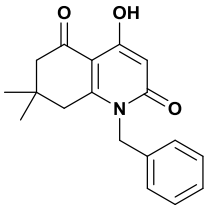

1-benzyl-4-hydroxy-7,7-dimethyl-7,8-dihydroquinoline-2,5(1H,6H)-dione III.7i

$C_{18}H_{19}NO_3$. **M**: 297,14 g.mol^{-1}. **Aspect:** Crystal. **Yield** = 69 %. **M.p** = 168 – 170 °C. **R_f** = 0.64 ($CH_3CO_2C_2H_5$/petroleum ether, 60:40).

IR (KBr, cm^{-1}): ν =3350 (OH), 3031, 2954, 1659 (C=O), 1632 (C=O), 1586 (C=C), 1443 (C=C); **^{1}H NMR (400 MHz, DMSO-*d*$_6$): δ** = 0.92 (s, 6H, 2CH_3), 2.48 (s, 2H, CH_2-C), 2.84 (s, 2H, CH_2-CO), 5.37 (s, 2H, N-CH_2), 5.68 (s, 1H, CH), 7.13 (d, 2H, *J* = 7.2 Hz, Ar-H), 7.25-7.30 (m, 1H, Ar-H), 7.36 (dd, 2H, *J* = 4.6, 10.1 Hz, Ar-H), 12.65 (s, 1H, OH); **^{13}C NMR (101 MHz, DMSO-*d*$_6$): δ** = 27.33, 31.85, 45.70, 48.78, 95.58 (CH), 104.08, 125.91, 127.21, 128.69, 136.27, 160.56, 162.70 (N-C=O), 166.71 (C-OH), 202.00 (C=O); **MS: (m/z)** = 298 (M+1); **Anal. Calc. for $C_{18}H_{19}NO_3$** C, 72.71; H, 6.44; N, 4.71; Found: C, 72.74; H, 6.40; N, 4.65.

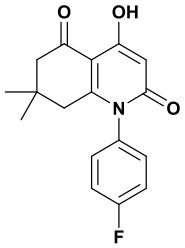

1-(4-fluorophenyl)-4-hydroxy-7,7-dimethyl-7,8-dihydroquinoline-2,5(1H,6H)-dione III.7j

$C_{17}H_{16}FNO_3$. **M**: 301,11 g.mol^{-1}. **Aspect:** Poudre jaune. **Yield** = 70 %. **M.p** = 193 – 195 °C. **R_f** = 0.66 ($CH_3CO_2C_2H_5$/petroleum ether, 60:40).

IR (KBr, cm^{-1}): ν =3373 (OH), 2956, 1665 (C=O), 1625 (C=O), 1526 (C=C), 1508 (C=C); **^{1}H NMR (400 MHz, $CDCl_3$): δ** = 1.04 (s, 6H, 2CH_3), 2.31 (s, 2H, CH_2-C), 2.44 (s, 2H, CH_2-CO), 5.85 (s, 1H, CH), 7.11-7.14 (m, 2H, Ar-H), 7.20 – 7.25 (m, 2H, Ar-H), 12.37 (s, 1H, OH); **^{13}C NMR (101 MHz, $CDCl_3$): δ** = 28.15, 32.63, 42.89, 50.07, 97.84 (CH), 105.11, 117.27, 117.50, 129.92, 133.20, 158.68, 161.63, 164.11 (N-C=O), 167.67 (C-OH), 201.27 (C=O); MS: (m/z) = 302 (M+1); **Anal. Calc. for $C_{17}H_{16}FNO_3$** C, 67.76; H, 5.35; N, 4.65; Found: C, 67.71; H, 5.34; N, 4.61.

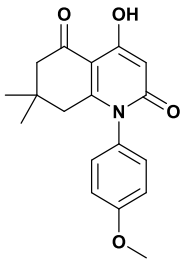

4-hydroxy-1-(4-methoxyphenyl)-7,7-dimethyl-7,8-dihydroquinoline-2,5(1H,6H)-dione III.7k

$C_{18}H_{19}NO_4$. **M**: 313,13 g.mol^{-1}. **Aspect:** Crystal. **Yield** = 71 %. **M.p** = 186 – 188 °C. **R_f** = 0.44 ($CH_3CO_2C_2H_5$/petroleum ether, 60:40).

IR (KBr, cm^{-1}): ν =3431 (OH), 2960, 1676 (C=O), 1609 (C=O), 1534 (C=C), 1510 (C=C), 1457, 1403; **^{1}H NMR (400 MHz, $CDCl_3$): δ** = 1.03 (s, 6H, $2CH_3$), 2.34 (s, 2H, CH_2-C), 2.43 (s, 2H, CH_2-CO), 3.86 (s, 3H, CH_3), 5.86 (s, 1H, CH), 7.04 (s, 4H, Ar-H), 12.37 (s, 1H, OH); **^{13}C NMR (101 MHz, $CDCl_3$): δ** = 28.15, 32.58, 42.87, 50.13, 55.68, 97.79 (CH), 104.98, 115.48, 128.98, 129.85, 159.26, 160.16, 164.41 (N-C=O), 167.55 (C-OH), 201.28 (C=O); **MS: (m/z)** = 314 (M+1); **Anal. Calc. for $C_{18}H_{19}NO_4$** C, 69.00; H, 6.11; N, 4.47; Found: C, 69.04; H, 6.13; N, 4.49.

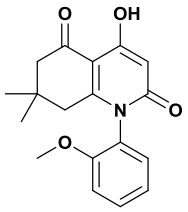

4-hydroxy-1-(2-methoxyphenyl)-7,7-dimethyl-7,8-dihydroquinoline-2,5(1H,6H)-dione III.7l

$C_{18}H_{19}NO_4$. **M**: 313,13 g.mol^{-1}. **Aspect:** Poudre jaune. **Yield** = 61 %. **M.p** = 176 – 178 °C. **R_f** = 0.52 (EtOAc/Petroleum ether, 60:40).

IR (KBr, cm^{-1}): ν =3236 (OH), 1738 (C=O), 1668 (C=O), 1532 (C=C); **^{1}H NMR (400 MHz, $CDCl_3$): δ** = 1.03 (d, 6H, *J* = 2.2 Hz, $2CH_3$), 2.23 (d, 1H, *J* = 17.6, CH-C), 2.36 (d, 2H, *J* = 17.6, CH-C), 2.43 (s, 2H, CH_2-CO), 3.80 (s, 3H, CH_3), 5.86 (s, 1H, CH), 7.04 – 7.17 (m, 3H, Ar-H), 7.47 (ddd, 1H, *J* = 3.5, 5.8, 8.3 Hz, Ar-H), 12.38 (s, 1H, OH); **^{13}C NMR (101 MHz, $CDCl_3$): δ** = 27.7, 28.6, 32.4, 41.8, 50.2, 56.0, 97.7, 104.9, 112.5, 121.6, 125.9, 129.3, 131.1, 154.4, 159.7, 163.8, 167.6, 201.3; **MS: (m/z)** = 314 (M+1); **Anal. Calc. for $C_{18}H_{19}NO_4$** C, 69.00; H, 6.11; N, 4.47; Found: C, 69.05; H, 6.17; N, 4.50.

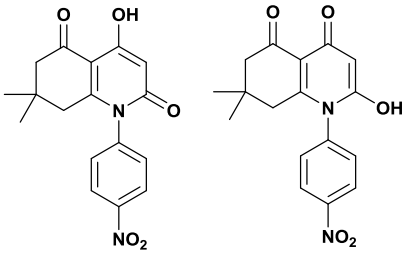

4-hydroxy-7,7-dimethyl-1-(4-nitrophenyl)-7,8-dihydroquinoline-2,5(1H,6H)-dione + 2-hydroxy-7,7-dimethyl-1-(4-nitrophenyl)-7,8-dihydroquinoline-4,5(1H,6H)-dione III.7m

$C_{17}H_{16}N_2O_5$. **M**: 328,11 g.mol^{-1}. **Aspect:** Huileux. **Yield** = 53 %. **R_f** = 0.6 (EtOAc/Petroleum ether, 60:40).

IR (KBr, cm^{-1}): ν =3449 (OH), 3380 (OH), 2962, 1737 (C=O), 1663 (C=O), 1598 (C=O), 1563 (C=O), 1529 (C=C), 1510 (C=C); **^{1}H NMR (400 MHz, $CDCl_3$): (III.7m$_1$:III.7m$_2$) (5:1); III.7m$_1$ δ** = 1.06 (s, 6H, $2CH_3$), 2.30 (s, 2H, CH_2-C), 2.47 (s, 2H, CH_2-CO), 5.88 (s, 1H, CH),

7.30–7.43 (m, 2H, Ar-H), 8.38–8.46 (m, 2H, Ar-H), 12.37 (s, 1H, OH); **III.7m$_2$ δ** = 1.09 (s, 6H, 2CH_3), 2.33 (s, 2H, CH_2-C), 2.67 (s, 2H, CH_2-CO), 5.52 (s, 1H, CH), 6.96–7.04 (m, 2H, Ar-H), 8.26–8.32 (m, 2H, Ar-H), 13.59 (s, 1H, OH); **^{13}C NMR (101 MHz, $CDCl_3$): δ** = 28.0, 28.1, 31.7, 32.8, 41.4, 42.9, 50.0, 62.4, 90.5, 98.0, 104.8, 105.3, 119.6, 125.1, 125.6, 129.7, 142.9, 143.4, 148.4, 151.7, 157.5, 163.6, 167.9, 170.0, 170.1, 170.4, 171.2, 201.2, 204.4; **Anal. Calc. for $C_{17}H_{16}N_2O_5$** C, 62.19; H, 4.91; N, 8.53; Found: C, 62.23; H, 4.97; N, 8.58.

2.4. Synthesis of imino-acridine derivatives

In a microwave reactor with a volume of 10 mL, a mixture comprising β-enaminone (2 eq, 1 mmol), aldehyde (1 eq, 0.5 mmol), and a minimal amount of ethanol (0.2 mL) to dissolve the reaction components was prepared. Subsequently, the reaction mixture was subjected to microwave irradiation for an appropriate duration ranging from 3 to 12 minutes. Upon completion of the reaction, as confirmed by TLC analysis, 3 mL of methanol were added to the mixture, and the pure products were allowed to crystallize overnight at 6°C. The resulting products were then filtered, dried, and obtained in excellent yields.

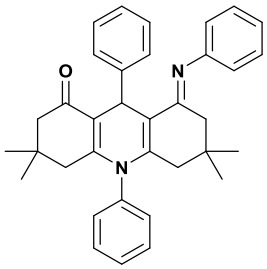

(E)-3,3,6,6-tetramethyl-9,10-diphenyl-8-(phenylimino)-3,4,5,6,7,8,9,10-octahydroacridin-1(2H)-one III.9a

$C_{35}H_{36}N_2O$. **M**: 500,69 g.mol^{-1}. **Aspect:** Yellow powder. **Yield =** 89%. **M.p** = 227 – 229 °C (lit: 230–232 °C [106]), **R_f** = 0.33 (Petroleum ether EtOAc, 8:2).

IR (KBr, cm^{-1}) ν = 3026, 2956, 1711 (C=O), 1638 (C=N), 1607, 1590 (C=C), 1576 (C=C), 1483, 1451, 1366, 1302; **^{1}H NMR (400 MHz, DMSO-*d*$_6$) δ** = 0.62 (s, 3H, CH_3), 0.73 (s, 3H, CH_3), 0.78 (s, 3H, CH_3), 0.90 (s, 3H, CH_3), 1.66 (d, 1H, *J* = 17.3 Hz, CH_2), 1.77 (d, 1H, *J* = 17.3 Hz, CH_2), 1.94 – 2.12 (m, 4H, 2CH_2), 2.23 (dd, 2H, *J* = 16.7, 13.2 Hz, CH_2), 5.46 (s, 1H, CH*), 6.46 – 6.55 (m, 2H, H_{Ar}), 6.96 (t, 1H, *J* = 7.5 Hz, H_{Ar}), 7.10 (t, 1H, *J* = 7.3 Hz, H_{Ar}), 7.25 (td, 4H, *J* = 7.5, 4.0 Hz, H_{Ar}), 7.40 (q, 4H, *J* = 7.8, 7.1 Hz, H_{Ar}), 7.52 – 7.64 (m, 3H, H_{Ar}); **^{13}C NMR (101 MHz, DMSO-*d*$_6$) δ =** 25.97, 26.01, 29.19, 29.44, 30.87, 31.86, 32.47, 40.43, 40.91, 40.99, 49.71, 111.56, 113.09, 119.36, 122.14, 125.43, 127.57, 127.65, 128.73, 129.10, 129.88, 138.82, 142.82, 146.61, 150.67, 151.78, 163.39, 194.84; **MS: (m/z)** = 501 (M+1); **Anal. Calc. for $C_{35}H_{36}N_2O$** C, 83.96; H, 7.25; N, 5.60; Found C, 83.98; H, 7.29; N, 5.63.

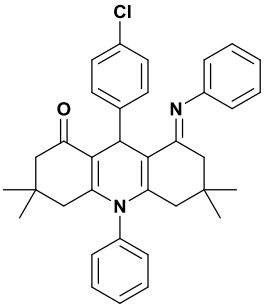

(E)-9-(4-chlorophenyl)-3,3,6,6-tetramethyl-10-phenyl-8-(phenylimino)-3,4,5,6,7,8,9,10-octahydroacridin-1(2H)-one III.9b

$C_{35}H_{35}ClN_2O$. **M**: 535,13 g.mol^{-1}. **Aspect:** Yellow powder. **Yield** = 80%. **M.p** = 252 – 254 °C (lit: 252–254°C [106]); $\mathbf{R_f}$ = 0.78 (CH_2Cl_2).

IR (KBr, cm^{-1}) ν = 2957, 2930, 1640 (C=O), 1591 (C=N), 1485 (C=C), 1367; **^{1}H NMR (400 MHz, DMSO-*d*$_6$) δ** = 0.62 (s, 3H, CH_3), 0.72 (s, 3H, CH_3), 0.77 (s, 3H, CH_3), 0.89 (s, 3H, CH_3), 1.65 (d, 1H, *J* = 17.4 Hz, CH_2), 1.76 (d, 1H, *J* = 17.4 Hz, CH_2), 1.94 – 2.12 (m, 4H, $2CH_2$), 2.22 (dd, 2H, *J* = 16.7, 9.7 Hz, CH_2), 5.42 (s, 1H, CH*), 6.51 (d, 2H, *J* = 7.7 Hz, H_{Ar}), 6.96 (t, 1H, *J* = 7.4 Hz, H_{Ar}), 7.25 (t, 2H, *J* = 7.7 Hz, H_{Ar}), 7.32 (d, 2H, *J* = 8.4 Hz, H_{Ar}), 7.41 (d, 4H, *J* = 8.0 Hz, H_{Ar}), 7.58 (dq, 3H, *J* = 14.3, 7.2 Hz, H_{Ar}); **^{13}C NMR (101 MHz, DMSO-*d*$_6$) δ** = 25.97, 26.06, 29.20, 29.40, 30.89, 31.91, 32.34, 40.36, 40.93, 40.99, 49.63, 111.16, 112.65, 119.43, 122.27, 127.59, 128.78, 129.19, 129.55, 129.87, 138.70, 143.06, 145.63, 150.86, 151.65, 163.35, 194.87; **Anal. Calc. for $C_{35}H_{35}ClN_2O$** C, 78.56; H, 6.59; N, 5.24; Found C, 78.58; H, 6.60; N, 5.29.

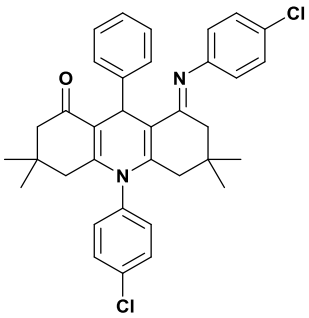

(E)-10-(4-chlorophenyl)-8-((4-chlorophenyl)imino)-3,3,6,6-tetramethyl-9-phenyl-3,4,5,6,7,8,9,10-octahydroacridin-1(2H)-one III.9c

$C_{35}H_{34}Cl_2N_2O$. **M**: 569,57 g.mol^{-1}. **Aspect:** Yellow powder. **Yield =** 88%. **M.p** = 255 – 257 °C (lit: 259–262°C [106]); $\mathbf{R_f}$ **=** 0.6 (Petroleum ether/EtOAc, 70:30).

IR (KBr, cm^{-1}) ν = 2958, 1641 (C=O), 1606 (C=N), 1580 (C=C), 1482 (C=C), 1367; **^{1}H NMR (400 MHz, DMSO-*d*$_6$) δ** = 0.63 (s, 3H, CH_3), 0.74 (s, 3H, CH_3), 0.80 (s, 3H, CH_3), 0.91 (s, 3H, CH_3), 1.68 (d, 1H, *J* = 17.3 Hz, CH_2), 1.79 (d, 1H, *J* = 17.4 Hz, CH_2), 1.93 – 2.11 (m, 4H,

2CH_2), 2.22 (dd, 2H, *J* = 16.7, 12.8 Hz, CH_2), 5.41 (s, 1H, CH*), 6.52 (d, 2H, *J* = 8.6 Hz, H_{Ar}), 7.10 (t, 1H, *J* = 7.5 Hz, H_{Ar}), 7.26 (dd, 4H, *J* = 18.5, 8.1 Hz, H_{Ar}), 7.35 – 7.45 (m, 4H, H_{Ar}), 7.66 (d, 2H, *J* = 8.8 Hz, H_{Ar}); **^{13}C NMR (101 MHz, DMSO-*d*$_6$) δ** = 25.88, 25.99, 29.12, 29.38, 30.96, 31.90, 32.49, 40.44, 40.83, 40.90, 49.70, 111.89, 113.11, 121.23, 125.50, 126.26, 127.61, 127.63, 128.64, 129.94, 131.67, 133.64, 137.64, 143.13, 146.38, 150.41, 150.53, 164.22, 194.89; **Anal. Calc. for $C_{35}H_{34}Cl_2N_2O$** C, 73.81; H, 6.02; N, 4.92; Found C, 73.85; H, 6.09; N, 4.96.

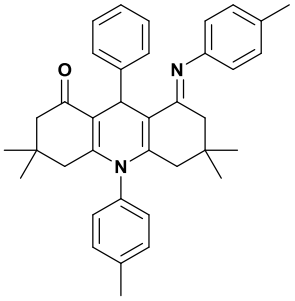

(E)-3,3,6,6-tetramethyl-9-phenyl-10-(p-tolyl)-8-(p-tolylimino)-3,4,5,6,7,8,9,10-octahydroacridin-1(2H)-one III.9d

$C_{37}H_{40}N_2O$. **M**: 528,74 g.mol^{-1}. **Aspect:** Yellow crystal. **Yield =** 85%. **M.p** = 205 – 207 °C (lit: 224–226°C [106]); **R_f =** 0.58 (Petroleum ether/EtOAc, 70:30).

IR (KBr, cm^{-1}) ν = 2955, 2927, 1639 (C=O), 1603 (C=N), 1501 (C=C), 1367; **^{1}H NMR (400 MHz, $CDCl_3$) δ** = 0.69 (s, 3H, CH_3), 0.80 (s, 3H, CH_3), 0.83 (s, 3H, CH_3), 0.95 (s, 3H, CH_3), 1.64 – 1.95 (m, 4H, 2CH_2), 1.95 – 2.14 (m, 4H, 2CH_2), 2.28 (s, 3H, CH_3), 2.46 (s, 3H, CH_3), 5.62 (s, 1H, CH*), 6.43 (d, 2H, *J* = 3.0 Hz, H_{Ar}), 7.01 (d, 2H, *J* = 7.9 Hz, H_{Ar}), 7.10 (d, 3H, *J* = 7.8 Hz, H_{Ar}), 7.21 (d, 2H, *J* = 7.9 Hz, H_{Ar}), 7.30 (d, 2H, *J* = 7.7 Hz, H_{Ar}), 7.50 (d, 2H, *J* = 7.5 Hz, H_{Ar}); **^{13}C NMR (101 MHz, $CDCl_3$) δ =** 20.89, 21.36, 26.81, 26.87, 29.60, 29.80, 30.04, 30.98, 31.50, 32.45, 33.69, 40.95, 41.91, 42.00, 50.56, 113.18, 115.15, 119.62, 125.49, 127.67, 128.47, 129.26, 130.51, 131.38, 137.16, 139.07, 141.88, 147.17, 149.89, 150.83, 163.06, 195.93; **Anal. Calc. for $C_{37}H_{40}N_2O$** C, 84.05; H, 7.63; N, 5.30; Found C, 84.10; H, 7.67; N, 5.33.

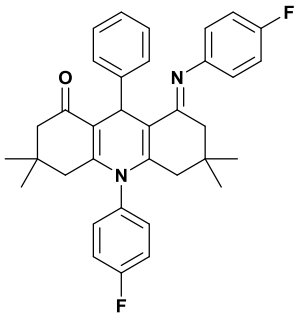

(E)-10-(4-fluorophenyl)-8-((4-fluorophenyl)imino)-3,3,6,6-tetramethyl-9-phenyl-3,4,5,6,7,8,9,10-octahydroacridin-1(2H)-one III.9e

$C_{35}H_{34}F_2N_2O$. **M**: 536,67 g.mol^{-1}. **Aspect:** Yellow powder. **Yield =** 84%. **M.p** = 231 – 233 °C (lit: 233–234°C [106]); **R_f =** 0.63 (Petroleum ether/EtOAc, 70:30).

IR (KBr, cm^{-1}) ν = 3068, 2949, 2868, 1640 (C=O), 1614 (C=N), 1582 (C=C), 1507 (C=C), 1496 (C=C), 1369; **^{1}H NMR (400 MHz, DMSO-*d*$_6$) δ** = 0.62 (s, 3H, CH_3), 0.74 (s, 3H, CH_3), 0.80 (s, 3H, CH_3), 0.91 (s, 3H, CH_3), 1.67 (d, 1H, *J* = 17.3 Hz, CH_2), 1.79 (d, 1H, *J* = 17.4 Hz, CH_2), 1.95 – 2.11 (m, 4H, $2CH_2$), 2.22 (dd, 2H, *J* = 16.8, 12.9 Hz, CH_2), 5.43 (s, 1H, CH*), 6.52 (dd, 2H, *J* = 8.7, 5.1 Hz, H_{Ar}), 7.08 (q, 3H, *J* = 8.8, 8.3 Hz, H_{Ar}), 7.25 (t, 2H, *J* = 7.5 Hz, H_{Ar}), 7.41 (dd, 6H, *J* = 15.2, 8.2 Hz, H_{Ar}); **^{13}C NMR (101 MHz, DMSO-*d*$_6$) δ** = 25.91, 26.00, 29.21, 29.42, 30.90, 31.86, 32.46, 40.38, 40.87, 40.93, 49.70, 111.77, 113.18, 115.21, 115.43, 116.65, 116.87, 120.83, 120.91, 125.45, 127.46, 127.59, 127.64, 135.05, 135.08, 143.04, 146.51, 147.97, 148.00, 150.68, 156.87, 160.45, 164.21, 194.86; **MS: (m/z)** = 537 (M+1); **Anal. Calc. for $C_{35}H_{34}F_2N_2O$** C, 78.33; H, 6.39; N, 5.22; Found C, 78.39; H, 6.43; N, 5.27.

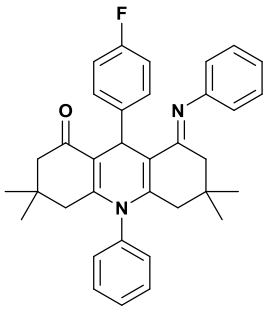

(E)-9-(4-fluorophenyl)-3,3,6,6-tetramethyl-10-phenyl-8-(phenylimino)-3,4,5,6,7,8,9,10-octahydroacridin-1(2H)-one III.9f

$C_{35}H_{35}FN_2O$. **M**: 518,68 g.mol^{-1}. **Aspect:** Yellow powder. **Yield =** 81%. **M.p** = 224 – 226 °C; **R_f =** 0.61 (Petroleum ether/EtOAc, 70:30).

IR (KBr, cm^{-1}) ν = 3061, 2957, 2870, 1713 (C=O), 1641 (C=N), 1591 (C=C), 1578 (C=C), 1503 (C=C), 1484 (C=C), 1417, 1368, 1302; **^{1}H NMR (400 MHz, DMSO-*d*$_6$) δ =** 0.62 (s, 3H, CH_3), 0.73 (s, 3H, CH_3), 0.77 (s, 3H, CH_3), 0.89 (s, 3H, CH_3), 1.65 (d, 1H, *J* = 17.3 Hz, CH_2), 1.78 (d, 1H, *J* = 17.4 Hz, CH_2), 2.02 (dt, 4H, *J* = 27.2, 16.7 Hz, CH_2), 2.22 (dd, 2H, *J* = 16.7, 10.0 Hz, CH_2), 5.43 (s, 1H, CH*),6.47 – 6.54 (m, 2H, H_{Ar}), 6.96 (t, 1H, *J* = 7.4 Hz, H_{Ar}), 7.07 (t, 2H, *J* = 8.9 Hz, H_{Ar}), 7.25 (t, 2H, *J* = 7.8 Hz, H_{Ar}), 7.36 – 7.45 (m, 4H, H_{Ar}), 7.57 (dd, 3H, *J* = 16.6, 7.5 Hz, H_{Ar}); **^{13}C NMR (101 MHz, DMSO-*d*$_6$)** δ = 25.94, 26.04, 29.18, 29.38, 30.87, 31.88, 32.02, 40.37, 40.90, 40.98, 49.65, 111.43, 112.98, 114.06, 114.27, 119.37, 122.20, 128.74, 129.14, 129.29, 129.37, 129.87, 138.74, 142.83, 142.87, 150.69, 151.70, 158.73,

161.41, 163.34, 194.85; **MS: (m/z)** = 519 (M+1); **Anal. Calc. for $C_{35}H_{35}FN_2O$** C, 81.05; H, 6.80; N, 5.40; Found C, 81.10; H, 6.83; N, 5.44.

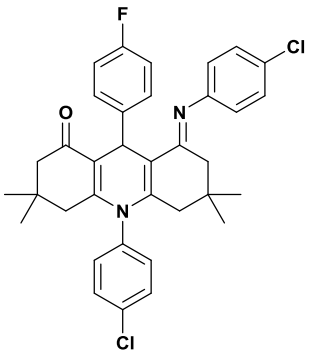

(E)-10-(4-chlorophenyl)-8-((4-chlorophenyl)imino)-9-(4-fluorophenyl)-3,3,6,6-tetramethyl-3,4,5,6,7,8,9,10-octahydroacridin-1(2H)-one III.9g

$C_{35}H_{33}Cl_2FN_2O$. **M**: 587,56 g.mol^{-1}. **Aspect:** Yellow powder. **Yield =** 90%. **M.p** = 245 – 247 °C; **R_f =** 0.68 (CH_2Cl_2).

IR (KBr, cm^{-1}) ν = 2956, 1712 (C=O), 1641 (C=N), 1603, 1580 (C=C), 1490 (C=C), 1482 (C=C), 1367, 1303; **^{1}H NMR (400 MHz, DMSO-d_6) δ** = 0.63 (s, 3H, CH_3) 0.74 (s, 3H, CH_3), 0.80 (s, 3H, CH_3), 0.91 (s, 3H, CH_3), 1.68 (d, 1H, *J* = 17.3 Hz, CH_2), 1.80 (d, 1H, *J* = 17.4 Hz, CH_2), 1.96 – 2.12 (m, 4H, $2CH_2$), 2.21 (dd, 2H, *J* = 16.6, 9.4 Hz, CH_2), 5.39 (s, 1H, CH*),6.48 – 6.56 (m, 2H, H_{Ar}), 7.05 (t, 2H, *J* = 8.9 Hz, H_{Ar}), 7.28 (d, 2H, *J* = 4.6 Hz, H_{Ar}), 7.36 – 7.47 (m, 4H, H_{Ar}), 7.66 (d, 2H, *J* = 8.8 Hz, H_{Ar}); **^{13}C NMR (101 MHz, DMSO-d_6) δ** = 25.85. 26.02, 29.11, 29.33, 30.96, 31.92, 32.04, 40.39, 40.83, 49.65, 111.76, 112.98, 114.10, 114.31, 121.25, 126.32, 128.65, 129.32, 129.39, 129.92, 133.69, 137.57, 142.64, 143.18, 150.44, 150.46, 164.18, 194.90; **Anal. Calc. for $C_{35}H_{33}Cl_2FN_2O$** C, 71.55; H, 5.66; N, 4.77; Found C, 71.60; H, 5.68; N, 4.81.

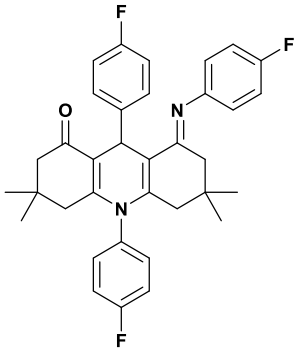

(E)-9,10-bis(4-fluorophenyl)-8-((4-fluorophenyl)imino)-3,3,6,6-tetramethyl-3,4,5,6,7,8,9,10-octahydroacridin-1(2H)-one III.9h

$C_{35}H_{33}F_3N_2O$. **M**: 554,66 g.mol^{-1}. **Aspect:** Yellow powder. **Yield =** 88%. **M.p** = 240 – 242 °C; **R_f =** 0.55 (Petroleum ether/EtOAc, 70:30).

IR (KBr, cm^{-1}) ν = 3060, 2958, 2870, 1641 (C=O), 1602 (C=N), 1508 (C=C), 1498 (C=C), 1368, 1304; **^{1}H NMR (400 MHz, CDCl$_3$) δ** = 0.71 (s, 3H, CH_3), 0.81 (s, 3H, CH_3), 0.86 (s, 3H, CH_3), 0.96 (s, 3H, CH_3), 1.71 (d, 1H, *J* = 17.2 Hz, CH_2), 1.82 (d, 1H, *J* = 17.2 Hz, CH_2), 1.99 (dd, 4H, *J* = 31.5, 18.0 Hz, CH_2), 2.13 – 2.25 (m, 2H, CH_2), 5.56 (s, 1H, CH*), 6.44 (s, 2H, H_{Ar}), 6.91 (t, 4H, *J* = 7.1 Hz, H_{Ar}), 7.22 (d, 4H, *J* = 6.5 Hz, H_{Ar}), 7.42 (s, 2H, *J* = 6.9 Hz, H_{Ar}), **^{13}C NMR (101 MHz, CDCl$_3$) δ** = 26.81, 29.64, 29.82, 29.99, 31.56, 32.51, 33.17, 40.94, 42.04, 50.43, 114.30, 115.26, 115.49, 116.95, 120.72, 129.73, 136.60, 136.98, 142.33, 142.70, 148.42, 151.06, 163.73, 196.08; **Anal. Calc. for $C_{35}H_{33}F_3N_2O$** C, 75.79; H, 6.00; N, 5.05; Found C, 75.84; H, 6.06; N, 5.09.

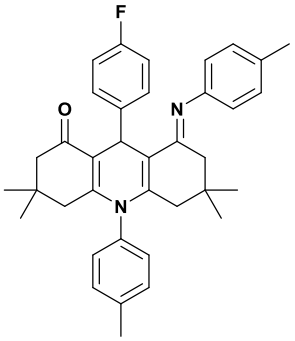

(E)-9-(4-fluorophenyl)-3,3,6,6-tetramethyl-10-(p-tolyl)-8-(p-tolylimino)-3,4,5,6,7,8,9,10-octahydroacridin-1(2H)-one III.9i

$C_{37}H_{39}FN_2O$. **M**: 546,73 g.mol^{-1}. **Aspect:** Yellow powder. **Yield =** 90%. **M.p** = 194 – 196 °C; **R_f =** 0.71 (Petroleum ether/EtOAc, 70:30).

IR (KBr, cm^{-1}) ν = 2956, 1641 (C=O), 1602 (C=N), 1579 (C=C), 1503 (C=C), 1368, 1302; **^{1}H NMR (400 MHz, DMSO-*d*$_6$) δ** = 0.60 (s, 3H, CH_3), 0.73 (s, 3H, CH_3), 0.77 (s, 3H, CH_3), 0.90 (s, 3H, CH_3), 1.66 (d, 1H, *J* = 17.3 Hz, CH_2), 1.79 (d, 1H, *J* = 17.4 Hz, CH_2), 1.95 – 2.09 (m, 4H, CH_2), 2.16 – 2.23 (m, 2H, CH_2), 2.24 (s, 3H, CH_3), 2.41 (s, 3H, CH_3), 5.42 (s, 1H, CH*), 6.41 (2H, d, *J* = 7.8 Hz, H_{Ar}), 7.03 – 7.09 (m, 4H, H_{Ar}), 7.24 (d, 2H, *J* = 8.0 Hz, H_{Ar}), 7.37 – 7.42 (m, 4H, H_{Ar}); **^{13}C NMR (101 MHz, DMSO-*d*$_6$) δ** = 20.33 20.72, 25.95, 26.05, 29.23, 29.41, 30.84, 31.86, 31.93, 49.67, 111.33, 113.05, 114.03, 114.24, 119.39, 129.19, 129.25, 129.33, 130.95, 136.15, 138.57, 142.80, 149.10, 150.93, 163.36, 194.81; **MS: (m/z) =** 569 (M+23). **Anal. Calc. for $C_{37}H_{39}FN_2O$** C, 81.28; H, 7.19; N, 5.12; Found C, 81.31; H, 7.21; N, 5.16.

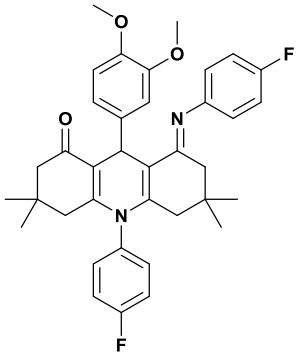

(E)-9-(3,4-dimethoxyphenyl)-10-(4-fluorophenyl)-8-((4-fluorophenyl)imino)-3,3,6,6-tetramethyl-3,4,5,6,7,8,9,10-octahydroacridin-1(2H)-one III.9j

$C_{37}H_{38}F_2N_2O_3$. **M**: 596,72 g.mol^{-1}. **Aspect:** Yellow powder. **Yield =** 87%. **M.p** = 168 – 170 °C; **R_f =** 0.51 (Cyclohexane/EtOAc, 80:20).

IR (KBr, cm^{-1}) ν = 2956, 2833, 1639 (C=O), 1602 (C=N), 1508 (C=C), 1498 (C=C), 1464 (C=C), 1368; **^{1}H NMR (400 MHz, DMSO-*d*$_6$) δ** = 0.65 (s, 3H, CH_3), 0.79 (s, 6H, $2CH_3$), 0.92 (s, 3H, CH_3), 1.65 (d, 1H, *J* = 17.3 Hz, CH_2), 1.80 (d, 1H, *J* = 17.4 Hz, CH_2), 2.02 (dd, 4H, *J* = 19.1, 11.3 Hz, $2CH_2$), 2.23 (t, 2H, *J* = 15.5 Hz, CH_2), 3.70 (d, 6H, *J* = 4.8 Hz, $2(OCH_3)$), 5.39 (s, 1H, CH*),6.54 – 6.58 (m, 1H, H_{Ar}), 6.87 (t, 1H, *J* = 8.7 Hz, H_{Ar}), 6.98 (s, 1H, H_{Ar}), 7.08 (d, 2H, *J* = 8.7 Hz, H_{Ar}), 7.43 (t, 3H, *J* = 6.4 Hz, H_{Ar}); **^{13}C NMR (101 MHz, DMSO-*d*$_6$) δ** = 25.90, 26.06, 29.26, 29.53, 30.65, 30.92, 31.51, 31.88, 40.47, 40.90, 40.96, 49.72, 55.21, 55.31, 111.24, 111.73, 111.79, 113.43, 115.30, 115.51, 119.27, 120.86, 120.94, 139.15, 142.90, 146.66, 147.88, 150.67, 160.39, 164.43, 195.03, 206.42; **Anal. Calc. for $C_{37}H_{38}F_2N_2O_3$** C, 74.48; H, 6.42; N, 4.69; Found: C, 74.50; H, 6.46; N, 4.71.

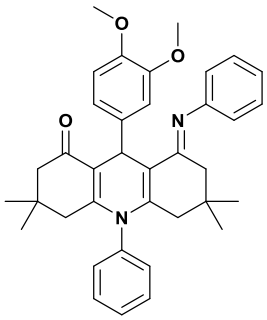

(E)-9-(3,4-dimethoxyphenyl)-3,3,6,6-tetramethyl-10-phenyl-8-(phenylimino)-3,4,5,6,7,8,9,10-octahydroacridin-1(2H)-one III.9k

$C_{37}H_{40}N_2O_3$. **M**: 560,74 g.mol^{-1}. **Aspect:** Yellow powder. **Yield =** 81%. **M.p =** 106 – 108 °C; **R_f =** 0.55 (Cyclohexane/EtOAc, 80:20).

IR (KBr, cm^{-1}) ν 2953, 2926, 1638 (C=O), 1573 (C=N), 1510 (C=C), 1367; **^{1}H NMR (400 MHz, DMSO-*d*$_6$) δ** = 0.64 (s, 3H, CH_3), 0.79 (s, 6H, $2CH_3$), 0.91 (s, 3H, CH_3), 1.63 (d, 1H, *J* = 16.8 Hz, CH_2), 1.72 (d, 1H, *J* = 17.6 Hz, CH_2), 1.96 – 2.09 (m, 2H, CH_2), 2.20 – 2.30 (m, 2H,

CH_2), 3.70 (d, 6H, *J* = 4.8 Hz, 2(OCH_3)), 5.41 (s, 1H, CH*), 6.54 (d, 2H, *J* = 8 Hz, H_{Ar}), 6.65 – 6.69 (m, 1H, H_{Ar}), 6.84 – 6.91 (m, 2H, H_{Ar}), 6.94 – 7.00 (m, 2H, H_{Ar}), 7.18 (d, 1H, *J* = 13.2 Hz, H_{Ar}), 7.26 (t, 2H, *J* = 7.6 Hz, H_{Ar}), 7.48 – 7.62 (m, 3H, H_{Ar}); **^{13}C NMR (101 MHz, DMSO-*d*$_6$) δ** = 26.46, 26.59, 29.76, 30.06, 31.40, 32.04, 32.39, 50.26, 55.70, 55.82, 111.73, 111.73, 112.07, 113.81, 119.80, 119.90, 124.90, 125.68, 129.32, 129.69, 139.34, 147.15, 148.43, 151.11, 198.61, 206.66; **Anal. Calc. for $C_{37}H_{40}N_2O_3$** C, 79.25; H, 7.19; N, 5.00; Found C, 79.27; H, 7.21; N, 5.01.

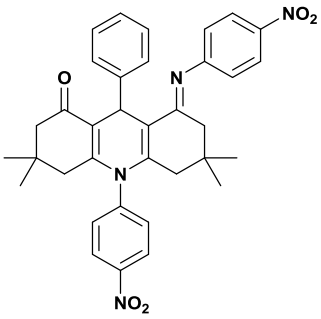

(E)-3,3,6,6-tetramethyl-10-(4-nitrophenyl)-8-((4-nitrophenyl)imino)-9-phenyl-3,4,5,6,7,8,9,10-octahydroacridin-1(2H)-one III.9l

$C_{35}H_{34}N_4O_5$. **M**: 590,68 g.mol^{-1}. **Aspect:** Yellow powder. **Yield =** 77%. **M.p =** 225 – 227 °C; **R_f =** 0.7 (CH_2Cl_2).

IR (KBr, cm^{-1}) ν = 2925, 2853, 1645 (C=O), 1579 (C=N), 1368 (C=C), 1335; **^{1}H NMR (400 MHz, DMSO-*d*$_6$) δ** = 0.65 (s, 3H, CH_3), 0.74 (s, 3H, CH_3), 0.80 (s, 3H, CH_3), 0.91 (s, 3H, CH_3), 1.75 – 1.83 (m, 2H, CH_2), 1.93 – 2.05 (m, 2H, CH_2), 2.14 – 2.32 (m, 3H, CH_2), 2.54 – 2.67 (m, 1H, CH_2), 5.38 (s, 1H, CH*), 6.69 (d, 2H, *J* = 8 Hz, H_{Ar}), 7.11 – 7.13 (m, 2H, H_{Ar}), 7.22 – 7.29 (m, 2H, H_{Ar}), 7.39 (d, 2H, *J* = 6.8 Hz, H_{Ar}), 7.71 (s, 1H, H_{Ar}), 8.14 – 8.20 (m, 3H, H_{Ar}), 8.44 (d, 1H, *J* = 8 Hz, H_{Ar}); **Anal. Calc. for $C_{35}H_{34}N_4O_5$** C, 71.17; H, 5.80; N, 9.49; Found C, 71.19; H, 5.83; N, 9.52.

2.5. Synthesis of hydroxylated acridine derivatives

In a microwave reactor with a volume of 10 mL, a mixture containing β-enaminone (2 eq, 1 mmol), *ortho*-substituted aromatic aldehyde (1 eq, 0.5 mmol), and a minimal amount of ethanol (0.2 mL) to facilitate dissolution was prepared. Subsequently, the reaction components were exposed to microwave irradiation for an appropriate duration ranging from 4 to 5 minutes. Upon completion of the reaction, as confirmed by TLC analysis, the resulting hydroxylated acridines were purified using column chromatography with an eluent composed of a 6:4 mixture of petroleum ether and ethyl acetate. The pure fractions were then concentrated under vacuum.

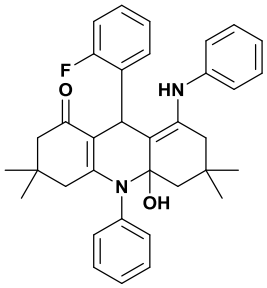

9-(2-fluorophenyl)-10a-hydroxy-3,3,6,6-tetramethyl-10-phenyl-8-(phenylamino)-3,4,5,6,7,9,10,10a-octahydroacridin-1(2H)-one III.14a

$C_{35}H_{37}FN_2O_2$. **M**: 536,69 g.mol^{-1}. **Aspect:** Brown powder. **Yield** = 75%. **M.p** = 179 – 181 °C; **R_f** = 0.91 (Petroleum ether/EtOAc, 50:50).

IR (KBr, cm^{-1}) ν = 3226 (OH), 3062, 2958, 2868, 1714 (C=O), 1588 (C=C), 1574 (C=C), 1492 (C=C), 1391; **^{1}H NMR (400 MHz, DMSO-*d*$_6$) δ** = 0.77 (s, 3H, CH_3), 0.79 (s, 3H, CH_3), 0.91 (s, 3H, CH_3), 0.95 (s, 3H, CH_3), 1.78 (d, 1H, *J* = 18.9 Hz, CH_2), 1.90 (d, 1H, *J* = 15.9 Hz, CH_2), 2.01 (d, 1H, *J* = 15.8 Hz, CH_2), 2.07 (d, 1H, *J* = 8.1 Hz, CH_2), 2.13 (d, 2H, *J* = 17.6 Hz, CH_2), 2.25 – 2.33 (m, 2H, CH_2), 2.85 (d, 1H, *J* = 16.0 Hz, CH_2), 5.02 (s, 1H, CH*),5.94 – 5.99 (m, 1H, H_{Ar}), 6.81 – 6.89 (m, 2H, H_{Ar}), 6.92 – 6.98 (m, 1H, H_{Ar}), 7.10 (t, 1H, *J* = 7.3 Hz, H_{Ar}), 7.19 (d, 2H, *J* = 7.8 Hz, H_{Ar}), 7.36 – 7.48 (m, 3H, H_{Ar}), 7.53 – 7.59 (m, 1H, H_{Ar}), 7.65 (s, 2H, H_{Ar}), 7.84 (s, 1H, OH), 10.26 (s, 1H, NH); **^{13}C NMR (75 MHz, DMSO-*d*$_6$) δ** = 25.25, 26.26, 28.12, 29.44, 31.07, 31.29, 32.47, 41.37, 48.81, 50.91, 106.28, 114.78, 119.61, 121.71, 122.32, 122.57, 125.55, 126.92, 128.13, 128.53, 128.96, 139.82, 140.41, 140.55, 154.40, 193.39, 195.30; **^{19}F NMR (282 MHz, DMSO-*d*$_6$) δ** = –117.68. **Anal. Calc. for $C_{35}H_{37}FN_2O_2$** C, 78.33; H, 6.95; N, 5.22; Found C, 78.36; H, 6.99; N, 5.27.

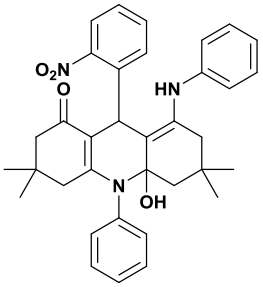

10a-hydroxy-3,3,6,6-tetramethyl-9-(2-nitrophenyl)-10-phenyl-8-(phenylamino)-3,4,5,6,7,9,10,10a-octahydroacridin-1(2H)-one III.14b

$C_{35}H_{37}N_3O_4$. **M**: 563,70 g.mol^{-1}. **Aspect:** Brown powder. **Yield** = 72%. **R_f** = 0.84 (Petroleum ether/EtOAc, 50:50).

IR (KBr, cm^{-1}) ν = 3368 (C=O), 3104, 3075, 2958, 2928, 2868, 1699 (C=O), 1607, 1575 (C=C), 1529 (C=C), 1508 (C=C), 1448, 1392, 1347, 1316; **^{1}H NMR (400 MHz, DMSO-d$_6$) δ**

= 0.78 (s, 6H, $2CH_3$), 0.92 (s, 6H, $2CH_3$), 1.75 – 1.99 (m, 4H, $2CH_2$), 2.17 – 2.49 (m, 2H, CH_2), 2.63 – 2.73 (m, 2H, CH_2), 5.02 (s, 1H, CH*), 5.98 (d, 1H, *J* = 9.2 Hz, H_{Ar}), 6.87 – 7.00 (m, 4H, H_{Ar}), 7.22 – 7.40 (m, 6H, H_{Ar}, OH), 7.47 – 7.51 (m, 3H, H_{Ar}), 7.90 (d, 2H, *J* = 9.2 Hz, H_{Ar}), 10.11 (s, 1H, NH); **Anal. Calc. for $C_{35}H_{37}N_3O_4$** C, 74.58; H, 6.62; N, 7.45; Found C, 74.60; H, 6.64; N, 7.49.

2.6. Synthesis of sulfamide derivatives

In a 2-neck round bottom flask, equipped with a nitrogen flux, and placed in an ice-bath, introduced 1 mmol of CSI dissolved in anhydrous acetone (5 mL). 1 mmol of sulfanilamide was liquefied in 5 mL of anhydrous acetone. The solution of sulfanilamide was added dropwise to the stirring CSI, and then the reaction components were stirred for 30 min. After completion of the reaction monitored by TLC that indicated the formation of a carbamate intermediate, 1 mmol of trimethylamine was added to a stirring mixture of amine (1 mmol) and anhydrous acetone (5 mL). After 15 min of stirring, this latter was added dropwise to the formed carbamate intermediate. The completion of the reaction indicated by TLC was followed by an *in vacuo* evaporation. The obtained dry substance was then purified by column chromatography eluted with a 94:06 mixture of dichloromethane/methanol. Obtained pure fractions were then concentrated and dried yielding pure sulfamide derivatives.

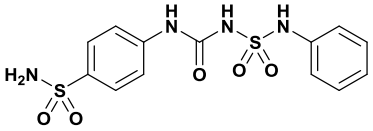

4-(3-(N-phenylsulfamoyl)ureido)benzenesulfonamide III.17a

$C_{13}H_{14}N_4O_5S_2$. **M**: 370,40 g.mol^{-1}. **Aspect:** Yellow powder. **Yield =** 80%. **M.p =** 184 – 186 °C; **R_f** = 0.35 (DCM/Methanol, 94:06).

IR (KBr, cm^{-1}) ν = 3238 (NH), 3075, 2924, 1707 (C=O), 1682, 1601, 1465, 1416, 1363 (SO_2), 1225, 1159 (SO_2); **^{1}H NMR (400 MHz, DMSO-*d*$_6$) δ** = 6.60 (d, 2H, *J* = 8.8 Hz, $2H_{Ar}$ (Sulfanilamide)), 6.86 (s, 2H, NH_2), 7.16 – 7.24 (m, 3H, $3H_{Ar}$ (Aniline)), 7.36 – 7.40 (m, 2H, H_{Ar} (Aniline)), 7.45 (d, 2H, *J* = 8.4 Hz, $2H_{Ar}$ (Sulfanilamide)); **^{13}C NMR (101 MHz, DMSO-*d*$_6$) δ** = 113.08, 121.44, 127.87, 130.08, 130.69, 152.17; **Anal. Calc. for $C_{13}H_{14}N_4O_5S_2$** C, 42.16; H, 3.81; N, 15.13; Found C, 42.18; H, 3.84; N, 15.15.

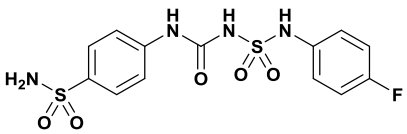

4-(3-(N-(4-fluorophenyl)sulfamoyl)ureido)benzenesulfonamide III.17b

$C_{13}H_{13}FN_4O_5S_2$. **M**: 388,39 g.mol^{-1}. **Aspect:** Yellow powder. **Yield =** 75%. **M.p =** 172 – 174 °C; **R_f =** 0.36 (DCM/Methanol, 94:06).

IR (KBr, cm^{-1}) ν = 3242 (NH), 2927, 1681 (C=O), 1600, 1509, 1415, 1370 (SO_2), 1230, 1168 (SO_2); **^{1}H NMR (400 MHz, DMSO-*d*$_6$) δ** = 6.66 – 6.69 (m, 4H, 4H_{Ar} (4-fluoroaniline)), 7.34 (s, 1H), 7.35 – 7.42 (m, 2H), 7.47 (d, 1H, *J* = 1.2 Hz), 7.49 – 7.51 (m, 6H); **^{13}C NMR (101 MHz, DMSO-*d*$_6$) δ** = 113.08, 121.44, 127.87, 130.08, 130.69, 152.17; **Anal. Calc. for $C_{13}H_{13}FN_4O_5S_2$** C, 40.20; H, 3.37; N, 14.43; Found C, 40.22; H, 3.41; N, 14.50.

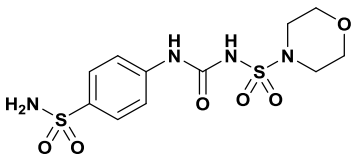

N-((4-sulfamoylphenyl)carbamoyl)morpholine-4-sulfonamide III.17c

$C_{11}H_{16}N_4O_6S_2$. **M**: 364,39 g.mol^{-1}. **Aspect:** Yellow powder. **Yield =** 80%. **M.p =** 184 – 186 °C; **R_f =** 0.30 (DCM/Methanol, 94:06).

IR (KBr, cm^{-1}) ν = 3220 (NH), 3070, 2900, 1704 (C=O), 1674, 1661, 1475, 1420, 1360 (SO_2), 1277, 1160 (SO_2); **^{1}H NMR (400 MHz, DMSO-*d*$_6$) δ** = 2.96 (t, 4H, 2CH_2), 3.64 (t, 4H, 2CH_2), 6.00 (s, 1H, NH-SO_2), 6.89 (s, 2H, NH_2), 7.64 (d, 2H, 2H_{Ar}), 7.70 (d, 2H, 2H_{Ar}), 8.9 (s, NH-CO); **^{13}C NMR (101 MHz, DMSO-*d*$_6$) δ** = 44.30, 65.00, 118.00, 129.40, 136.50, 142.60, 152.00; **Anal. Calc. for $C_{11}H_{16}N_4O_6S_2$** C, 36.26; H, 4.43; N, 15.38; Found C, 36.29; H, 4.49; N, 15.41.

3. Biological evaluation methods

3.1. DPPH assay

The radical scavenging activity of newly synthesized compounds was determined using the DPPH (2,2-diphenyl-1-picrylhydrazyl) assay, following the protocol outlined by Blois *et al.* [91]. A DPPH solution at a concentration of 0.1 mM was prepared by dissolving 4 mg of DPPH in 100 mL of methanol and stored at -20°C in the dark. For each compound, 40 µL of the compound solution (dissolved in methanol, except for compounds **III.9c** and **III.9g**, which were dissolved in a 8:2 mixture of CH_3OH/DMSO due to poor solubility in methanol) was mixed with 160 µL of the prepared DPPH solution, and the mixture was left at room temperature for 30min in the dark. The DPPH test was conducted on different concentration of the synthesized compounds (3.2, 1.6, 0.8, 0.4, 0.2, 0.1, 0.05 mM) and was repeated 3 times for each concentration. BHA (butylhydroxyanisole) and BHT (butylhydroxytoluene) were employed as positive

controls. The absorbance values were measured at 517 nm using a microplate reader (PerkinElmer (Enspire)).

The inhibition percentage was calculated using the formula:

Inhibition (%) = (A0 - As) / A0 × 100

where A0 is the absorbance of the negative control (mixture of 160 µL of methanol and 40 µL of product) and As is the absorbance of the tested sample. A mixture of 160 µL of methanol and 40 µL of product was used as blank.

Finally, IC_{50} values, representing the concentration at which 50% inhibition occurred, were determined based on the calculated inhibition percentages.

3.2. ABTS assay

ABTS was dissolved in water to a 7 mM concentration. ABTS radical cation ($ABTS^{\bullet 1}$) was produced by reacting ABTS solution with 2.45 mM potassium persulfate (final concentration) solution. The mixture was allowed to stand in the dark for about 12 to 16h [100].

Absorbance of final ABTS solution was adjusted to 0.7 ± 0.02 at 734 nm.

160 µL of ABTS solution is added to 40 µL of dissolved product and left for 10 min in the dark at room temperature. Synthesized compounds were dissolved in methanol. BHA (butylhydroxyanisole) and BHT (butylhydroxytoluene) were employed as positive controls. The ABTS test was conducted on different concentration of the products (3.2, 1.6, 0.8, 0.4, 0.2, 0.1, 0.05 mM)) and was repeated 3 times. Different absorbance values were measured at 734 nm using a microplate reader (PerkinElmer (Enspire)).

IC_{50} values were determined based on the inhibition percentages calculated employing the following formula:

Inhibition (%) = (A0 - As)/A0 × 100

In which A0 and As corresponds respectively to the absorbance of the negative control and the absorbance of the tested products.

3.3. α-amylase inhibition test

α-amylase inhibitory activity was evaluated using the iodine/potassium iodide (IKI) method [107] with some modifications.

The iodine/potassium iodide (IKI) solution was prepared by adding 3 g of potassium iodide to 100 mL of H_2O resulting in a homogeneous KI solution to which was added 127 mg of iodine. The enzyme was prepared in a buffer phosphate solution (pH: 6.9) with 6 mM of NaCl (35.1 mg in 100 mL of buffer phosphate solution).

The test was performed on solutions of the synthesized products with different concentrations (1.6, 0.8, 0.4, 0.2, 0.1, 0.05, 0.025 mM) and repeated 3 times for each concentration.

In a 96-well microplate, was added 25µL of the dissolved product and 50µL of enzyme (1U). Then, the mixture was incubated for 10 min at a temperature of 37°C. Afterwards, 50µL of amidon solution (0.1%) was added to the mixture. This step was followed by a second incubation of 10 min at 37°C. Finally, 25µl of HCl (1M) and 100µl of the previously prepared IKI solution were added, and the absorbance was lectured at a wavelength of 630 nm.

IC_{50} values were determined based on the inhibition percentages calculated employing the following formula:

Inhibition (%) = $1-[(A_c-A_e)-(A_s-A_b)/(A_c-A_e)]$

with: $\mathbf{A_c}$=Absorbance [Amidon + IKI + HCl + volume of solvent in which the product is solubilized + volume of buffer phosphate]

$\mathbf{A_e}$=Absorbance [Enzyme + Amidon + IKI + HCL + volume of solvent in which the product is solubilized]

As=Absorbance [Enzyme + product +Amidon + IKI + HCl]

$\mathbf{A_b}$=Absorbance [Product +IKI + 125µl buffer phosphate]

4. *In silico* methods

4.1. Molecular docking studies

The X-ray crystal structures of the Quercetin-Xanthine oxidase (PDB: 3NVY) [101], Hypoxanthine-Xanthine oxidase (PDB: 3NRZ) [92] and Acarbose-α-amylase (PDB: 1B2Y) [93]. (Obtained from the Protein Data Bank) were utilized in this study. The protein structures underwent preparation using the Protein Preparation Wizard within the Schrödinger Suites software package. Three-dimensional structures of the synthesized compound derivatives were generated using Maestro software and further refined through optimization with Ligprep, employing the OPLS3e force field [108].

Subsequently, the prepared PDB files for both proteins and synthesized compounds were subjected to the docking process. Docking simulations were performed using Glide software using extra precision [109]. The output files containing the docked compounds bound to their respective proteins were visualized using Chimera X [110] giving the disposition of studied compounds within the receptors as well as the interactions with the active sites.

4.2. Density Functional Theory (DFT)

DFT calculations were performed using Gaussian 09 package [98].

The molecular geometry of all synthesized compounds was optimized in the gas phase using Density Functional Theory (DFT) with the B3LYP method. Optimization utilized the 6-31G (d,p) basis set. Additionally, Frontier Molecular Orbitals (FMOs) and global reactivity descriptors, including the Highest Occupied Molecular Orbital (HOMO) and Lowest Unoccupied Molecular Orbital (LUMO) were computed. These calculations involved determining the energy gap and chemical reactivity descriptors at the DFT/B3LYP/6-31G (d,p) level of theory [111].

Conclusions and perspectives

Given the continuous evolution of pathologies and the increasing resistance of certain diseases to drugs, the synthesis of new compounds that could have pharmacological activities remains a major priority for researchers worldwide, particularly for chemists. This is aimed at increasing human life expectancy and protecting public health.

The development of a therapeutically active molecule can be achieved through several ways, including the modification of existing molecules or even the combination and modification of structural motifs already known for their activities against certain diseases.

The development of potential drug-candidates through modification of known pharmacophores was the main axis of this study that led to the easy synthesis of four different groups of compounds, three of them derived from β-enaminone and one derived from sulfamide.

The biological evaluation gave promising results for 4-hydroxyquinolone analogues as antioxidant agents, in addition, the same activity was found to be encouraging in several derivatives of the β-enaminocarboxamide series, the hydroxylated derivative of acridine and one sulfamide-derived molecule.

Antidiabetic acitivity evaluation of β-enaminocarboxamides screened by α-amylase inhibition measurement revealed that these molecules holds a high potential as α-amylase inhibitors with results better then the standard Acarbose.

As future perspectives and in view of the obtained results, it would be encouraging to continue these studies by:

- Conducting a molecular dynamics simulation study for compounds exhibiting the best activities.
- Carrying out an *in vivo* evaluation of the effect of β-enaminocarboxamides giving the best α-amylase inhibition.
- Biological evaluation of the synthesized compounds activities against other drug targets that match with the exhibited activities of their analogues.
- The synthesis of further derivatives of sulfamide-based molecules and their antioxidant evaluation.
- The synthesis of a new series of acridines analogous to the hydroxylated acridine derivative that showed promising antioxidant activity.
- Evaluation of the antioxidant activity of 4-hydroxyquinolone analogues and β-enaminocarboxamides using other described and efficient assays to confirm the potency of these series as antioxidant agents.

On the other hand, the use of microwave in the synthesis of bioactive entities showed a great interest in the field of green chemistry, with its ability to overcome many problems related to

conventional chemistry, from minimizing toxic wastes and the employment of hazardous solvents and reagents, to the production of different structural cores in improved yields within a very short reaction time.

The high interest of microwave-assited synthesis was clearly shown in this manuscript since it was employed as a new procedure to generate both 4-hydroxyquinolone and acridine analogues.

As a future perspective, we look forward elaborating synthetic protocols that involve the beneficial use of microwaves.

Bibliography

1. (a) C.O. Kappe, Angewandte *Chemie International Edition*. **2004**, 43, 6250. (b) B.L. Hayes, *Aldrichimica Acta*. **2004**, 37, 66. (c) B. Stanovnik, J. Svete, *Chemical Reviews*. **2004**, 104, 2433.

2. D.J. Hogenkamp, T.B.C. Johnstone, J-C. Huang, W-Y. Li, M. Tran, E.R. Whittemore, R.E. Bagnera, K.W. Gee, *Journal of Medicinal Chemistry*. **2007**, 50, 3369.

3. P. Subramamiam, C. Ramasubbu, S. Athiramu, S. Arumugam, M. Alagumuthu, *Archiv der Pharmazie - Chemistry in Life Science*. **2018**, 352, 1800244.

4. P. Beauverger, G. Begis, S. Biscarrat, O. Duclos, G. McCort, US8975250B2. (**2015**).

5. (a) J. Jampilek, *Molecules*, **2019**, 24, 3839. (b) T. Su, J. Zhu, R. Sun, H. Zhang, Q. Huang, X. Zhang, R. Du, L. Qiu and R. Cao, *European Journal of Medicinal Chemistry*. **2019**, 178, 154. (c) M. Vilková, M. Hudáčová, N. Palušeková, R. Jendželovský, M. Almáši, T. Béres, P. Fedoročko and M. Kožurková, *Molecules*. **2022**, 27, 2883.

6. T. Khamkhenshorngphanuch, K. Kulkraisri, A. Janjamratsaeng, N. Plabutong, A. Thammahong, K. Manadee, S. Na Pombejra and T. Khotavivattana, *Molecules*. **2020**, 25, 3059.

7. S. Banu, R. Bollu, R. Bantu, L. Nagarapu, S. Polepalli, N. Jain, R. Vangala and V. Manga, *European Journal of Medicinal Chemistry*. **2017**, 125, 400.

8. I.V. Ukrainets, O.V. Mospanova, N.L. Bereznyakova and O.O. Davidenko, *Journal of Organic and Pharmaceutical Chemistry*. **2015**, 13, 41.

9. H. Takagaki, Y. Aoki and M. Ishiwara, US8980914, (**2015**).

10. K. Arya and M. Agarwal, *Bioorganic Medicinal Chemistry Letters*. **2007**, 17, 86.

11. a) W. Denny, *Current Medicinal Chemistry*. **2002**, 9, 1655. b) M. Alvala, S. Bhatnaga, A. Ravi, V.U. Jeankumar, T.H. Manjashetty, P. Yogeswari, D. Sriram, *Bioorganic Medicinal Chemistry Letters*. **2012**, 22, 3256. (c) J. Hornedo, D.A. Van Echo, *Pharmacotherapy*. **1985**, 5, 78.

12. K.H. Oudah, M.A. Najm, A.B. Roomi, H.A. Al-saidy, F.M. Awadallah, *Systematic Reviews in Pharmacy*, **2020**, 11, 1473.

13. A. Ovung, J. Bhattacharyya, *Biophysical reviews*. **2021**, 13, 259.

14. P. Saha, *Diabetes*. **2020**, 2, 2605.

15. F.M. Hamed, B.A. Hassan, M.M. Abdulridha, *International Journal of Pharmaceutical Research*. **2020,** 12, 2512.

16. P.K. Bangalore, S.K. Vagolu, R.K. Bollikanda, D.K. Veeragoni, P.C. Choudante, S. Misra, D. Sriram, B. Sridhar, S. Kantevari, *Journal of Natural Products*. **2020**, 83, 1, 26.

17. R. Kumar, N. Saha, P. Purohit, S.K. Garg, K. Seth, V.S. Meena, S. Dubey, K. Dave, R. Goyal, S.S. Sharma, U.C. Banerjee, A.K. Chakraborti, *European Journal of Medicinal Chemistry*. **2019**, 182, 111601.

18. (a) N.D. Eddington, D.S. Cox, R.R. Roberts, J.P. Stables, C.B. Powell, K.R. Scott, *Current Medicinal Chemistry*. **2000**, 7, 417. (b) T. Heinbockel, Z-J. Wang, P.L. Jackson-Ayotunde, *Pharmaceuticals*. **2014**, 7, 1069.

19. Z.J. Wang, L. Sun, P.L. Jackson, K.R. Scott, T. Heinbockel, *Journal of Pharmacology and Experimental Therapeutics*. **2011**, 336, 916.

20. (a) I.J. Amaye, T. Heinbockel, J. Woods, Z. Wang, M. Martin-Caraballo, P. Jackson-Ayotunde, *International Journal of Environmental Research and Public Health*. **2018**, 15, 1784. (b) Isis J. Amaye, Patrice L. Jackson-Ayotunde, Miguel Martin-Caraballo, *Bioorganic Medicinal Chemistry*. **2022**, 65, 116766.

21. B. Kumar, S. Singh, I. Skvortsova, V. Kumar, *Current Medicinal Chemistry*. **2017**, 24, 4729.

22. M.M. Ghorab, F.A. Ragab, H.I. Heiba, M.G. El-Gazzar, M.G.M. El-Gazzar, *Bioorganic Medicinal Chemistry Letters*. **2018**, 28, 1464.

23. C.T. Supuran, *Current topics in medicinal chemistry*. **2007**, 7, 825.

24. W.M. Eldehna, M.F. Abo-Ashour, E. Berrino, D. Vullo, H.A. Ghabbour, S.T. Al-Rashood, G.S. Hassan, H.M. Alkahtani, A.A. Almehizia, A. Alharbi, H.A. Abdel-Aziz, C.T. Supuran, *Bioorganic Chemistry*. **2019**, 83, 549.

25. A.A. Alkhaldi, M.M. Al-Sanea, A. Nocentini, W.M. Eldehna, Z.M. Elsayed, A. Bonardi, M.F. Abo-Ashour, A.K. El-Damasy, M.S. Abdel-Maksoud, T. Al-Warhi, P. Gratteri, H.A. Abdel-Aziz, C.T. Supuran, R. El-Haggar, *European Journal Medicinal Chemistry.* **2020**, 207, 112745.

26. N.D. Eddington, D.S. Cox, M. Khurana, N.N. Salama, J.P. Stables, S.J. Harrison, A. Negussie, R.S. Taylor, U.Q. Tran, J.A. Moore, *European journal of medicinal chemistry*. **2003**, 38, 49.

27. J. Apraku, C.O. Okoro, *Bioorganic Medicinal Chemistry*. **2019**, 27, 161.

28. H.A. Stefani, I.M. Costa, D. de O Silva, *Synthesis*, **2000**, 2000, 1526.

29. K. Prabakaran, M. Sivakumar, M.S. Perumal, *Chemistry*. **2017**, 2, 2363.

30. M.M. Khodaei, A.R. Khosropour, M. Kookhazadeh, *Canadian journal of chemistry*. **2005**, 83, 209.

31. M.M. Khodaei, A.R. Khosropour, M. Kookhazadeh, *Synlett*, **2004**, 2004, 1980.

32. Z.H. Zhang, J.Y. Hu, *Journal of the Brazilian Chemical Society*. **2006**, 17, 1447.

33. R. Lenin, R.M. Raju, *Arkivoc*, **2007**, 13, 204.

34. M. Paira, R. Misra, S.C. Roy, *Indian Journal of Chemistry.* **2008**, 47B, 966.

35. I. Hideo, Y. Yoshifumi, K. Chihiro, *Journal of Organic Chemistry.* **1980**, *45*, 2938.

36. Y.L.N. Murthy, R. Venu, B. Govindh, B.S. Diwakar, K. Naga Lakshmi, E.R. Singh, *Asian Journal of Chemistry.* **2010**, 22, 3047.

37. A. Arcadi, G. Bianchi, S. Di Giuseppe, F. Marinelli, *Green Chemistry*. **2003**, 5, 64.

38. A. Shekhar, D.D. Pathak, *Journal of Chemistry*. **2011**, 8, 1632.

39. N. Sharma, U.K. Sharma, E.V. Van der Eycken, *Green techniques for organic synthesis and medicinal chemistry*. **2018**, 441.

40. C.K.Z. Andrade, A.S. Barreto, W.A. Silva, *Arkivoc*. **2008**, 12, 226.

41. B. Rechsteiner, F. Texier-Boullet, J. Hamelin, *Tetrahedron Lett.* **1993,** 34, 5071.

42. M.E.F. Braibante, H.T.S. Braibante, A.F. Morel, C.C. Costa, M.G. Lima, *Journal of the Brazilian Chemical Society*. **2006**, 17, 184.

43. H.T.S Braibante, M.E.F. Braibante, G.B. Rosso, D.A. Oriques, *Journal of the Brazilian Chemical Society*. **2003**, 14, 994.

44. S.A. Paveliev, O.O Segida, O.M. Mulina, I.B. Krylov, A.O. Terent'ev, *Organic Letters.* **2022**, 24, 8942.

45. T. Miura, Y. Funakoshi, M. Morimoto, T. Biyajima, M. Murakami, *Journal of the American Chemical Society.* **2012**, 134, 17440.

46. X. Kong, Y. Liu, L. Lin, Q. Chen, B. Xu, *Green Chemistry.* **2019**, 21, 3796.

47. E. Gayon, M. Szymczyk, H. Gérard, E. Vrancken, J.-M. Campagne, *Journal of Organic Chemistry*. **2012**, 77, 9205.

48. S. Karabiyikoglu, Y. Kelgokmen, M. Zora, *Tetrahedron.* **2015**, 71, 4324.

49. Q.H. To, Y.R. Lee, S.H. Kim, *Bulletin of the Korean Chemical Society*. **2012**, 33, 1170.

50. T.S. Jiang, Y. Zhou, L. Dai, X. Liu, X. Zhang, *Tetrahedron Lett*. **2019**, 60, 2078.

51. C. Caubere, P. Caubere, S. Ianelli, M. Nardelli, B. Jamart-Gregoire, *Tetrahedron.* **1994**, 50, 11903.

52. B. Jiang, Q.Y. Li, S.J. Tu, G. Li, *Organic Letters.* **2012**, 14, 5210.

53. H. Iida, Y. Yuasa, C. Kibayashi, *Journal of Organic Chemistry*, **2003**, 45, 2938.

54. F. Carta, A. Scozzafava, C.T. Supuran, *Expert opinion on therapeutic patents*. **2012**, 22, 747.

55. (a) A.S. Kalgutkar, R. Jones, A. Sawant, *RSC Drug Discovery Series.* **2010**, 1, 210. (b) J. Tréfouel, T.J. Tréfouel, *Revue des deux mondes, Hommes et mondes***. 1947**, 2, 132.

56. R. Hamdi, *Tetrahedron*. **2019**, 75, 6.

57. Y-F. Chen, P. Jobanputra, P. Barton, S. Bryan, A. Fry-Smith, *Health Technology Assessment.* **2008**, 12, 1.

58. J.C. Henquin, *Diabetologia.* **1992,** 35, 907.

59. W. Lv, X. Wang, Q. Xu, W. Lu, *Current topics in medicinal chemistry*. **2020**, 20, 37.

60. N.B. Arslan, et al. *Acta Crystallographica Section E.* **2011**, 67, 1736.

61. Z. Atlı Şekeroğlu, A. Gediz Ertürk, S. Kontaş Yedier, V. Şekeroğlu, *Drug and Chemical Toxicology*. **2019**, 44, 595.

62. S.K. Danek, D.P. Kelly, *Journal of Organic Chemistry.* **1991,** 56, 2031.

63. M. Abdaoui, G. Dewyenter, N-E. Aouf, G. Favre, A. Morère, J.L. Montero, *Bioorganic Medicinal Chemistry.* **1996,** 4, 1227.

64. K.F. Suzdalev, S.V. Den'kina, *Russian Journal of Organic Chemistry***. 2009,** 45, 1675.

65. A.V. Leontiev, H.V. Rasika Dias, D.M. Rudkevich, *Chemical Communications*. **2006**, 2006, 2887.

66. S.D. McDermott, W.J. Spillane, *New Journal for Organic Synthesis*. **1984,** 16, 49.

67. N. Khettache, A. Bendjeddou, M. Berredjem, Z. Regainia, V. Montero, C. Menut, J.Y. Winum, N-E. Aouf, *Synthetic Communication.* **2006**, 36, 2305.

68. A. Bouzina, M. Berredjem, B. Belhani, S. Bouacida, C. Marminon, M. Le Borgne, Z. Bouaziz and M. Aissaoui, *Research on Chemical Intermediates.* **2021**, 47, 1359.

69. A. Bouzina, A. Djemel, O. Sekiou, I. Kadi, Y.O. Bouone, R. Mansouri, Z. Aouf, M. Ibrahim-Ouali, and N.E. Aouf, *Journal of Molecular Structure.* **2023**, 1285, 135527.

70. (a) M. Zhang, A. Abdukader, Y. Fu, C. Zhu, *Molecules*. **2012**, 17, 2812. (b) A.P. Prakasham, M.K. Gangwar, P. Ghosh, *European Journal of Inorganic Chemistry*. **2019**, 2019, 295.

71. (a) D. Sharma, M. Kumar, S. Kumar, D. Bhattacherjee, A.K. Shil, M. Mehta, P. Das, *Synthetic Communications*. **2023**, 53, 953. (b) I.J. Amaye, R.D. Haywood, E.M. Mandzo, J.J. Wirick, P.L. Jackson-Ayotunde, *Tetrahedron*. **2021**, 83, 12, 131984.

72. S.B. Christensen, *Molecules*. **2021**, 26, 6057.

73. H.Turkmen, G. Zengin, B. Buyukkircali, *Bioorganic Chemistry.* **2011**, 39, 114.

74. R. Redjemia, A. Bouzina, Y.O. Bouone, A. Mansouri, R. Bahadi, M. Berredjem, *Research on Chemical Intermediates*. **2022**, 48, 4947.

75. A.R. Khosropour, M.M. Khodaei, M. Kookhazadeh, *Tetrahedron Letters.* **2004**, 45, 1725.

76. (a) T.B.C. Johnstone, H.S. McCarren, J. Spampanato, F.E. Dudek, J.H. McDonough, D. Hogenkamp, K.W. Gee, *Frontiers in Pharmacology*. **2019**, 10, 560. (b) S.H. Ruah, A. Hazlewood, P.D.J. Grootenhuis, F. Van Goor, A. Singh, J. Zhou, San Diego, J. McCartney, US8324242B2, (**2012**).

77. N.Y. Gorobets, S.A. Yermolayev, T. Gurley, A.A. Gurinov, P.M. Tolstoy, I.G. Shenderovich, N.E. Leadbeater, *Journal of Physical Organic Chemistry*. **2012**, 25, 287.

78. C.F. Macrae, I. Sovago, S.J. Cottrell, P.T.A. Galek, P. McCabe, E. Pidcock, M. Platings, G.P. Shields, J.S. Stevens, M. Towler, P.A. Wood, *Journal of Applied Crystallography*. **2020**, 53, 226.

79. (a) A. Mukherjee, S. Tothadi, S. Chakraborty, S. Ganguly, G.R. Desiraju, *CrystEngComm*. **2013**, 15, 4640. (b) H. Torii, T. Tatsumi, T. Kanazawa, M. Tasumi, *Journal of Physical Chemistry B.* **1998**, 102, 309.

80. J.M. Bothwell, S.W. Krabbe and R.S. Mohan, *Chemical Society Reviews*, **2011**, 40, 4649.

81. E. Lopez, S.C. Thorp and R.S. Mohan, *Polyhedron*. **2022**, 222, 115765.

82. S.R. Chia, S. Nomanbhay, J. Milano, K.W. Chew, C-H. Tan and K.S. Khoo, *Energies*. **2022**, 15, 7984.

83. W.A. Denny, *Medicinal Chemistry Reviews*. **2004**, 1, 257.

84. (a) M.A.P. Martins, C.P. Frizzo, D.N. Moreira, L. Buriol, P. Machado, *Chemical Reviews*. **2009**, 109, 4140. (b) A. Albert, The Acridines, second ed., Edward Arnold Ltd, London, 1996.

85. S. Lotfi, T. Rahmani, M. Hatami, B. Pouramiri, E. Tavakolinejad Kermani, E. Rezvannejad, M. Mortazavi, S. Fathi Hafshejani, N. Askari, N. Pourjamali, M. Zahedifar, *Bioorganic Chemistry*. **2020**, 105, 104457.

86. G.F. Makhaeva, S.V. Lushchekina, N.P. Boltneva, O.G. Serebryakova, E.V. Rudakova, A.A. Ustyugov, S.O. Bachurin, A.V. Shchepochkin, O.N. Chupakhin, V.N. Charushin, R.J. Richardson, *Bioorganic & Medicinal Chemistry*. **2017**, 25, 5981.

87. M. Elmusa, S. Elmusa, S. Mert, R. Kasımoğulları, F. Türkan, M.N. Atalar, E. Bursal, *Journal of Molecular Structure*. **2023**, 1274, 134553.

88. P. Varakumar, K. Rajagopal, B. Aparna, K. Raman, G. Byran, C.M. Gonçalves Lima, S. Rashid, M.H. Nafady, T.B. Emran, S. Wybraniec, *Molecules*. **2022**, 28 193.

89. M. Fonte, N. Tassi, P. Gomes, C. Teixeira, *Molecules*. **2021**, 26, 600.

90. A.B. Reitz , G.R. Smith, M.H. Parker, *Expert Opinion on Therapeutic Patents*, **2009**, 19, 1449.

91. M.S. Blois, *Nature*. **1958**, 181, 1199.

92. H. Cao, J.M. Pauff, R. Hille, *Journal of Biological Chemistry*. **2010**, 285, 28044.

93. V. Nahoum, G. Roux, V. Anton, P. Rouge, A. Puigserver, H. Bischoff, B. Henrissat, F. Payan, *Biochemical Journal*. **2000**, 346, 201.

94. A. Daina, O. Michielin, V. Zoete, *Scientific Reports.* **2017**, 7, 42717.

95. C.P. Chen, C.C. Chen, C.W. Huang, Y.C. Chang, *Molecules.* **2018**, 23, 911.

96. M.J. Waring, *Expert Opinions in Drug Discovery.* **2010**, 5, 235

97. C.A. Lipinski, *Drug Discovery Today: Technologies*. **2004**, 1, 337.

98. M.J. Frisch, Gaussian-09 Revision A.02, Gaussian Inc, Wallingford CT, **2009**.

99. M.A. Al-Mamary, Z. Moussa, *Antioxidants: Benefits, sources, mechanisms of action*. **2021**, 50, 318.

100. R. Re, N. Pellegrini, A. Proteggente, A. Pannala, M. Yang, C. Rice-Evans, *Free Radical Biology and Medicine*. **1999**, 26, 1231.

101. H. Cao, J.M. Pauff, R. Hille, *Journal of Natural Products*. **2014**, 77: 1693.

102. G.M. Sheldrick, *Acta Crystallographica*. **2015**, A71, 3.

103. O.V. Dolomanov, L.J. Bourhis, R.J. Gildea, J.A.K. Howard, H. Puschmann, *Journal of Applied Crystallography*. **2009**, 42, 339.

104. G.M. Sheldrick, *Acta Crystallographica*. **2015**, C71, 3.

105. CrysAlisPro Software System, Rigaku Oxford Diffraction. (**2022**).

106. F-J. Liu, T-T. Sun, Y-G. Yang, C. Huang, X-B. Chen, *RSC Advances*. **2018**, 8, 12635.

107. (a) G. Zengin, C. Sarikurkcu, A. Aktumsek, R. Ceylan, O. Ceylan, *Industrial Crops and Products.* **2014**, 53, 244. (b) R. Randhir, K. Shetty, *Asia Pacific Journal of Clinical Nutrition.* **2007**, 16, 382.

108. Release S, 2 LigPrep, version 3.4. Schrödinger, LLC, New York, NY, **2015**, 26400175.

109. R.A. Friesner, J.L. Banks, R.B. Murphy, T.A. Halgren, J.J. Klicic, D.T. Mainz, M.P. Repasky, E.H. Knoll, D.E. Shaw, M. Shelley, J.K. Perry, P. Francis, P.S. Shenkin, *Journal of Medicinal Chemistry*. **2004**, 47, 1739.

110. (a) E.C. Meng, T.D. Goddard, E.F. Pettersen, G.S. Couch, Z.J. Pearson, J.H. Morris, T.E. Ferrin, *Protein Science*. **2023**, 32, 4792. (b) E.F. Pettersen, T.D. Goddard, C.C. Huang, E.C. Meng, G.S. Couch, T.I. Croll, J.H. Morris, T.E. Ferrin, *Protein Science*. **2021**, 30, 70.

111. A.D. Becke, *The Journal of Chemical Physics*. **1993**, 98, 5648. (b) G. Zhang, C.B. Musgrave, *Journal of Physical Chemistry A*. **2007**, 111, 1554. (c) M.M. Francl, W.J. Pietro, W.J. Hehre, J.S. Binkley, M.S. Gordon, D.J. DeFrees, J.A. Pople, *The Journal of Chemical Physics*. **1982**, 77, 3654.

Appendix: Spectra

Spectra indexes

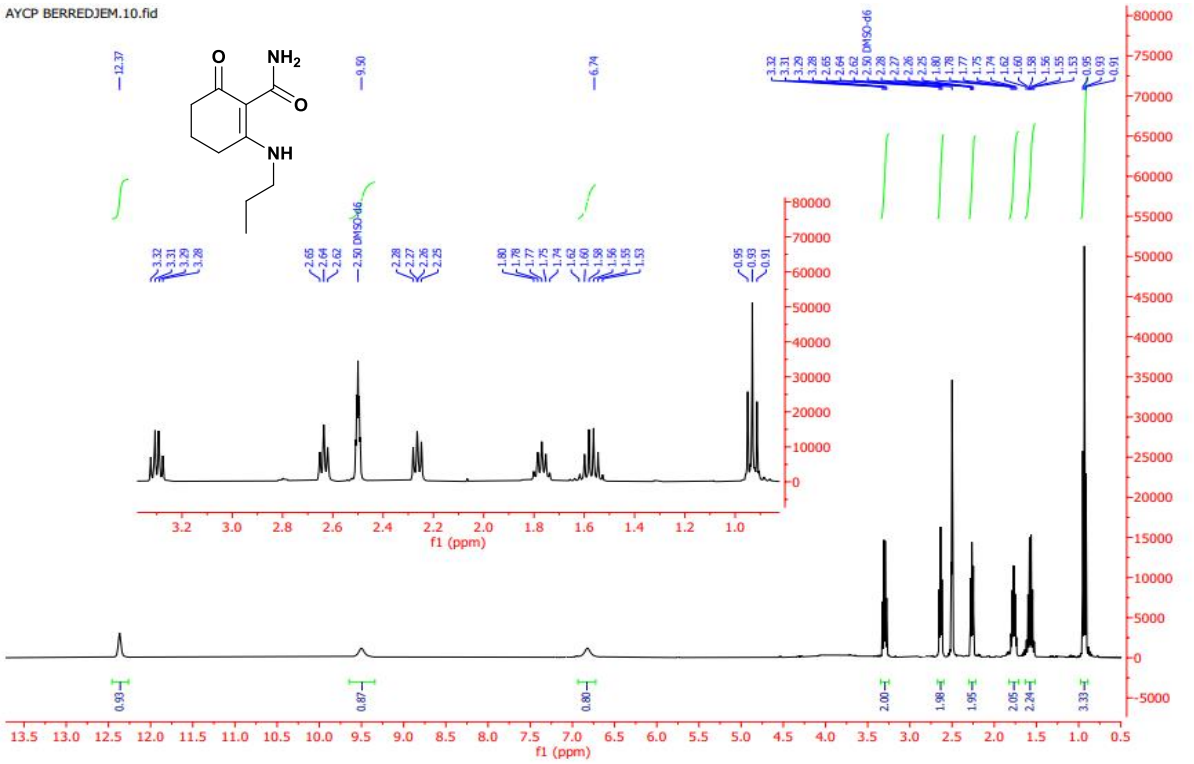

S1. ^{1}H NMR III.5a.

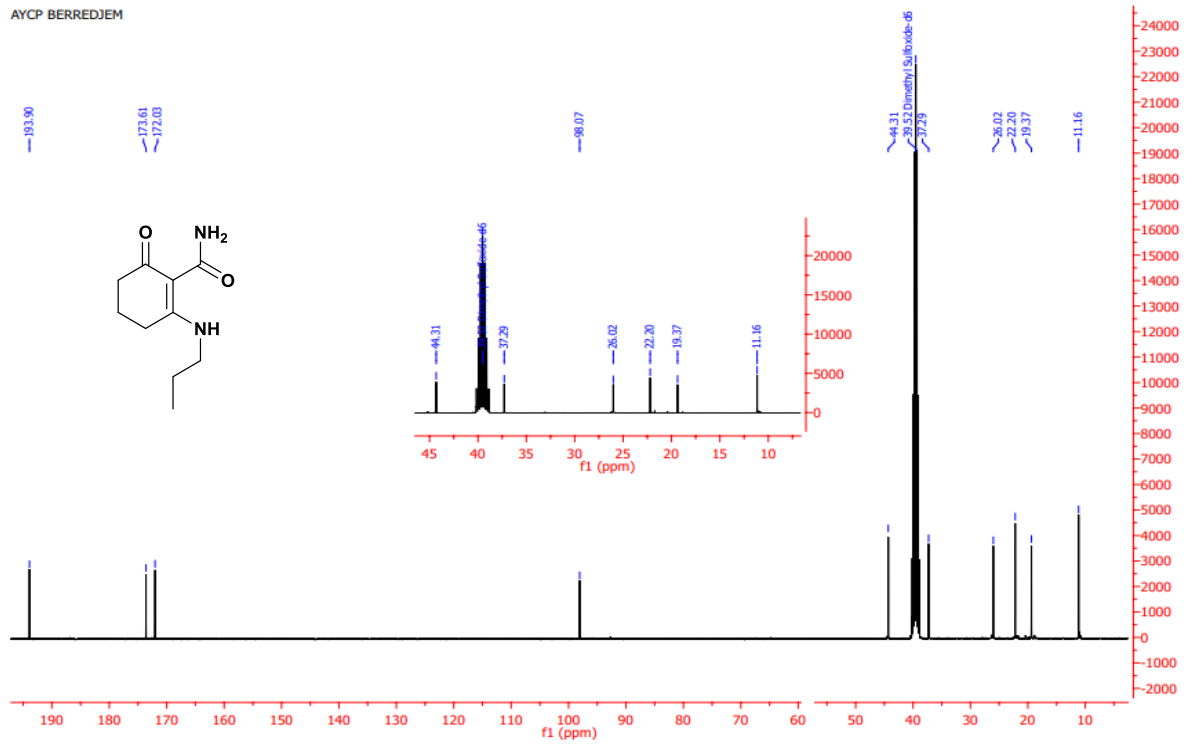

S2. ^{13}C NMR III.5a.

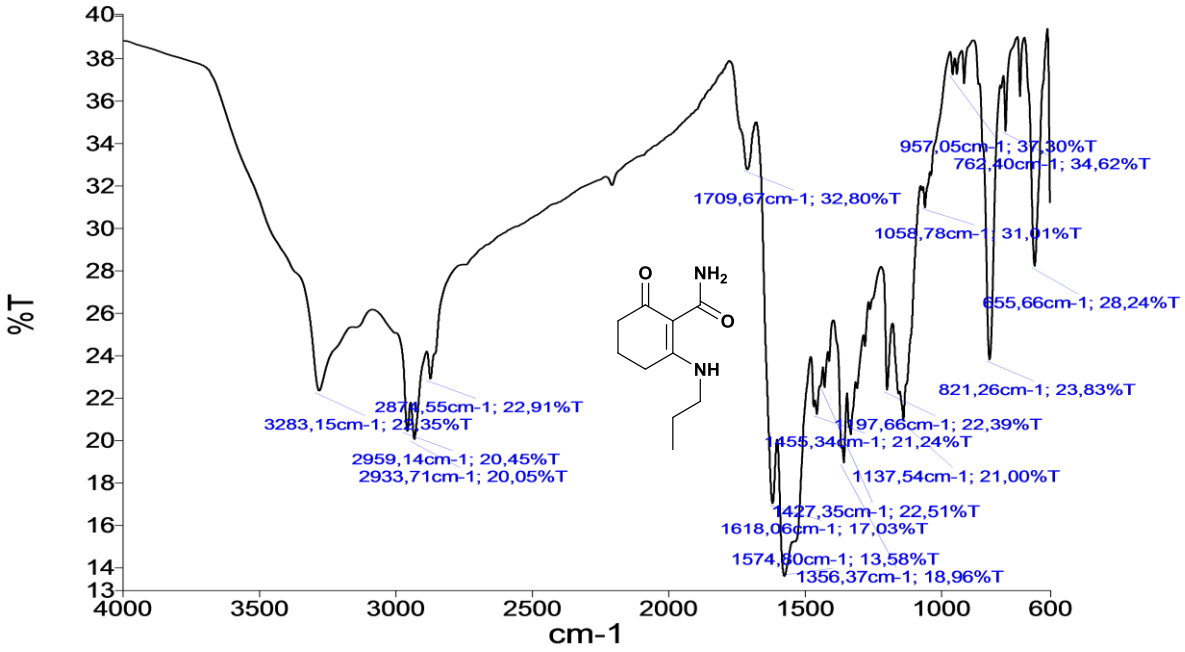

S3. IR III.5a.

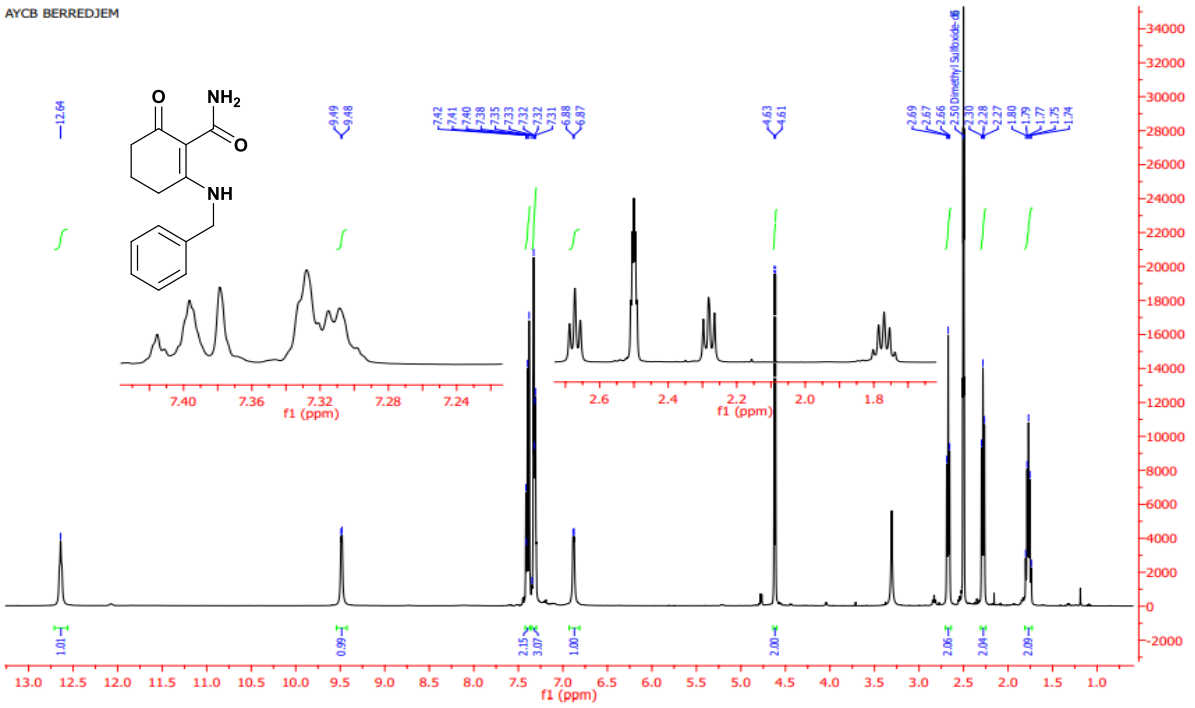

S4. ^{1}H NMR III.5d.

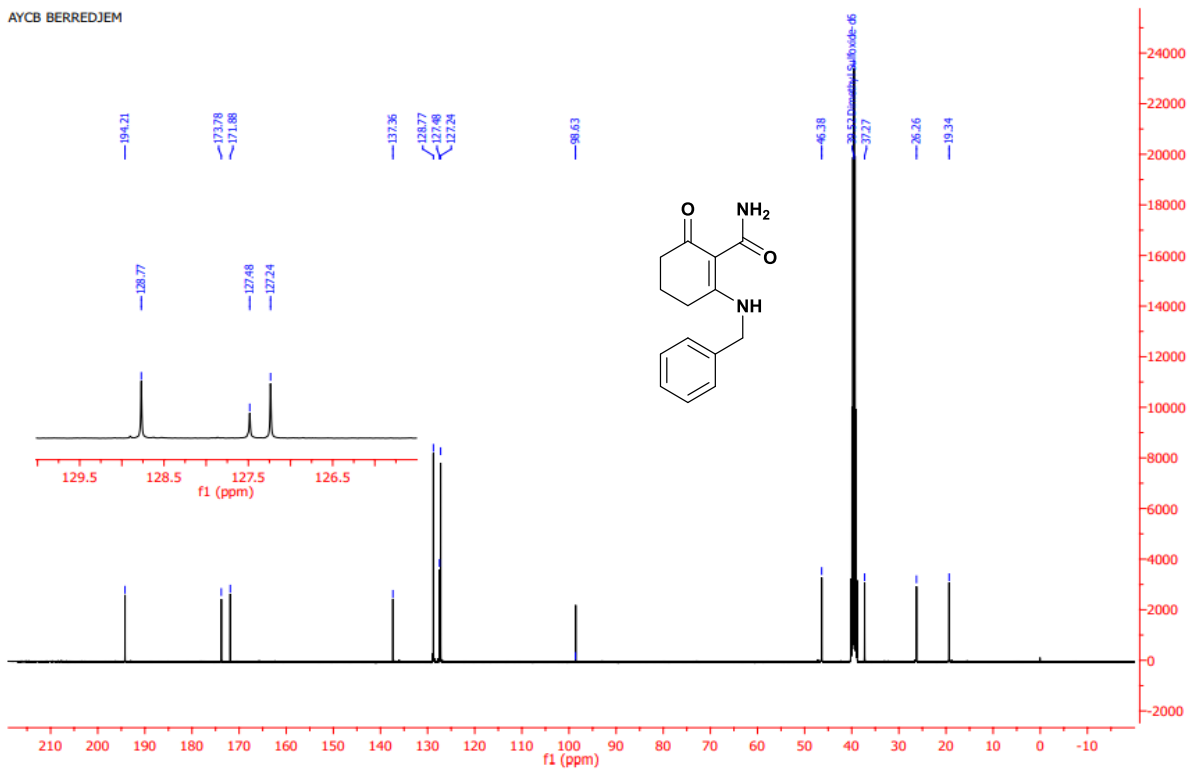

S5. ^{13}C NMR III.5d.

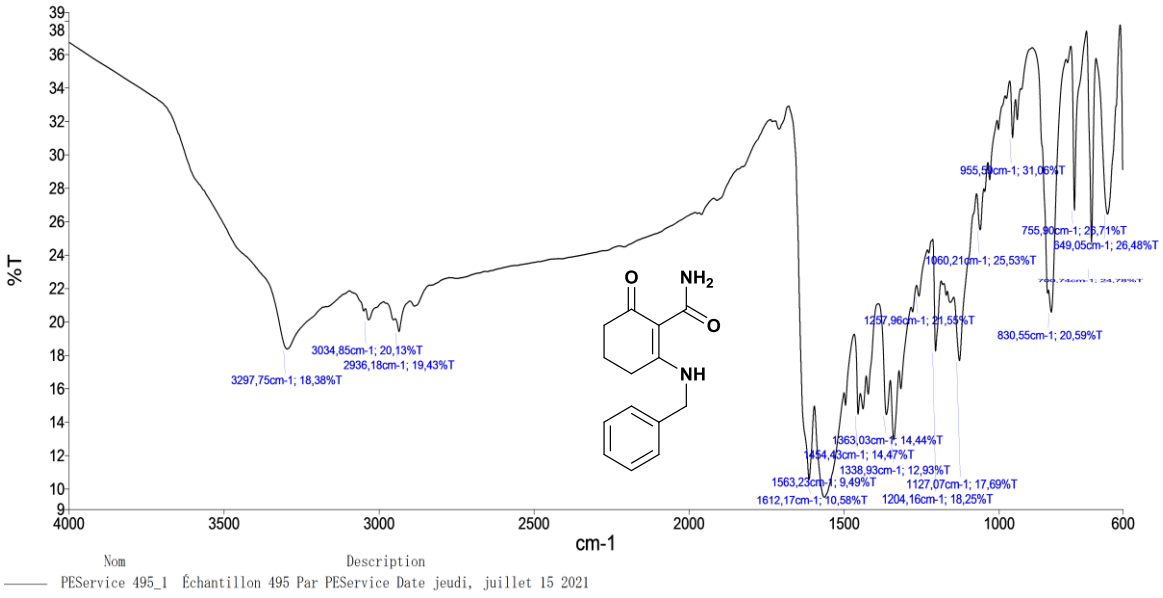

S6. IR III.5d.

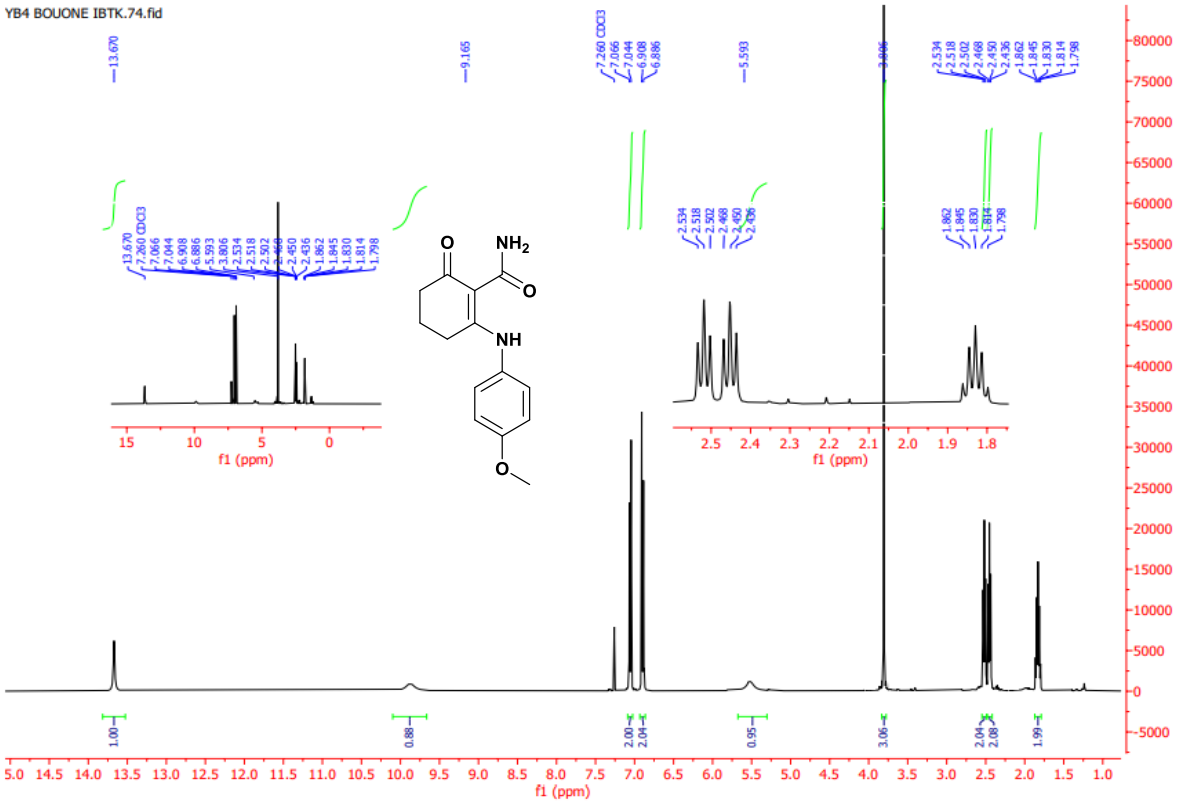

S7. ^{1}H NMR III.5h.

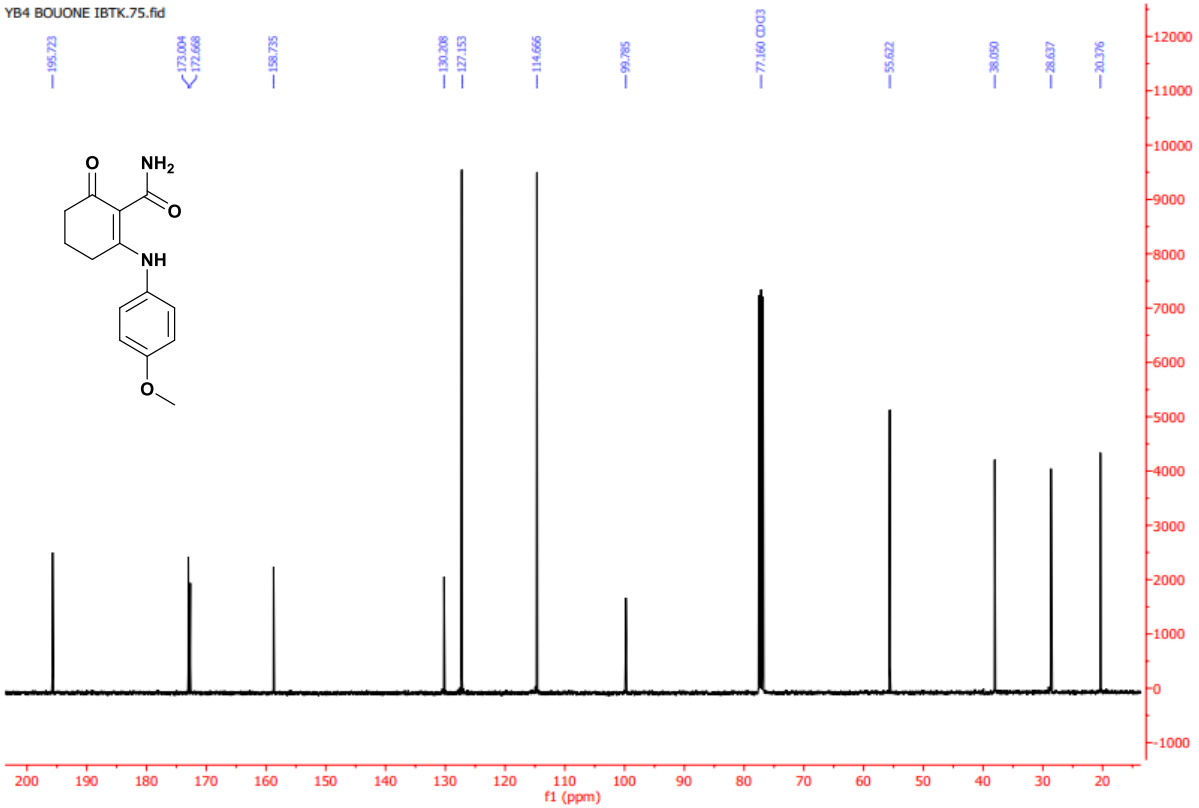

S8. ^{13}C NMR III.5h.

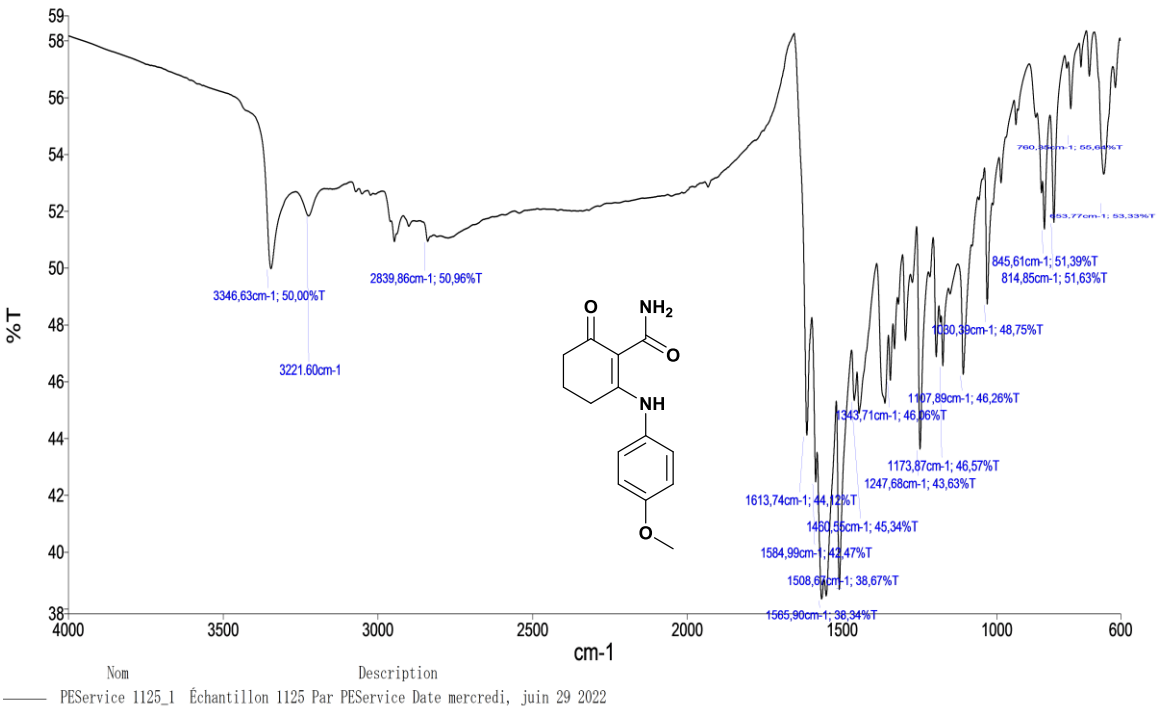

S9. IR III.5h.

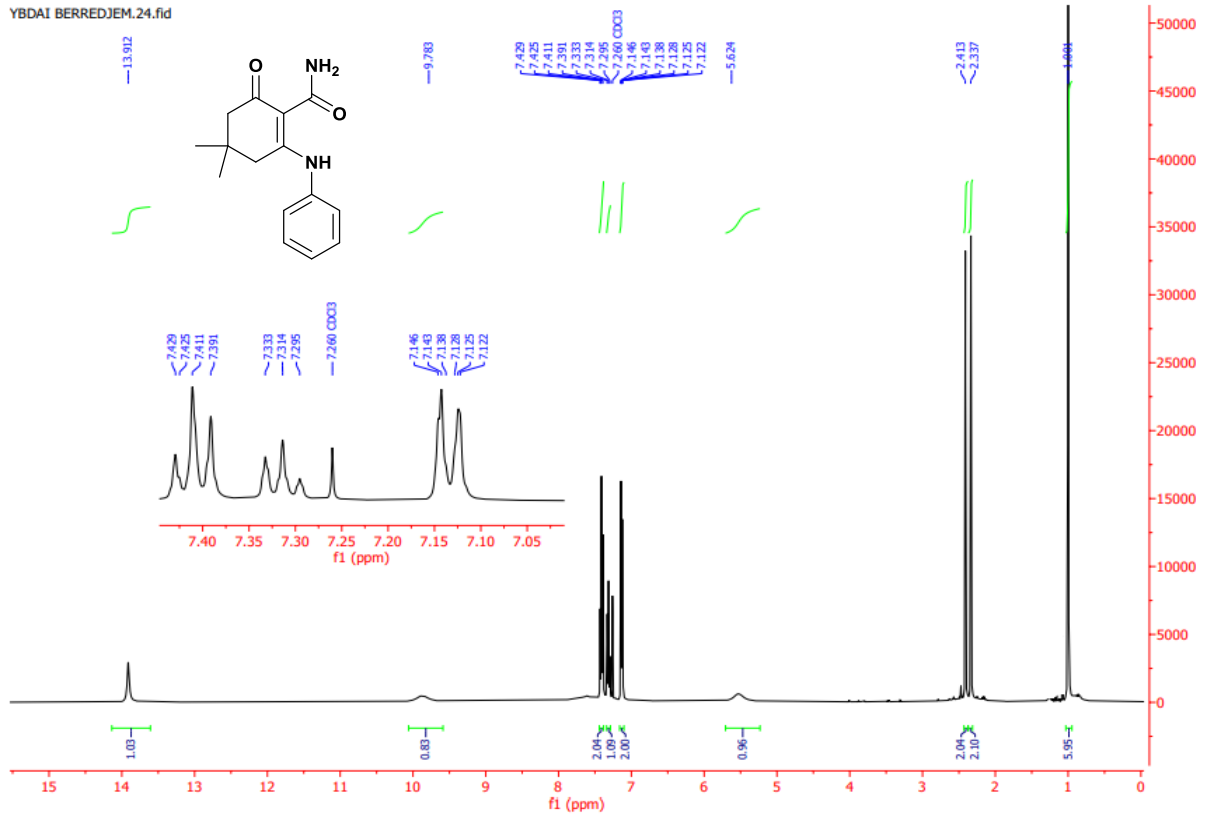

S10. ^{1}H NMR III.5k.

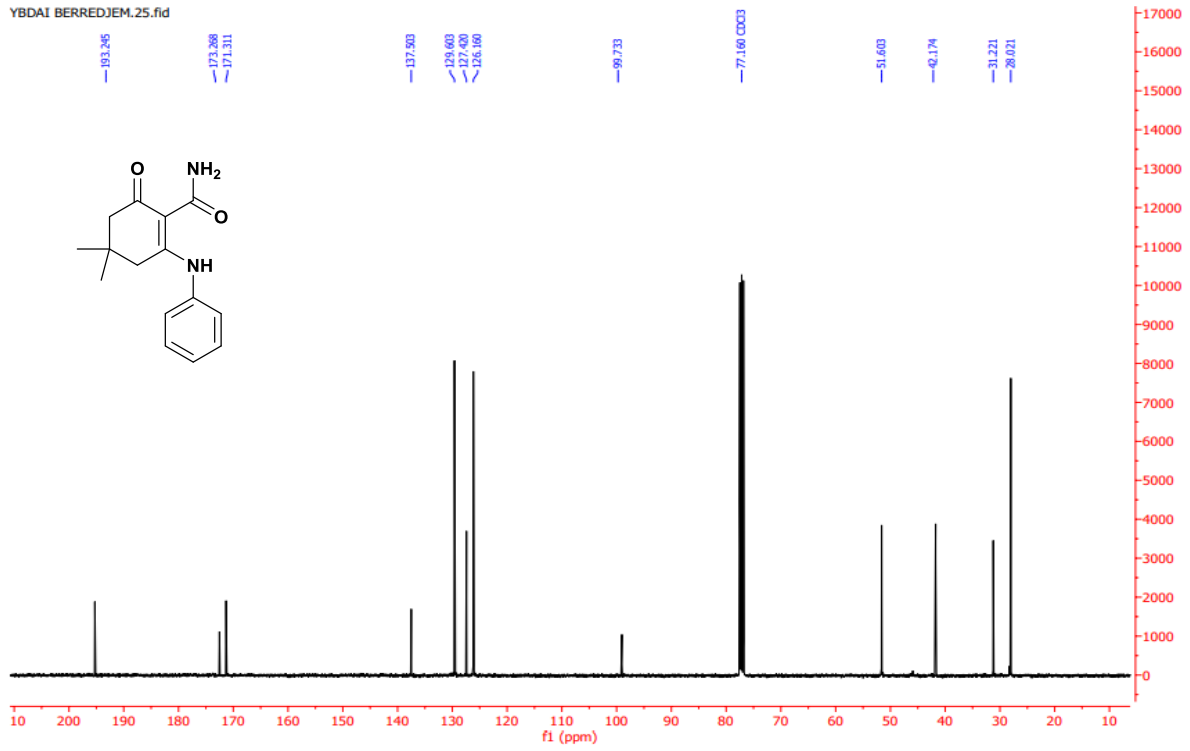

S11. ^{13}C NMR III.5k.

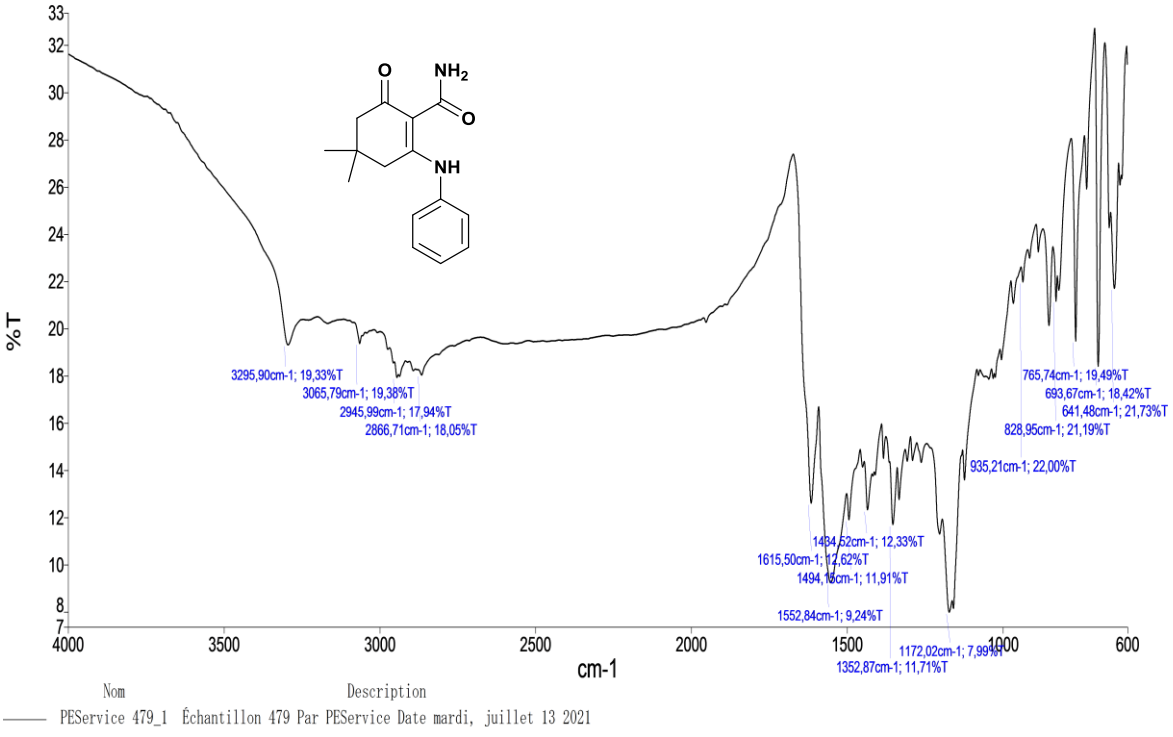

S12. IR III.5k.

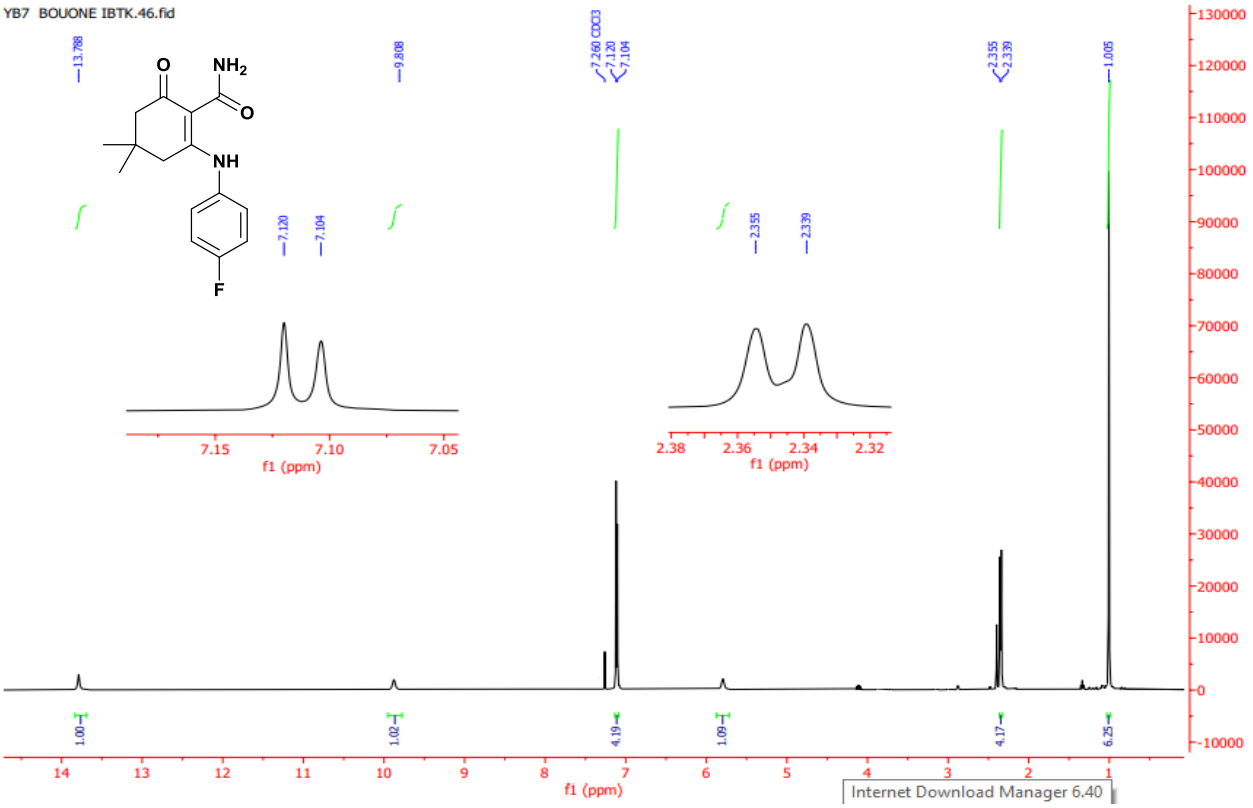

S13. ^{1}H NMR III.5m.

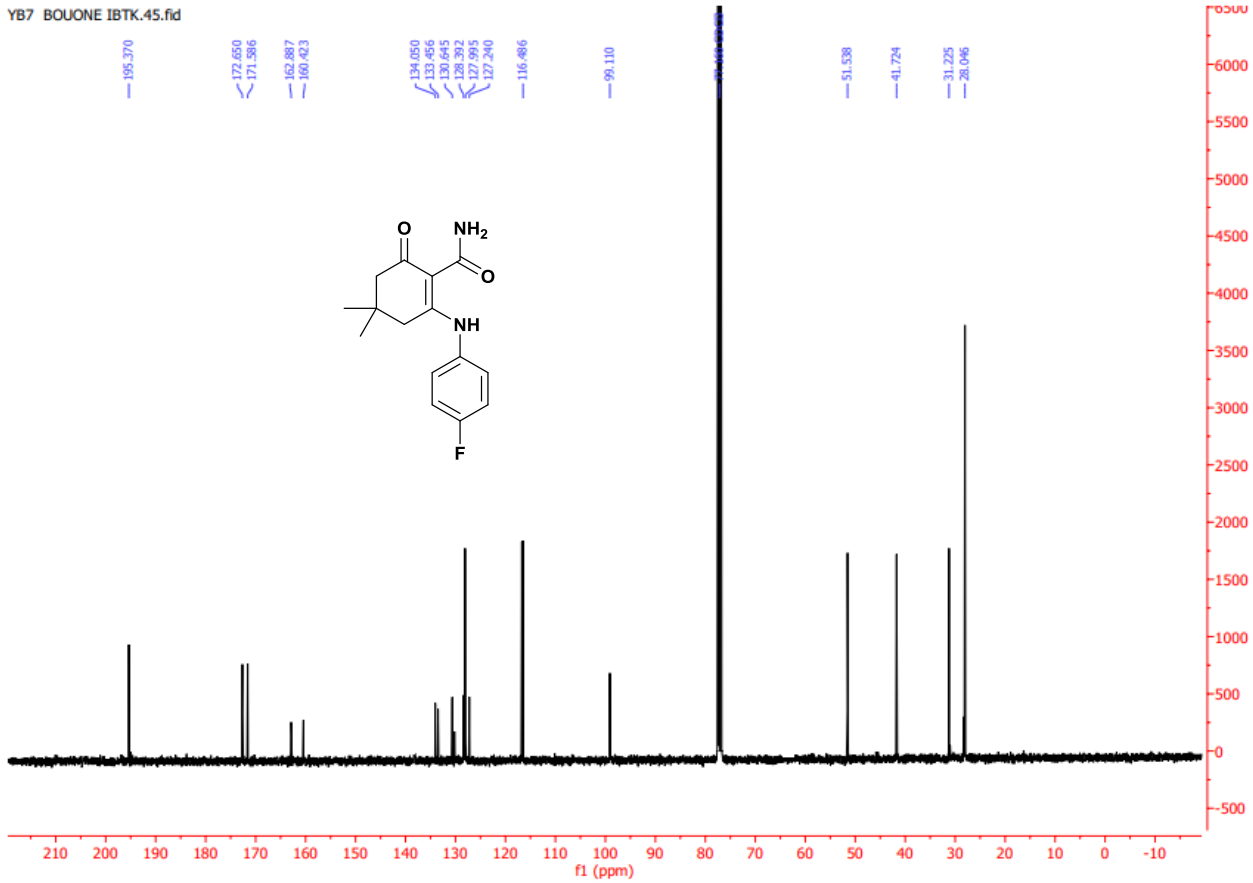

S14. ^{13}C NMR III.5m.

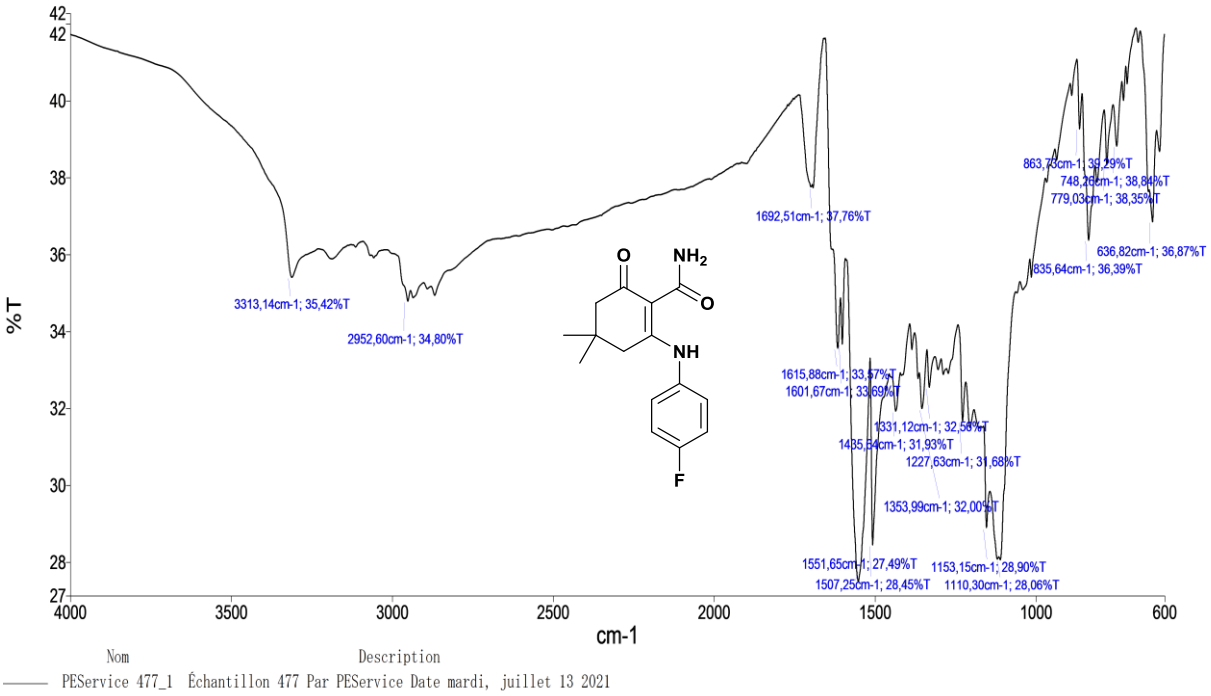

S15. IR III.5m.

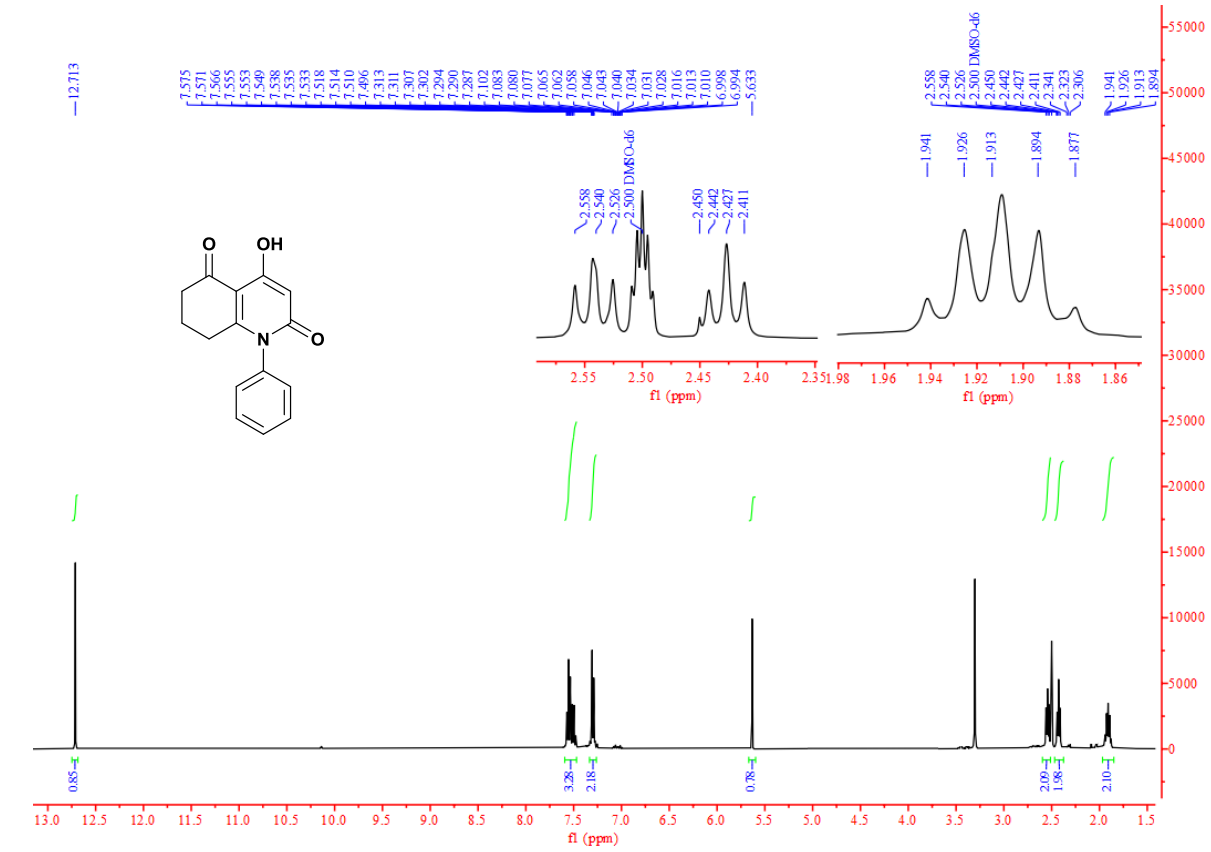

S16. ^{1}H NMR III.7a.

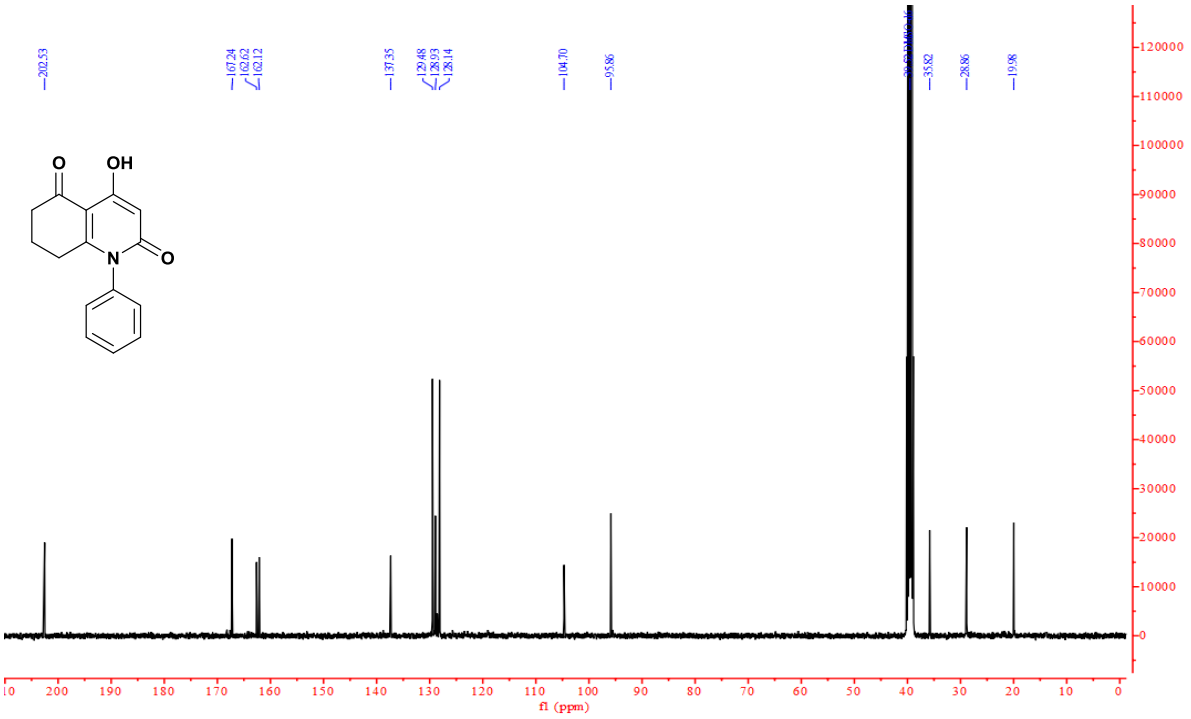

S17. ^{13}C NMR III.7a.

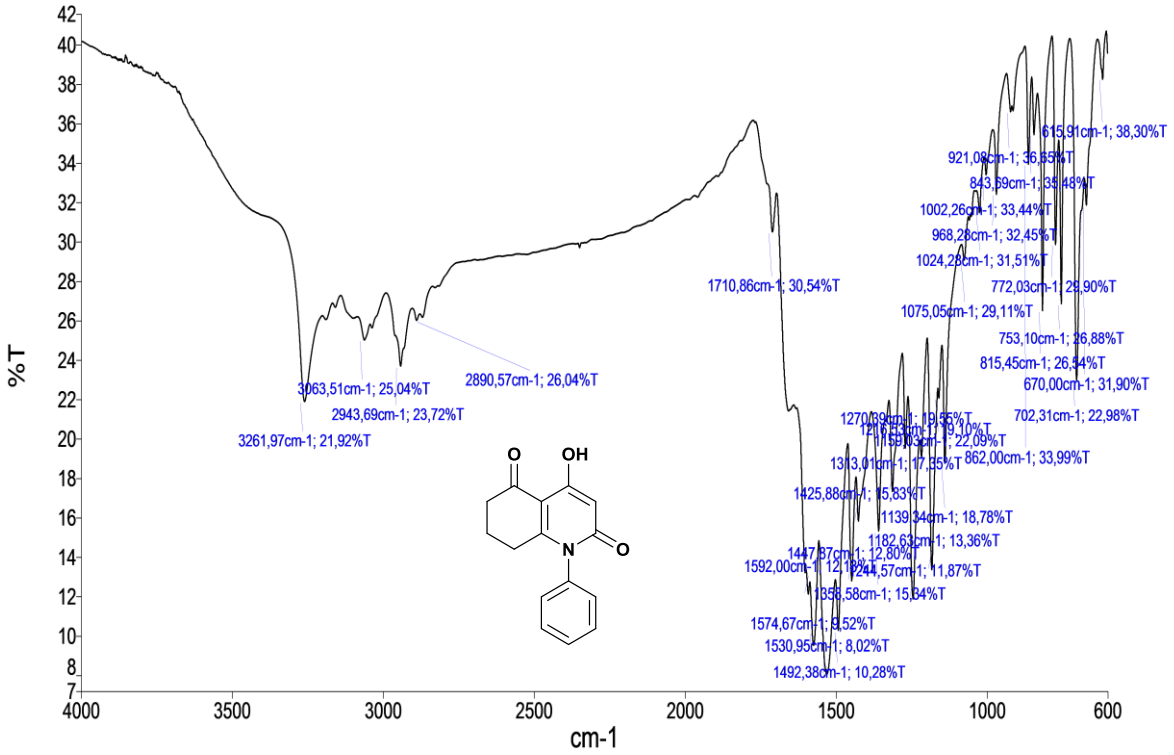

S18. IR III.7a.

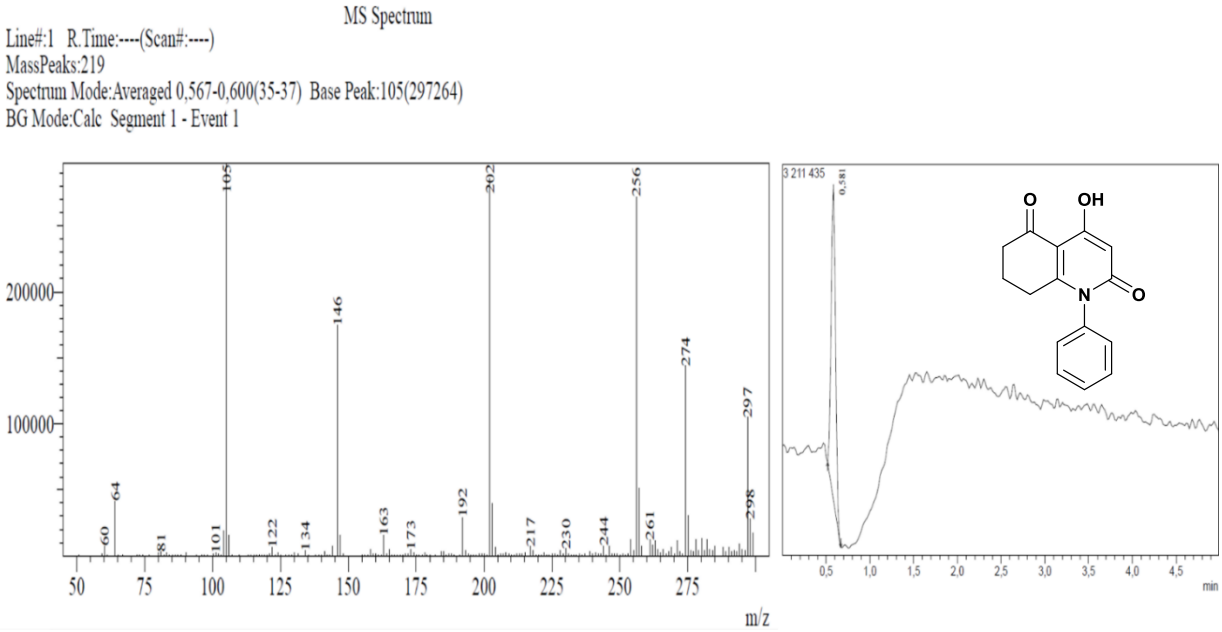

S19. LC-MS III.7a.

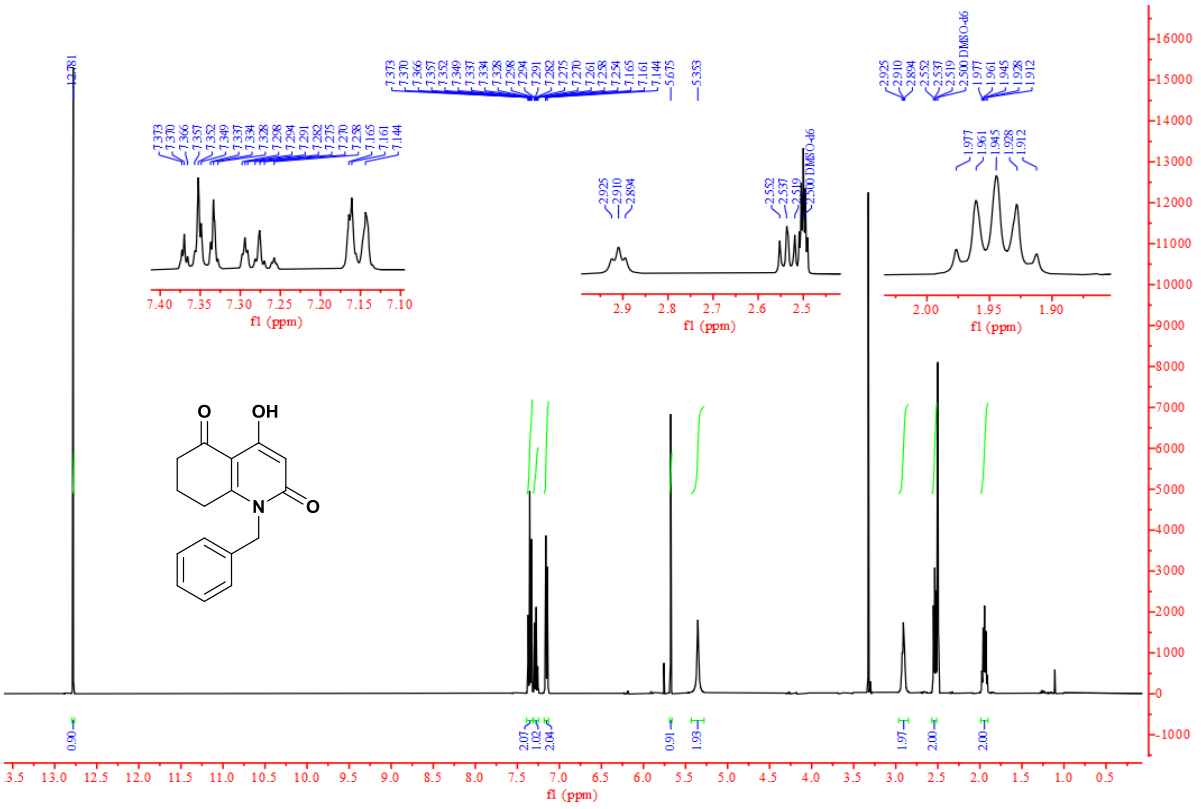

S20. ^{1}H NMR III.7b.

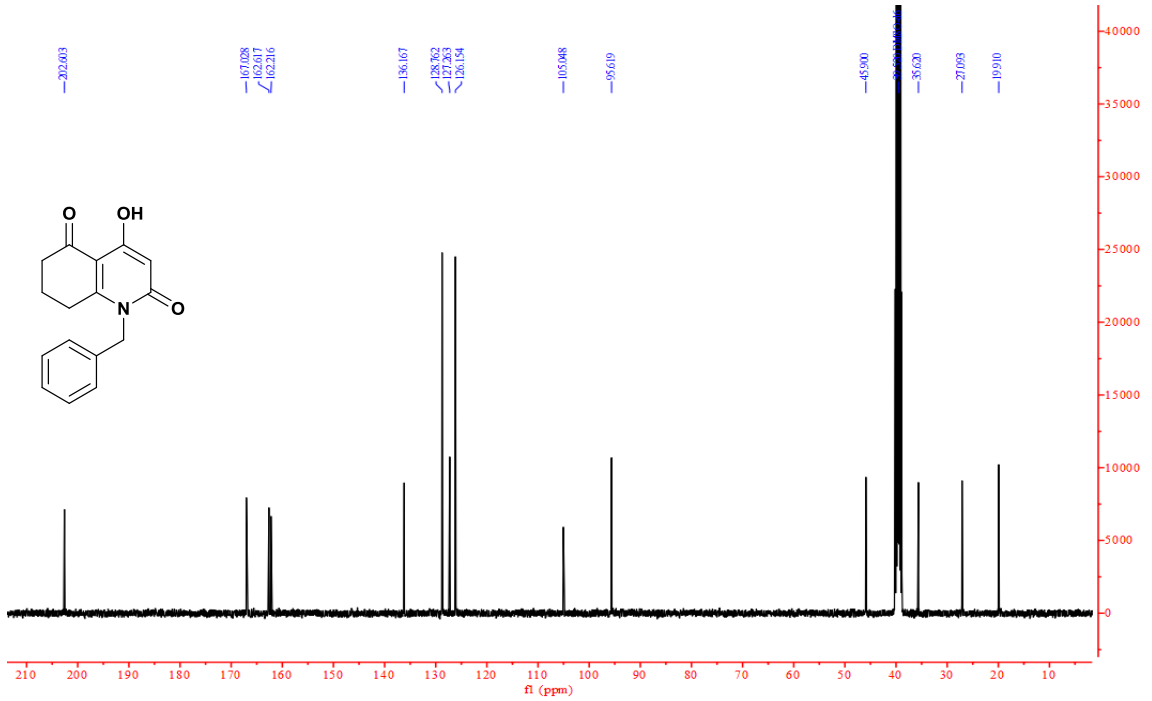

S21. ^{13}C NMR III.7b.

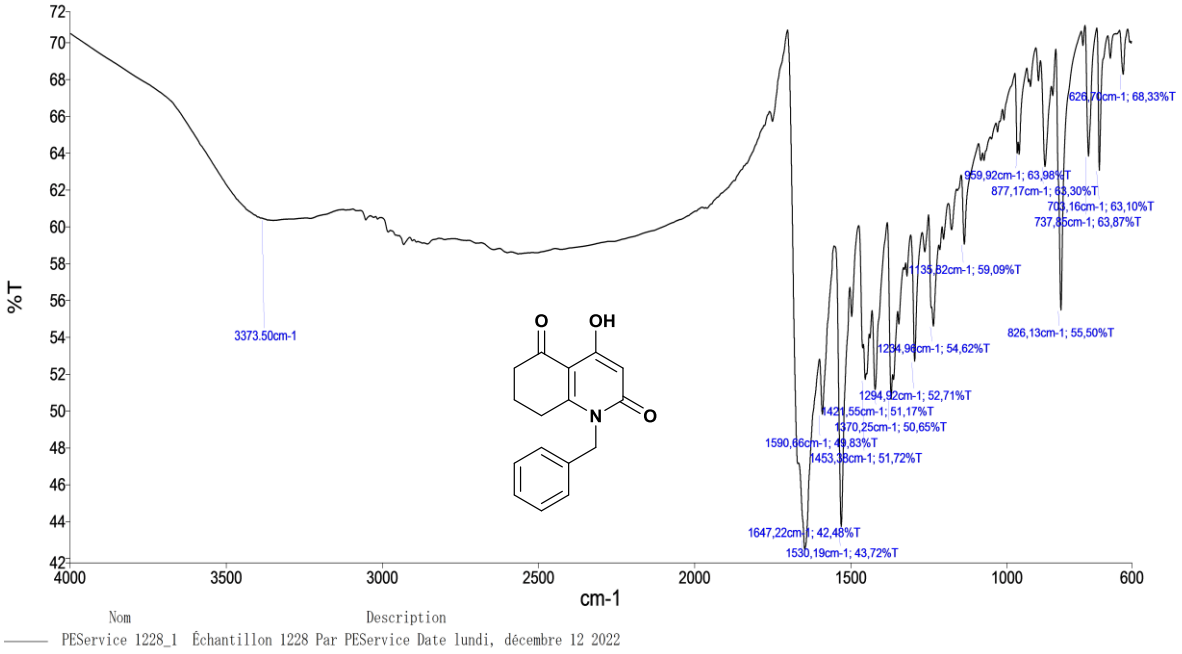

S22. IR III.7b.

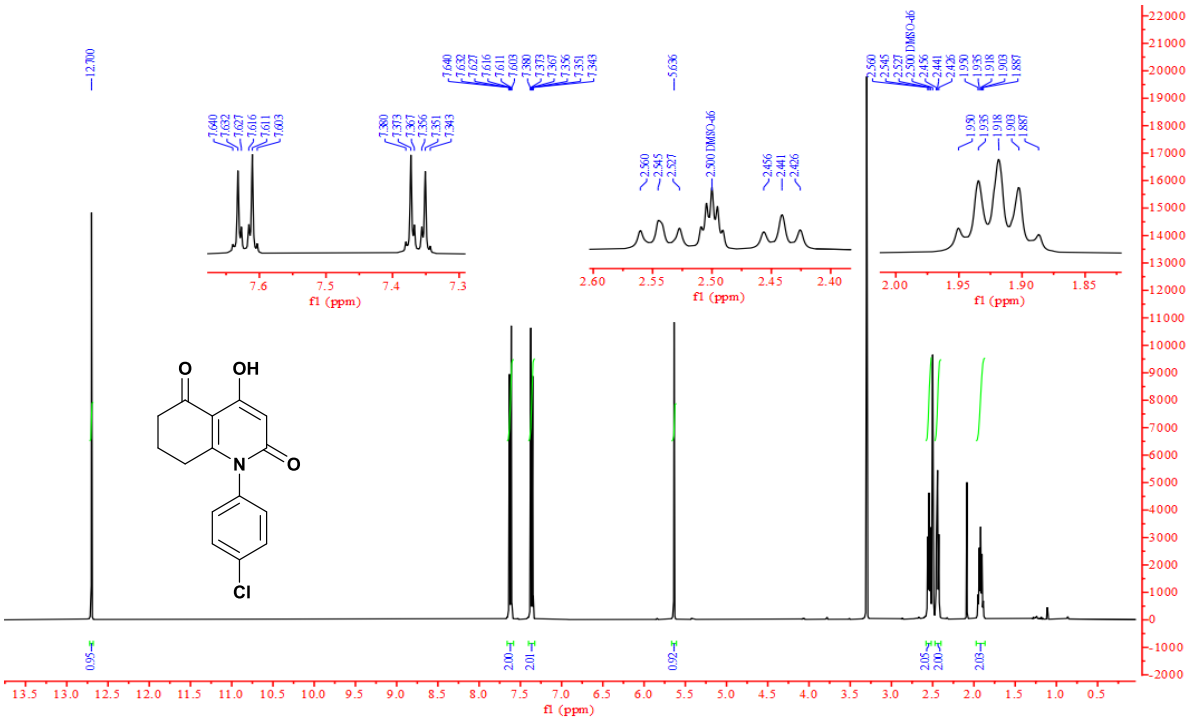

S23. ^{1}H NMR III.7d.

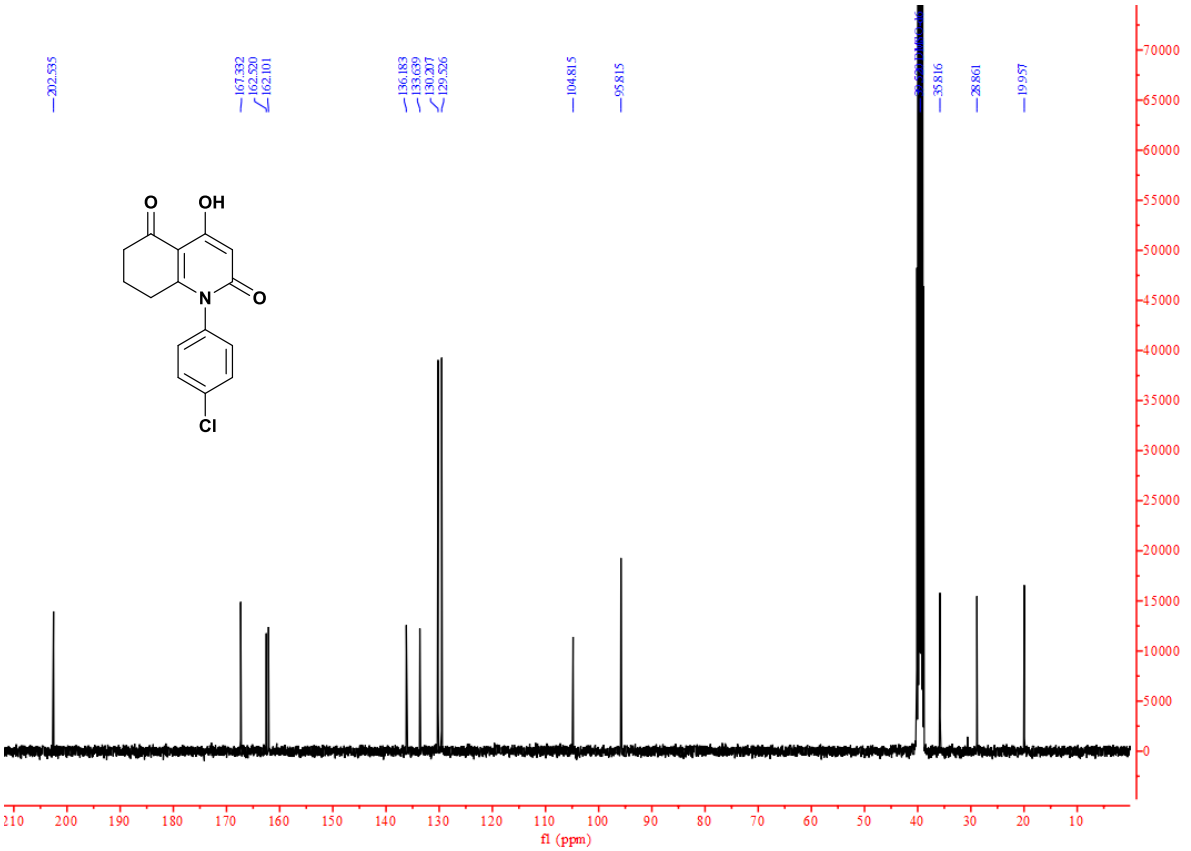

S24. ^{13}C NMR III.7d.

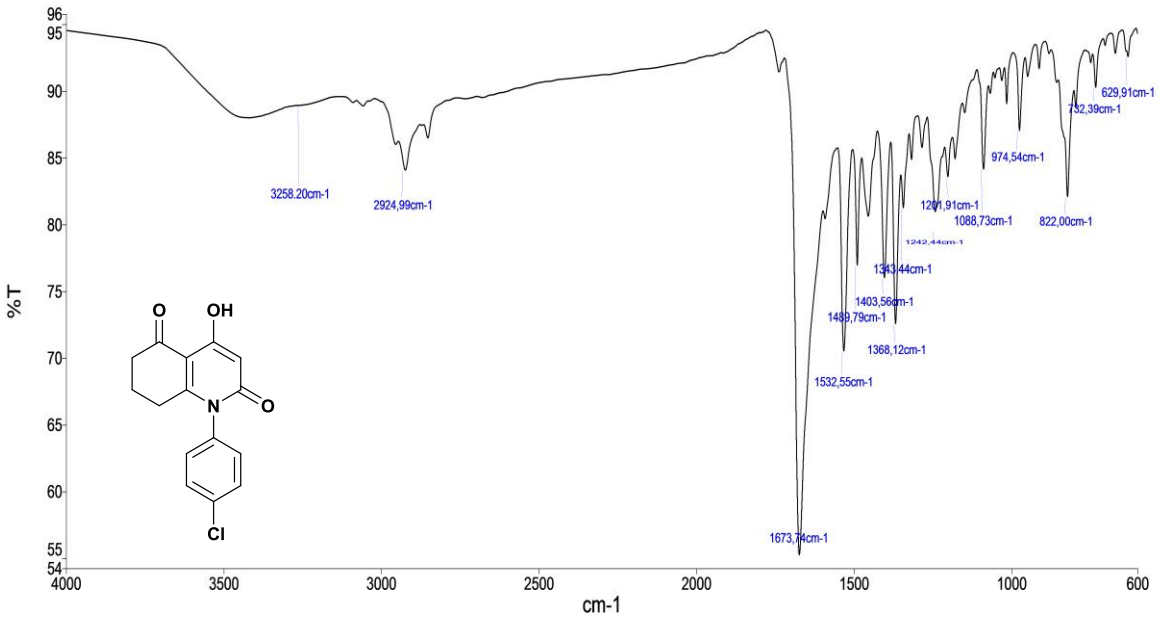

S25. IR III.7d.

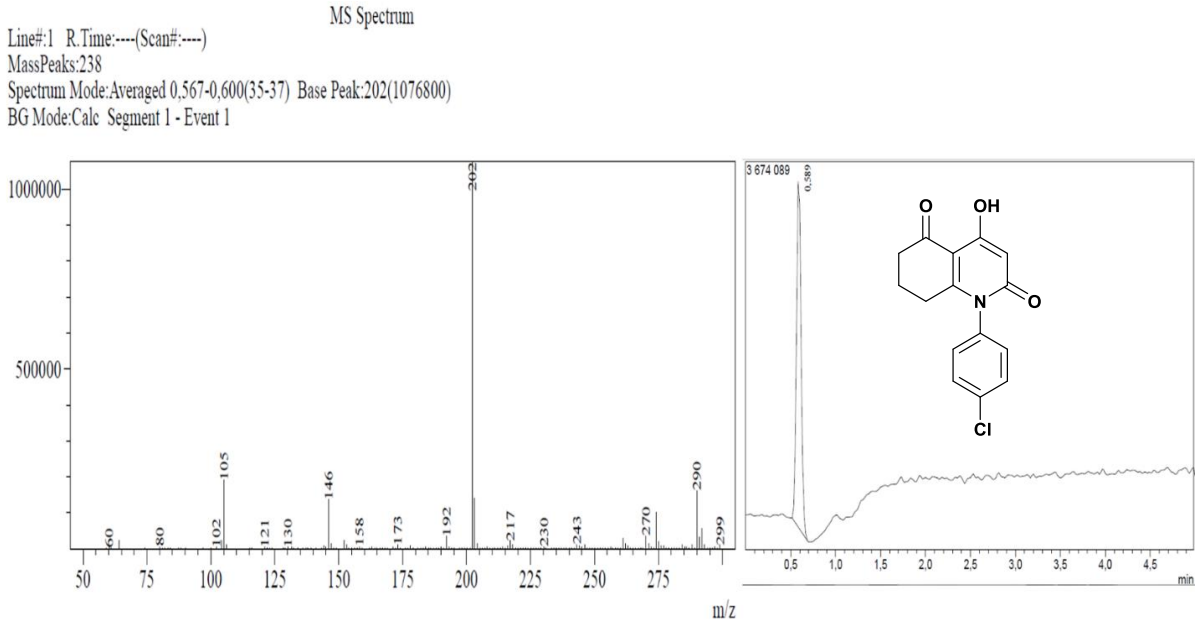

S26. LC-MS III.7d.

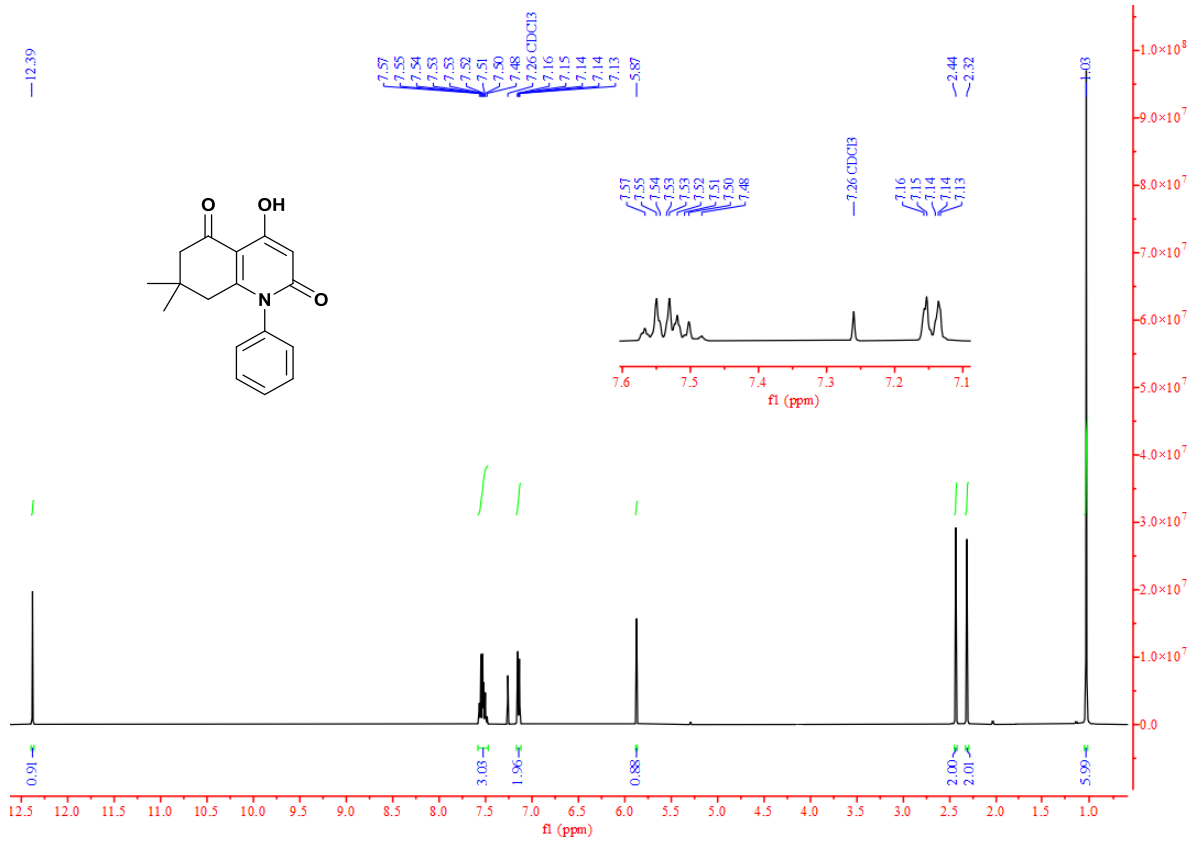

S27. ^{1}H NMR III.7h.

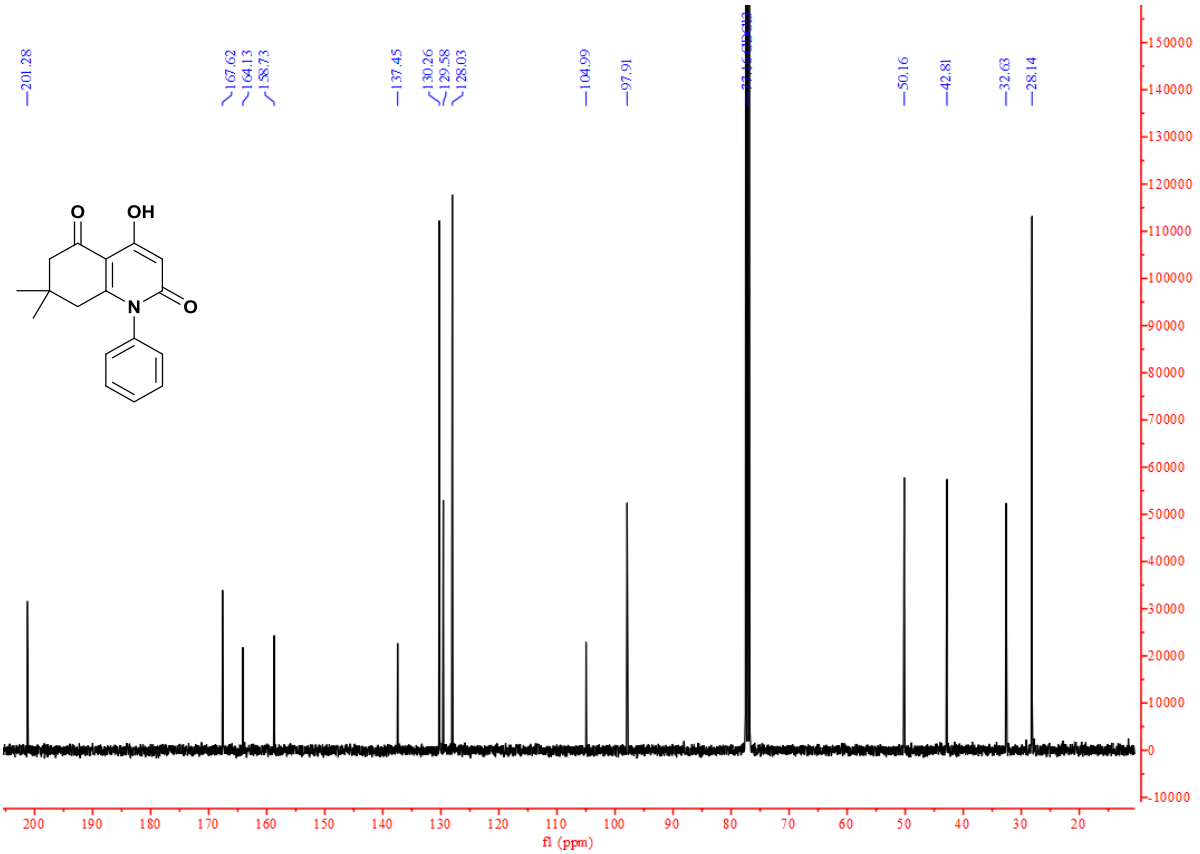

S28. ^{13}C NMR III.7h.

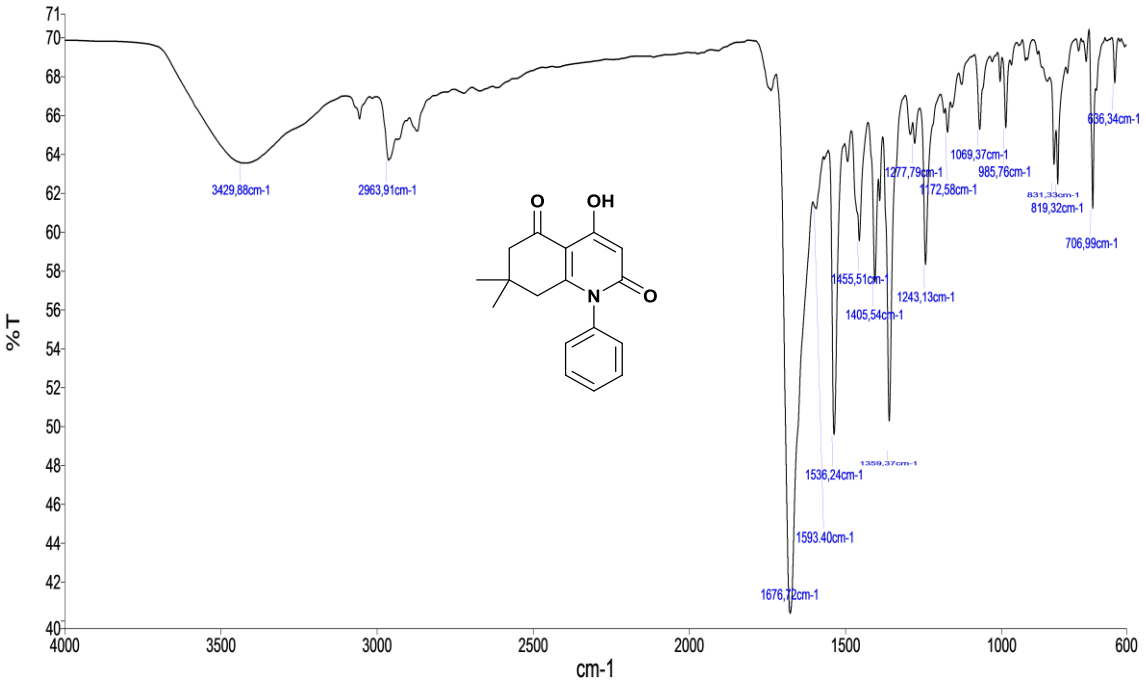

S29. IR III.7h.

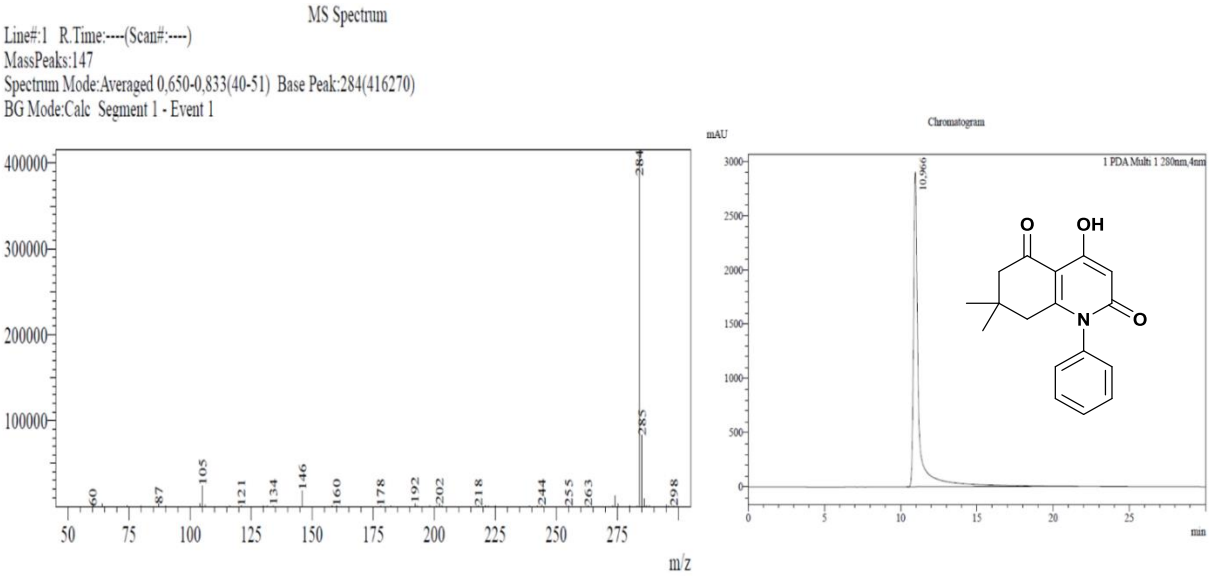

S30. LC-MS III.7h.

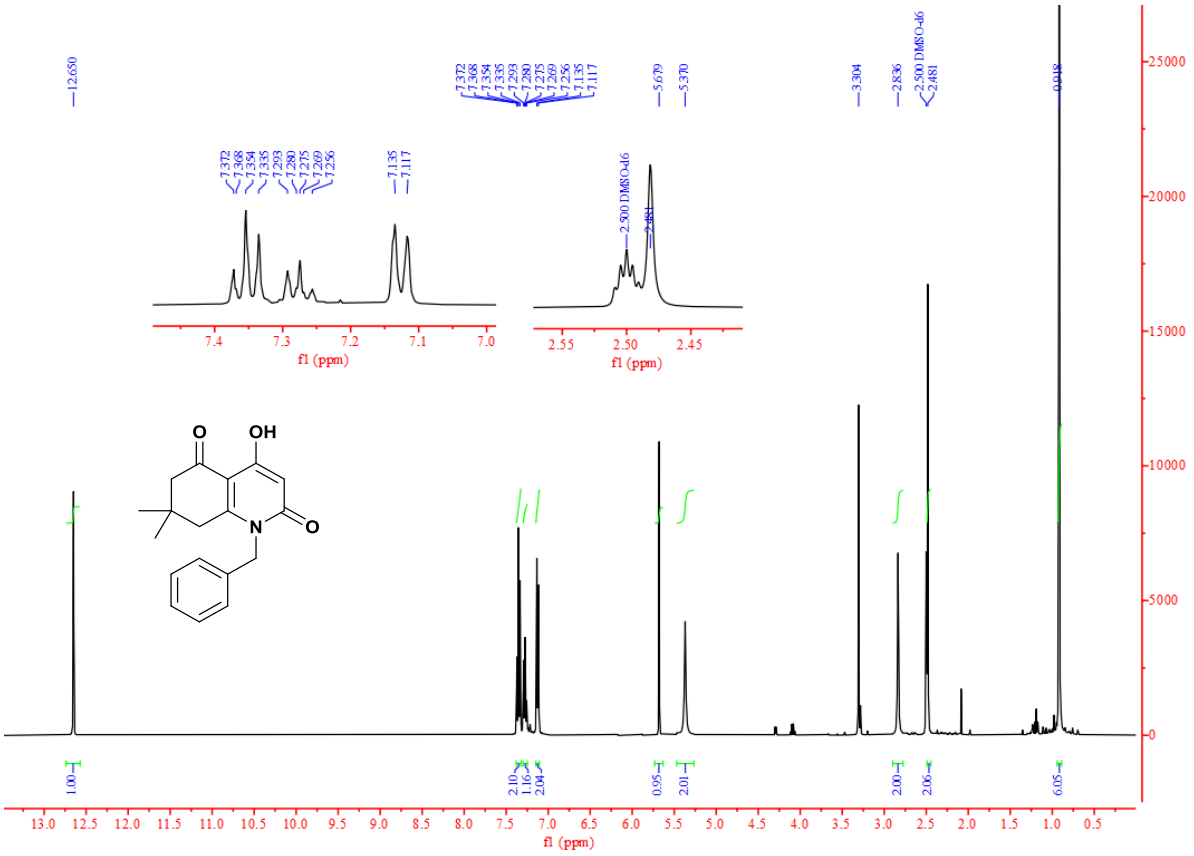

S31. ^{1}H NMR III.7i.

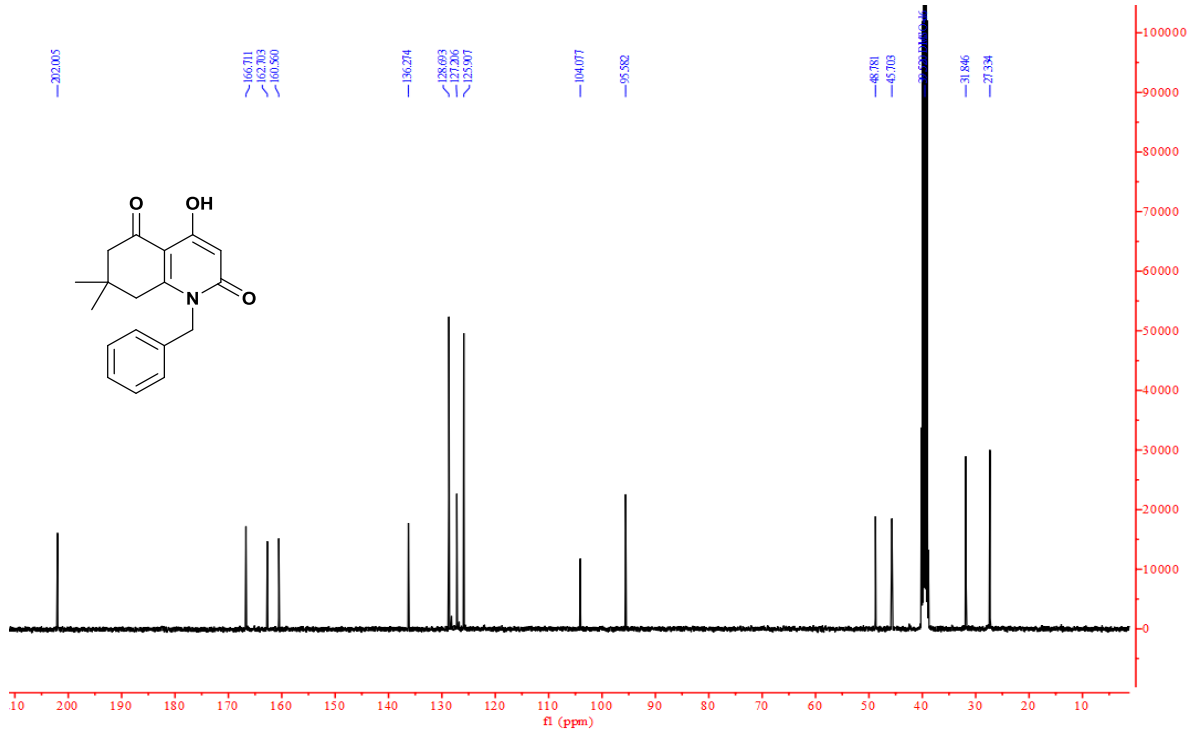

S32. ^{13}C NMR III.7i.

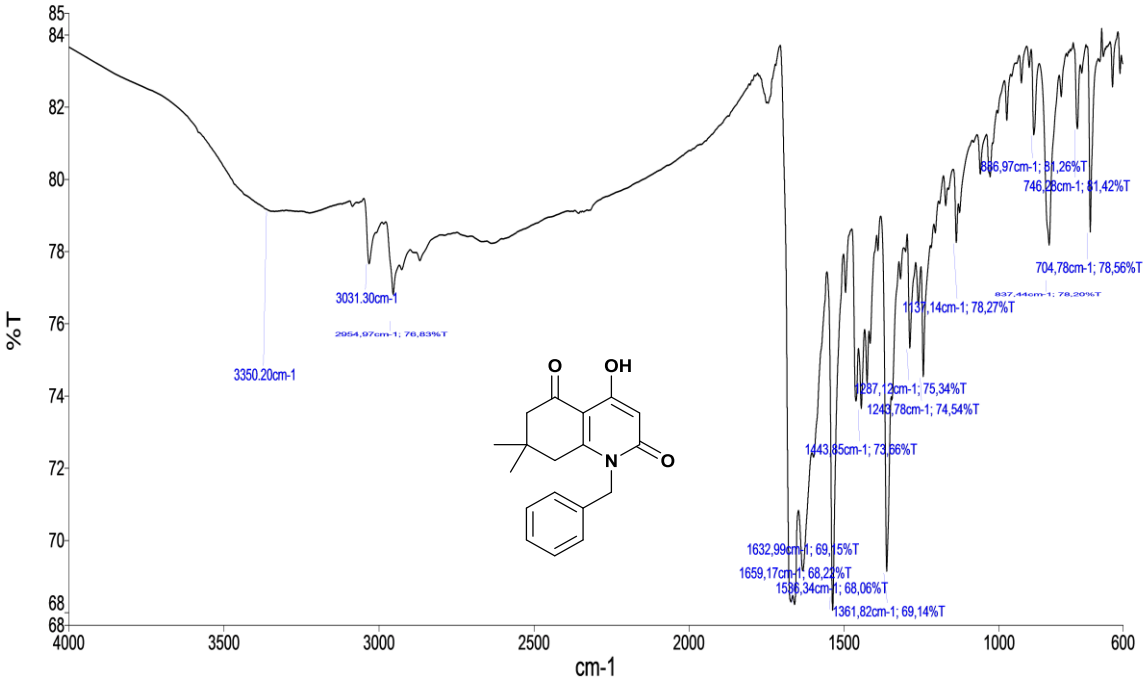

S33. IR III.7i.

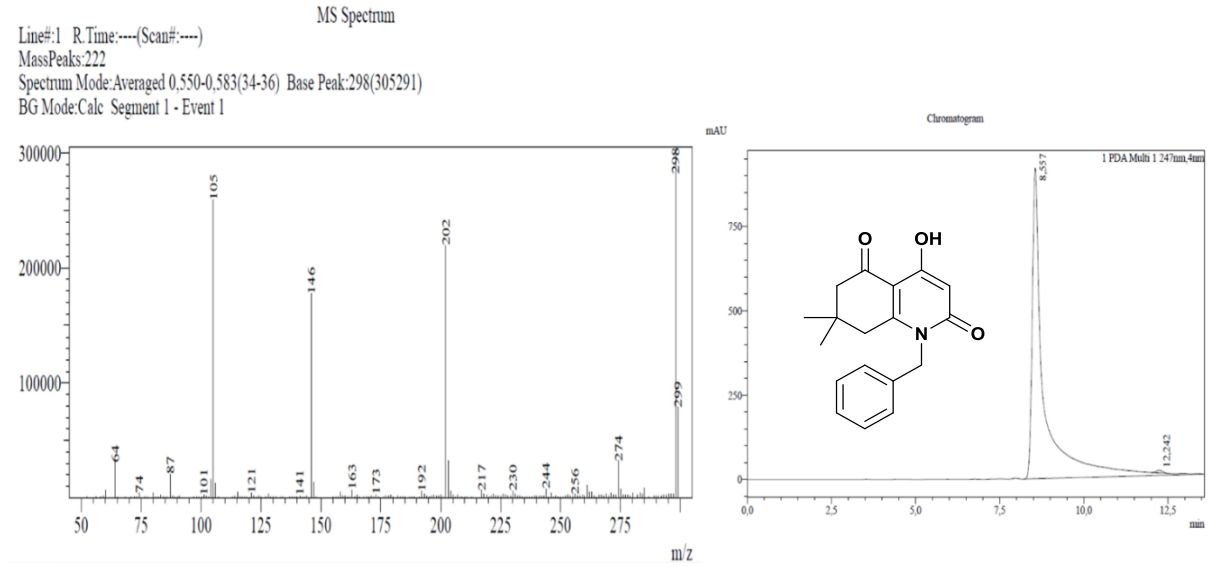

S34. LC-MS III.7i.

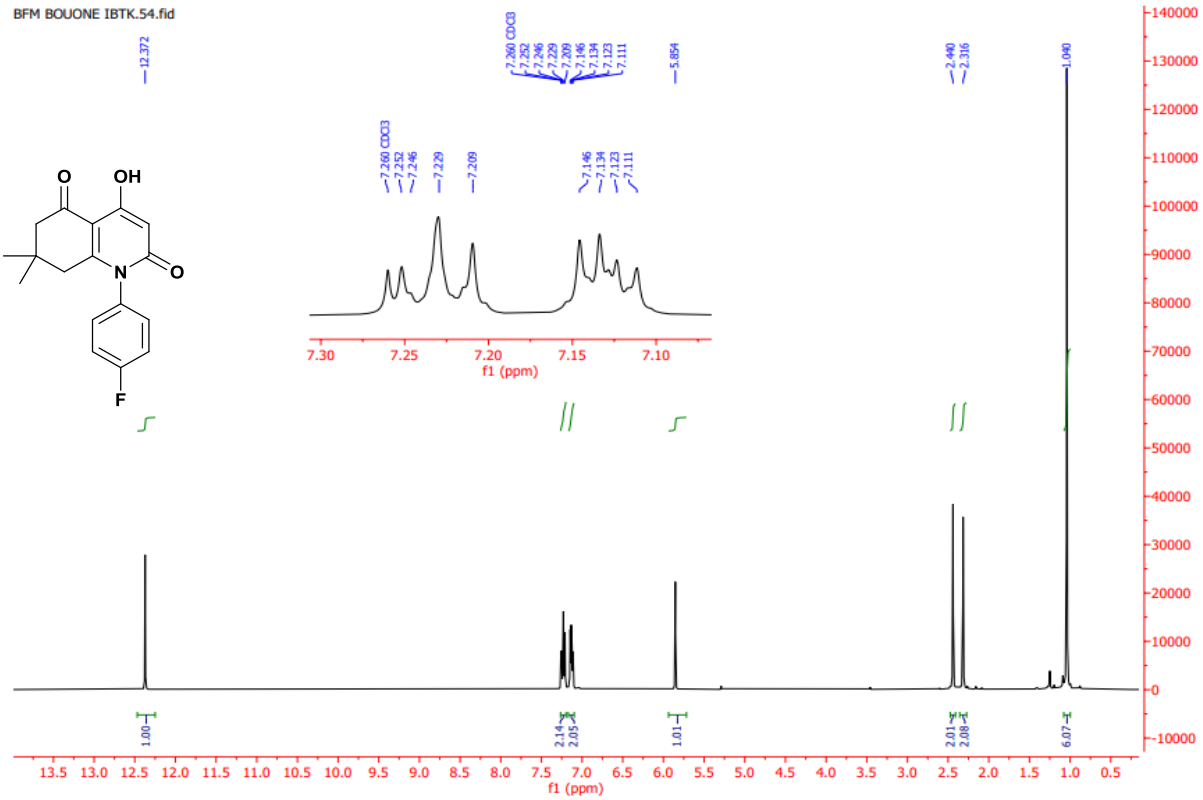

S35. ^{1}H NMR III.7j.

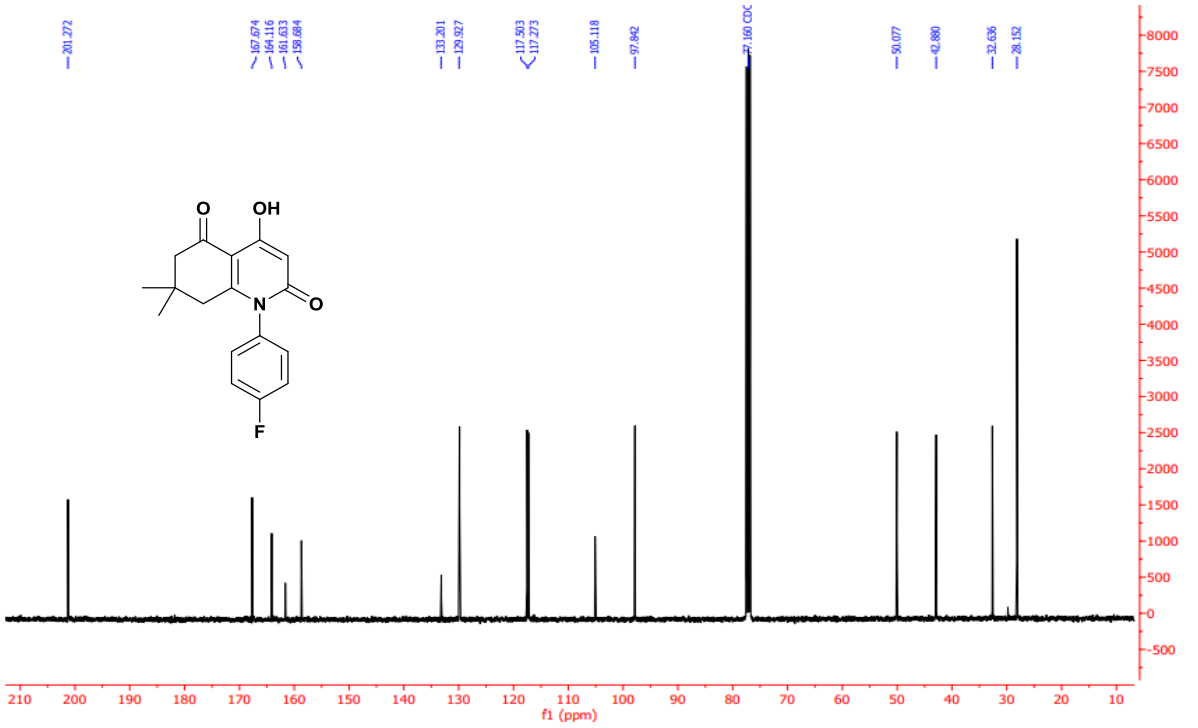

S36. ^{13}C NMR III.7j.

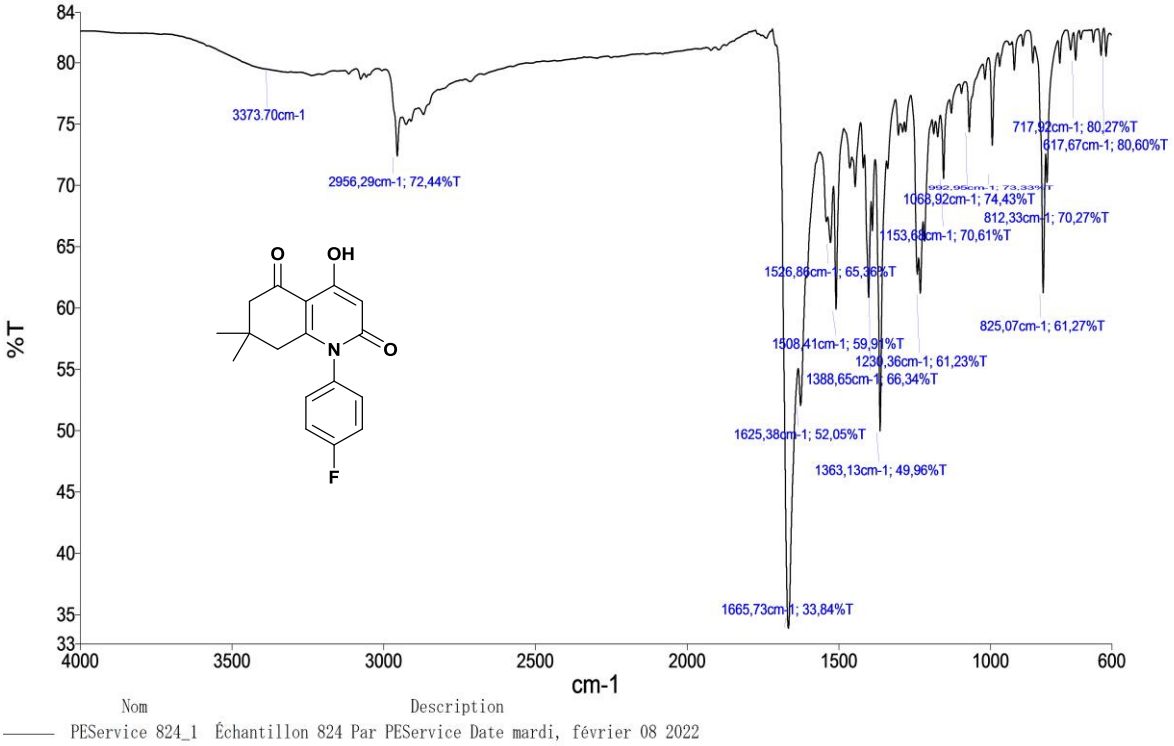

S37. IR III.7j.

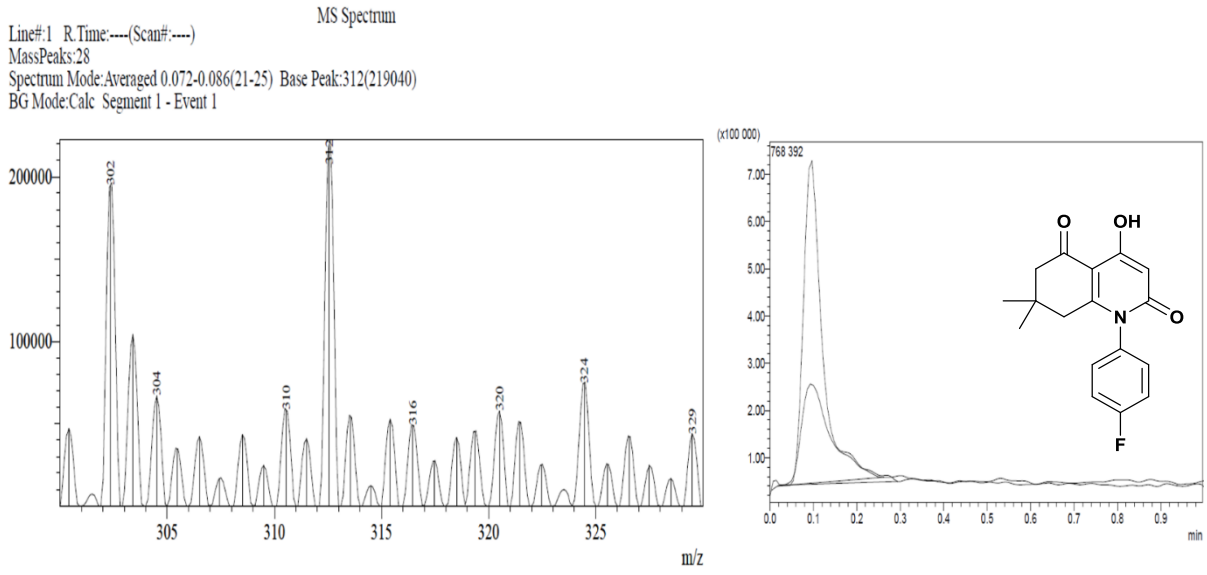

S38. LC-MS III.7j.

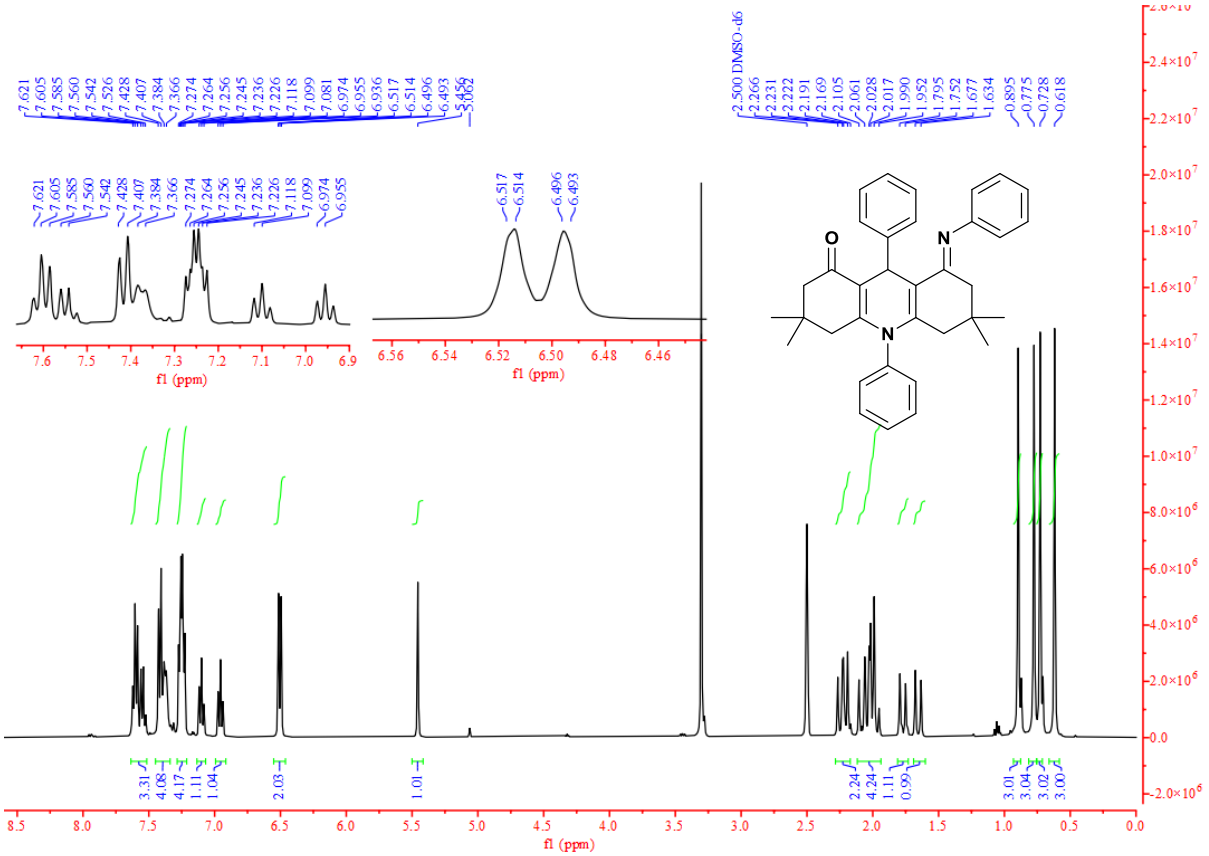

S39. ^{1}H NMR III.9a.

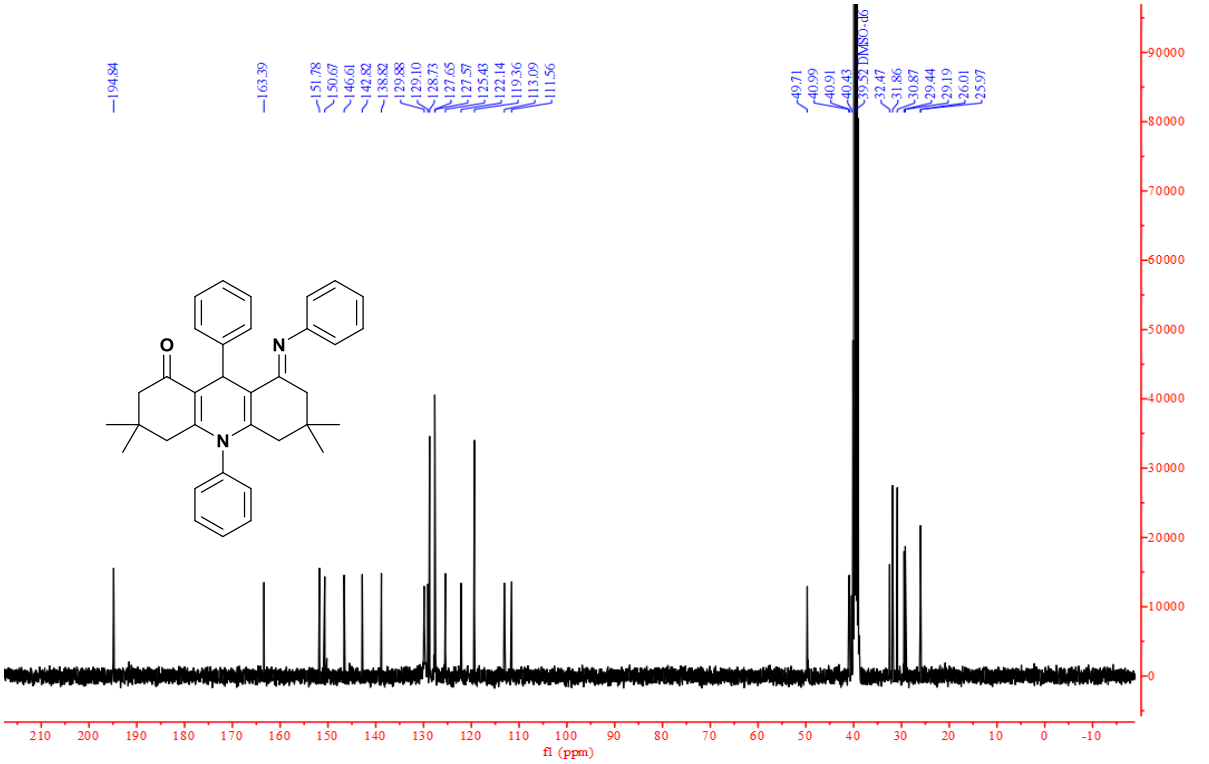

S40. ^{13}C NMR III.9a.

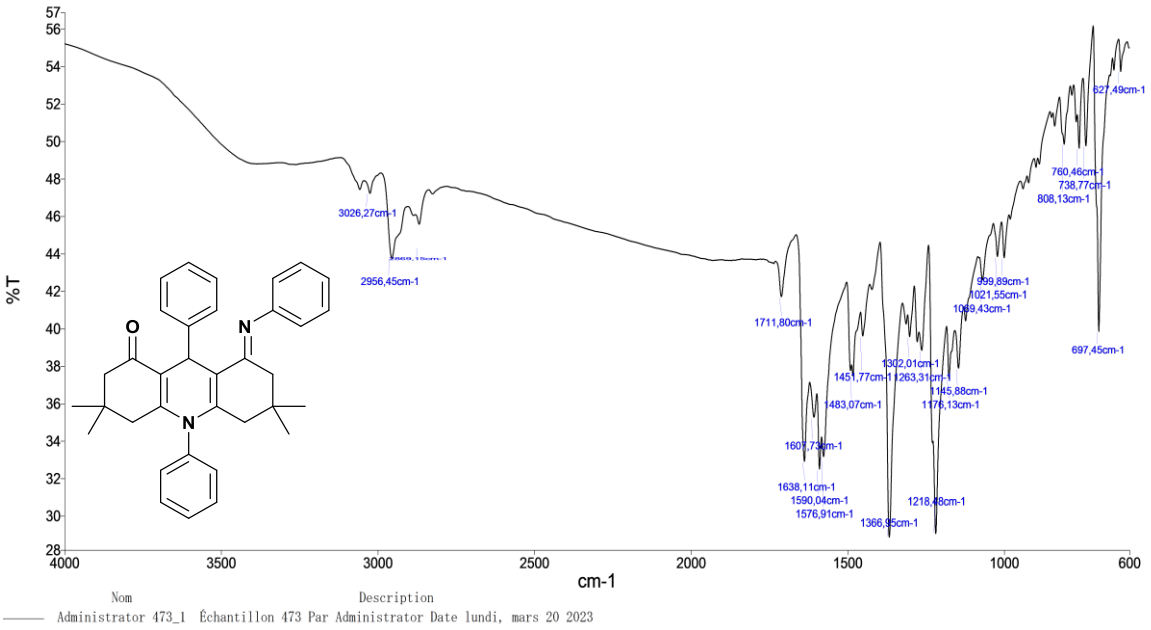

S41. IR III.9a.

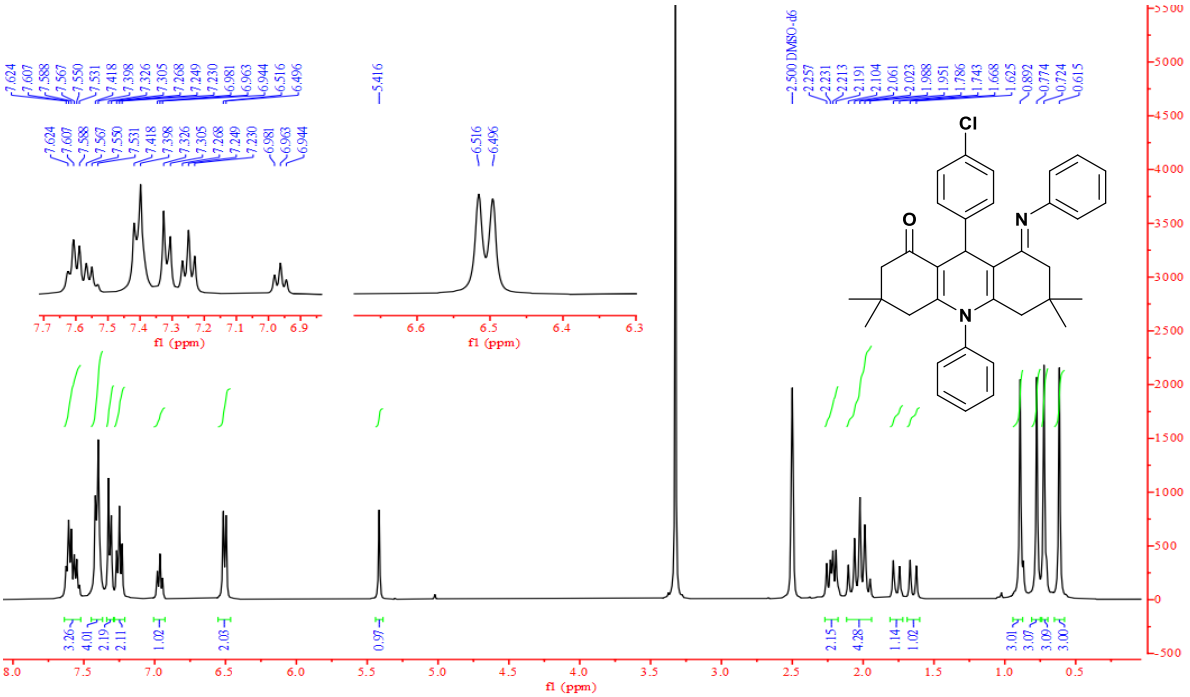

S42. ^{1}H NMR III.9b.

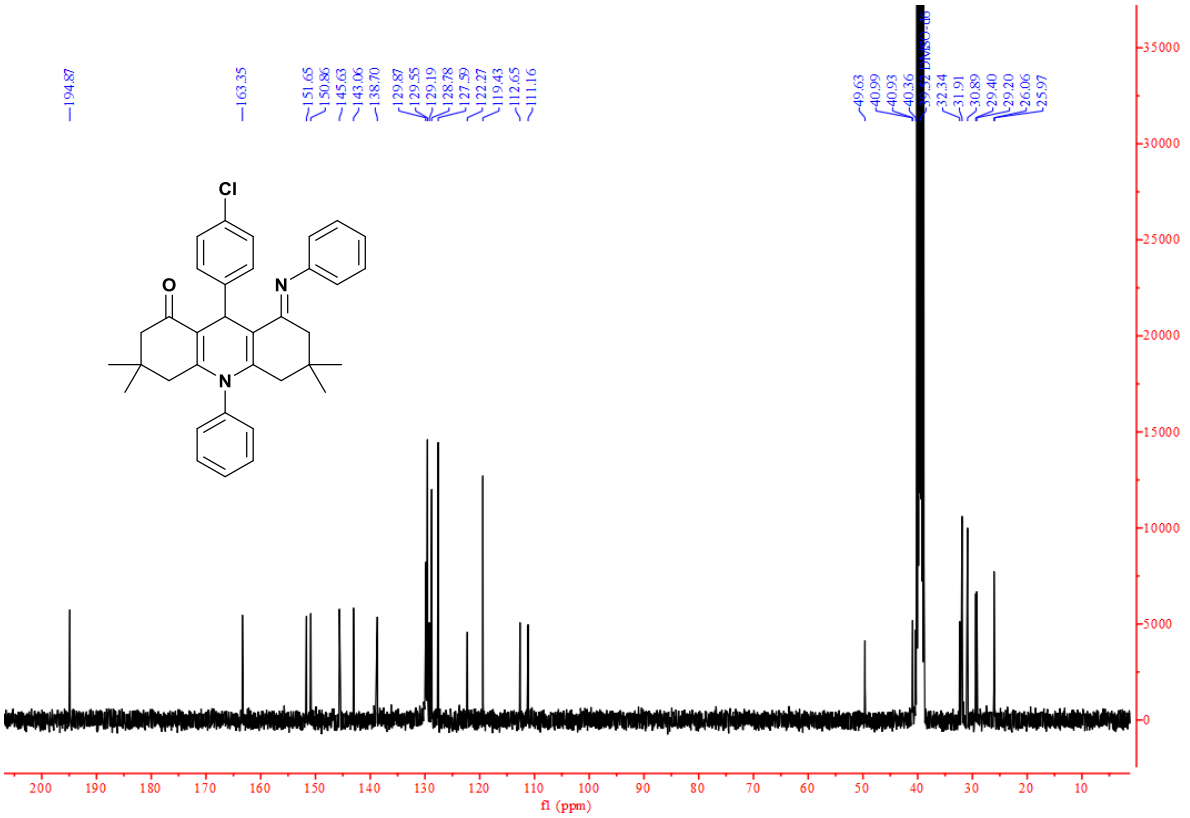

S43. ^{13}C NMR III.9b.

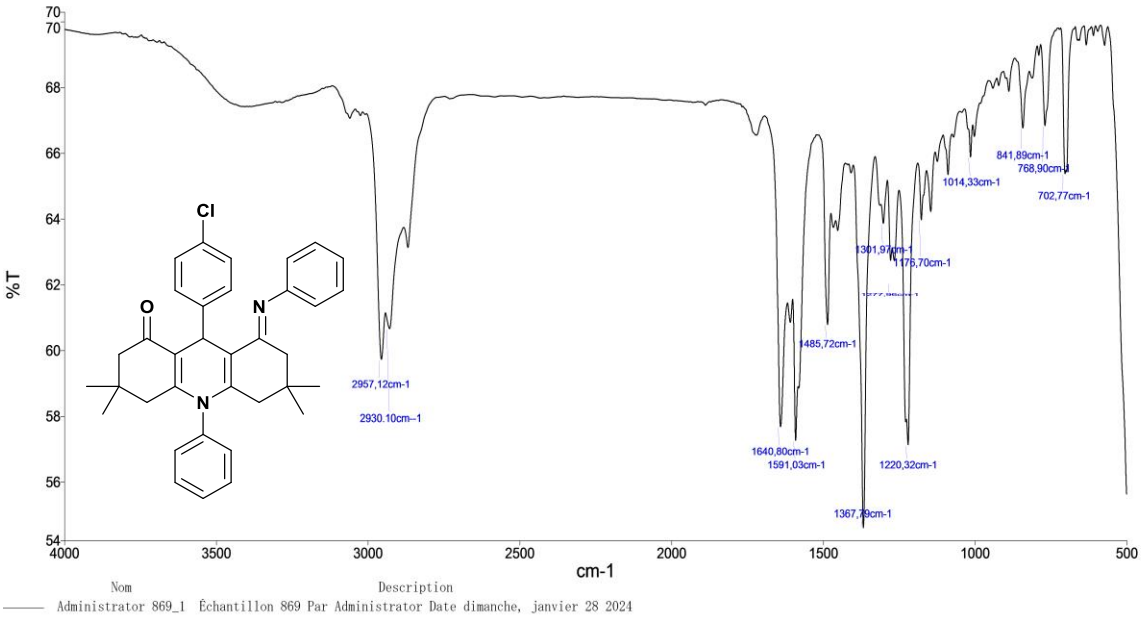

S44. IR III.9b.

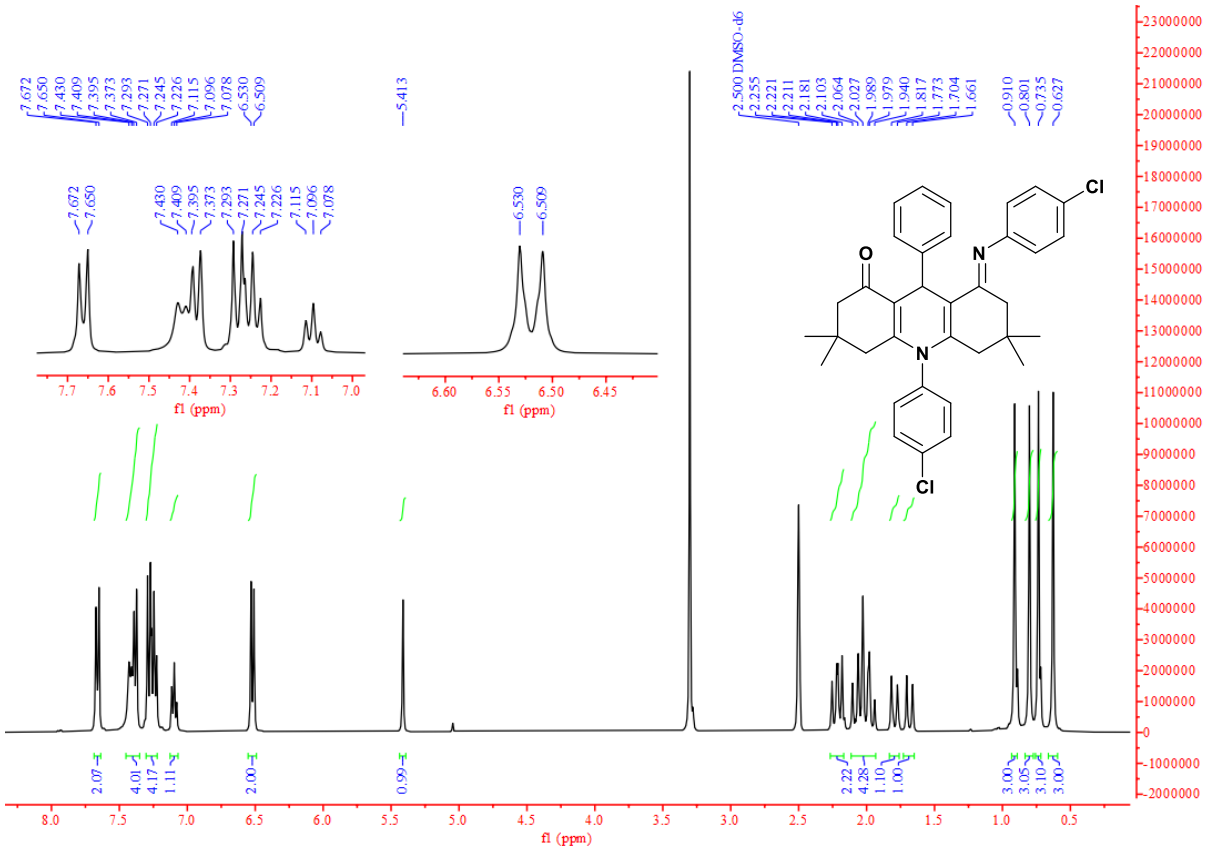

S45. ^{1}H NMR III.9c.

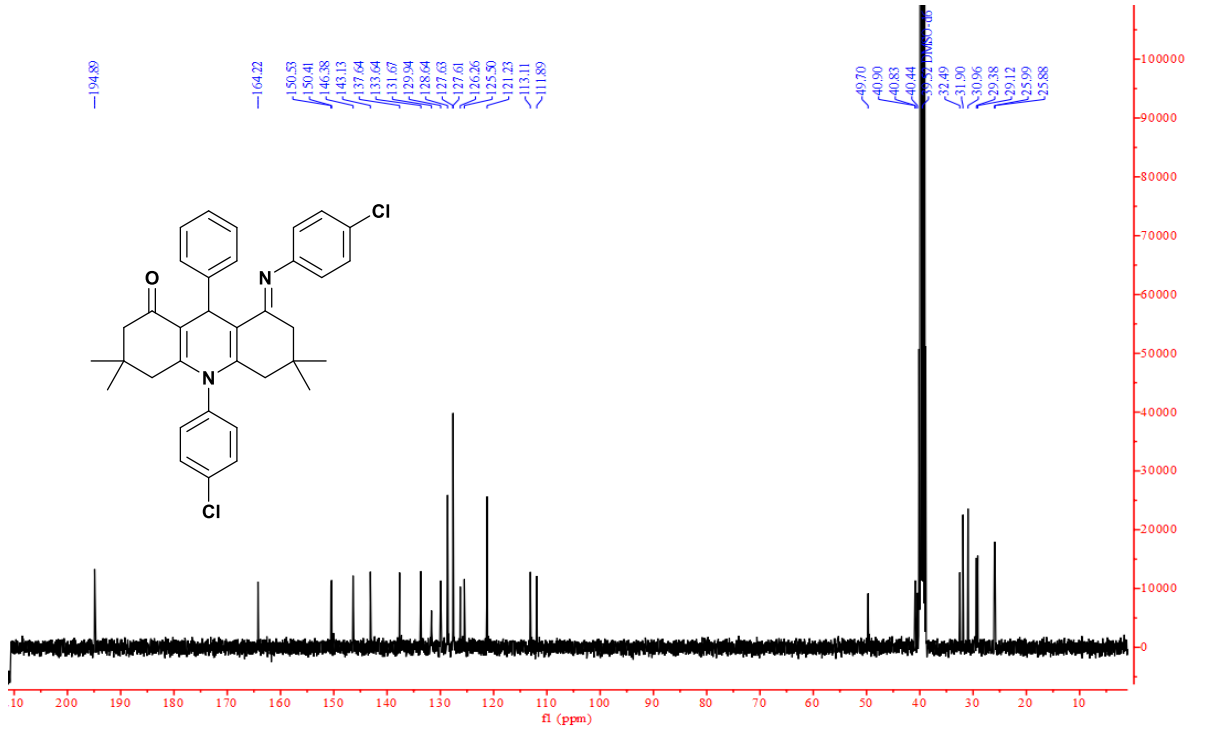

S46. ^{13}C NMR III.9c.

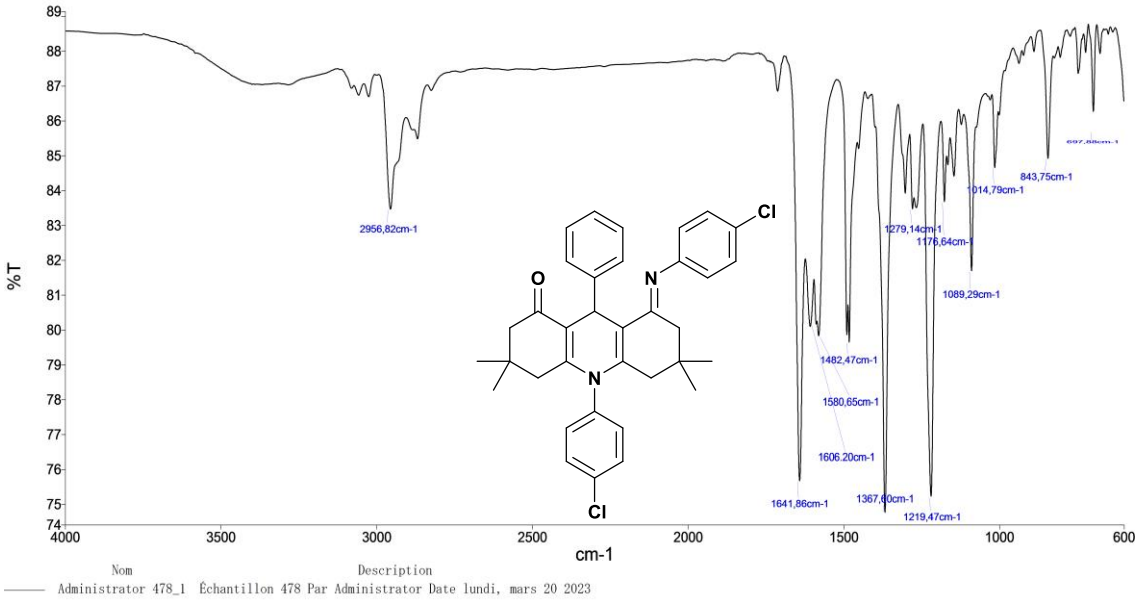

S47. IR III.9c.

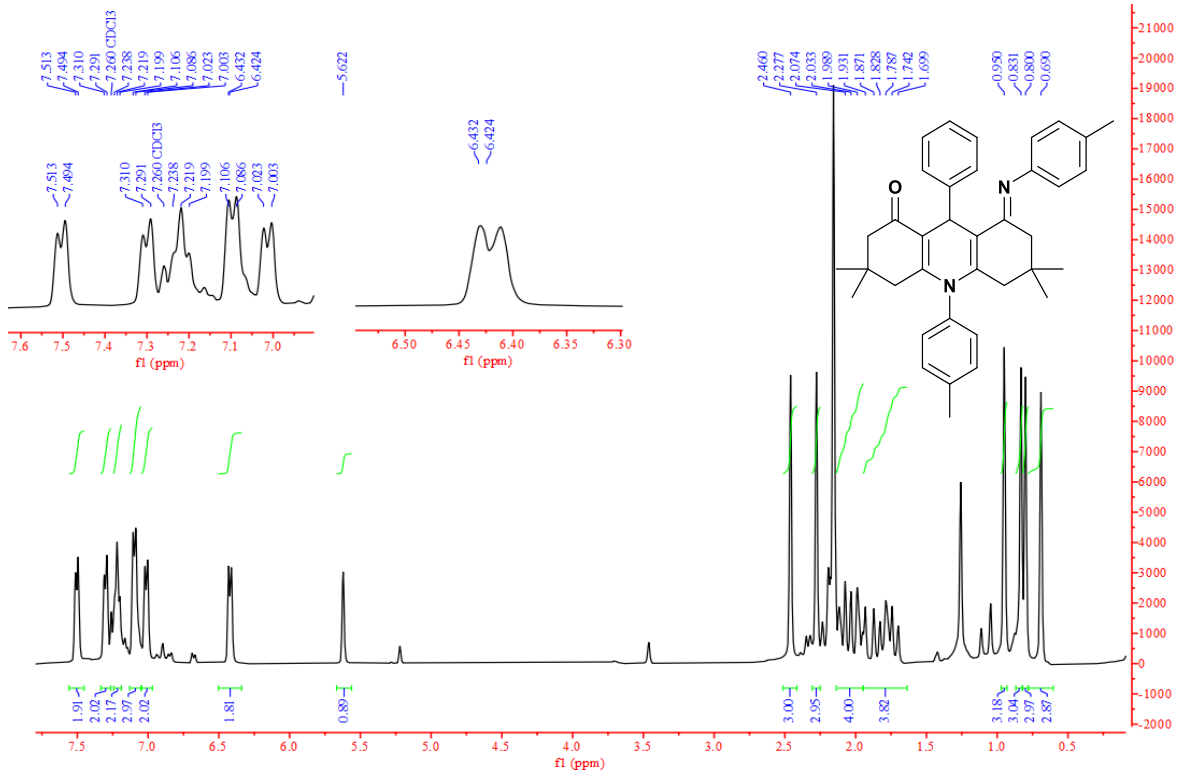

S48. ^{1}H NMR III.9d.

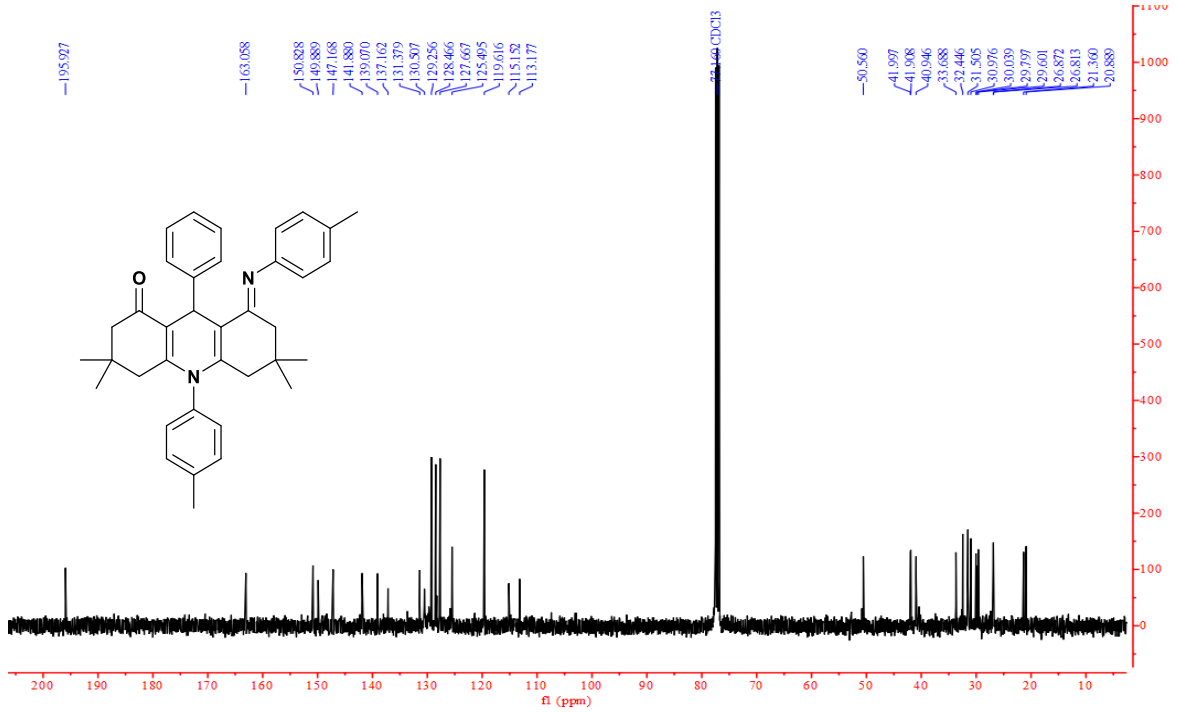

S49. ^{13}C NMR III.9d.

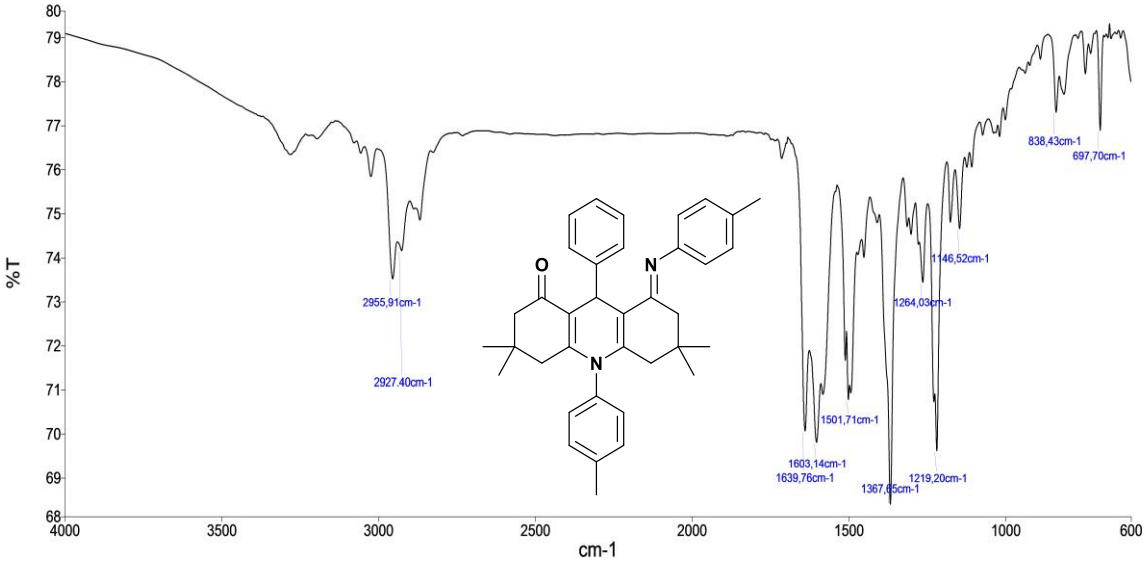

S50. IR III.9d.

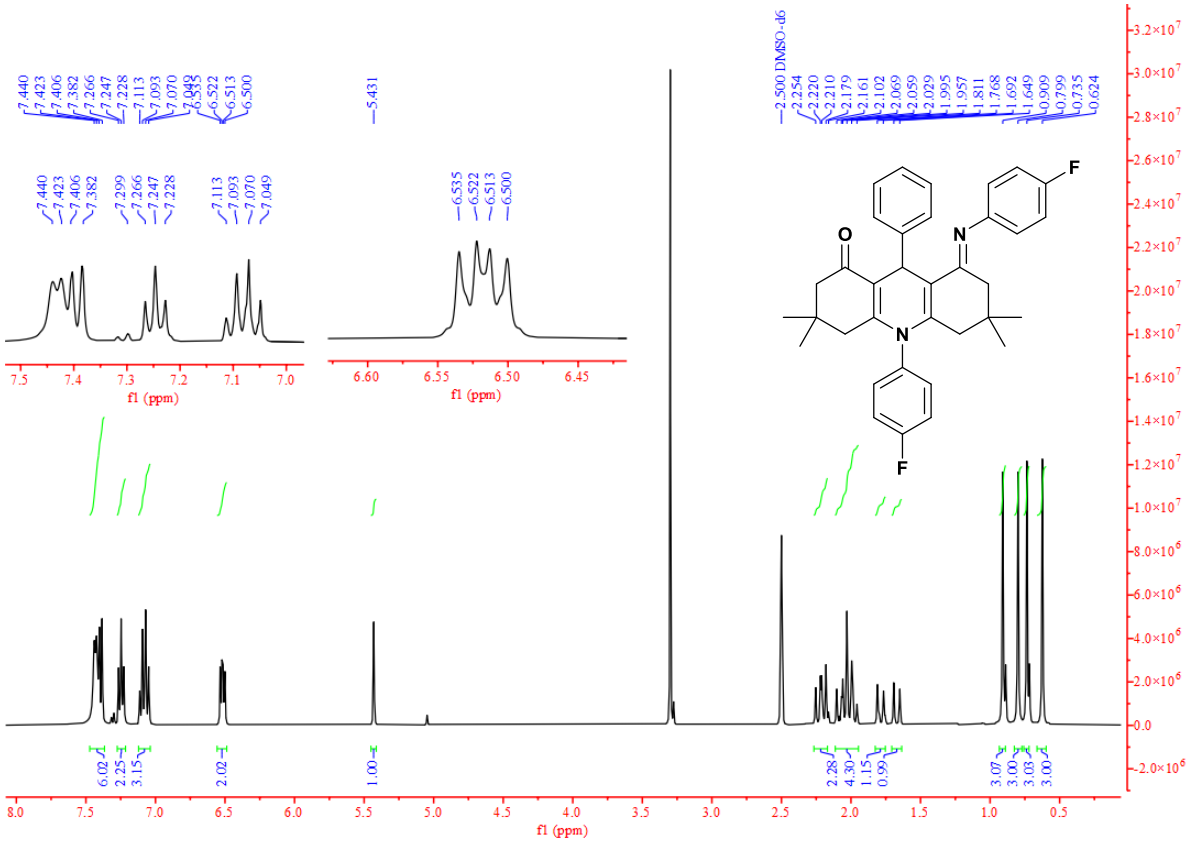

S51. ^{1}H NMR III.9e.

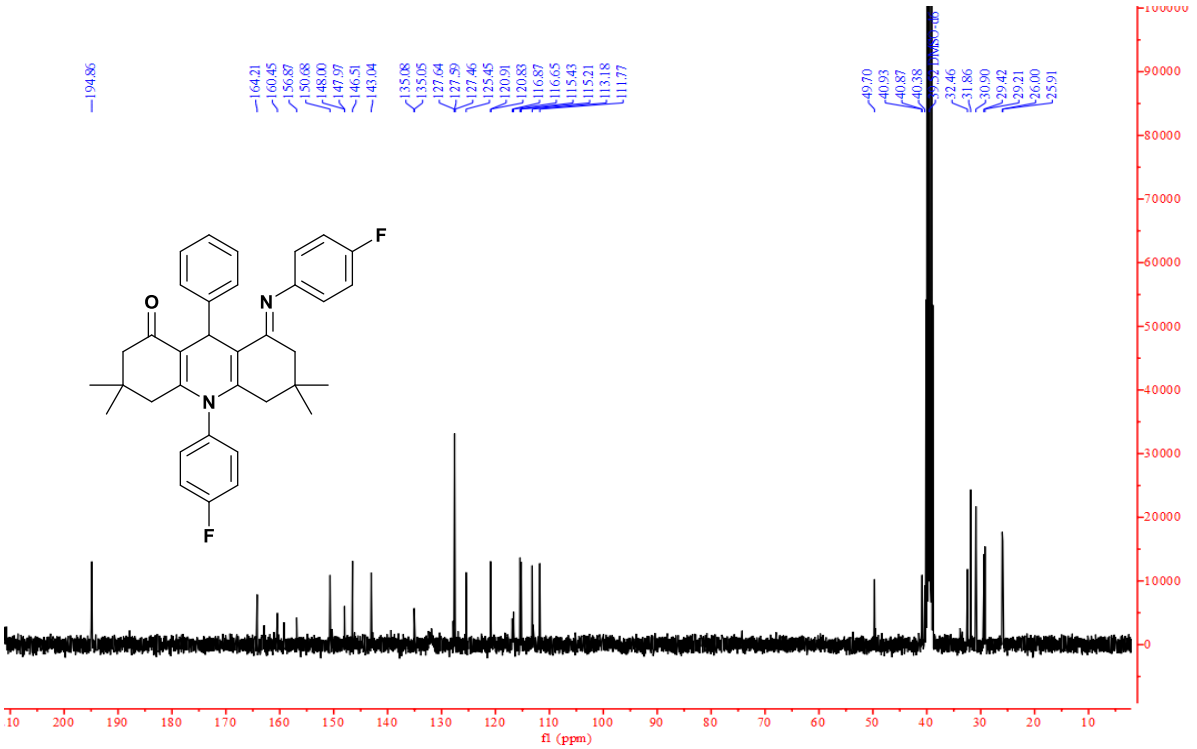

S52. ^{13}C NMR III.9e.

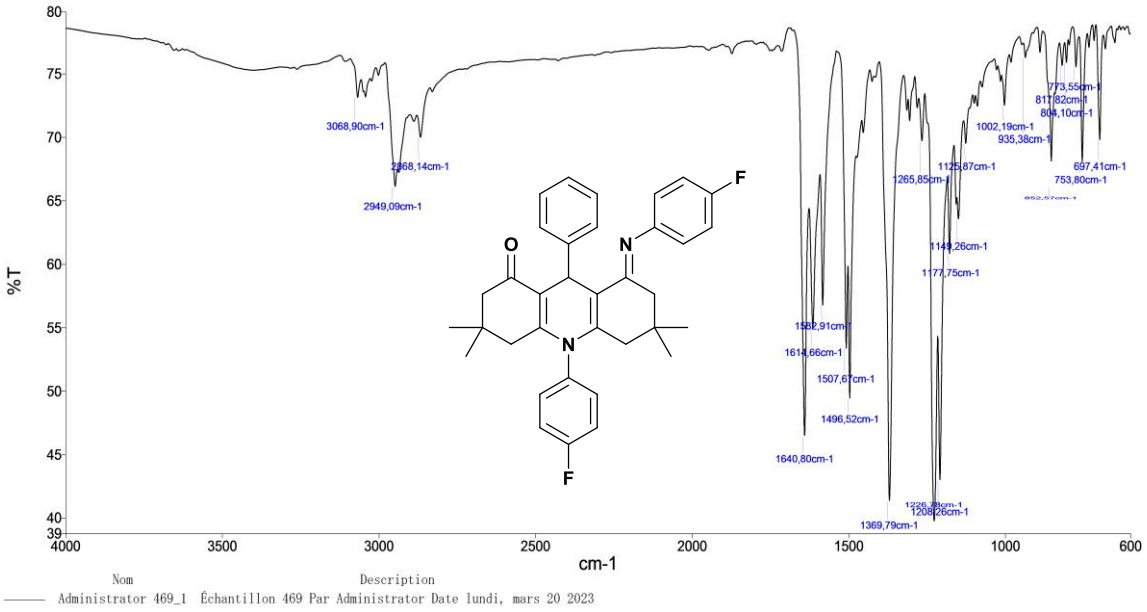
%T
cm-1
3068,90cm-1
2949,09cm-1
1640,80cm-1
1614,66cm-1
1507,67cm-1
1496,52cm-1
1369,79cm-1
1265,85cm-1
1177,75cm-1
1149,26cm-1
1125,87cm-1
1002,19cm-1
935,38cm-1
817,82cm-1
808,10cm-1
753,80cm-1
697,41cm-1
O
N
N
F
F
Nom
Description
Administrator 469_1 Échantillon 469 Par Administrator Date lundi, mars 20 2023

S53. IR III.9e.